

The *glmS* ribozyme is an antibacterial target

Mode of action analysis, investigation of potential metabolite analogs and characterization of *glmS* ribozyme variants of human pathogens

Dissertation

zur
Erlangung des Doktorgrades (Dr. rer. nat.)
der
Mathematisch-Naturwissenschaftlichen Fakultät
der
Rheinischen Friedrich-Wilhelms-Universität Bonn
vorgelegt von

Anna Katharina Schüller

aus

Bonn

Bonn 2017

Angefertigt mit Genehmigung der Mathematisch-
Naturwissenschaftlichen Fakultät der Rheinischen Friedrich-
Wilhelms-Universität Bonn

1. Gutachter: Prof. Dr. Günter Mayer
2. Gutachter: Prof. Dr. Tanja Schneider
Tag der Promotion: 10.04.2018
Erscheinungsjahr: 2018

Parts of this thesis have been published in:

- Schüller, A.; Matzner, D.; Lünse, C. E.; Wittmann, V.; Schumacher, C.; Unsleber, S.; Brötz-Oesterhelt, H.; Mayer, C.; Bierbaum, G.; Mayer, G., Activation of the glmS Ribozyme Confers Bacterial Growth Inhibition. *ChemBioChem* **2017**, 18 (5), 435-440
- Matzner, D.; Schüller, A.; Seitz, T.; Wittmann, V.; Mayer, G., Fluoro-carba-sugars are glycomimetic activators of the glmS ribozyme. *Chemistry – A European Journal* **2017**, 23 (51), 12604-12612.
- Lünse, C. E.; Schüller, A.; Mayer, G., The promise of riboswitches as potential antibacterial drug targets. *Int J Med Microbiol* **2013**.

Contents

Contents	i
List of Figures	v
List of Tables.....	viii
List of Abbreviations.....	ix
Abstract.....	1
Zusammenfassung	3
1 Introduction	4
1.1 Bacteria of relevance for this thesis	4
1.2 Identification of antibiotics.....	5
1.2.1 The problem of antibiotic resistance.....	7
1.2.2 The bacterial cell wall as antibiotic drug target.....	8
1.3 RNA as drug target.....	11
1.4 Non-coding regulatory RNAs and their role in antibacterial processes ..	12
1.5 Natural ribozymes.....	15
1.6 Riboswitches.....	17
1.6.1 Riboswitches as drug targets	21
1.7 The glmS riboswitch is a self-cleaving ribozyme.....	24
1.7.1 The glmS ribozyme and its metabolites.....	24
1.7.2 The glmS ribozyme and its dependency on divalent cations.....	29
1.7.3 2D and 3D structure of the glmS ribozyme.....	30
1.7.4 The glmS ribozyme employs a self-cleavage mechanism.....	32
1.7.5 The glmS ribozyme regulates the expression of the glmS gene	34
1.8 The GlmS enzyme	34
2 Aim of the study	37
3 Results.....	38
3.1 Screening of potential glmS ribozyme modulators with 3D shape similarity to the natural metabolite, GlcN6P.....	38
3.1.1 Structure activity relationship of Reymond compound D2 and its isomers	41
3.1.2 Refinement of screening compounds with a similar 3D shape to GlcN6P for modulation of glmS ribozyme activity	44
3.2 Mode of action analysis of CGlcN on B. subtilis.....	46
3.2.1 Antibacterial effect of CGlcN on B. subtilis	48

3.2.2	Investigation of potential uptake and subsequent phosphorylation of CGlcN by bacterial phosphoenol-pyruvate transport systems (PTSs).....	49
3.2.3	Quantitative real-time PCR analysis to determine the intracellular effect of CGlcN on glmS levels in <i>B. subtilis</i>	53
3.2.4	Quantitative real-time PCR analysis to determine the intracellular effect of CGlcN on glmS levels in <i>S. aureus</i>	59
3.2.5	Induction of stress inducible promoters by CGlcN	62
3.2.6	Antibacterial effect of CGlcN on <i>B. subtilis</i> in LB-medium	64
3.3	Experimental validation of glmS ribozymes of pathogenic bacteria.....	65
3.3.1	Screening of different sugars to identify activating metabolites of <i>C. difficile</i> and <i>L. monocytogenes</i> glmS ribozyme	69
3.3.2	Concentration-dependent analysis of self-cleavage induction by GlcN6P and GlcN in <i>C. difficile</i> and <i>L. monocytogenes</i> glmS ribozymes	72
3.3.3	Investigation of different metal ions participating in glmS ribozyme self-cleavage of <i>C. difficile</i> and <i>L. monocytogenes</i>	74
3.3.4	pH-dependency of glmS ribozyme variants of <i>C. difficile</i> and <i>L. monocytogenes</i>	76
3.3.5	Determination of glmS ribozyme cleavage rates of <i>C. difficile</i> and <i>L. monocytogenes</i>	77
3.3.6	Influence of the temperature on the glmS ribozyme self-cleavage of <i>C. difficile</i> and <i>L. monocytogenes</i>	79
3.3.7	Kinetics of <i>L. monocytogenes</i> glmS self-cleavage at 6 °C.....	80
3.4	Screening and Mode of Action analysis of novel carba-sugar variants ..	81
3.4.1	Screening of carba-sugar derivative for glmS ribozyme activation ..	82
3.4.2	Concentration-dependent analysis of FC- α -D-GlcN6P-induced cleavage of glmS ribozymes	84
3.4.3	Kinetic analysis of FC- α -D-GlcN6P-induced cleavage of glmS ribozymes.....	85
3.4.4	Antibacterial effect of FC- α -D-GlcN on <i>B. subtilis</i>	86
3.4.5	Analysis of the uptake of FC- α -D-GlcN by PTS	87
3.4.6	Induction of stress inducible promoters by FC- α -D-GlcN.....	89
4	Discussion.....	91
4.1	glmS ribozyme modulators with shape similarity to GlcN6P	91
4.1.1	In silico screening of glmS ribozyme modulators.....	91
4.1.2	In silico screening of glmS ribozyme modulators.....	94
4.2	MoA analysis CGlcN	98

4.2.1	Uptake of CGlcN	100
4.2.2	CGlcN reduces glmS ribozyme and gene levels intracellularly	101
4.2.3	CGlcN treatment can be linked to bacterial cell wall biosynthesis.	102
4.2.4	Perspectives based on the findings of CGlcN as antibacterial targeting the glmS ribozyme	103
4.3	Experimental validation of in silico predicted glmS ribozymes	104
4.3.1	Activators of <i>C. difficile</i> and <i>L. monocytogenes</i> glmS ribozyme self-cleavage	106
4.3.2	Divalent metal ions participating in glmS ribozyme self-cleavage of <i>C. difficile</i> and <i>L. monocytogenes</i>	106
4.3.3	pH dependency of glmS ribozyme self-cleavage of <i>C. difficile</i> and <i>L. monocytogenes</i>	108
4.3.4	Kinetic of glmS ribozyme self-cleavage of <i>C. difficile</i> and <i>L. monocytogenes</i>	108
4.3.5	Temperature-dependency of glmS ribozyme self-cleavage of <i>C. difficile</i> and <i>L. monocytogenes</i>	109
4.4	carba-sugar derivatives.....	110
5	Outlook	112
5.1	glmS ribozyme modulators with in silico predicted 3D shape similarity to GlcN6P.....	112
5.2	The glmS ribozyme activators CGlcN6P and FC- α -D-GlcN6P and their MoA	112
5.3	Validation and characterization of novel glmS ribozyme variants	114
6	Material & Methods.....	116
6.1	Material	116
6.1.1	Equipment.....	116
6.1.2	Chemicals	117
6.1.3	Solutions, Buffers	120
6.1.4	Kits	120
6.1.5	Chemically defined medium	121
6.1.6	Bacterial strains.....	122
6.1.7	Standards, nucleotides.....	123
6.1.8	Synthetic oligos	123
6.1.9	Sequences of glmS ribozymes.....	124
	<i>S. aureus</i> Mu50	124

6.1.10	Software	127
6.2	Methods	128
6.2.1	Preparation of DEPC water	128
6.2.2	PCR	128
6.2.3	Quantitative real-time PCR	129
6.2.4	Agarose gel electrophoresis	131
6.2.5	Polyacrylamide gel electrophoresis (PAGE)	132
6.2.6	In vitro transcription	133
6.2.7	RNA work up after in vitro transcription	134
6.2.8	RNA work up by electroelution used for non-cleaving <i>S. aureus</i> FRET leader strand	134
6.2.9	5' Dephosphorylation	135
6.2.10	Phenol-chloroform extraction	135
6.2.11	5' radioactive phosphorylation.....	136
6.2.12	Determination of nucleic acid concentration	136
6.2.13	RNA isolation of Gram-positive bacteria.....	136
6.2.14	Reverse Transcription for real-time PCR.....	137
6.2.15	Radioactive metabolite induced glmS ribozyme self-cleavage assay	138
6.2.16	Fluorescence based glmS ribozyme self-cleavage assays utilizing Förster resonance energy transfer (FRET) assay	139
6.2.17	Cultivation of <i>S. aureus</i> Mu50	141
6.2.18	Cultivation of <i>B. subtilis</i> 168	141
6.2.19	Minimal inhibitory concentration (MIC)	141
6.2.20	Growth curve	142
6.2.21	Δ PTS mutants	142
6.2.22	Promotor-gene assay	143
7	Appendix	144
8	References.....	153
	Acknowledgment.....	168

List of Figures

Figure 1: Cellular bacterial targets addressed by antibiotics	8
Figure 2: Illustration of bacterial cell wall biosynthesis and the corresponding cell wall inhibiting antibiotics modified after Schneider & Sahl 2010. ⁴⁷	9
Figure 3: ncRNA based regulatory mechanisms.....	13
Figure 4: Catalytic strategies of natural ribozymes regarding the transfer of a phosphate group, modified after Lilley 2017. ⁹⁰	15
Figure 5: Riboswitch based gene regulatory mechanisms.....	18
Figure 6: Chemical structures of analogs and non-active analogs of GlcN6P regarding glmS ribozyme activation	25
Figure 7: Recognition of the natural metabolite, GlcN6P by the glmS ribozyme taken from Cochrane et al. ¹³⁰	27
Figure 8: Chemical structures of CGlcN6P and CGlcN	28
Figure 9: Comparison of active sites of glmS ribozymes modified after Lau and Ferré D´ Amaré 2013 ¹⁶¹	29
Figure 10: Consensus sequence and crystal structure of the glmS ribozyme taken from McCown et al. 2012 ¹⁶⁷	31
Figure 11: Gene regulatory mechanism employed by the glmS ribozyme	33
Figure 12: Self-cleavage mechanism employed by the glmS ribozyme modified after Viladoms et al. ¹⁷⁷	33
Figure 13: Screening for activation of glmS ribozyme self-cleavage by 1 st generation Reymond compounds	39
Figure 14: Screening for inhibition of GlcN6P-induced glmS ribozyme cleavage by 1 st generation Reymond compounds	40
Figure 15: Concentration-dependent inhibition of GlcN6P-induced glmS ribozyme self-cleavage by Reymond compound D2 and isomers	42
Figure 16: Screening of compounds structurally similar to D2	43
Figure 17: Screening of the 2 nd generation Reymond compounds for induction of glmS ribozyme self-cleavage	45
Figure 18: Screening for inhibition of GlcN6P-induced glmS ribozyme self-cleavage by the 2 nd generation of Reymond compounds	46
Figure 19: Growth of <i>S. aureus</i> in the presence of CGlcN in CDM	47
Figure 20: Scheme of proposed MoA of CGlcN	47
Figure 21: Growth of <i>B. subtilis</i> in the presence of CGlcN in CDM	49
Figure 22: Schematic drawing of PTS modified after Deutscher et al 2006 ⁵⁶	50
Figure 23: Growth curve analysis of <i>B. subtilis</i> 168 wt and PTS knock out strains in the presence of GlcN and CGlcN	51
Figure 24: Growth curve analysis of PTS deleted strains in presence of CGlcN	52
Figure 25: Growth curve analysis of PTS deleted strains in presence of CGlcN monitored for 23.75 h (1425 min).....	52
Figure 26: Growth curve analysis of PTS deleted strains with the addition of CGlcN after 270 min.....	53
Figure 27: Shema of sample preparation for qPCR analysis	54

Figure 28: Growth curve of <i>B. subtilis</i> pre-grown to OD ₆₀₀ ~0.35 and then incubated in the presence of CGlcN to define the timepoint at which the effect of treatment becomes visible for later RNA extraction experiments	55
Figure 29: Agarose gel of total RNA isolated from <i>B. subtilis</i>	56
Figure 30: Representative qPCR analysis.....	56
Figure 31: Analysis of qPCR products of <i>B. subtilis</i>	57
Figure 32: Amplification efficacy of qPCR constructs	58
Figure 33: Quantitative real-time PCR analysis of glmS gene and glmS ribozyme levels in the presence of CGlcN of <i>B. subtilis</i>	59
Figure 34: Growth curve of <i>S. aureus</i> pre-grown to an OD ₆₀₀ ~0.3 and then incubated in the presence of CGlcN to define the timepoint at which the effect of treatment becomes visible for later RNA extraction experiments	60
Figure 35: Agarose gel of total RNA isolated from <i>S. aureus</i>	61
Figure 36: Analysis of qPCR products of <i>S. aureus</i>	61
Figure 37: qPCR analysis of glmS gene+ribozyme levels in <i>S. aureus</i> in the presence of CGlcN or GlcN.....	62
Figure 38: Induction of stress inducible promoters by the corresponding reference antibiotics	63
Figure 39: Stress inducible promoter gene assay in the presence of CGlcN	64
Figure 40: Growth curve of <i>B. subtilis</i> in the presence of CGlcN in LB-medium..	65
Figure 41: PCR products of glmS ribozymes	66
Figure 42: PAGE gel of radioactive metabolite-induced cleavage assay to study glmS ribozyme activity.....	67
Figure 43: Screening for glmS ribozyme activity by radioactive metabolite induced self-cleavage assay.....	68
Figure 44: Secondary structure prediction of glmS ribozyme cores of <i>C. difficile</i> and <i>L. monocytogenes</i>	69
Figure 45: Chemical structures of sugars screened for <i>C. difficile</i> and <i>L. monocytogenes</i> glmS ribozyme self-cleavage induction	70
Figure 46: Screening of various sugars for the induction of glmS ribozyme cleavage of <i>C. difficile</i> and <i>L. monocytogenes</i>	71
Figure 47: EC ₅₀ value determination for GlcN6P- and GlcN-induced self-cleavage of the glmS ribozyme of <i>C. difficile</i> and <i>L. monocytogenes</i>	73
Figure 48: Self-cleavage of glmS ribozymes in the presence of GlcN6P and different divalent ions	74
Figure 49: EC ₅₀ value determination of GlcN6P-induced cleavage of glmS ribozymes in the presence of different divalent ions.....	75
Figure 50: Analysis of pH-dependency of glmS ribozyme cleavage.....	76
Figure 51: Determination of k _{obs} values for glmS ribozymes in the presence of GlcN6P and GlcN.....	78
Figure 52: Analysis of the effect of different temperatures on the cleavage of glmS ribozymes.....	80
Figure 53: Determination of k _{obs} values for <i>L. monocytogenes</i> glmS ribozyme in the presence of GlcN6P at 6 °C	81

Figure 54: Chemical structures of carba-sugar derivatives	82
Figure 55: Screening of novel carba-sugar variants for glmS ribozyme activation	83
Figure 56: Concentration-dependent analysis of glmS ribozyme cleavage induced by FC- α -D-GlcN6P	84
Figure 57: Cleavage kinetics of glmS ribozymes in the presence of FC- α -D-GlcN6P	85
Figure 58: Growth curve analysis of <i>B. subtilis</i> in the presence of FC- α -D-GlcN	87
Figure 59: Growth curve analysis of <i>B. subtilis</i> 168 wt and PTS knock out strains in the presence of FC- α -D-GlcN	88
Figure 60: Growth curve analysis of PTS deletion strains in the presence of FC- α -D-GlcN	89
Figure 61: Stress inducible promotor gene assay in the presence of FC- α -D-GlcN	90
Figure 62: Chemical structures of glmS ribozyme self-cleavage inhibitors identified by screening the 1 st generation Reymond compounds	92
Figure 63: Chemical structures of glmS ribozyme self-cleavage inhibitors Reymond compound D2, the isomer D2.2 and the bioisosteres 2-hydroxy-4-trifluoromethyl-aniline	94
Figure 64: Chemical structures of potential glmS ribozyme self-cleavage activators identified by screening the 2 nd generation Reymond compounds	96
Figure 65: Chemical structures of potential glmS ribozyme self-cleavage inhibitors identified by screening the 2 nd generation Reymond compounds	97
Figure 66: Chemical structure of phosphate and phosphate mimicking moieties	101
Figure 67: Chemical structures of 1 st generation Reymond compounds.....	146
Figure 68: Chemical structures of 2 nd generation Reymond compounds	151
Figure 69: Induction of stress inducible promotors by the corresponding reference antibiotics	152

List of Tables

Table 1: Classes of riboswitches. Modified after McCown et al. 2017 ¹¹⁰	19
Table 2: Riboswitch ligand analogs that exert antibacterial activity	23
Table 3: EC ₅₀ values for GlcN6P- and GlcN-induced cleavage of glmS ribozymes of <i>C. difficile</i> and <i>L. monocytogenes</i>	73
Table 4: EC ₅₀ values for GlcN6P-induced self-cleavage mediated by different divalent ions	76
Table 5: k _{obs} values for glmS ribozyme of <i>C. difficile</i>	78
Table 6: k _{obs} values for glmS ribozyme of <i>L. monocytogenes</i>	79
Table 7: k _{obs} values for glmS ribozyme of <i>L. monocytogenes</i> in the presence of GlcN6P at 6 °C.....	81
Table 8: Comparison of EC ₅₀ values regarding the self-cleavage induction by GlcN6P, CGlcN6P and FC- α -D-GlcN6P for <i>S. aureus</i> and <i>B. subtilis</i> glmS ribozymes.....	85
Table 9: k _{obs} values for FC- α -D-GlcN6P induced cleavage of glmS ribozyme of <i>S. aureus</i>	86
Table 10: k _{obs} values for FC- α -D-GlcN6P induced cleavage of glmS ribozyme of <i>B. subtilis</i>	86
Table 11: Pipetting scheme for PCR reactions.....	128
Table 12: PCR cycling program	129
Table 13: Annealing temperatures for PCR reactions	129
Table 14: Pipetting scheme real-time PCR reactions.....	130
Table 15: PCR cycles for qPCR reactions amplifying glmS ribozyme- <i>B. subtilis</i>	130
Table 16: PCR cycles for qPCR reactions amplifying the glmS gene- <i>B. subtilis</i>	130
Table 17: PCR cycles for qPCR reactions amplifying 16S rRNA- <i>B. subtilis</i>	130
Table 18: PCR cycles for qPCR reactions amplifying glmS gene- <i>S. aureus</i>	130
Table 19: PCR cycles for qPCR reactions amplifying glmS gene+ribozyme- <i>S. aureus</i>	131
Table 20: PCR cycles for qPCR reactions amplifying 16S rRNA <i>S. aureus</i>	131
Table 21: Composition of PAGE-PAA gels.....	133
Table 22: Pipetting scheme of in vitro transcription.....	133
Table 23: Pipetting scheme for dephosphorylation reactions	135
Table 24: Pipetting scheme for radioactive phosphorylation	136
Table 25: Pipetting and reaction scheme for reverse transcription.....	137
Table 26: Temperature profile for annealing of fluorescence-based cleavage assay of <i>S. aureus</i> glmS ribozyme	140
Table 27: Pipetting scheme for positive control FRET reactions	140
Table 28: Pipetting scheme for control of FRET reactions without GlcN6P.....	140
Table 29: Pipetting scheme for FRET reactions without glmS leader sequence	140
Table 30: Pipetting scheme for FRET reactions without MgCl ₂	141

List of Abbreviations

APS	ammonium persulfate
ATP	adenosine triphosphate
bp	base pairs
BSA	bovine serum albumin
<i>B. subtilis</i>	<i>Bacillus subtilis</i> , gram positive bacterium
BGSC	Bacillus genetic stock center
CDM	chemically defined medium
CIAP	calf intestine alkaline phosphatase
cpd	compound
Δ	delta, difference
dH ₂ O	distilled water
DNA	deoxyribonucleic acid
dNTP	deoxyribonucleoside triphosphate
DTT	dithiotheritol
EC ₅₀	half maximal effective concentration
EDTA	ethylenediaminetetraacetic acid
e.g.	exempli gratia (for example)
FL	full-length
GlcN	glucosamine
GlcN6P	glucosamine-6-phosphate
GlmS	glutamine-fructose-6-amidotransferase
IC ₅₀	half maximal inhibitory concentration
IPP	inorganic pyrophosphatase
k _{obs}	observed rate constant
l	litre

M	molar
mA	milli-Ampere
max.	maximal
MgCl ₂	magnesium chloride
min	minute
mRNA	messenger RNA
NaCl	sodium chloride
NaOAc	sodium acetate
NaOH	sodium hydroxide
NH ₄ OAc	ammonium acetate
nt	nucleotide(s)
NTC	no template control of PCR reactions
NTP	nucleoside triphosphate
o/n	over night
PAA	polyacrylamide
PAGE	polyacrylamide gel electrophoresis
PCR	polymerase chain reaction
pH	negative decade logarithm of the hydrogen ion concentration
RNA	ribonucleic acid
rpm	rounds per minute
RT	room temperature
s	second
SD	standard deviation
SDS	sodium dodecyl sulphate
T7 promotor	promotor for T7 polymerase
TBE	Tris-Borate-EDTA buffer

TEMED

N,N,N',N'-tetramethyl-ethane-1,2-diamine

tRNA

transfer RNA

V

volt

Abstract

Bacteria increasingly develop resistances to the known antibiotics, this threatens human health. Thus, novel antibiotics are urgently needed. The currently used antibiotics mainly target five bacterial processes and are therefore limited in the target structures they address. This problem calls for the development of antibiotics that address new targets.

Riboswitches are RNA elements mostly found in the non-coding region of bacterial mRNA molecules. Several classes of riboswitches regulate the expression of essential bacterial genes by the recognition of their cognate metabolites. Compounds that exhibit at least part of their activity through the action as metabolite analogs of riboswitches corroborate the suitability of riboswitches as antibacterial targets.

The *glmS* riboswitch constitutes a unique class of riboswitches that regulate the expression of the essential *glmS* gene by a self-cleavage mechanism, resulting in the degradation of the *glmS* mRNA. This mechanism is induced by the metabolite glucosamine 6-phosphate (GlcN6P) and magnesium ions, consequently, the *glmS* riboswitch is also a co-factor dependent ribozyme. The thesis at hand deals with the analysis of different aspects regarding *glmS* ribozymes from different bacteria.

The investigation of potential modulators of *glmS* ribozyme activity is displayed in **section 3.1** and revealed insights into the interaction of the *glmS* ribozyme RNA with putative metabolite analogs. This section analyses the activity of compounds that originate from an *in silico* prediction based on the 3D shape of the ribozyme's natural metabolite, GlcN6P. **Section 3.2** studies the potential of the *glmS* ribozyme as antibacterial target. The investigation of the intracellular mode of action of the metabolite analog carba-glucosamine (CGlcN) is displayed. It is demonstrated that the antibacterial activity of CGlcN is based on the *in vivo* activation of the *glmS* ribozyme, presumably by carba-glucosamine 6-phosphate (CGlcN6P). Apart from the analysis of potential *glmS* ribozyme activators, different *glmS* ribozyme variants and their properties were studied. The analysis and characterization of putative novel *glmS* ribozyme sequences and the differential recognition of already known *glmS* ribozyme activators by those validated *glmS* ribozymes is displayed in **section 3.3**. In a similar manner as described for the *in silico* predicted GlcN6P analogs (**section 3.1**) putative *glmS* ribozyme activators, originating from a focused library based on the scaffold of an already described activator, are analyzed regarding their potential activation of *glmS* ribozyme variants (**section 3.3**) in **section 3.4**. The mode of action of the in **section 3.4** identified novel *glmS* ribozyme activator was subsequently analyzed utilizing the same approach as described in **section 3.2**.

This study underlines the potential of riboswitches as antibacterial targets and furthermore represents the first proven study on ribozymes as antibacterial targets.

Zusammenfassung

Die steigende Zahl resistenter Bakterien stellt ein zunehmendes Problem für das Gesundheitssystem dar. Die meisten der zur Verfügung stehenden Antibiotika adressieren nur fünf verschiedene bakterielle Prozesse und daher auch nur eine limitierte Anzahl an Zielstrukturen. Diese Tatsache macht die Entwicklung neuer antibiotischer Substanzen, die andere Zielstrukturen adressieren, zu einer Notwendigkeit.

RNA-Schalter sind RNA Elemente, die in den nicht kodierenden Bereichen von meist bakteriellen mRNAs lokalisiert sind. Die verschiedenen Klassen RNA-Schalter regulieren die Expression essentieller Gene und derer Genprodukte, die Metaboliten. Metabolit-Analoga, die zumindest einen Teil ihrer antibiotischen Aktivität über RNA-Schalter vermitteln, sind bereits beschrieben und bilden die Basis für die These, dass RNA-Schalter neue antibiotische Zielstrukturen darstellen können. Der *glmS* RNA-Schalter nutzt einen speziellen Regulationsmechanismus der Selbstspaltung, um die Expression des essentiellen *glmS* Gens zu regulieren. Dieser Prozess wird initiiert durch den Metaboliten Glucosamin 6-Phosphat (GlcN6P). Aufgrund der Selbstspaltung wird der *glmS* RNA-Schalter auch als *glmS* Ribozym bezeichnet. Die vorliegende Arbeit befasst sich mit verschiedenen Aspekten des *glmS* Ribozyms.

Es wird beschrieben, dass die antibakterielle Aktivität von Carba-glucosamin (CGlcN), ein beschriebenes Metabolit-Analagon, auf der *in vivo* Aktivierung des *glmS* Ribozyms basiert, vermutlich vermittelt durch Carba-glucosamin 6-phosphate (CGlcN6P). Dies unterstützt die These, dass RNA-Schalter antibakterielle Zielstrukturen sind und ist darüber hinaus das erste Beispiel für ein Ribozym, welches als antibiotische Zielstruktur fungiert.

Der zweite Teil dieser Arbeit untersucht neue Modulatoren des *glmS* Ribozyms. Dazu wurden Moleküle analysiert, die aus einem *in silico* Screening stammen und basierend auf der 3D-Struktur-Ähnlichkeit zu dem natürlichen Metaboliten GlcN6P ausgesucht wurden.

Weiterhin wurden *glmS* Ribozym-Varianten aus humanen Pathogenen charakterisiert. Es konnte gezeigt werden, dass das *glmS* Ribozym aus *L. monocytogenes* einzigartige Eigenschaften aufweist.

Ein weiterer Abschnitt befasst sich mit der Aufklärung der Wirkweise einer weiteren Carba-Zucker-Variante namens FC- α -D-GlcN6P. Entsprechend wird FC- α -D-GlcN als neuer *glmS* Ribozym-Aktivator mit antibiotischer Aktivität charakterisiert.

1 Introduction

1.1 Bacteria of relevance for this thesis

Nowadays, we are confronted with the problem of an increasing number of resistant and even multidrug resistant (MDR) bacteria.¹⁻² The problem of antimicrobial resistance is associated with annual ~ 50,000 deaths in Europe and the US.³ Infections with the so called ESKAPE pathogens, *Enterococcus faecium*, *Staphylococcus aureus*, *Klebsiella pneumoniae*, *Acinetobacter baumannii*, *Pseudomonas aeruginosa* and *Enterobacter* species are of high concern.⁴⁻⁵ The ESKAPE pathogens are highly pathogenic, have high transmission frequencies and are resistant to at least one of the major classes of antibiotics. All of them are nosocomial pathogens, meaning that they are present in high numbers in hospitals and intensive care units.⁴ The pathogens *K. pneumoniae*, *A. baumannii*, *P. aeruginosa* and *Enterobacter* species belong to the gram-negative bacteria, while *E. faecium* and *S. aureus* represent gram-positive bacteria. The gram-positive *S. aureus* mainly rose attention because of the acquired resistance to methicillin (MRSA) and vancomycin (VRSA/VISA). The main risk for public health regarding *E. faecium* infections is given by the vancomycin resistant (VRE) strains. Some of the MDR bacteria have mortality rates of 50-80%.⁶ In conjunction with the observation that more than 70% of these evolved resistances to the majority of clinically used antibiotics results in an urgent need for the development of novel antibacterial substances, curing life-threatening infections.^{1-2, 6-8}

Relevant for this thesis are the following bacteria: *S. aureus*, *Clostridium difficile*, *Listeria monocytogenes* and the non-pathogenic gram-positive model organism, *Bacillus subtilis*.⁹ All those bacterial species have in common that they are gram-positive bacteria belonging to the phylum *Firmicutes*. Moreover, the gram-positive *Enterococcus faecalis*, *E. faecium*, *Clostridium perfringens* as well as the gram-negative *Fusobacterium nucleatum* and *Fusobacterium periodonticum* play a minor role in this thesis. All of these were chosen for analysis because they are human pathogens harboring a putative *glmS* ribozyme.

The gram-positive, facultative anaerobic bacterium, *S. aureus* belongs to the ESKAPE pathogens and is referred to as one of the major causes of healthcare associated diseases.¹⁰ *S. aureus* is often present in the nasal cavity and on the skin of healthy individuals.¹¹ However, it can bring about severe and hard to treat diseases ranging from superficial skin lesions and invasive inflammation to life-threatening diseases like pneumoniae or endocarditis.¹⁰ Among the infections caused by MDR bacteria, MRSA are regarded as most widespread and are incidental with annual 11,000 deaths.¹²⁻¹³ The occurrence of VISA and VRSA strains represent another threatening progression. Infections caused by these strains are difficult to treat and are known to come along with thickened cell walls, prolonged doubling times, and decreased susceptibility to lysostaphin.¹⁴⁻¹⁵

The gram-positive bacterium *C. difficile* is an obligate anaerobe spore forming prominent nosocomial pathogen that can be found in the human colon.¹⁶⁻¹⁷ Although it can live in the colon in devoid of symptoms it can cause severe and life-threatening forms if the commensal gut microbiota is impaired, e.g. after antibiotic treatment.¹⁸ Unlike *S. aureus*, *C. difficile* does not belong to the ESKAPE pathogens. Nevertheless, the center of disease control (CDC) classifies *C. difficile* as “microorganism with a threat level of urgent”.¹² Infections caused by *C. difficile* yearly account for ~14,000 – 20,000 deaths in the US.^{12, 18} Some reports claim that infections caused by *C. difficile* are even more prevalent than infections caused by MRSA.¹⁹ *C. difficile* is the causative pathogen of pseudomembranous colitis, a severe intestinal disease. Symptoms are mediated by the production of two cytotoxins and range from mild diarrhea and abdominal pain with fever to inflammatory lesions and sepsis.^{16, 18, 20} The anaerobic lifestyle of *C. difficile* within the human guts necessitates the transmission through dormant spores. Spores are intrinsically resistant to antibiotics and are not recognized by the hosts immune system.²¹⁻²² Moreover, the antibiotic treatment of *C. difficile* is associated with high recurrence rates.²³

L. monocytogenes is a gram-positive, facultative anaerobic rod-shaped bacterium. It is found in a variety of different environments like soil, decaying vegetation, ground-water, faeces of animals as well as on food and in food processing units.²⁴⁻²⁷ In some environments, e.g. soil *L. monocytogenes* does not grow very well, but persists as saprophyte.²⁸ The fact that *L. monocytogenes* can persist in different environments is based on the ability to make use of diverse carbohydrates.²⁹ Of note, *L. monocytogenes* can grow at refrigerating temperatures and can even survive at temperatures of -0.4 °C,³⁰ albeit growth at low temperatures comes along with prolonged doubling time of about 50 h.³¹ In addition to the ability to survive at low temperatures, *L. monocytogenes* can also withstand low pH and high salt concentrations, which are both associated with food processing environments.^{25, 32} *L. monocytogenes* is the cause of the disease, listeriosis. Infections can cause mild flu-like symptoms, vomiting and diarrhea in healthy individuals. In immune-compromised, individuals it can lead to meningitis and septicemia. Listerial infections are known to induce spontaneous abortion in pregnant women.^{27, 33} Today infections with *L. monocytogenes* are still comparably rare but they are associated with a high mortality rate of 30%.^{27, 34}

1.2 Identification of antibiotics

The period from 1950 to 1960 was the golden age of antibiotic discovery. Almost all major classes have been discovered within this time period.² In course, it was believed that the problem of bacterial infections is solved. A lot of the since the 1960s developed antibiotics are basically reformulations of these already known antimicrobial drugs. In turn, the term “innovation gap” has been coined to describe

the lack of novel antimicrobials that belong to a new structural class since the 1960s.³⁵⁻³⁶

Due to the massive use of antibiotics in the clinics, in agriculture and food processing environments we nowadays have to deal with life-threatening infections caused by drug and multidrug resistant strains (**section 1.1**). Pathogenic as well as commensal bacteria have equipped themselves with various defense systems, employing a huge arsenal of resistance mechanisms against antibiotics. Commonly employed mechanisms include the expression of drug efflux pumps, enzyme deactivation as well as the modification of the cellular target or the formation of biofilms.³⁷⁻³⁸

In general, two conceptionally different methods are employed to discover novel drugs: activity-based screenings and target-based approaches. In activity-based screenings, compounds are administered to bacterial cells and successful growth inhibitors are then further validated and characterized including target identification. An obvious advantage of this approach is the fact that research starts with accessing the final effect of antibiotic activity, meaning that the final goal is met already in the beginning. Nonetheless, most often this leads to the identification of substances that address already known targets, which is as formerly mentioned associated with the risk of comparably fast resistance development. In contrast, the target-based approach starts with a novel target essential for bacterial growth and/or survival. Usually *in vitro* assays are performed to identify specific modulators of the chosen target. Although this approach has the benefit that a novel target is addressed, it is most often very time and cost consuming if it is at all possible to transfer *in vitro* effects to a whole cell system.

To identify antimicrobial drugs, mainly natural products, i.e. compounds that are produced by microorganisms as defense mechanisms were assessed. This approach was mainly followed in the 1960s and due to the extensive use of this strategy it leaves us nowadays with almost inability to further identify natural product antibiotics by this traditional way. The other approach concerns the screening of compounds with chemical origin. However, the initial hopes that this approach can fill the gap in antibiotic discovery did not accomplish as successful. Nevertheless, a few agents exhibiting narrow spectrum activity were identified in high-throughput screening (HTS).³⁹⁻⁴¹ A review article focusing on the perspective of pharmaceutical industry and their efforts to identify novel antibacterials illustrates how difficult and cost as well as time consuming it is to discover novel antibiotics and sheds light on the fact that pharmaceutical industry left this research area. It is reported that 67 HTS against 260,000-530,000 compounds were performed, both target as well as activity based screenings were employed and collectively yielded only 5 lead molecules within a timeframe of 6 years.⁴² So both approaches either screening for natural products or synthetics are nowadays of limited success.⁶

Virtual screenings are computer based approaches, commonly used to identify binding partners, interactors or drug like compounds. Drug discovery is a time-consuming process that usually takes more than 10 years. It starts with the identification of a lead structure, which then undergoes several optimization cycles. Finally, with entering and completing a clinical trial study ~ 800 million US \$ are spend. ⁴³ In classical empirical drug discovery, the identified hit compounds often do not yield successful drug candidates due to problems in the optimization cycle. However, it was realized in the beginning of the 1990s that combinatorial chemistry together with HTS represents a powerful tool to optimize potential hit compounds and to screen libraries of several thousand compounds in shorter time. In combination with virtual screening this represents a promising strategy to identify a collection of optimized drug candidates in a comparably short timeframe and cost-effective manner.^{43 44}

On the other hand, a novel promising method was developed which allows to enlarge the group of culturable bacterial species under laboratory conditions. Actually, scientists are only capable to culture a fraction as small as 1% of all bacterial species at laboratory conditions. A novel technology called iChip was developed quite recently. The cultivation in the so-called iChip device allows for growth of a single bacterial cells in a diffusion chamber. The semi-permeable membranes of the chamber allow for interaction with the soil, the habitat the sample originates from and the device is placed back in for cultivation.⁴⁵ This procedure makes it possible to cultivate bacteria that so far could not be cultured under standard laboratory conditions.⁴⁵ The ability to expand the spectrum of culturable bacteria potentially allows the identification of so far unknown natural products that exhibit antimicrobial activities.

1.2.1 The problem of antibiotic resistance

One part of the problem associated with drug resistance is the fact that currently used antibiotics mainly address five different cellular processes and therefore a limited number of targets. Traditional targets are the cell wall, protein synthesis, DNA replication and folate coenzyme biosynthesis.⁴⁶ Besides, classes targeting the RNA polymerase as well as the cytoplasmic membrane are known. The common bacterial targets and classes of antibiotics effective against those are illustrated in **Figure 1**.

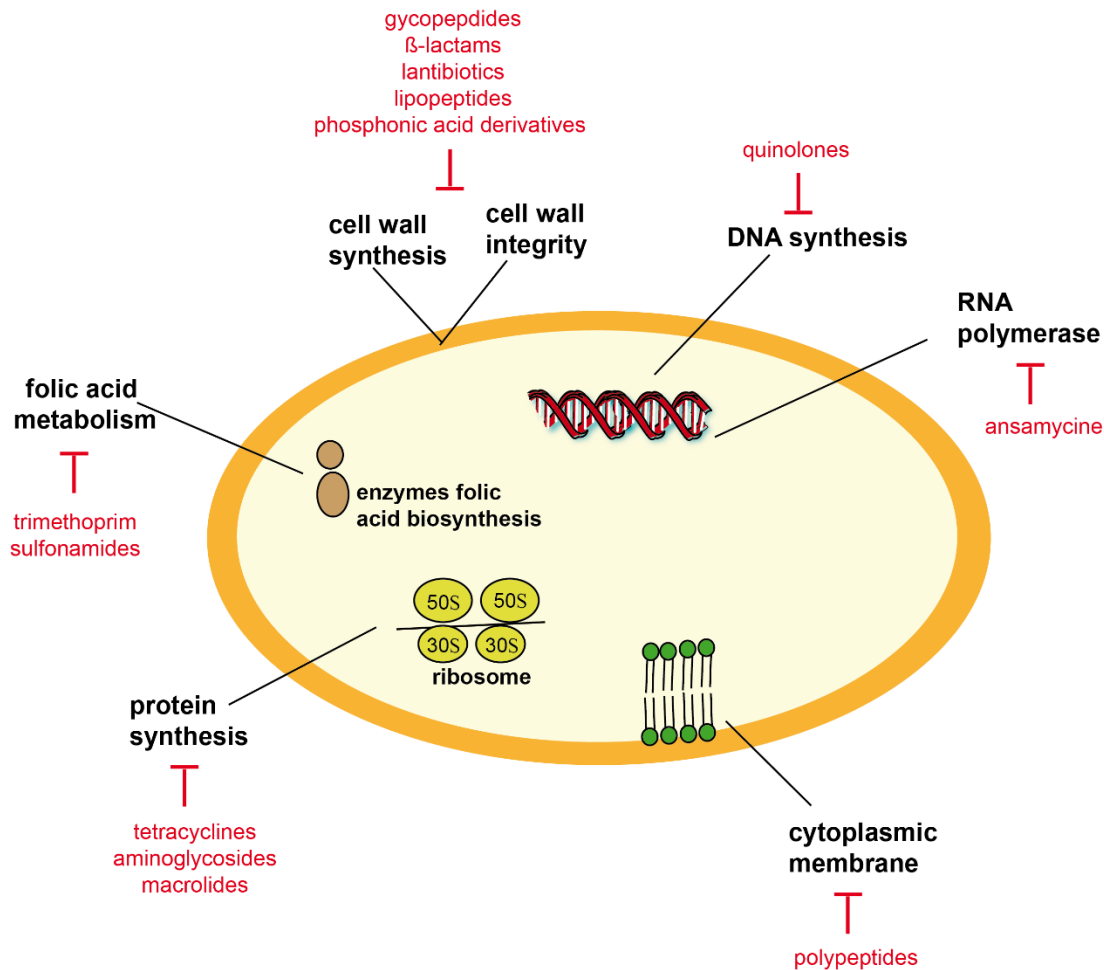


Figure 1: Cellular bacterial targets addressed by antibiotics

Depicted are the targets commonly addressed by traditional antibiotics. The corresponding classes of antibiotics against these targets are shown in red.

1.2.2 The bacterial cell wall as antibiotic drug target

About 50% of the clinically used drugs inhibit cell wall biosynthesis. Some of these antibiotics have already been discovered in the 1940s and still show favorable therapeutical properties.⁴⁷⁻⁴⁸ One explanation for the overrepresentation of cell wall inhibitors among antibiotics is that this structure is unique to bacteria.⁴⁸ The absence of such a structure in mammals potentially accounts for a higher specificity. All in all the bacterial cell wall still provides a suitable antibacterial target structure with good prospect regarding the identification of novel antibacterial drugs.⁴⁸

Bacterial cell wall biosynthesis is the metabolic pathway of interest for this thesis and, therefore, the mechanisms of those antibiotics inhibiting cell wall biosynthesis are explained here in more detail. **Figure 2** describes some of the most important antibacterial cell wall agents and their mode of action (MoA).

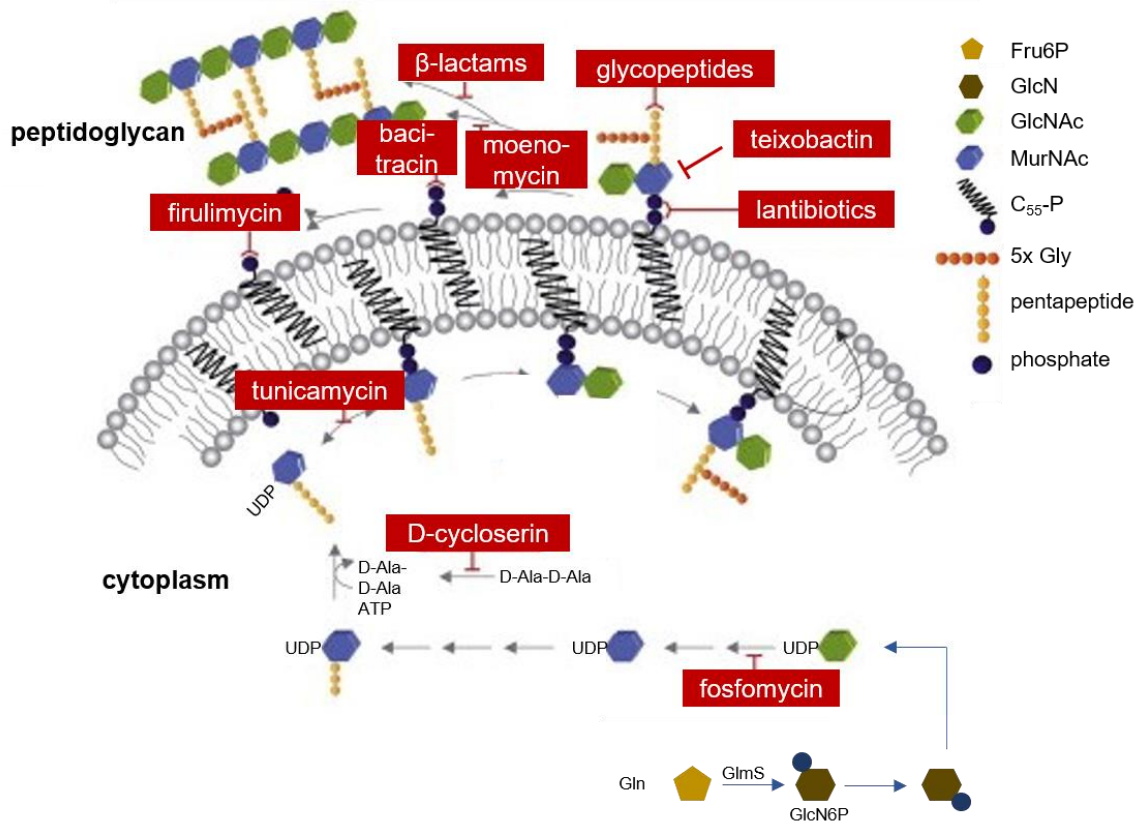


Figure 2: Illustration of bacterial cell wall biosynthesis and the corresponding cell wall inhibiting antibiotics modified after Schneider & Sahl 2010.⁴⁷

Beginning with the formation of GlcN6P by GlmS through the reaction of Fru6P and Gln synthesis of UDP-GlcNAc proceeds by conversion of GlcN6P to GlcN1P by the enzyme GlmM and the subsequent bifunctional action of GlmU UDP-GlcNAc is built. The antibiotic fosfomycin is known as inhibitor of the next biosynthetic step, namely the transformation of UDP-GlcNAc to UDP-MurNAc. The intermediate UDP-MurNAc is converted to its soluble form UDP-MurNAc-pentapeptide by the help of the Mur enzymes (Mur A-F). After lipid I (undecaprenylphosphate-MurNAc-pentapeptide) is formed at the cell wall UDP-MurNAc-pentapeptide is assigned to the lipid carrier undecaprenylphosphate (C55-P). The conjugation of UDP-GlcNAc to lipid I finally yields lipid II (undecaprenylphosphate-GlcNAc-MurNAc-pentapeptide). After translocation of lipid II the peptidoglycan subunits are connected to the growing peptidoglycan structure. Here the cell wall biosynthesis in *S. aureus* is illustrated, in this case lipid II is further modified by a 5-glycine containing motif. However, this kind of modification differs between different species. Different cell wall targeting molecules are indicated by red boxes at their place of action within cell wall biosynthesis pathway.

Penicillin, one of the early discovered antibiotics belongs to the class of β -lactam antibiotics and targets a family of D-D-transpeptidases and D-D-carboxypeptidases, the so-called penicillin-binding-proteins (PBPs).⁴⁷ Among penicillin the cephalosporins, monobactams and carbapenems belong to the most important class of cell wall inhibitors, the β -lactam antibiotics.⁴⁹ However, bacteria have evolved β -lactamases that induce resistance to this class of antibiotics functioning by hydrolysis of the common β -lactam ring.⁵⁰

Vancomycin and teicoplanin are prominent representatives of the class of glycopeptides. They bind the D-Ala-D-Ala motif of the pentapeptide peptidoglycan precursor lipid II (**Figure 2**) and thereby block subsequent transglycosylation and transpeptidation steps.^{47, 51} Although vancomycin is a drug of last-resort and was economically used in the clinics, resistance by the *vanA* transposon has evolved. This operon codes for nine polypeptides that all contribute to the modification of the cellular target, namely the D-Ala-D-Ala to either a D-Ala-D-Lac or a D-Ala-D-Ser motif. Thereby the recognition by glycopeptides is impaired. Resistant enterococci have already been described in 1988⁵² and since 2002 vancomycin resistant MRSA strains have been reported.⁵³ It is evident that the *vanA* plasmid that was isolated from those MRSA strains originated from the transfer from enterococci.⁵¹

The class of lantibiotics is characterized by the common structural element, the lanthionines thioether. This class of antibiotic specifically binds to the pyrophosphorylated carbohydrate structure of lipid II (**Figure 2**) and thereby prevents the insertion of the precursors into the peptidoglycan.⁴⁷

Although moenomycin and tunicamycin exhibit antibacterial activity by competitive binding of cell wall biosynthesis enzymes, both of these have shown to have toxic effects and thereof will not make their way in the clinics.⁴⁷

The natural product based antibiotics, bacitracin and frulimycin inhibit steps in the cell wall biosynthesis pathways by blocking the global carbohydrate carrier C₅₅ (**Figure 2**). However, the carrier is also involved in the teichoic acid and capsule biosynthesis pathways.⁴⁷

The antibacterial agent teixobactin was discovered recently by making use of a novel method aiming at the cultivation of so far unculturable bacterial species.⁵⁴ By making use of this approach Ling & Schneider and coworkers identified the antibacterial substance teixobactin. Teixobactin has very good activity against gram-positive pathogens as for instance *S. aureus* or *Mycobacterium tuberculosis* and was detected in a screening of 10,000 natural product extracts.⁵⁴ The resistance development to teixobactin was not detected even after 27 days of cultivation. Together with the fact that teixobactin was shown to be non-toxic in mammalian cell culture and the demonstrated efficacy in a mouse infection model rises hopes for this compound to turn out as novel antibiotic that can be used by clinicians to treat MDR pathogens.⁵⁴

Regarding the MoA of this cell wall inhibitory agent it was revealed in biochemical assays that it interacts with pyrophosphorylated-sugar group of lipid II and lipid III (**Figure 2**) and interestingly can also recognize modified lipid II moieties which have evolved as resistance mechanism to glycopeptides such as vancomycin. From the structural point of view teixobactin is an unusual depsipeptide isolated from a β -proteoobacterium and commences a new class of antibiotics.⁵⁴

So far, the action of cell wall targeting antibiotic substances that act on the extracellular side has been described. The two antibacterials D-cycloserine and fosfomycin (**Figure 2**) are inhibitors of the early steps of cell wall biosynthesis and have effects within the cytoplasm.

The mode of action of fosfomycin relies on blocking the formation of an essential peptidoglycan precursor, namely the N-acetylmuramic acid by inhibiting MurA function. In order to enter the cell fosfomycin makes use of two distinct bacterial transporter systems, the glycerol phosphate transporter and a hexose phosphate transporter.^{55 56-57} Bacterial modification of the cognate PTS operon lead to the development of resistances to fosfomycin.^{55, 58} Moreover, resistances to fosfomycin achieved by modification of the cellular target and inactivation of the antibiotic itself are known.

D-cycloserine is a long-known natural product with antibiotic activity, which is widely used to treat tuberculosis. As it is a cyclic analog of D-alanine it inhibits formation and conjunction of D-alanine molecules that are crucial precursors in cell wall biosynthesis.⁵⁹⁻⁶⁰

So far, resistances to the main classes of antibiotics in clinical use are known.^{2, 42, 46} This fact, calls for the development of novel antibiotics that address novel targets. With its biochemical function RNA represents one vulnerable class of target structure.

1.3 RNA as drug target

Most drugs in clinical use target proteins. However, RNA is known as drug target exhibiting antifungal, anticancer, antiviral or antibacterial activity. Albeit RNA is composed of only four building blocks being planar bases with a negatively charged phosphate, it is equipped to adopt diverse structural conformations.⁶¹⁻⁶² RNA can exhibit explicit formations like pockets or cavities that allow for shape specific recognition of diverse ligands.⁶² These features make RNA an attractive drug target.

Indeed, several antiviral strategies are built on ribozymes as mediating molecules. Ribozymes are catalytically active RNA molecules and are described in more detail in **section 1.5**. One antiviral approach based on ribozyme function has already been tested in a phase II clinical trial. This approach relies on the hammerhead ribozyme (HHR) and targets the proteins vpr and tat. Vpr is involved in the import of HIV1 and tat in transcription.⁶³⁻⁶⁴ The anti-HER2-ribozyme, which is also based on the features of the HHR was described to be a potential aid in anti-breast cancer research. By use of this approach downregulation of HER2 mRNA, p185 and the oncogene k-ras could be detected in transfected breast cancer cells.⁶⁵ Another

example utilizes the HHR in an adenovirus approach to target the antiapoptotic factor survivin which is overexpressed in all types of cancer.⁶⁶

Of interest for the thesis at hand are cases in which RNA is employed as antibacterial drug target. Most of the translation inhibiting antibiotics (**Figure 1**) actually act by interfering with the rRNA instead of the protein components involved in translational steps of initiation or elongation. For example, aminoglycoside antibiotics that have been shown to target ribosomal RNA instead of ribosomal proteins.^{62, 67} Aminoglycoside and tetracycline antibiotics affect the 16S rRNA component, while the 23S rRNA is targeted by oxazolidinones or macrolides.^{46, 68} Moreover, numerous regulatory RNAs have been shown to play a role in diverse metabolic processes as well as mediating virulence and in bacterial defense against antibiotics.⁶⁸

1.4 Non-coding regulatory RNAs and their role in antibacterial processes

Besides the classical RNA molecules involved in protein synthesis (mRNA, tRNA, rRNA) a broad variety of non-coding RNAs (ncRNAs) exerting regulatory functions are known.⁶⁹⁻⁷⁰

Bacteria need to adapt to a variety of ever-changing biochemical and biophysical conditions. One mechanism employed to do so relies on ncRNAs. In comparison to protein regulation, RNA-based mechanisms are faster and the metabolic burden is lower.⁷¹⁻⁷³ The class of ncRNAs comprises a heterogeneous collection of RNA molecules with different origins and structures as well as regulatory mechanisms applied.⁷⁴⁻⁷⁵

Some ncRNAs of interest include temperature sensitive RNA thermometers (**Figure 3A**), antibiotic sensing riboregulators (**Figure 3B**), catalytically active ribozymes (**section 1.5**) (**Figure 3C**), small regulatory RNAs (sRNAs) (**Figure 3D**) and metabolite-responsive riboswitches (**Figure 5**) (**sections 1.6, 1.6.1**).

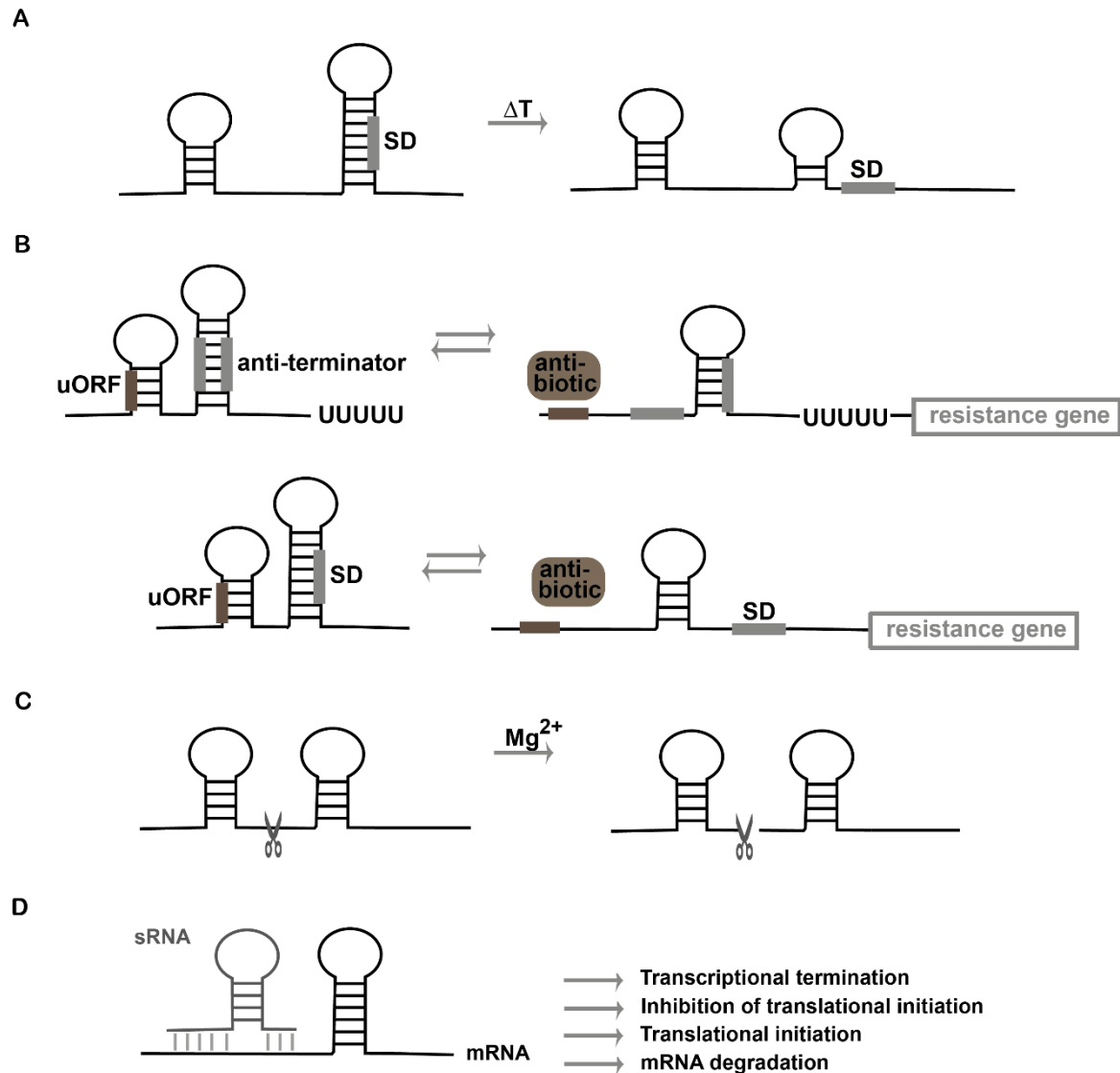


Figure 3: ncRNA based regulatory mechanisms.

Regulation of gene expression by RNA thermometers is shown in A. An increase in temperature leads to melting of the corresponding ncRNA structure, which make the Shine Dalgarno (SD) sequence accessible for the ribosome binding site and subsequently translation is initiated. In B, the two mechanisms antibiotic sensing riboregulators make use of are depicted. In the upper scheme the transcription is attenuated. In the presence of the cognate antibiotic the uORF inhibits the formation of anti-terminator and transcription of the resistance gene can occur. In the lower scheme the presence of the cognate antibiotic leads to the formation of an accessible SD and subsequently translation of the resistance gene can occur. D illustrates the diverse regulatory mechanisms employed by sRNAs mediated by base-pairing of the sRNA with the cognate mRNA.

RNA thermometers are ncRNAs located in the 5' untranslated region (UTR) of various bacterial mRNAs.⁷⁶ They control transcriptional regulation in a temperature-dependent manner (**Figure 3A**). At low temperatures (30 °C and below) the RNA adopts a structure that sequesters the Shine Dalgarno (SD) sequence so that the ribosome binding site (RBS) is not accessible and translation cannot occur. With increasing temperatures, the sequestering stem-loop structure

melts and allows initiation of translation.⁷⁷ In *L. monocytogenes*, the PrfA gene is controlled by such an RNA thermometer. PrfA is a known key player regulating numerous virulence factors. In condition of acute bacterial infection (37 °C), the hairpin structure of the RNA thermometer melts and allows initiation of PrfA transcription.

One class of molecules providing protection against antibiotics are the so called riboregulators, antibiotic-sensing RNAs that have recently been identified within various bacterial species. These ncRNAs are mostly found in the 5'UTR and are cis encoded. In the presence of antibiotic they adopt alternative structures to regulate the expression of resistance genes (**Figure 3B**).^{78,70} Interestingly, most of the riboregulators recognize antibiotics that inhibit translation. Moreover, for most of the translation inhibiting antibiotics riboregulators have been identified.⁷⁸ These observations qualify ncRNA as perspicuous target for antibacterial research.

The sRNAs comprise the so far broadest class of ncRNAs and are usually acting in trans. Therefore, they are distantly located from the genes they regulate on independent transcripts (**Figure 3D**). Although sRNAs affecting proteins and mRNA stability are known, most sRNAs modulate translational processes through antisense-base pairing with their target mRNAs.^{72-73, 79} In general, sRNAs are associated with regulation under nutrient reduced conditions as well as pathogenesis and virulence.⁸⁰ For instance, the sRNA SgrS was shown to regulate a PTS responsible for the uptake of glucose in *E. coli*. This regulation has evolved to protect the bacterial cell from the toxic accumulation of phosphorylated sugars, e.g. Glc6P, which otherwise could cause DNA damage and inhibit bacterial growth.⁸¹⁻⁸³ SgrS was identified in 2004 in a microarray study analyzing interaction partners of Hfq, the global bacterial RNA binding protein, which is known to assist in sRNA activities in gram-negatives.⁸⁴ Further insights into the SgrS mediated regulation of ptsG mRNA showed that both Hfq-mediated recruitment of RNase E and the haloacid dehalogenase-like enzyme YigL are important for the dephosphorylation of sugar-phosphates and eventually lead to the efflux of non-phosphorylated sugar molecules.⁸³

Diverse studies in *Salmonella*, *Escherichia coli* and *S. aureus* have provided a connection between antibiotic exposure and the expression of small regulatory RNAs (sRNAs).⁷² Moreover, complex regulatory networks, sRNA regulons, in which numerous sRNAs act in accordance to modulate the activity of regulatory proteins have been uncovered and shown to function in a similar manner to transcription factors.⁷³

An sRNA based regulatory system restricted to gram-negatives concerns the concerted regulation of GlmS by the two sRNAs GlmY and GlmZ. These two sRNAs promote GlmS synthesis. GlmY activates GlmZ in situations of low intracellular GlcN6P levels. In turn, GlmZ allows translation of GlmS.^{81, 85} Interestingly, gram-positives widely use another RNA-based mechanism to control

the essential *GlmS*. This mechanism is based on a metabolite-sensing riboswitch that exerts catalytic function to control the expression of the *glmS* mRNA. Riboswitches are a class of metabolite-responsive ncRNAs, which have already been found to have implications in antibacterial research (**section 1.6.1**). The thesis at hand focuses on the *glmS* riboswitch, which is actually a natural ribozyme and its potential as antibacterial target.

1.5 Natural ribozymes

The finding that RNA has catalytic activity and can function similarly to proteins changed the prevailing view of biologists in 1980s, when natural ribozymes were discovered.⁸⁶⁻⁸⁷ These publications were that seminal that Sidney Altman and Thomas R. Cech got the Nobel prize for their discovery of the catalytic properties of RNA in 1989.

Today 14 classes of natural ribozymes are known and although the biological implication has not been revealed for all of them it has been demonstrated that they participate in protein synthesis or RNA processing.⁸⁸⁻⁹¹

Ribozymes commonly catalyze the biochemical reaction of transferring a phosphate group without the help of any protein based factor (**Figure 4**).⁸⁹⁻⁹⁰

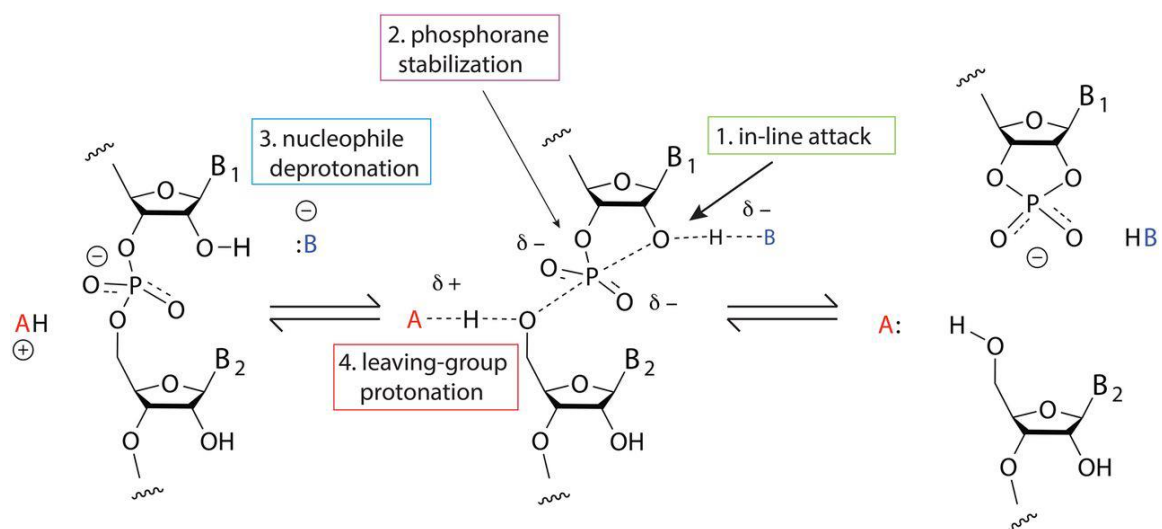


Figure 4: Catalytic strategies of natural ribozymes regarding the transfer of a phosphate group, modified after Lilley 2017.⁹⁰

The four different common mechanisms employed by natural ribozymes are depicted. A indicates acids involved in the cleavage reactions while B denotes bases participating in general-acid base catalysis. The first described mechanism (1.) shows the so-called process of in-line attack, in which the 2'-oxygen initiates a nucleophilic attack on the phosphorous atom yielding the O5 leaving group. This mechanism requires a specific geometry of the reaction partners and is for instance seen in hairpin ribozymes. In 2., the stabilization of the phosphorane transition state is depicted. This stabilization is in most cases achieved by electrostatic, e.g. ionic interactions. In 3., a general base

deprotonates the 2'OH group while in 4., the protonation of the oxyanion is shown; these two mechanisms are known as general acid-base catalysis.

Ribozymes can be divided by size, larger ribozyme as RNase P and group I and II introns longer than 300 nt. Those large ribozymes are also regarded as “metalloenzymes” as their activity is dependent on metal ions.⁹¹⁻⁹² RNase P is a ribonucleoprotein though it was demonstrated that the RNA part alone is functional regarding the cleavage of precursor RNAs.⁹³ Group I and II introns confer two step based self-splicing reactions involving cleavage and ligation reactions. In case of large ribozymes, the nucleophile and the phosphate moiety involved in cleavage are usually carried by different molecules accounting for the necessity of precise folding.

Small ribozymes are shorter than 300 nt and include the hammerhead (HHR), hairpin, hepatitis delta virus (HDV), varkud satellite (VS), twister, pistol, hatchet, *glmS* ribozyme.⁸⁸ Of the small ribozymes HHR is the most well studied. A common mechanism employed by natural self-cleaving ribozymes to catalyze RNA cleavage is internal phosphoester transfer. The mechanism occurring at the cleavage sites by the nucleophilic attack of the 2' oxygen on the neighboring phosphate leads to a cleavage product with a 2'3'-cyclic phosphate and a product with a 5' hydroxyl (**Figure 4**).⁹⁴

RNA provides only a limited number of chemically functional groups and the pKa value at physiological pH does not support general-acid base catalysis. The “two metal ion model” provides an explanation for the fact that ribozymes indeed are capable of performing catalytic reactions. One of the two metal ions supports the activation of a nucleophile, while the other metal ion stabilizes the transition state by coordination of the leaving group.⁹⁵

All of the so far described natural ribozymes require the help of metal ions for proper folding. For a limited number of ribozymes metal ions are crucial for catalysis as for instance the large ribozymes or the HDV ribozyme.⁹⁵⁻⁹⁶ In cases where metal ions are only involved in folding preferably divalent ions are used.^{91, 95} However, monovalent and even multivalent ions can take over the job although efficacy might be impaired.⁹⁷ In a cellular context divalent ions most likely play the important role in assisting folding of natural ribozymes. Most commonly Mg²⁺ ions are utilized by ribozymes. However, in several cases Ca²⁺ and Mn²⁺ and sometimes also Cd²⁺ can be functional replacements of Mg²⁺.^{91, 94}

Although this thesis focuses only on natural ribozymes it should be mentioned that a whole research area focuses on engineered ribozymes and some examples are already mentioned earlier in the introduction reporting on HHR variants being implemented in therapeutic applications (**section 1.3**).

1.6 Riboswitches

Riboswitches sense and respond to metabolites that are fundamental for various cellular functions within an organism. As common for ncRNAs, modulation of gene expression occurs without the help of protein factors. In comparison to proteins, riboswitches exemplify complex folding patterns.⁹⁴ Riboswitches mainly reside within the 5'UTR of bacterial mRNAs but can also be found in archaea, fungi or plants and phages.⁹⁸⁻¹⁰¹ Heretofore, riboswitches have not been discovered in humans.¹⁰²

Riboswitches are composed of an aptamer domain that selectively recognizes the cognate ligand, and an expression platform that upon conformational change regulates gene expression (**Figure 5**). While the aptamer domain is usually conserved, the sequence of the expression platform contains variable regions. Mechanisms employed to regulate gene expression are mostly transcriptional termination or inhibition of translational initiation (**Figure 5**). A third unique mechanism to regulate gene expression is employed by the *glmS* riboswitch, upon binding of the metabolite self-cleavage is induced concomitantly resulting in the degradation of the *glmS* mRNA (**section 1.7**). In case gene expression is regulated by termination of transcription, binding of the metabolite to the aptamer domain induces a conformational change. In cases of an “off” switching riboswitch, the anti-terminator sequence within the expression platform is released, thereby a stretch of Us is freed and causes the polymerase to stop transcription (**Figure 5A**). The opposite phenomenon is known as “on” switch. In those cases, the terminator is released upon ligand binding. Riboswitches, which regulate gene expression by translational, sequester the ribosome-binding site (RBS), the Shine-Dalgarno sequence upon binding of their corresponding metabolite (“off” switches) (**Figure 5B**). As introduced for riboswitches regulating transcription, “on” switches working on the translational level are also known.

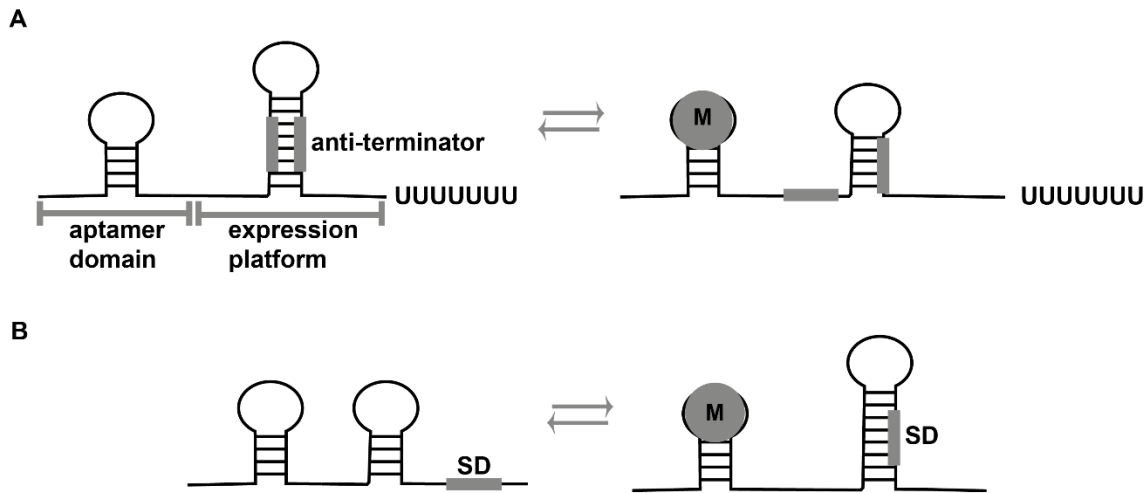


Figure 5: Riboswitch based gene regulatory mechanisms

Regulation of gene expression by riboswitches utilizing transcriptional termination is shown in A. The transcriptional terminator is sequestered by an anti-terminator. Upon metabolite (M) binding the terminator sequence in combination with a stretch of uridines (usually 5-9 Us) leads to transcriptional termination. In B, inhibition of translational initiation is shown: Upon metabolite binding, the Shine-Dalgarno (SD) sequence is sequestered.

Although there are examples of riboswitches that use positive feedback regulation, the predominant mechanism utilized by riboswitches to regulate gene expression is negative feedback regulation. The adenine and glycine riboswitch employs positive feedback regulation meaning that upon encountering the cognate ligand expression of genes involved in transport or deamination are induced. Interestingly, a few examples of tandem riboswitches, so the conjunction of two riboswitches are known, which exhibit a greater complexity of gene regulation.¹⁰³

Regarding the identification of riboswitches, rather long intergenic regions (IGRs) give a first hint at the presence of potential riboswitches. The average length of a *B. subtilis* IGR is 152 nt, but the median length of a riboswitch containing IGR comprises 330 nt.¹⁰⁴ First entries of riboswitches in literature can be found in 2002 when the groups of Breaker and Nudler reported on metabolite sensing RNAs.¹⁰⁵⁻¹⁰⁸ 15 years later we know almost 40 distinct classes and several orphan riboswitches.¹⁰⁹⁻¹¹⁰ Riboswitches respond to a variety of different molecules like coenzymes, amino acids, ions, nucleobase containing molecules or a phosphorylated amino sugar (**Table 1**). Riboswitches are qualified to discriminate between closely related metabolites within a complex cellular environment and by doing so they control gene expression, even of essential genes. The discriminative power of riboswitches is remarkable as they unveil specificity of 100-1000 fold or more for their metabolite versus chemically closely related compounds.^{107, 111-112}

Table 1: Classes of riboswitches. Modified after McCown *et al.* 2017¹¹⁰

Type of ligand	Riboswitch classes
Coenzymes	Adenosylcobalamin Aquacobalamin Thiamine pyrophosphate (TPP) Flavin mononucleotide (FMN) S-Adenosylmethionine Molybdenum cofactor Tungsten cofactor Tetrahydrofolate S-Adenosylhomocystein
Amino acids	Lysine Glycine Glutamine
Ions	Mg ²⁺ Mn ²⁺ F ⁻ Ni ²⁺ /Co ²⁺
Signaling molecules	Cyclic di-GMP Cyclid di-AMP Cyclic AMP-GMP ZTP
Nucleobases and derivatives	Guanine Adenine Prequeosine-1 (preQ) 2'-Deoxyguanosine (2'- dG)
others	Glucosamine 6-phosphate Azaaromatics Guanidine

In general, riboswitch classes recognizing either coenzymes or signaling molecules represent the most widespread classes, while so far for the riboswitch classes recognizing variants of preQ and 2'-dG only few representatives have been identified.¹¹⁰

The TPP riboswitch class should be highlighted as it has the broadest distribution. TPP riboswitches are besides in bacteria and archaea also found in eukaryotes like fungi, algae or plants. Thiamine (vitamin B1) transport and biosynthesis genes are regulated by TPP riboswitches.^{107, 113} Thiamine undergoes intracellular phosphorylation yielding the TPP inside the bacterial cell. TPP functions as coenzyme and is involved in the processing of carbon-carbon bonds in preparation for essential pathways like glycolysis, the citric acid cycle or the pentose phosphorylation pathway.¹¹³ The participation in those pathways accounts for the essentiality of TPP to all living organism. Furthermore, it implies the need for regulation to sustain satisfactory levels of TPP.¹¹³ Most TPP riboswitches recognize TPP with high specificity and high selectivity by contacts through a thiamine sensory helix and a pyrophosphate sensor helix.¹¹⁴⁻¹¹⁶ Nevertheless,

variants are known that recognize thiamine monophosphate or TPP analogs as for instance benfotiamine, pyrithiamine (PT) or triazolthiamine (TT).^{107, 113-114, 116} Recently, TPP riboswitch variants recognizing thiamine have been identified and it could be shown that distinct mutations within the aptamer domain account for this altered recognition specificity.¹¹⁸

In contrast to the recognition of TPP by the TPP riboswitches or the example of THF sensing riboswitches that also only sense parts of their metabolites, some lysine and purine recognizing riboswitches sense proportions of up to ~98% of their cognate metabolites.¹¹⁹⁻¹²¹ They use a recognition strategy that is based on shape complementarity and discriminate their ligands by size.¹¹⁹

In order to enable highly specific and selective binding of their metabolites, riboswitches employ a series of other strategies. The recognition of their metabolites by π - π interactions is extensively used by TPP, FMN, and some preQ riboswitches as their metabolites all contain aromatic ring systems favoring this stacking interaction.^{114-115, 122-124}

Adenine and guanine riboswitches make use of direct H-bonding to sense their metabolites. By those H-bonds, the RNA makes contact to the oxygens and nitrogen atoms of their metabolites.¹²⁵⁻¹²⁶ Interestingly, the conversion of U74 to C turns the adenine riboswitch into a guanine riboswitch. This finding is explained by the fact that this specific residue 74 is directly involved in Watson-Crick base pairing.¹¹¹ Several riboswitches recognize their cognate metabolites through electrostatic interactions, e.g. the recognition of the metabolite's ammonium group by lysine riboswitches.¹²⁷⁻¹²⁸

A serious challenge for riboswitches as RNA molecules with a negatively charged backbone is the recognition of metabolites that are negatively charged.¹¹⁹ Several metabolites contain negatively charged phosphate groups e.g. TPP, GlcN6P or, FMN. To allow specific recognition of these metabolites, riboswitches make use of positively charged cations like Mg^{2+} . The three formerly mentioned riboswitch classes all coordinate their metabolites by two Mg^{2+} cations in a water-based manner.^{114-115, 122, 129-130} A similar principle is employed by lysine riboswitches which utilize K^+ cations to coordinate the negatively charged carboxylate group of lysine.¹²⁸ The F^- riboswitch is a kind of special as three Mg^{2+} cations are necessary to mediate recognition, however, no direct interaction between the riboswitch RNA and the metabolite could be observed. The whole coordination seems to depend on the bridging cations.¹³¹ Interestingly, a riboswitch class whose ligand are Mg^{2+} cations is known. These riboswitches regulate the expression of ion transport genes.¹³²

Regarding the affinity for their metabolites tremendous differences were discovered between the different riboswitch classes. The most sensitive riboswitch that has been identified so far senses its metabolite c-di-GMP with a k_d of ~10 pM.

On the other side of the scale for some *glmS* riboswitches experiments determining cleavage kinetics in the presence of its natural metabolite revealed values in the high micromolar range.^{94, 133} The c-di-GMP riboswitches are involved in regulation of biofilm formation and the regulation of virulence gene expression.¹³⁴

However, not only the affinity to their metabolites is an important feature of riboswitches. Aspects like the kinetic of the reaction and the ability to discriminate between closely related analogs also account for riboswitch function.

1.6.1 Riboswitches as drug targets

To serve as promising antimicrobial target riboswitches have to fulfill certain requirements as for instance the regulation of an essential gene or pathway having implementation in organisms' growth or survival.

Indeed, it was uncovered that the long-known antibiotics, L-aminoethylcystein (AEC) and pyrithiamine (PT), mediate at least part of their antibacterial activity through the interactions with riboswitches.^{113, 135}

Another example for the potential of riboswitches as antibacterial targets are the lysine analogs DL-oxalysine and AEC (**Table 2**). These two metabolite analogs have been shown to inhibit growth of *B. subtilis* or *E. coli*.¹³⁵⁻¹³⁷ Furthermore, it has been demonstrated that mutations within the riboswitch region led to resistance against AEC.¹³⁶

The guanine riboswitch targeting compound 2,5,6-triminopyrimidin-4-one (PC1) (**Table 2**)¹³⁸ was thought to be the most prominent, best studied and of utmost relevance due to its clearance of *S. aureus* infected cows.¹³⁹ However, in 2016, it was uncovered that targeting of these guanine riboswitches in *S. aureus* is not sufficient to cure from infection.¹⁴⁰

The TPP analog pyrithiamine pyrophosphate (PTPP) was initially developed as PT to study thiamine metabolism (**Table 2**). Promptly, it was realized that PT has antimicrobial activity.¹⁴¹⁻¹⁴² The MoA remained elusive until in 2005, Sudarsan and coworkers linked PT action to the class of TPP riboswitches.¹¹³ In their in-line probing studies, they could demonstrate *in vitro* that the TPP riboswitch upstream of the *tenA* operon, which encodes for a variety of genes involved in thiamine metabolism in *B. subtilis*, is similarly responsive to TPP and PTPP.¹¹³ They concluded that the probability is high that PTPP binds TPP riboswitches *in vivo*. They collected several PT resistant bacterial strains of *B. subtilis* and *E. coli*, for which the existence of a TPP riboswitch in front of the *thiC* operon had been demonstrated beforehand. Sequencing of those PT resistant strains revealed that all of the *B. subtilis* sequences carried a mutation in the aptamer domain of the *tenA* controlling TPP riboswitch. In subsequent *in vitro* assays, they could confirm their hypothesis and validated that those riboswitch mutants show reduced affinity

for PTPP and TPP. Concerning the PT resistant *E. coli* strains they sequenced, only 9 showed mutations in TPP riboswitches, while the resistance of the remaining 14 clones could not be attributed to mutations within TPP riboswitch regions.¹¹³

Triazolthiamine (TT) (**Table 2**) was shown to be another activator of the TPP riboswitch.¹¹⁷ TT activity depends on the uptake through the bacterial thiamine uptake system. This uptake event is associated with phosphorylation of TT yielding TTPP.

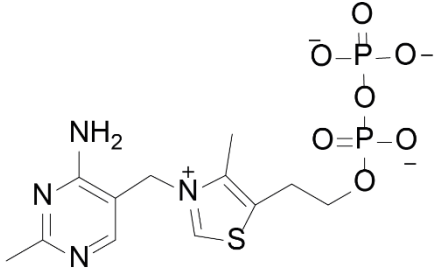
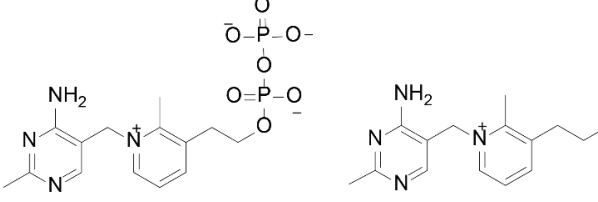
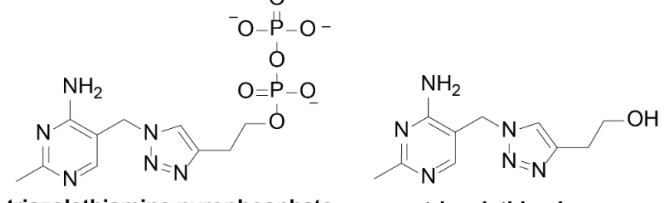
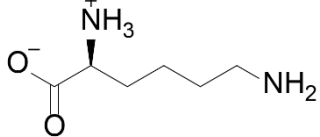
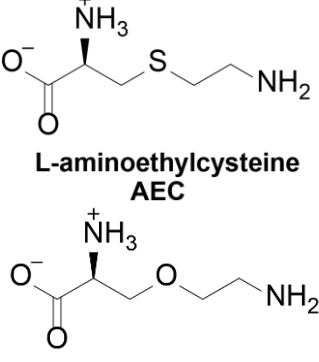
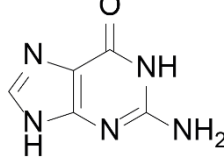
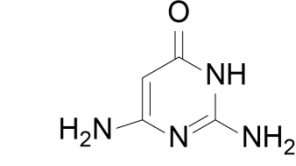
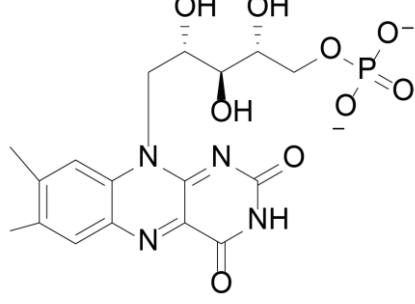
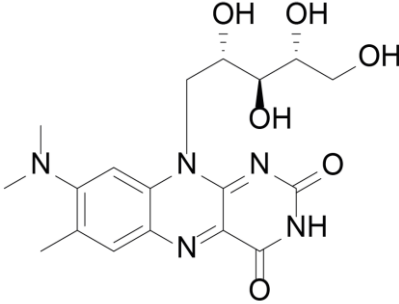
Another approach called fragment-based screening was utilized to identify binding partners of the TPP riboswitch aptamer domain. Screening a library of 13,000 fragments comprising diverse functional groups and molecule shapes led to the identification of several potent binders. The most potent identified fragment binds to the TPP aptamer domain with a K_d in the nM range.¹⁴³⁻¹⁴⁶

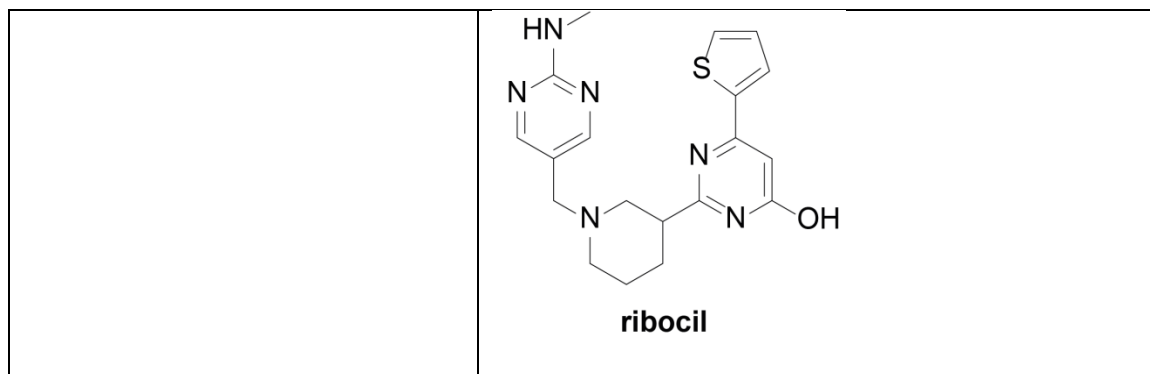
Moreover, roseoflavin (**Table 2**) an activator of FMN riboswitches is naturally produced by the soil microbe *Streptomyces davawensis*.¹⁴⁷ Compared to the riboswitch's natural metabolite riboflavin, roseoflavin harbors an additional dimethylamino group. However, crystal structure analysis showed that this does not disturb the metabolite binding pocket.¹²² The example of roseoflavin makes it reasonable to believe that nature has already realized the potential of riboswitches as antibacterial target structure.

The most recent identified compound that exhibits antibacterial activity through action on a riboswitch is called ribocil.¹⁴⁸ The synthetic small molecule, ribocil was identified in a target based approach. From a chemical point of view ribocil represents the most dissimilar activator of a riboswitch class in comparison to the natural metabolite (**Table 2**). Besides its selectivity for FMN riboswitches it was shown to have implication in animal models, more precisely in mice infected by *E. coli*.¹⁴⁸

Inspired by the already known riboswitch targeting antibiotics and the urgent need for the development of novel antibiotics, several strategies were followed to identify compounds that by activating riboswitches exert antibacterial activities. Strategies to identify such compounds are rational structure guided design, HTSs or fragment based approaches. The so far known artificial riboswitch activators that are capable of inhibiting bacterial growth are summarized in **Table 2**.

Table 2: Riboswitch ligand analogs that exert antibacterial activity

Riboswitch class and natural metabolite	Artificial compound
 <p style="text-align: center;">thiamine pyrophosphate TPP</p>	 <p style="text-align: center;">pyriothiamine pyrophosphate PTPP</p> <p style="text-align: center;">pyriothiamine PT</p>  <p style="text-align: center;">triazothiamine pyrophosphate TTTP</p> <p style="text-align: center;">triazothiamine TT</p>
 <p style="text-align: center;">L-lysine</p>	 <p style="text-align: center;">L-aminoethylcysteine AEC</p> <p style="text-align: center;">L-4-oxalysine</p>
 <p style="text-align: center;">guanine</p>	 <p style="text-align: center;">2,6-diaminopyrimidin-4-one</p>
 <p style="text-align: center;">flavin mononucleotide FMN</p>	 <p style="text-align: center;">roseoflavin</p>



Regarding the distribution of riboswitches TPP, AdoCbl, SAM I and FMN, riboswitches are most abundant.¹¹⁰ Moreover, targeting riboswitches that also regulate essential genes in fungi potentially provides the clinicians with novel antifungal drugs.

Riboswitch classes, for which only a limited number of representatives in human pathogens are known nevertheless have potential implication as drug targets. Potential antibiotics relying on targeting these classes could serve as narrow-spectrum antibiotics.¹⁰² Those antibiotics potentially benefit from the fact that they do not harm the hosts microbiota.

1.7 The *glmS* riboswitch is a self-cleaving ribozyme

The *glmS* ribozyme was identified by a computational search for conserved structural elements in intergenic regions (IGR) of *B. subtilis* and 91 other genomes.¹⁰⁴ The *glmS* riboswitch is a GlcN6P responsive ribozyme that upon GlcN6P binding modulates the expression of the essential *glmS* gene, which encodes the fructose-6-phosphate amidotransferase (GlmS), the enzyme producing GlcN6P.^{94, 104}

The gene regulatory mechanism of self-cleavage is unique among the classes of riboswitches. Also among the natural ribozymes, the *glmS* ribozyme is outstanding as it is the only RNA catalyst known to require a co-factor for RNA self-cleavage. The *glmS* ribozyme is unique as it melts both ribozyme and riboswitch properties. On the one hand gene expression is controlled by recognition of a cognate ligand as riboswitches do and on the other hand the *glmS* ribozyme bears self-cleavage activity as ribozymes do.^{104, 149}

1.7.1 The *glmS* ribozyme and its metabolites

The *glmS* ribozyme requires, in comparison to other riboswitch classes rather high concentrations (EC₅₀ values in the μM range¹⁵⁰) of the natural metabolite, to initiate

gene regulation.⁹⁴ However, the *glmS* ribozyme exhibits remarkable discrimination between even closely related GlcN6P analog (Figure 6).

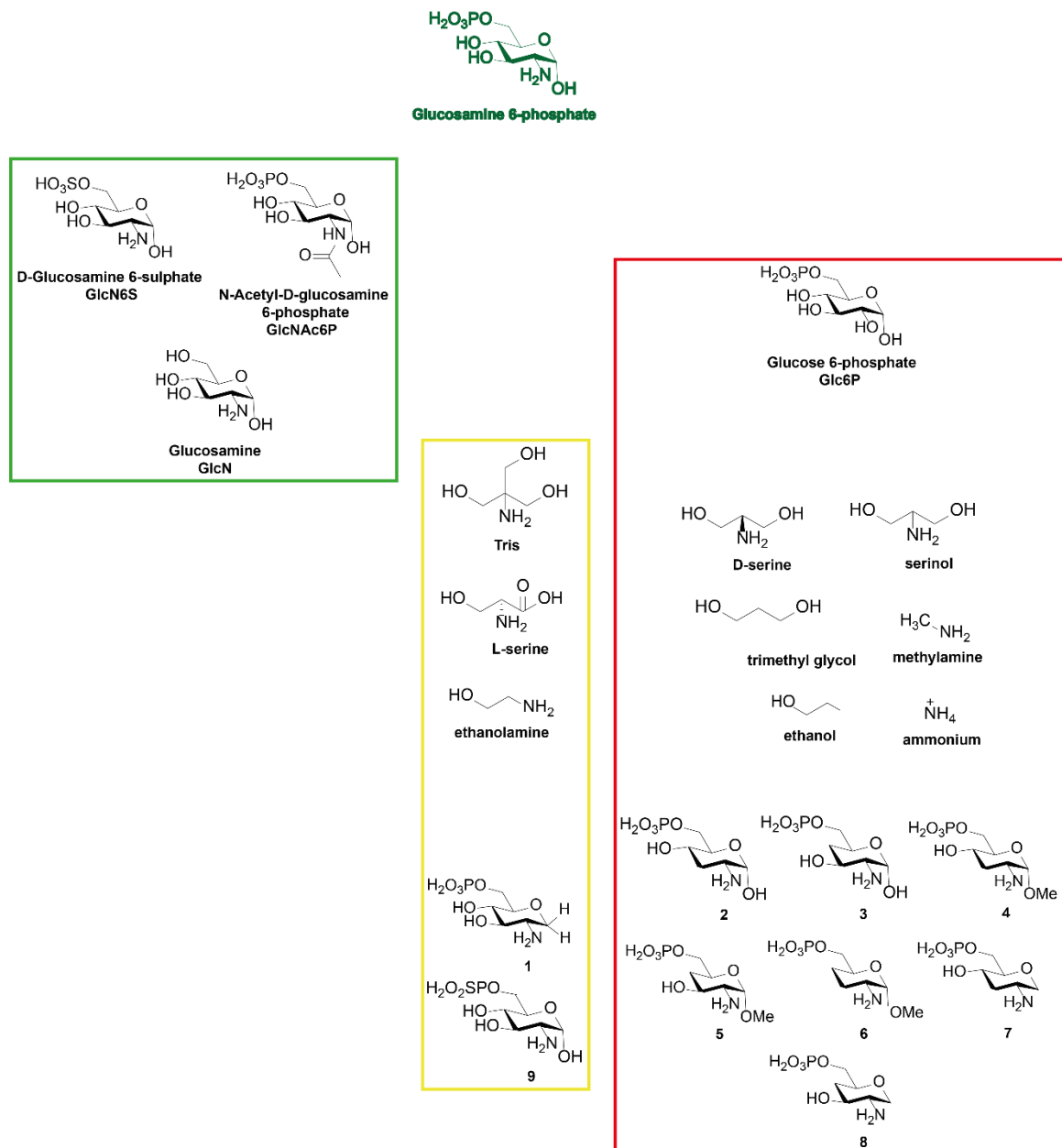


Figure 6: Chemical structures of analogs and non-active analogs of GlcN6P regarding *glmS* ribozyme activation

The chemical structure of the natural metabolite, GlcN6P, of the *glmS* ribozyme is depicted in dark green. In the lighter green box, the chemical structures of functional GlcN6P analogs are depicted. The chemical structures of moderate *glmS* ribozyme activators are shown in the yellow box. Analogs of GlcN6P that are not capable of inducing *glmS* ribozyme cleavage are shown in the red box.

For example, Glc6P differing from GlcN6P by the exchange of the amino group to a hydroxyl group (**Figure 6**) does not show ribozyme activating properties.^{94, 151} Although crystal structures strongly imply that Glc6P binds in the same position as GlcN6P, Glc6P fails to induce self-cleavage. However, Glc6P was shown to be a competitive inhibitor of metabolite-induced self-cleavage.^{129, 152} This finding accounts for the essentiality of the amine group for *glmS* ribozyme activators and builds the fundament for further investigations.^{104, 151} The observation that Tris (**Figure 6**) promotes *glmS* ribozyme cleavage while the corresponding buffer containing HEPES does not, was another hint for the fundamental necessity of the amine group of *glmS* ribozyme activators.^{94, 151, 153} Moreover, the comparison of L-serine and D-serine with L-serine (**Figure 6**) being an activator of *glmS* ribozyme cleavage in contrast to D-serine clearly indicates that the stereochemistry of the amine and anomeric hydroxyl groups is crucial for *glmS* ribozyme activation.¹⁵¹ Also serinol (**Figure 6**) resembles the minimal required motif and activates the *glmS* ribozyme, while trimethyl glycol (**Figure 6**) missing the amine fails in *glmS* ribozyme activation.¹⁵¹ Another finding on the activating ethanolamine and the non-active analogues ethanol, methylamine and ammonium (**Figure 6**) corroborates the finding on the minimal requirements for *glmS* ribozyme activators.¹⁵¹ Finally, it was shown that the pK_a value of the amine group of the natural metabolite GlcN6P is crucial for the catalytic reaction.¹⁵⁴⁻¹⁵⁵ The hydroxyl group of Glc6P in place of the amino group of GlcN6P has a higher pK_a value. Therefore, Glc6P is much less able to function as proton acceptor or donor, accounting for the inability of Glc6P to activate *glmS* ribozyme self-cleavage.¹⁵¹ Variants of molecules containing amine modifications disclosed that slight modifications of the amine moiety are tolerated as long as the general capability of the amine to accept and donate protons is retained.¹⁵⁶

Furthermore, Lim *et al.* showed that an GlcN6P analog lacking the hydroxyl group in position 1 (**Figure 6, 1**) serves as an activator of *glmS* ribozyme self-cleavage.¹⁵⁶ Analysis of additional rationally designed GlcN6P analog revealed that the hydroxyl group in position 4 (**Figure 6, 2**) is essential for binding while the hydroxyl group in position 3 (**Figure 6, 3**) has only minor effects on *glmS* ribozyme activation. Further studies analyzed the impact of the hydroxyl groups and it was shown that methylation of the hydroxyl group in position 1 in combination with the substitution of one or two hydroxyl groups in position 3 (**Figure 6, 4**) or 4 (**Figure 6, 5**) (**Figure 6, 6**) does not allow for *glmS* ribozyme activation.¹⁵⁰ The same is true for compounds lacking the hydroxyl group in position 1 plus the one in position 3 (**Figure 6, 7**) or 4 (**Figure 6, 8**). The acetylated analog of GlcN6P, GlcNAc6P (**Figure 6**) was shown to confer activation of the *glmS* ribozyme, however rather high concentration are required and the achieved cleavage rate is significantly lower as observed for GlcN6P.¹⁵⁰ Similar effects were observed for an analog bearing a phosphorothioate instead of a phosphate in position 6 (**Figure 6, 9**).¹⁵⁶ Nevertheless, the ribozyme activating properties of a phosphorothioate modified GlcN6P could not be reconfirmed in an HTS assay.¹⁵⁷ Another compound with an

cyclic phosphate completely failed regarding *glmS* ribozyme activation.¹⁵⁰ Although all of the so far mentioned activators are indeed capable of promoting *glmS* ribozyme cleavage, their impact is limited as comparably high concentrations are needed to confer the cleavage reaction. In addition, even if these high concentrations are used some of these compounds are orders of magnitudes less effective than GlcN6P.

GlcN, (**Figure 6**) which differs from GlcN6P only by the lack of the phosphate group, is known to be a moderate activator of *glmS* ribozyme cleavage.¹⁵⁰⁻¹⁵¹ In direct comparison to the natural metabolite GlcN6P, the potency of GlcN as *glmS* ribozyme activator is reduced, indicating the importance of the phosphate group for full ribozyme activation. GlcN6S (**Figure 6**) in which the phosphate is exchanged for a sulfate is a more potent *glmS* ribozyme activator than GlcN.¹⁵⁰ Although 100 times higher concentrations of GlcN6S are needed to induce cleavage comparable to GlcN6P.⁹⁴

Altogether, the *glmS* ribozyme interacts with almost all functional groups of the metabolite, GlcN6P (**Figure 7**).¹³⁰ This highly discriminative nature allows the *glmS* ribozyme to specifically function in a complex cellular environment. The recognition of their cognate ligands in case of other riboswitch classes is also highly specific but does not always involve the recognition of as many functional groups. For instance, the TPP riboswitch senses the pyrimidine moiety by one and the pyrophosphate moiety of TPP by another helix but it does not recognize the central thiazol ring of TPP.¹⁵⁸

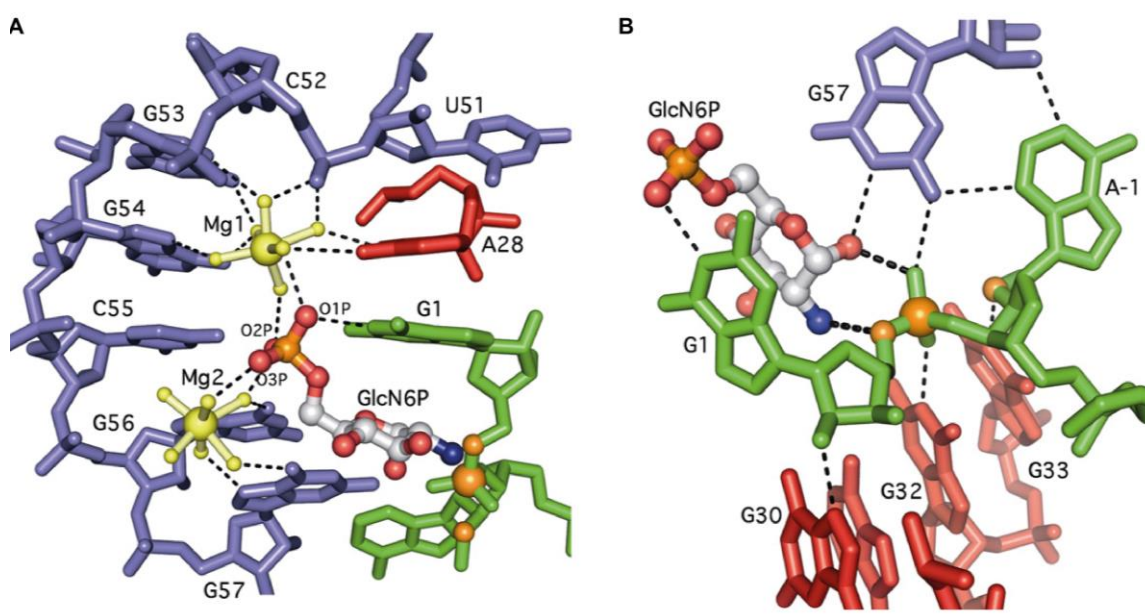


Figure 7: Recognition of the natural metabolite, GlcN6P by the *glmS* ribozyme taken from Cochrane *et al.*¹³⁰

In A the coordination of the phosphate group of GlcN6P by magnesium ions and the *glmS* ribozyme RNA of *B. anthracis* is shown. Displayed are the interactions (dashed lines) between the two fully hydrated Mg^{2+} ions (yellow) as well as the metabolite GlcN6P and the nucleotides of the ligand binding pocket that contribute to the coordination of the metabolites phosphate group. The cleavage site at G1 is highlighted in orange. B depicts the hydrogen bonding interactions at the cleavage site of GlcN6P bound to the *glmS* ribozyme from *B. anthracis*. The hydrogen bonds between the natural metabolite GlcN6P and the conserved nucleotides (G1, A-1, G30, G32, G33, G57) of the ligand binding pocket of the *glmS* ribozyme are displayed. The cleavage site is highlighted in orange.

The urgent need for novel antibiotics (**section 1.2**) and the demonstrated potential of riboswitches as antibacterial targets (**section 1.6.1**) inspired the work on the discovery of metabolite analogs as activators of the *glmS* ribozyme.

Attempts to identify *glmS* ribozyme activators by screening a library of 88 compounds did not reveal any novel activator.¹⁵⁹ The same approach was followed by screening a collection of more than 5000 drug like compounds, which as well did not yield any *glmS* ribozyme activator.¹⁵⁰ Another assay used a bimolecular construct composed of substrate strain and a leader sequence to enable FRET. In a HTS, 960 bioactive compounds were analyzed regarding their ability to induce *glmS* ribozyme self-cleavage. None of the initially identified hits besides GlcN could be confirmed.¹⁵⁷ Although HTS of compound libraries comprising drug like molecules has not been successful in identifying *glmS* ribozyme activators this approach represents a valuable tool in drug discovery.^{157, 159}

Finally, the construction of a small library of closely related GlcN6P analogues yielded the artificial *glmS* ribozyme activator, CGlcN6P¹⁵⁰ (**Figure 8**). CGlcN6P differs from the natural metabolite, GlcN6P by the exchange of the ring oxygen by a methylene. The analysis of the potency of CGlcN6P to induce *glmS* ribozyme self-cleavage showed that CGlcN6P is comparably active as GlcN6P with EC_{50} values of ~6 and 4 μM , respectively.¹⁵⁰

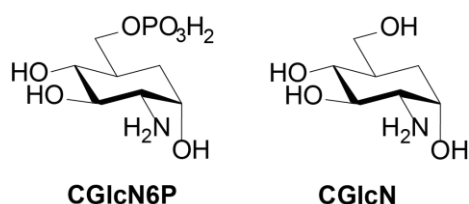


Figure 8: Chemical structures of CGlcN6P and CGlcN

So far, CGlcN6P is the only artificial *glmS* ribozyme activator known that induces self-cleavage almost as efficient as the natural metabolite, GlcN6P.

1.7.2 The *glmS* ribozyme and its dependency on divalent cations

The *glmS* ribozyme does require ions for structural organization.^{149, 160} The divalent cations Mg^{2+} , Mn^{2+} , and Ca^{2+} are well known to assist in self-cleavage reactions of the *glmS* ribozymes.^{94, 149, 153} Physiological concentrations of Mg^{2+} have been shown to promote sufficient self-cleavage.^{94, 153} Interestingly, an *in vitro* evolved *glmS* ribozyme variant that cleaves GlcN6P-independently in the presence of Ca^{2+} is known. Comparing the structural organization of the active sites of the wt *glmS* and this *in vitro* evolved variant reveals only minor differences (**Figure 9**). The main characteristic difference to the wt *glmS* ribozyme is a three nt mutation accounting for the name *glmS*^{AAA}.¹⁶¹⁻¹⁶²

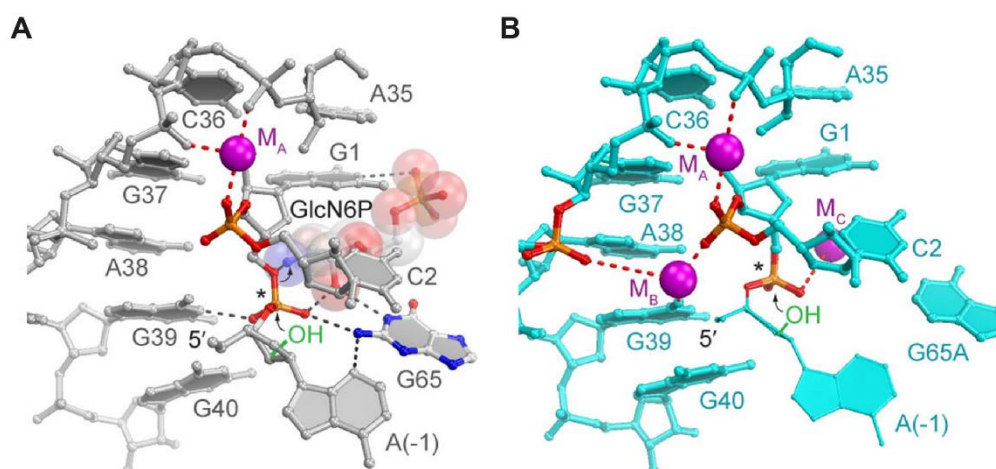


Figure 9: Comparison of active sites of *glmS* ribozymes modified after Lau and Ferré D' Amaré 2013¹⁶¹

The active site of *glmS* wt is depicted in A while the active site of the *in vitro* evolved Ca^{2+} dependent variant *glmS*^{AAA} is shown in B. The scissile phosphate is marked by an asterisk and the three metal ions participating in coordination are colored in magenta (M_A , M_B and M_C).

However, it was shown that transition ion metal complexes as well as monovalent ions and in some cases even polycationic molecules can replace the divalent ions, although their capacity in functionally replacing divalent cations, e.g. Mg^{2+} , Mn^{2+} , and Ca^{2+} is limited.¹⁴⁹ Experiments utilizing high non-physiological concentrations of the monovalent cation Na^+ showed that it can also promote self-cleavage.¹⁴⁹ Of note $Co(NH_3)_6^{3+}$, a mimic of hexahydrated Mg^{2+} , is also able to promote self-cleavage, but exhibits weak activity comparable to the monovalent ion Na^+ . Albeit the oxygen atoms of the phosphate moiety are potentially able to coordinate metal ions it seems implausible that this is the case for the *glmS* ribozyme. As cobalt hexamine ions can functionally substitute magnesium cations and $Co(NH_3)_6^{3+}$ although it cannot coordinate water molecules.^{149, 153} Cobalt hexamine however can solely build hydrogen bonds with the phosphate.^{153, 156}

The finding that monovalent ions and polycations can also promote self-cleavage to a certain extent accounts for an overall lack of ion specificity.

Nevertheless, ions are needed to confer the cleavage reaction, with Mg^{2+} , Mn^{2+} , and Ca^{2+} known to be most efficient.^{94, 149, 153} Interestingly, Mn^{2+} is the smallest known divalent cation while Ca^{2+} is the largest. However, Mg^{2+} , Mn^{2+} and Ca^{2+} , are all present in their hexahydrated form in aqueous environments and therefore have a more or less comparable geometry.¹⁴⁹

These observations indicate that the ions regarded as efficient in promoting *glmS* ribozyme self-cleavage do all mediate interactions with the RNA's nucleobases and the metabolite in aqueous solution (details are given in **section 1.7.3**).¹⁶³

1.7.3 2D and 3D structure of the *glmS* ribozyme

A common feature of most riboswitches is the conformational change upon metabolite binding. The *glmS* riboswitch is outstanding as it is preorganized for metabolite binding and upon recognition no major structural rearrangement was observed employing diverse biochemical analysis e.g. crosslinking or footprinting assays and crystal structures.^{129-130, 152-153, 164-166}

Structurally, the *glmS* ribozyme is comprised of four paired regions P1-4 (**Figure 10**).⁹⁴ Analysis of truncated *glmS* ribozyme variants revealed that the absence of the domains P3/4 impairs the self-cleavage activity but does not lead to a complete loss of ribozyme activity.^{94, 153} While regions P3 and P4 have been shown to mainly support structural stabilization, the domains P1 and P2 are highly conserved and involved in the recognition of GlcN6P. However, further truncation up to the catalytic core P2.1-P2.2 is possible without prevention of ribozyme activity. Nonetheless, the presence of all four structural domains is required for full ribozyme activity.¹⁵³

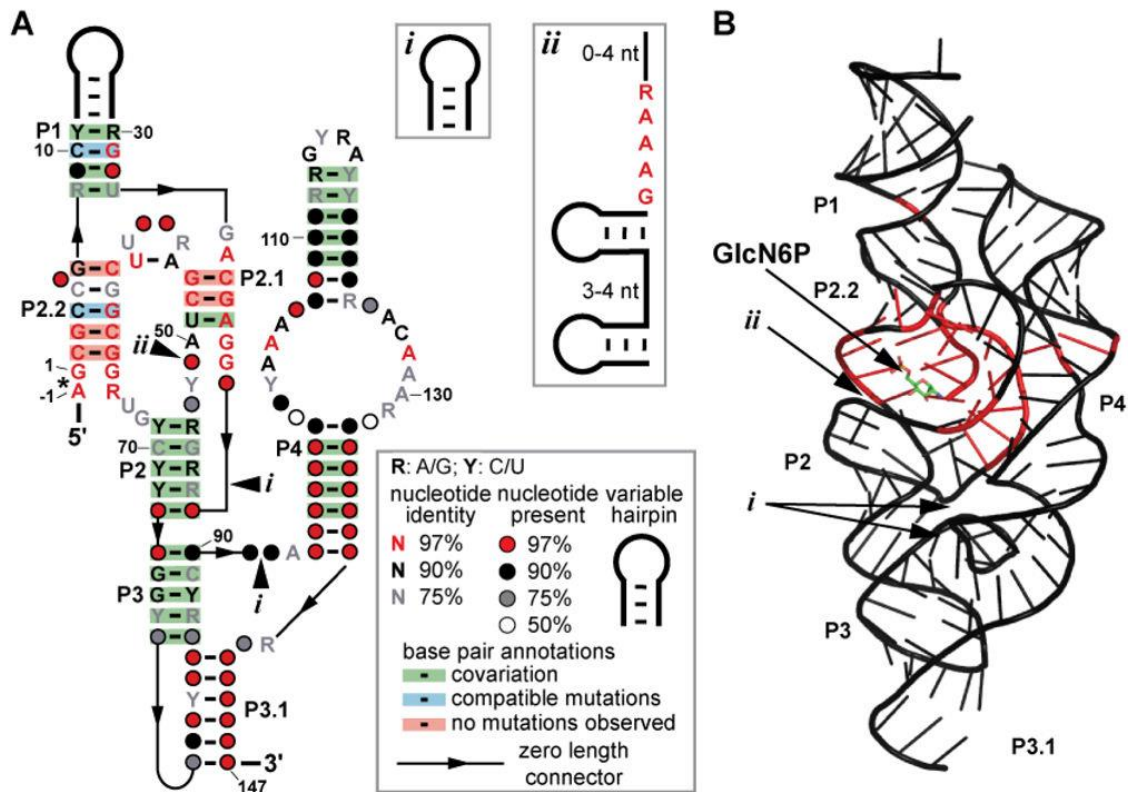


Figure 10: Consensus sequence and crystal structure of the *glmS* ribozyme taken from McCown *et al.* 2012¹⁶⁷

The consensus model shows the conserved cleavage site indicated by an asterisk and optional additional hairpins denoted with *i* or *ii* (A). In B, the crystal structure of the *glmS* ribozyme from *T. tengcongensis* is depicted, highly conserved nucleotide (at least 97% conservation) are colored in red.

The *glmS* ribozyme is composed of three helices that stack on each other and arrange side by side. P2.1 forms the central helical stack with the coaxial stacking helices P1, P2.2, P2, P3 and P3.1 on the one side and the helical stack of P4 and P4.1 on the other (**Figure 10B**). The ribozyme core consisting of P2.2 and P2.1 folds into a double pseudoknot structure.¹⁶⁸

Taking a closer look at the metabolite binding pocket uncovers that the *glmS* ribozyme does not engulf the metabolite, but rather senses it in a water accessible open form. Crystal structures implied that two fully hydrated Mg^{2+} ions are located in the metabolite binding pocket (**Figure 7A**).¹³⁰ The hydrated magnesium ions coordinate the nucleotides (A28, C52, G53, G54, G56 and G57) within the ligand binding pocket through hydrogen bonding interactions.¹³⁰ Moreover, the two hydrated Mg^{2+} ions as well as the N1 of nucleotide G1 are coordinating the phosphate moiety of GlcN6P through H-bonds (**Figure 7A**). Thereby, the Mg^{2+} ions in the water exposed ligand binding pocket compensate the negatively charged phosphate moiety.¹³⁰

The glucosamine moiety is sensed by the nucleotides of the ribozyme (**Figure 7B**).¹³⁰ The nucleotides A-1 and G1 directly participate in the cleavage reaction and carry the 2'-3' cyclic phosphate and the 5'OH group afterwards. The four guanines in positions 30, 32, 33 and 57 build hydrogen bonds and coordinate the ligand binding pocket (**Figure 7B**). The guanine in position 33 of the *glmS* ribozyme is highly conserved. It has been uncovered that the N1 imine of G33 forms H-bonds with the nucleophilic hydroxyl group of A1 (**Figure 7B**), which might indicate that G33 is involved in catalysis by acting as base in general acid-base catalysis. A quantum chemical/molecular mechanical calculation study published in 2015 provides evidence for this hypothesis and indicates that G33 acts as base.¹⁶⁹ However, other studies imply that the role of G33 is as base being involved in acid-base catalysis. Their hypothesis regarding the general acid-base catalysis mechanism utilized by the *glmS* ribozyme is that the amino group of GlcN6P acts as both base and acid.¹⁷⁰ This phenomenon has been similarly observed for other ribozymes, in which nucleotides assume the role of the base and acid in general acid-base catalysis.¹⁷¹⁻¹⁷² Although the role of G33 is not truly revealed, mutation of this conserved residue tremendously impairs ribozyme activity. In case of the G33A mutant, self-cleavage capability is completely lost.¹⁷³ Similar effects are observed regarding the guanine in position 57.^{130, 174}

1.7.4 The *glmS* ribozyme employs a self-cleavage mechanism

The *glmS* ribozyme utilizes self-cleavage as gene regulatory mechanism (**Figure 11**). Usually riboswitches control gene expression either by transcriptional termination or inhibition of translational initiation (**section 1.6, Figure 5**). However, self-cleavage is a mechanism well known to be employed by other ribozymes as for instance the HHR, VS ribozyme or HDV ribozyme.¹⁷⁵ Unlike other classes of ribozymes the *glmS* ribozyme employs neither divalent cations in the catalytic reaction nor the nucleotides in a general acid-base catalysis. The Mg²⁺ ions shield the negatively charged phosphate, but their location with a distance of ~10 Å from the scissile phosphate clearly indicate that the cations cannot be actively involved in the catalytic reaction.¹⁶⁸ Interestingly, GlcN6P acts as co-factor and is directly involved in the self-cleavage mechanism.^{129-130, 151, 153} This means that the *glmS* ribozyme exerts genetic control by metabolite, e.g. GlcN6P, induced self-cleavage (**Figure 11**).

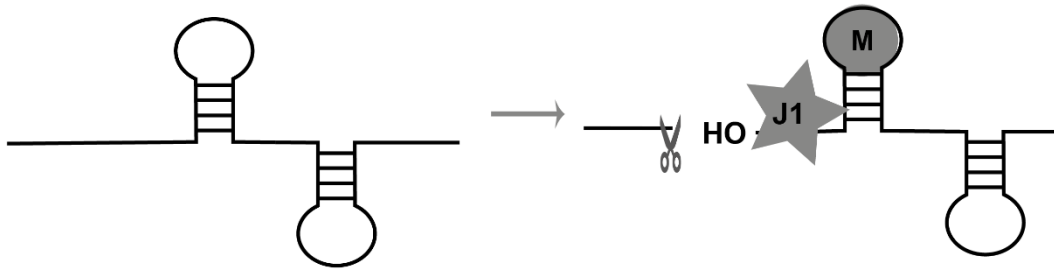


Figure 11: Gene regulatory mechanism employed by the *glmS* ribozyme

Schematic illustration of the unique self-cleavage mechanism employed by the *glmS* ribozyme. Upon binding of the metabolite (M) self-cleavage occurs and the free 5' OH group of the *glmS* ribozyme as well as the *glmS* mRNA become degraded by bacterial RNase J1 (J1).

Binding of the metabolite induces an internal phosphodiester transfer reaction resulting in cleavage of the scissile phosphodiester bond (**Figure 12**).¹⁶⁸ In phosphodiester transfer reactions as employed by the *glmS* ribozyme, the 2'-hydroxyl group located at the cleavage site attacks the adjacent phosphorous center by a nucleophilic attack yielding the 2'-3' cyclic phosphate and 5' hydroxyl cleavage products (**Figure 12**).⁹⁴ The cleavage reaction is catalyzed by general acid-base catalysis within the water accessible ligand binding pocket.^{154, 168, 176} The amine group is a known crucial requirement for *glmS* ribozyme activators and participates in the cleavage reaction by acting as proton donor and acceptor.¹⁷⁷

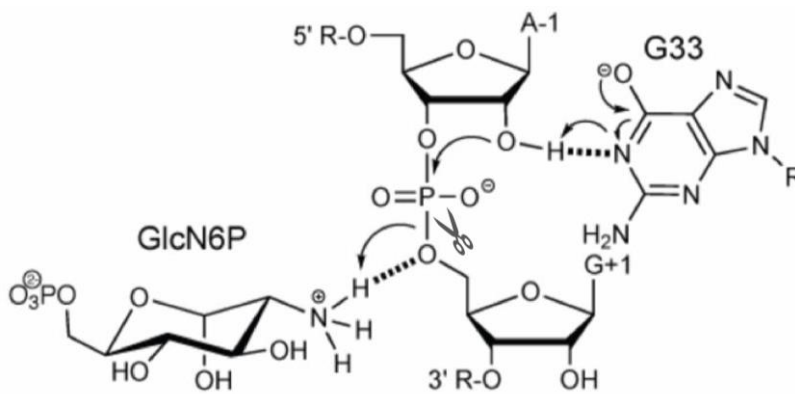


Figure 12: Self-cleavage mechanism employed by the *glmS* ribozyme modified after Viladoms *et al.*¹⁷⁷

Shown is the proposed self-cleavage mechanism utilizing general acid-base catalysis involving GlcN6P as co-factor. Depicted is the metabolite, GlcN6P, as well as the functional groups supporting self-cleavage of the bases G+1, A1 and G33. The scissor indicates the cleavage site.

The 6-phosphate as well as the 4-hydroxyl group of GlcN6P most likely participate by functioning as hydrogen acceptor and donor.¹⁵⁶ Subsequently to the cleavage

reaction, the cleavage product containing the 5'OH group is degraded by RNase J1.⁷¹ RNase J1 is a naturally occurring and widespread RNase exhibiting 5'-3' exonuclease activity and is specialized for degradation of 5'hydroxyl termini containing cleavage products within UTRs of regulatory RNAs.^{71, 178}

1.7.5 The *glmS* ribozyme regulates the expression of the *glmS* gene

The *glmS* ribozyme regulates the *glmS* gene involved in cell wall biosynthesis. Due to the essential role of the *glmS* gene for bacterial viability, targeting the *glmS* ribozyme with artificial metabolites, which induce the self-cleavage mechanism, presents a promising strategy to develop novel antibacterial compounds.^{158, 179} A study by Collins *et al.* already hints at the importance of the *glmS* ribozyme for bacterial metabolism and the suitability of the *glmS* ribozyme as antibacterial target. They investigated a mutated version of the *B. subtilis glmS* ribozyme that is not capable of self-cleavage and discovered that bacteria carrying this mutation are not able to sporulate or form biofilms. They concluded that this impairment in GlcN metabolism influences peptidoglycan biosynthesis and that the synthesis of polysaccharides is important in biofilm formation.⁷¹

1.8 The GlnS enzyme

The *glmS* gene codes for the enzyme L-glutamine: D fructose-6-phosphate amidotransferase.¹⁷⁹ This enzyme is responsible for the irreversible reaction of L-glutamine and D-fructose-6-phosphate (Fru6P), yielding glucosamine-6-phosphate (GlcN6P) and glutamate. Therefore, the enzyme is also called GlcN6P-synthase.¹⁸⁰ The reaction does not depend on other co-factors and proceeds without the consumption of ATP.¹⁸⁰ The GlnS enzyme (bacterial GlcN6P-synthase) is ubiquitously found as the product, GlcN6P, plays a key role in metabolism. GlcN6P-synthase participates in the synthesis of uridine 5'diphospho-N-acetyl-D-glucosamine (UDP-GlcNAc), the building block of diverse macromolecules crucial for prokaryotes and eukaryotes.¹⁷⁹ Due to the fact that GlnS is essential for survival, it requires a tight regulation. In eukaryotes, elevated levels of UDP-GlcNAc impede GlcN6P-synthase. In prokaryotes, millimolar concentrations of GlcN6P inhibit the *glmS* gene via the above explained *glmS* ribozyme.

In mammals the GlcN6P-synthase is called GFAT and two versions of GFAT are annotated.¹⁷⁹ The expression of GFAT1 and GFAT2 is known to highly vary depending on the analyzed tissue.¹⁸¹ Although the enzyme is also essential in mammals, the organism can circumvent short time periods of enzyme inhibition.¹⁸² However, in fungi, the GlcN6P-synthase is involved in chitin biosynthesis and deletion of the enzyme is lethal.¹⁸³

In bacteria, the GlmS enzyme assumes an essential role in the biosynthesis of peptidoglycan, lipopolysaccharides and teichoic acids. The enzyme converts the first step in the synthesis of UDP-GlcNAc.¹⁸⁴⁻¹⁸⁵ Diverse genetic knock out studies showed that GlmS is essential for bacterial survival and sporulation.^{179, 184, 186-190} However, the knock out can be rescued by the addition of GlcN or GlcNAc to growth medium.¹⁷⁹ A study in *E. coli* revealed that under specialized conditions, the GlcN6P deaminase can rescue the function of GlmS. However, this capability seems to be limited to the gram-negative bacterium *E. coli*.¹⁹¹ As the GlmS enzyme is essential for microorganisms, it represents a potential antimicrobial target. Indeed, certain *B. subtilis* strains are equipped with a defense mechanism that targets the GlmS enzyme. These strains produce the protein tetaïne, which is effective against bacteria and fungi by functioning as glutamine analog.¹⁹²⁻¹⁹³ Nonetheless, the downside of tetaïne is that it also has cytostatic effects in human cell culture.¹⁹⁴ Other examples of GlcN6P-synthase inhibitors are the N3-(4-methoxyfumaroyl)-L-2,3-diaminopropanoic acid (FMDP) peptides that have antimicrobial activity against fungi and gram-positive bacteria but do not seem to target the human homolog.¹⁹⁵

As already mentioned, the bacterial cell wall is composed of peptidoglycan. This heteropolymer consists of β 1-4 linked alternating GlcNAc and MurNAc molecules which form the glycan chains, that are connected by shorter peptides (**Figure 2**).¹⁹⁶ The synthesis of peptidoglycan is crucial for bacterial survival and includes at least 20 different chemical reactions at different sublocations within the cell.¹⁹⁴

This thesis focuses on the cytoplasmic steps of cell wall biosynthesis involving the GlmS enzyme. Further steps of bacterial cell wall biosynthesis at the inner and outer side of the membrane as well as the final polymerization of peptidoglycan at the outer side of the cytoplasmic membrane are nicely reviewed in.^{47, 197}

The GlmS enzyme is involved in the earliest steps of peptidoglycan synthesis and participates in the synthesis of UDP-GlcNAc in the cytoplasm. The synthesis of UDP-GlcNAc, one of the two molecules that later on build peptidoglycan, involves the three enzymes GlmS, GlmM and GlmU. A total of four enzymatic steps are needed for the formation of the precursor molecule UDP-GlcNAc. In the first step, GlmS converts Fru6P and L-glutamine to GlcN6P. GlcN6P is afterwards converted to GlcN1P by the phosphoglucosamine mutase, GlmM. Subsequently, GlmU carries out the acetylation of GlcN1P and then the formation of GlcNAc1P to UDP-GlcNAc (**Figure 2**).¹⁹⁴

As peptidoglycan and the genes associated with its formation are essential for cell wall formation and survival, these genes are a suitable antibacterial target. Several classes of antibiotics targeting peptidoglycan formation are known (**section 1.2.2**).

In bacteria, two different RNA based regulatory mechanisms regarding *glmS* expression are known. One is described in *E. coli* and is based on two small

RNAs.¹⁹⁸ The other gene regulatory mechanism is based on a riboswitch regulating gene expression by catalytic activity, namely the GlcN6P sensing *glmS* ribozyme, whose function is analyzed in detail in this thesis (**sections 1.7-1.7.5**).

2 Aim of the study

Resistances against almost all antibiotics in clinical use are known, nowadays drug and even MDR strains cause severe problems for human health. The rising problem of antibiotic resistance is associated with the fact that common antibiotics only address a limited number of cellular targets. Together, this calls for the urgent development of new antibiotics that address novel targets. The potential of riboswitches as antibacterial target structure has been demonstrated by a few reports. The aim of this thesis was to validate *glmS* riboswitches, whose utilizes a special gene regulatory mechanism, namely self-cleavage to regulate the expression of the essential *glmS* gene. By employing this self-cleavage mechanism, the *glmS* riboswitch can be classified as ribozyme, a class of RNA molecules for which it has not been described previously that they represent suitable antibacterial target structure properties. This thesis is based on the observation, that the *glmS* ribozyme of *S. aureus* is activated by CGlcN6P *in vitro*.^{150 199} Moreover, it was shown that CGlcN treatment leads to inhibition of *S. aureus* Mu50 cell growth.²⁰⁰ The question whether these findings are due to *in vivo* interaction of CGlcN and the *glmS* ribozyme was set out to be answered within this thesis. Besides the MoA analysis of CGlcN and its potential as antibiotic substance by targeting the *glmS* ribozyme it was aimed at a broader understanding of the *glmS* ribozyme per se and with a strong focus on the applicability of this RNA as antibiotic target. To gain further insights into the interaction of the *glmS* ribozyme and potential artificial metabolites, that could potentially exhibit antibacterial effects different approaches were followed. One approach was based on an *in silico* search. The potential of commercially available compounds that mimic the 3D shape of the ribozymes natural metabolite was analyzed in *in vitro* experiments. The analysis of a novel modified CGlcN variant as artificial metabolite, on the formerly known as well as on the herein validated *glmS* ribozymes and the MoA analysis of this monofluorinated CGlcN analog combines the potential of the mentioned approaches. Collectively different aspects on the *glmS* ribozyme were studied to gain more insights in the RNA biology of this special RNA and moreover, aiming at the demonstration that the *glmS* ribozyme represents a suitable antibiotic target structure. The MoA study on CGlcN was carried out with regard to the *glmS* ribozyme harboring bacterial species, *S. aureus* and *B. subtilis*. It was sought to expand our understanding of *glmS* ribozyme function by characterization and validation of *glmS* ribozymes of other relevant human pathogens.

3 Results

This chapter illustrates the results on the *glmS* ribozyme taking different aspects into account.

The interaction of the *glmS* ribozyme RNA with potential metabolites is presented in **section 3.1**. A screening of molecules with a 2D shape similarity to the natural metabolite GlcN6P was performed to identify modulators of *glmS* ribozyme self-cleavage.

Section 3.2 deals with the elucidation of the cellular MoA of a *glmS* ribozyme activator, namely CGlcN and demonstrates the suitability of the *glmS* ribozyme as antibacterial target.

Section 3.3 illustrates the validation and biochemical characterization of *glmS* ribozyme variants originated from high priority human bacterial pathogens.

In **section 3.4**, a combination of the approaches introduced in the former sections is depicted. The analysis of the effects of a chemically synthesized CGlcN derivative on different *glmS* ribozyme variants *in vitro* and its MoA analysis *in vivo* is displayed.

3.1 Screening of potential *glmS* ribozyme modulators with 3D shape similarity to the natural metabolite, GlcN6P

To identify *glmS* ribozyme modulators, an *in silico* screening based on the 3D shape of the natural metabolite GlcN6P was conducted in cooperation with the group of Prof. Louis Reymond (University of Berne). The approach to identify GlcN6P was ligand based virtual screening comparable to the one described in Montalbetti *et al.*²⁰¹ The aim of this approach was on the one hand to identify potential ribozyme activators that might also have antibacterial properties and on the other hand to identify inhibitory molecules that potentially reveal insights into the interaction with the *glmS* ribozyme RNA.

A screening analyzing the activation of *S. aureus glmS* ribozyme self-cleavage by a series of Reymond compounds (1st generation Reymond compounds) was performed (**Figure 13**). The chemical structures of the tested compounds, which were originating from a library of commercially available compounds can be seen in **Figure 67**. The compounds were analyzed in the metabolite-dependent self-cleavage assay (**section 6.2.15**), however none of the tested compounds activated *glmS* ribozyme cleavage.

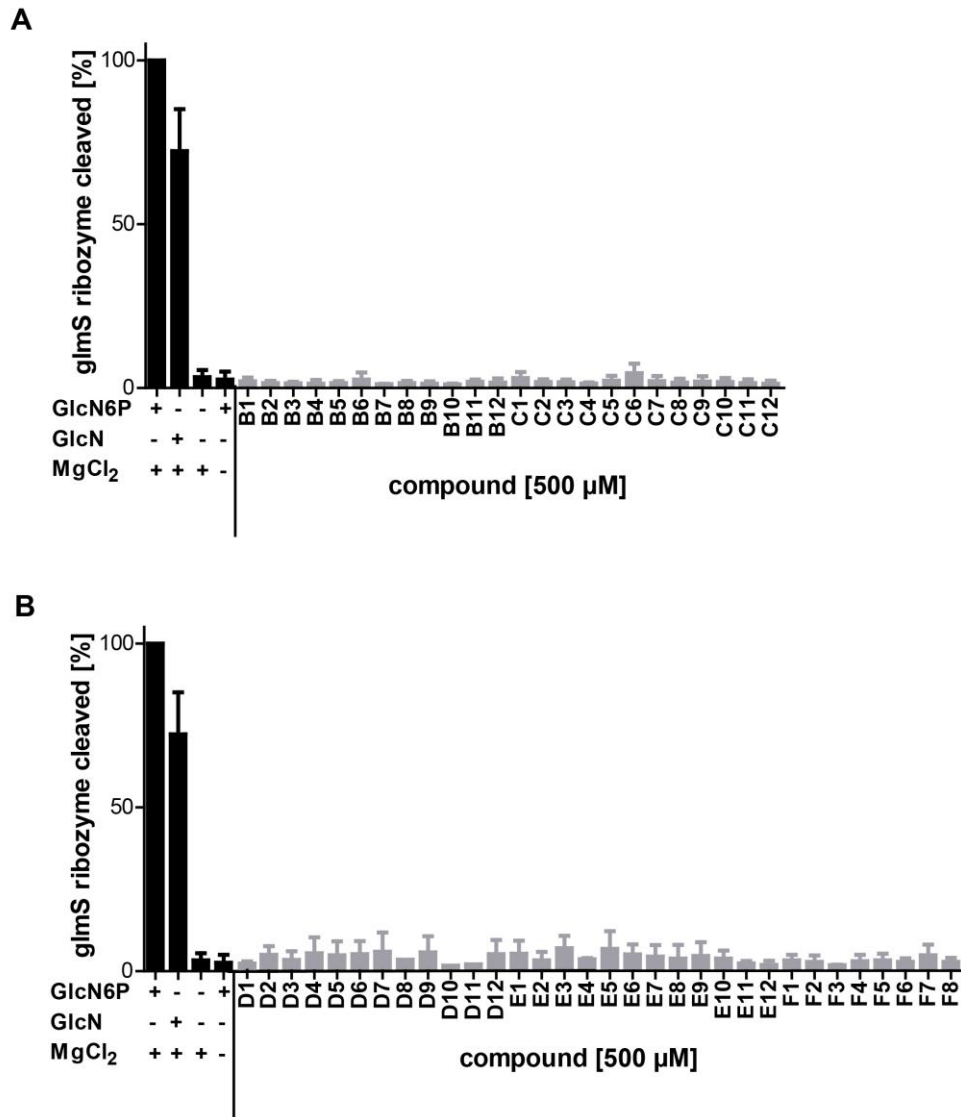


Figure 13: Screening for activation of *glmS* ribozyme self-cleavage by 1st generation Reymond compounds

Shown is the radioactive metabolite-induced self-cleavage assay to verify cleavage induction by Reymond compounds (500 μ M) in 0.5% DMSO (grey). Activation by compounds B1-C12 is depicted in A and activation of *glmS* ribozyme cleavage by compounds D1-F8 is depicted in B. Positive controls containing either 200 μ M GlcN6P or GlcN and negative controls without metabolite or MgCl₂ are depicted in black. All datasets are normalized to the control containing GlcN6P (n=1-3). Cleavage was monitored after 30 min of incubation at 37 °C.

As none of the tested compounds induces *glmS* ribozyme cleavage, it was analyzed if the compounds could inhibit GlcN6P-induced cleavage. To assess this, assays in the presence of 0.2 mM GlcN6P and 2 mM of compound in 2%DMSO were performed. **Figure 14** displays the results obtained for inhibition of *glmS* ribozyme cleavage by the 1st generation Reymond compounds. Of the 56 tested compounds, B7, C3, C8, C9, D2, D6, E4, E6, E8, E11, F6 and F7 show inhibition of cleavage.

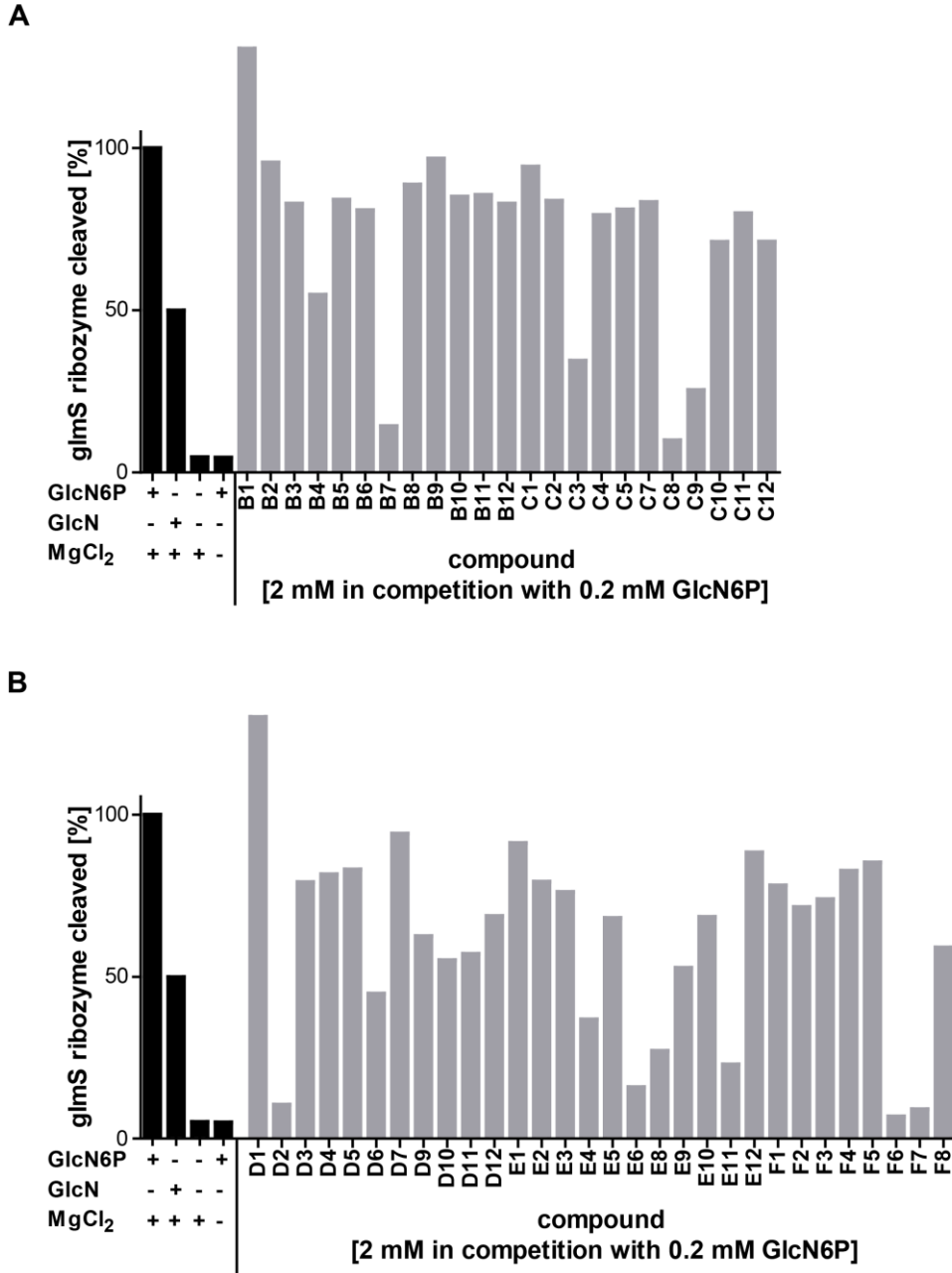


Figure 14: Screening for inhibition of GlcN6P-induced *glmS* ribozyme cleavage by 1st generation Reymond compounds

Shown is the radioactive metabolite-induced self-cleavage assay to identify inhibition of GlcN6P-induced *glmS* ribozyme cleavage by 2 mM Reymond compounds in 2% DMSO (grey). Inhibition by compounds B1-C12 is depicted in A and inhibition of GlcN6P-induced *glmS* ribozyme cleavage by compounds D1-F8 is depicted in B. Positive controls containing either 200 μM GlcN6P or GlcN and negative controls without metabolite or MgCl₂ are depicted in black. All datasets are normalized to the control containing GlcN6P (n=1). Cleavage was monitored after 30 min of incubation at 37 °C.

3.1.1 Structure activity relationship of Reymond compound D2 and its isomers

One of the GlcN6P-induced *glmS* ribozyme self-cleavage inhibitors identified in **Figure 14** is D2, 2, 4(-trifluoromethyl)benzol-1,2-diamin. The potential of D2 to inhibit *glmS* ribozyme cleavage was further analyzed in a concentration-dependent manner. The results are shown in **Figure 15A**. Having shown that D2 concentration-dependently inhibits cleavage, a literature search for chemical analogs of D2 was conducted to allow evaluation of the structure activity relationship. This search revealed 2,3-diaminobenzotrifluoride (D2.1) (**Figure 15B**) and 2,5-diaminobenzotrifluoride (D2.2) (**Figure 15C**). Subsequently, these two compounds were also analyzed regarding the inhibition of GlcN6P-induced *glmS* ribozyme cleavage (**Figure 15**). The obtained results show that D2.2 (**Figure 15C**) is the most potent inhibitor of GlcN6P-induced ribozyme cleavage, followed by the initially identified compound D2 (**Figure 15A**). The compound, D2.1 (**Figure 15B**) with the amino groups in *ortho* and *meta* position to the trifluoromethyl group is not capable of inhibiting *glmS* ribozyme cleavage.

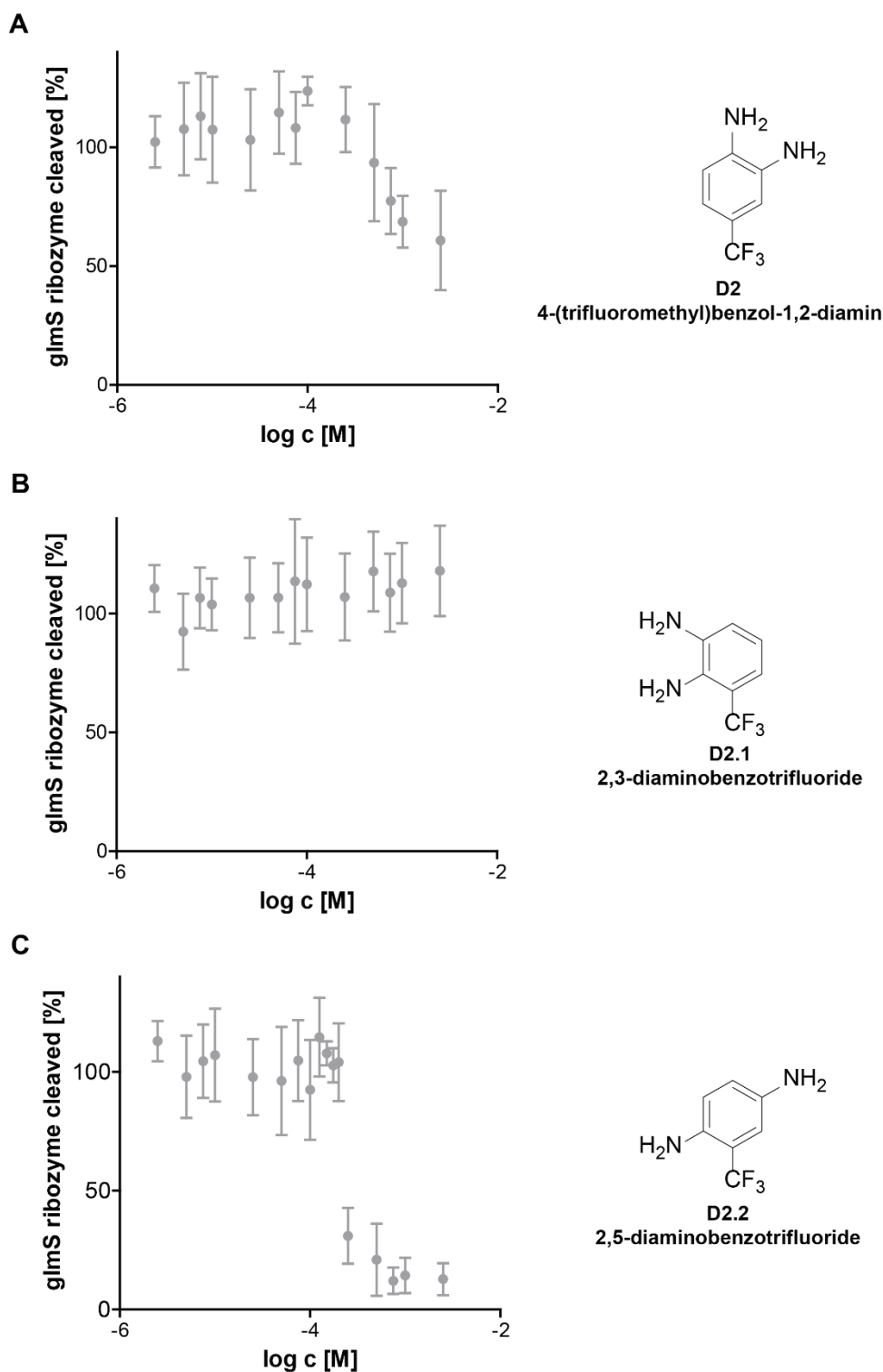


Figure 15: Concentration-dependent inhibition of GlcN6P-induced *glmS* ribozyme self-cleavage by Reymond compound D2 and isomers

Shown is the radioactive metabolite-induced self-cleavage assay of 200 μ M GlcN6P in the presence of increasing concentrations of Reymond compounds D2, 4-(trifluoromethyl)benzol-1,2-diamin (A), D2.1, 2,3-diaminobenzotrifluoride (B) and D2.2 2,5-diaminobenzotrifluoride (C). Depicted is the cleavage of the *S. aureus glmS* ribozyme RNA (n=3-6). All datasets are normalized to cleavage in the presence of only GlcN6P. Cleavage was monitored after 30 min of incubation at 37 $^{\circ}$ C.

3.1.1.1 Structure activity relationship of more distantly related variants of Reymond compound D2

Having assessed the ability of D2 and the isomer D2.2 to inhibit *glmS* ribozyme cleavage it was decided to gain more information about the interaction of the *glmS* ribozyme RNA and the chemically related D2 variants. It was searched for commercially available compounds that are substitutions or exchanges of D2 to elucidate the structure activity relationship. This search revealed the compounds depicted in **Figure 16A**. An initial screening of their ability to inhibit GlcN6P-induced *glmS* ribozyme self-cleavage is illustrated in **Figure 16B**. Of the five tested compounds, only 2-hydroxy-4-trifluoro-methyl-aniline showed inhibitory activity. 2-hydroxy-4-trifluoro-methyl-aniline (**Figure 16A**) differs from D2.2 (**Figure 15C**) by substitution of the amino- by a hydroxyl group at C5.

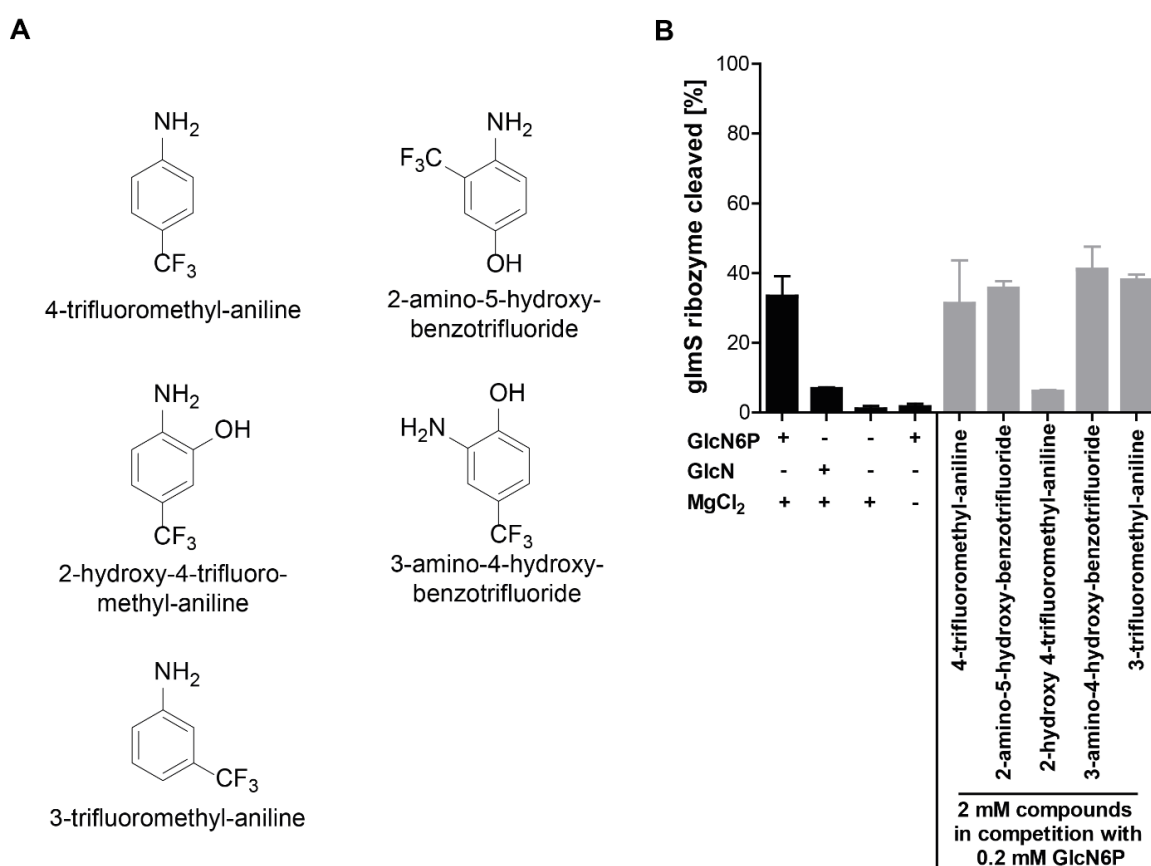


Figure 16: Screening of compounds structurally similar to D2

Radioactive metabolite-induced cleavage assay monitoring the inhibition of GlcN6P-induced *S. aureus glmS* ribozyme self-cleavage by 4-trifluoromethyl-aniline, 2-amino-5-hydroxy-benzotrifluoride, 2-hydroxy-4-trifluoro-methyl-aniline, 3-amino-4-hydroxy-benzotrifluoride or 3-trifluoromethyl-aniline are depicted in grey and shown in comparison to the controls. Positive controls containing either 200 μ M GlcN6P or GlcN and negative controls without metabolite or MgCl₂ are depicted in black (n=3). Cleavage was monitored after 30 min of incubation at 37 °C.

3.1.2 Refinement of screening compounds with a similar 3D shape to GlcN6P for modulation of *glmS* ribozyme activity

Based on the findings for the first series of Reymond compounds and taking more elevated computational algorithms into account, a second *in silico* screening for potential *glmS* ribozyme modulators was performed by the group of Prof. Reymond. In this second screening the phosphate group as well as the amino group of the natural metabolite GlcN6P and the findings on the compound D2 and its isomer D2.2 were considered. On this basis, a library of commercially available compounds was screened *in silico*.^a

The potential *glmS* ribozyme modulators were named 2nd generation of Reymond compounds and were analyzed in fluorescence-based metabolite-induced *glmS* ribozyme cleavage assays. This assay is based on Förster resonance energy transfer (FRET) and employs a bimolecular construct in which cleavage of the *glmS* ribozyme can be detected by fluorescence read out (for more details see **section 6.2.16**). This assay allows screening in 96-well plates and therefore is less time consuming compared to the radioactive-based metabolite-induced cleavage assay. The screening for activation is displayed in **Figure 17**. Compound H6 shows induction of self-cleavage, I3, K6, K8 N1 and N8 show moderate activation, while the capability of I8, J1, J3, J9, L7, M1, M5, N5, O1, O4, Q2 and R1 to induce cleavage needs re-evaluation and concentration-dependent analysis to confirm their activating properties. Compounds H6, K6, K8, J3, O1 and R1 should be re-evaluated in the radioactive metabolite induced self-cleavage assay as the fluorescence of the compounds potentially influences the results of this fluorescence based assay. The chemical structures of all tested compounds can be found in the appendix (**Figure 68**).

^a Personal communication Prof. Reymond

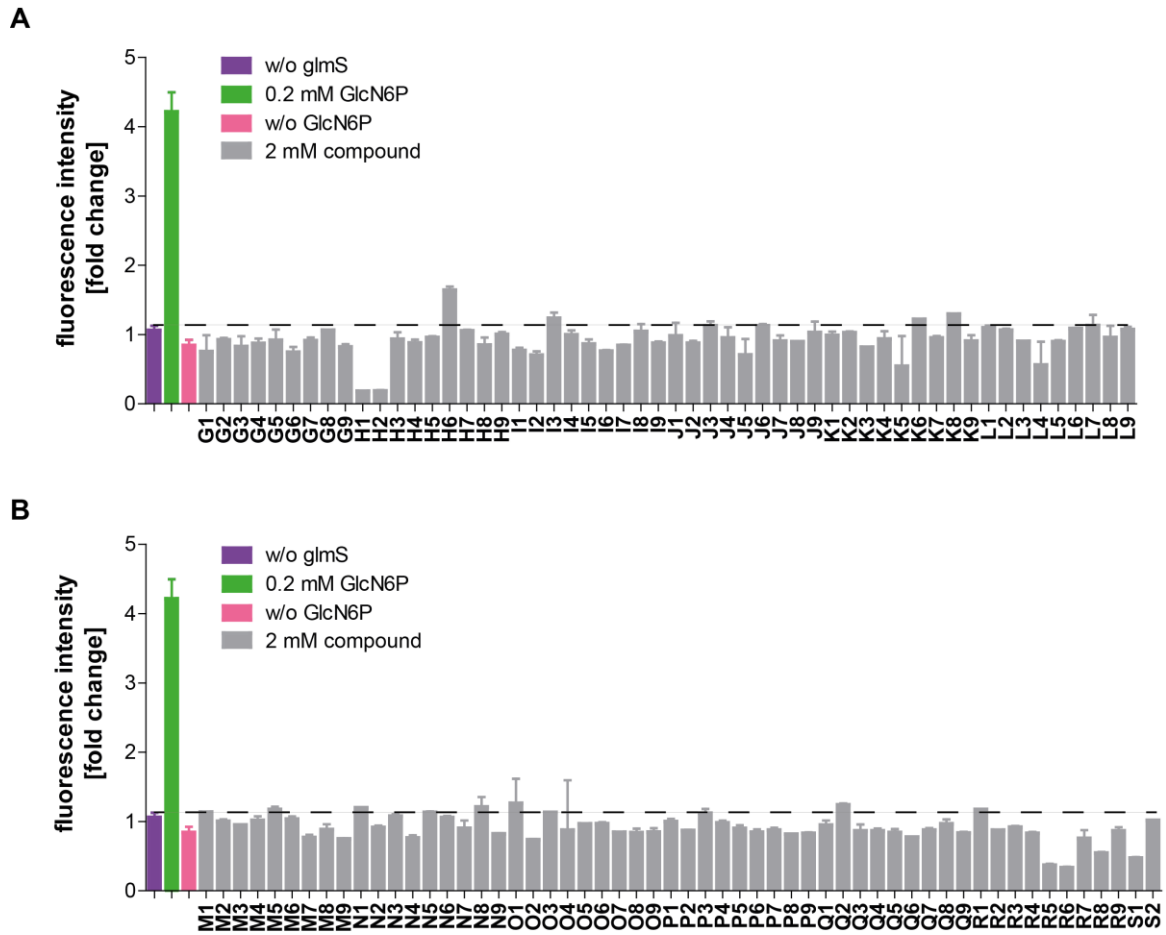


Figure 17: Screening of the 2nd generation Reymond compounds for induction of *glmS* ribozyme self-cleavage

Depicted are FRET assay results showing *S. aureus glmS* ribozyme self-cleavage in the presence of 2 mM Reymond compounds in 2% DMSO in grey and the positive control containing 0.2 mM GlcN6P as well as the negative controls lacking the metabolite or the leader sequence in black. Activation of self-cleavage by compounds G1-L9 is shown in A and compounds M1-S2 in B (compounds n=1-2; controls n=8). Cleavage was monitored after 19.5 min of incubation at 37 °C.

After testing the 2nd generation of Reymond compounds for *glmS* ribozyme activation in the FRET assay, a screening looking for potential inhibitors of GlcN6P-induced self-cleavage was performed. As shown in **Figure 18**, the inhibitors G1, H2, O4 and R5 were identified as *glmS* ribozyme inhibitors with H2 showing the strongest inhibition. The compounds G2, G3, H3, H4, H5, I1, J5, K3, K9, L5, M6, R4, R7 and S1 also showed moderate inhibition of *glmS* ribozyme cleavage. Re-evaluation of the inhibitory potency of compounds H2 and G2 would be needed by the radioactive metabolite-induced self-cleavage assay as the low fluorescence of the compounds alone might influence the results of this fluorescence based assay.

Results

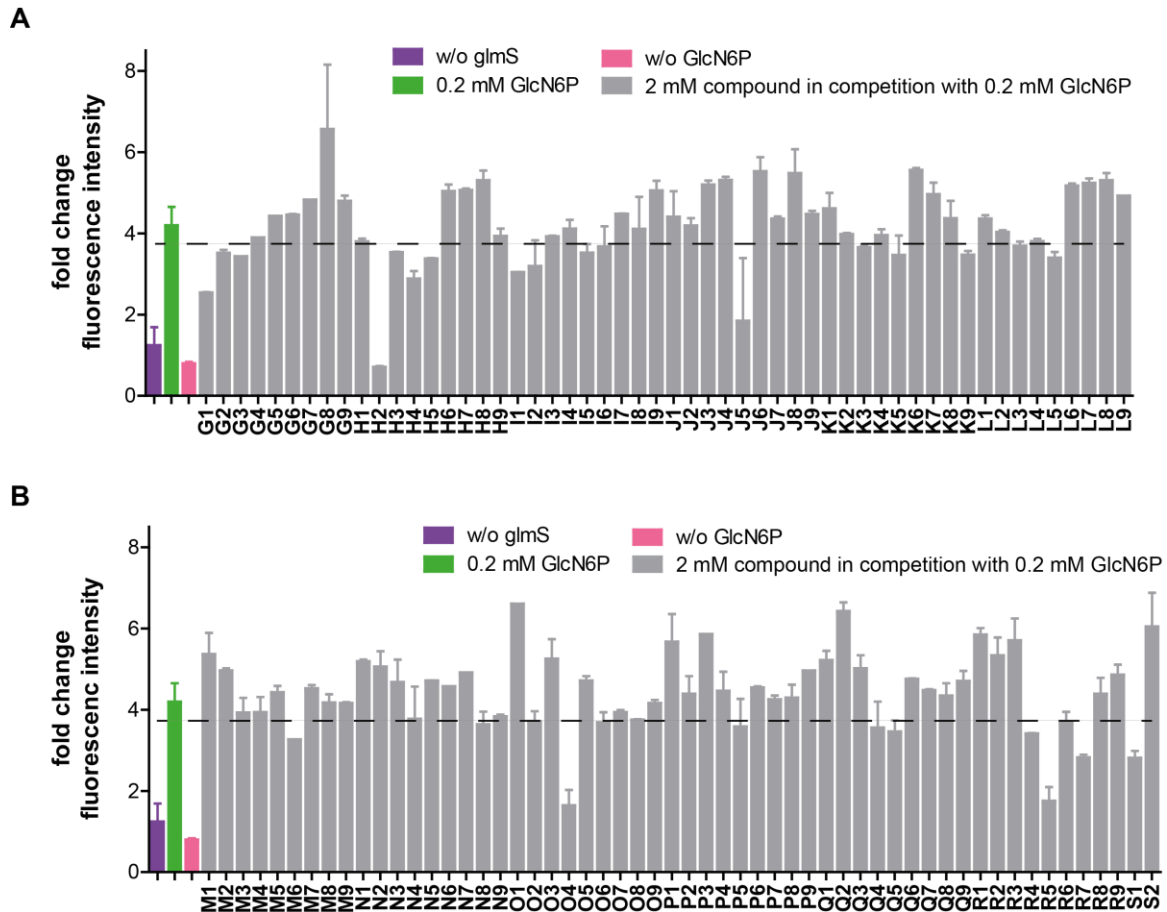


Figure 18: Screening for inhibition of GlcN6P-induced *glmS* ribozyme self-cleavage by the 2nd generation of Reymond compounds

Depicted is the fluorescence-based metabolite-induced self-cleavage assay monitoring the inhibition of GlcN6P induced *S. aureus glmS* ribozyme cleavage by 2 mM of 2nd generation of Reymond compounds in 2% DMSO shown in grey. The positive control containing 0.2 mM GlcN6P as well as the negative controls lacking the metabolite or the leader sequence are depicted in black. Inhibition by compounds G1-L9 is depicted in A and inhibition by compounds M1-S2 in B (Reymond compounds n=1-2; controls n=6-10). Cleavage was monitored after 19.5 min of incubation at 37 °C.

3.2 Mode of action analysis of CGlcN on *B. subtilis*

Based on the finding that CGlcN6P activates the *glmS* ribozyme as efficient as the natural metabolite GlcN6P¹⁵⁰ and the fact that growth of *S. aureus* is inhibited in the presence of the non-phosphorylated CGlcN (Figure 19)¹⁹⁹⁻²⁰⁰ the mode of action was to be analyzed.

*

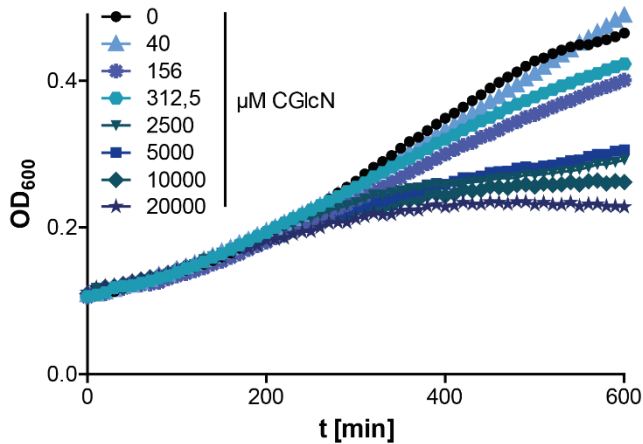


Figure 19: Growth of *S. aureus* in the presence of CGlcN in CDM

Growth in the presence of increasing concentrations of CGlcN is shaded in blue, for comparison growth in the absence of CGlcN is depicted in black (n=1). *199-200

The working hypothesis regarding the MoA of CGlcN involved the uptake and concomitant phosphorylation of the prodrug CGlcN as well as the intracellular activation of the *glmS* ribozyme by CGlcN6P, the subsequent loss of the GlmS mRNA that eventually causes an impairment of the bacterial cell and inhibition of bacterial growth (**Figure 20**).

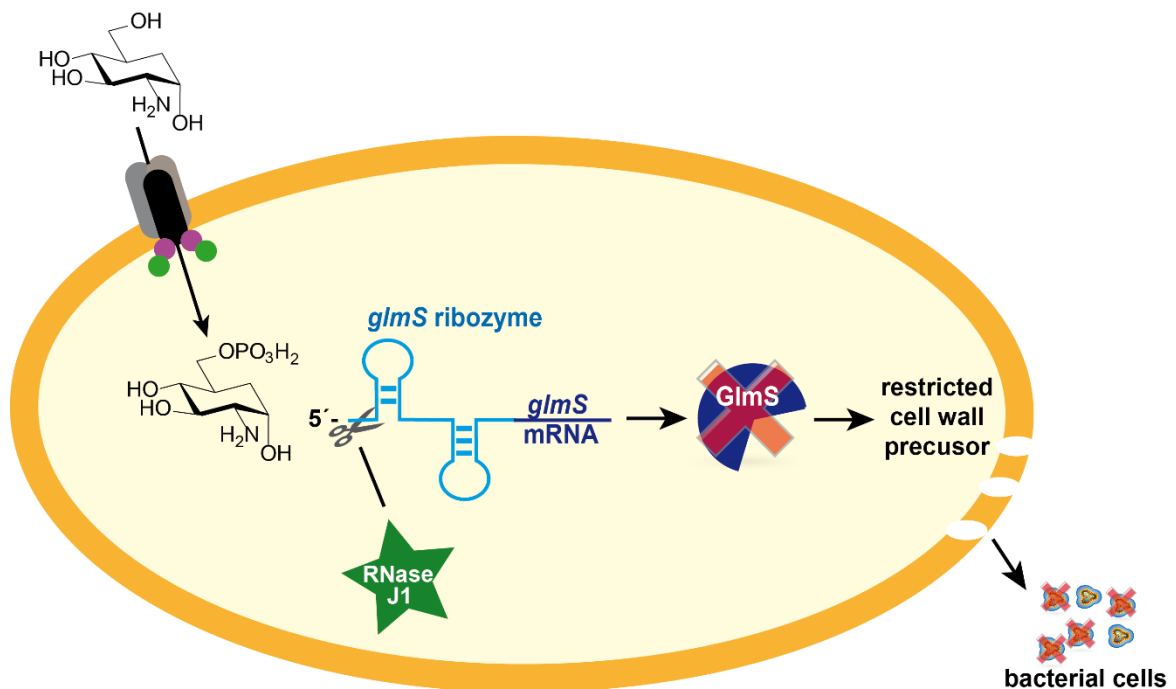


Figure 20: Scheme of proposed MoA of CGlcN

CGlcN is taken up by bacterial PTS. Depicted is the EII part of the PTS transporters with the membrane integral part (EIIC) in black and grey. The specificity for the sugars mainly reside in the EIIA/B part of the transporters here depicted in purple and green. PTS systems concomitantly phosphorylate their substrate during the uptake process, this would lead to the formation of CGlcN6P. The intracellularly phosphorylated carba-sugar presumably activates the *glmS* ribozyme (light blue) in the UTR of mRNA (dark blue) encoding the essential enzyme GlmS (dark blue symbol). The induction of *glmS* ribozyme self-cleavage leads to mRNA hydrolysis by RNase-J1 (green star). A reduction of the level of the GlmS enzyme would limit the amount of cell wall precursors; and thus, induce cell-envelope damage (white holes) and eventually confer bacterial growth inhibition.

B. subtilis is a well-studied bacterial gram-positive model organism.^{9, 202} Genetic manipulation of *B. subtilis* is more straightforward than it is for *S. aureus* and the Bacillus genetic stock center (BGSC.org) allows to directly obtain *B. subtilis* knock out strains. For these reasons, as well as the easier cultivation of *B. subtilis* 168 in chemically defined medium (CDM), it was decided to switch from *S. aureus* Mu50 to *B. subtilis* 168. It has already been shown that CGlcN6P also induces self-cleavage of the *B. subtilis glmS* ribozyme.¹⁵⁰

3.2.1 Antibacterial effect of CGlcN on *B. subtilis*

To use *B. subtilis* in further studies on the MoA of CGlcN, it had to be verified that CGlcN also inhibits growth of *B. subtilis* 168. For this, a minimal inhibitory concentration (MIC) of CGlcN was determined and a MIC value of 150 μ M (32 μ g/ml) was recorded. The respective MIC value for *S. aureus* Mu50 was 625 μ M (133 μ g/ml).¹⁹⁹ This means that CGlcN treatment is more effective in *B. subtilis* than in *S. aureus*, which moreover corroborates the decision of using *B. subtilis* for further studies. After assessing the MIC, growth of *B. subtilis* was measured over time and a growth curve of *B. subtilis* in the presence of different concentrations of CGlcN was recorded (**Figure 21**), a concentration-dependent inhibition of growth can be detected.

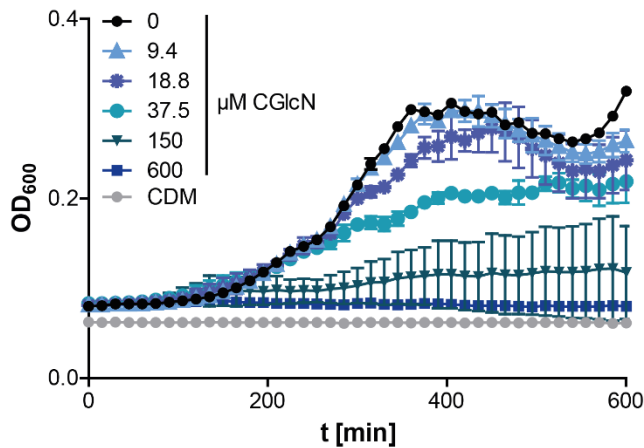


Figure 21: Growth of *B. subtilis* in the presence of CGlcN in CDM

Growth in the presence of increasing concentrations of CGlcN is shaded in blue, for comparison growth in the absence of CGlcN is depicted in black. The sterile control, in which no bacteria have been added to the medium, is shown in grey (n=2).

3.2.2 Investigation of potential uptake and subsequent phosphorylation of CGlcN by bacterial phosphoenol-pyruvate transport systems (PTs)

The non-phosphorylated variant, CGlcN, was used for cellular studies¹⁹⁹⁻²⁰⁰, as it is rather unlikely that a charged, phosphorylated molecule can pass the bacterial cell membrane.²⁰³ In order to prove the hypothesis (**Figure 20**) that CGlcN is taken up and phosphorylated by the bacterial cell PTS (phosphoenol-pyruvate transport systems) knock out strains were analyzed. PTs are natural bacterial sugar transport systems, which are three-enzyme based systems (EI-EIIA and EIIB/C) that in conjunction with a histidine rich protein (HPr) transport and simultaneously phosphorylate sugars. EI as well as HPr are common to all known PTs. The carbohydrate specificity resides within the EII complex (**Figure 22**).

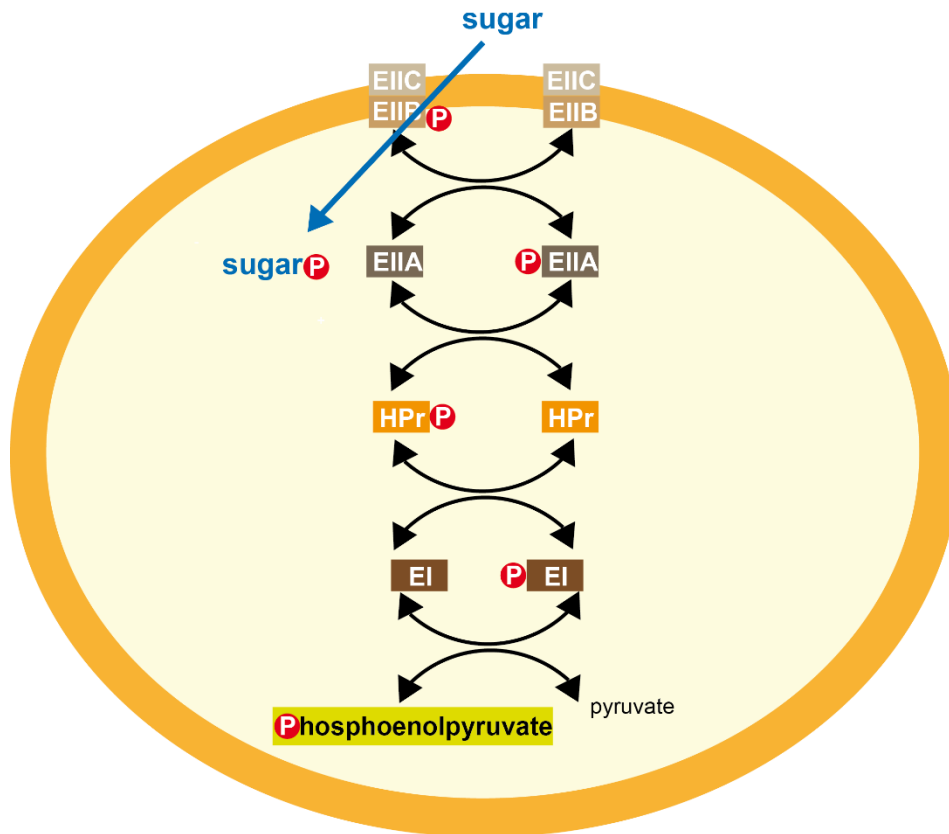


Figure 22: Schematic drawing of PTS modified after Deutscher et al 2006⁵⁶

PTSs transport and thereby phosphorylate sugars. The phosphoenolpyruvate originating from glycolysis transfers the phosphate group to EI, subsequently HPr is phosphorylated. The HPr transfers the phosphate to EIIA, which, through transfer to EIIB/C, allows for uptake and phosphorylation of the cognate sugar.

Herein, the effect of CGlcN treatment on knock out strains of the glucosamine specific transporter GamP as well as the GlcNAc specific transporter NagP and the global kinase PtsH was analyzed. GamP and NagP belong to the EII compartments of PTSs and are responsible for the recognition of the cognate sugar (**Figure 22**). PtsH is involved in the transfer of the phosphate from the histidine rich protein (HPr) and is therefore part of all transporters (**Figure 22**). *B. subtilis* strains lacking these transporters were analyzed in the presence of CGlcN, as well as in the presence of GlcN and in the absence of any additive. As expected cells overall grow better in the presence of GlcN, as sugar source as in CDM only. **Figure 23A** depicts the growth of *B. subtilis* wildtype (wt) cells without the addition as well as with the addition of GlcN and CGlcN in orange and blue, respectively. Wt cells were able to grow in the presence of GlcN as is for the control, where only medium was added. Wt cells treated with CGlcN show no increase of optical density corresponding to an inhibition of bacterial growth. Analyzing, the NagP mutant (**Figure 23B**) which is depleted in the transporter for GlcNAc, the same phenomenon was observed. In contrast, the Δ gamP strain growing in the presence of GlcN, the medium control and CGlcN (**Figure 23C**). *B. subtilis* cells lacking the global regulator PtsH (Δ ptsH)

(Figure 23D) are able to grow in the presence of CGlcN like the cells depleted for GamP.

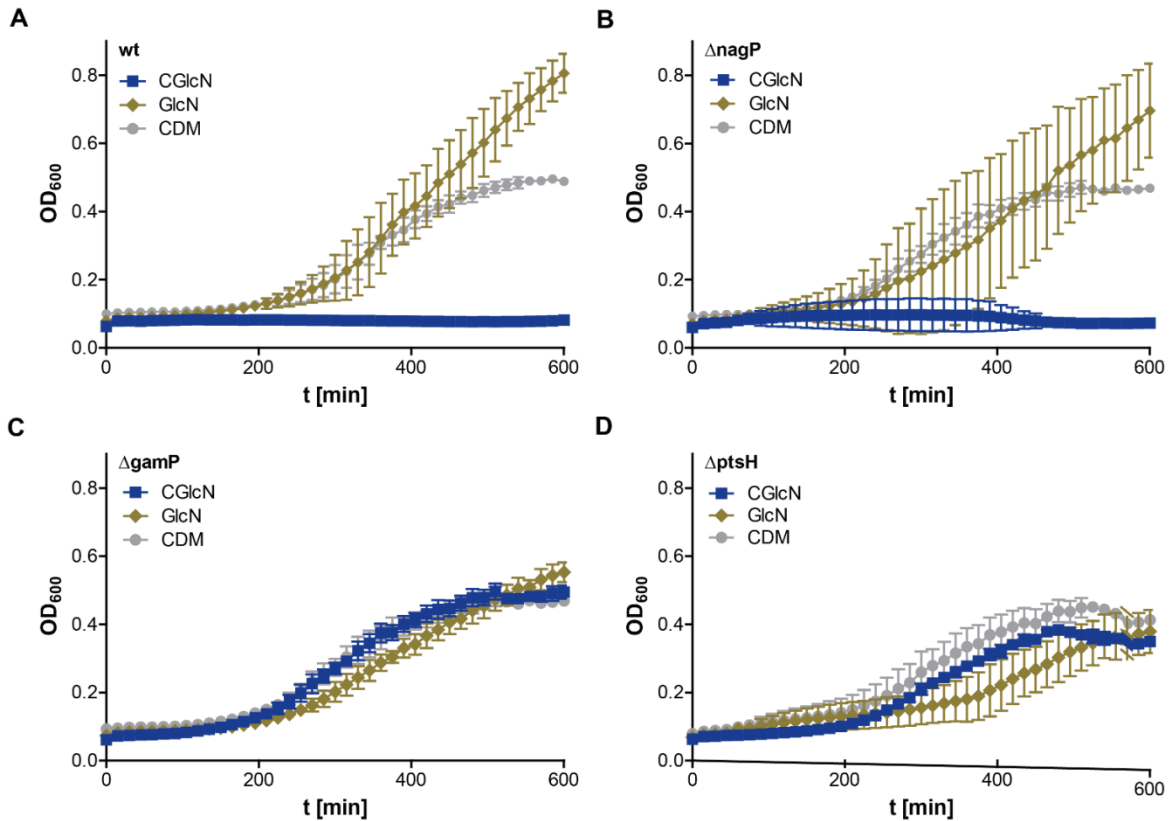


Figure 23: Growth curve analysis of *B. subtilis* 168 wt and PTS knock out strains in the presence of GlcN and CGlcN

The growth of *B. subtilis* 168 grown in CDM is depicted in grey. All cells are able to proceed growing. Cells grown in CDM and 300 μ M GlcN are depicted in orange and show growth in all tested strains. Growth of *B. subtilis* in the presence of 300 μ M (64 μ g/ml) CGlcN is represented in blue. Growth of *B. subtilis* wt is shown in A, growth of $\Delta nagP$ in B, $\Delta gamP$ in C and growth of $\Delta ptsH$ is shown in D (n=3).

Direct comparison of the CGlcN treated PTS deletion strains and the wt illustrates the ability of the $\Delta gamP$ and the $\Delta ptsH$ strain to grow in the presence of CGlcN, while neither the wt nor the $\Delta nagP$ mutant shows an increase in optical density (Figure 24).

Results

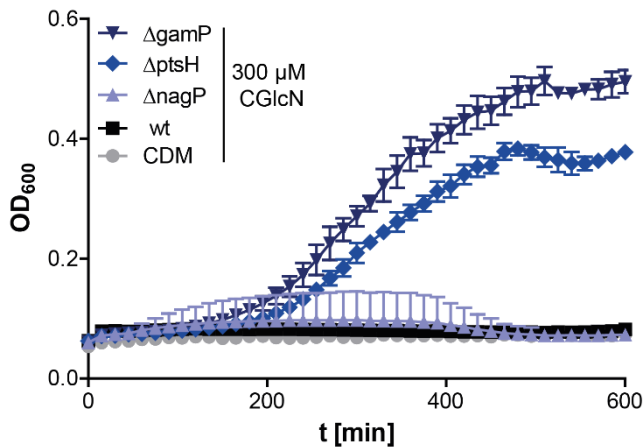


Figure 24: Growth curve analysis of PTS deleted strains in presence of CGlcN

Growth curve analysis of PTS deleted (ΔgamP , ΔptsH , ΔnagP , shades of blue) strains is shown in comparison to the wt *B. subtilis* 168 strain in black and sterile growth control (CDM) depicted in grey in the presence of 300 μM (64 $\mu\text{g/ml}$) CGlcN (n=3).

To gain better understanding of the time frame in which CGlcN can inhibit bacterial growth the effect was monitored over time. In **Figure 25** growth of the employed knock out strains as well as the wt *B. subtilis* monitored over a time frame of almost 24 h is depicted. It is evident from this graph that growth inhibition is countermanded after 11.25 h (670 min).

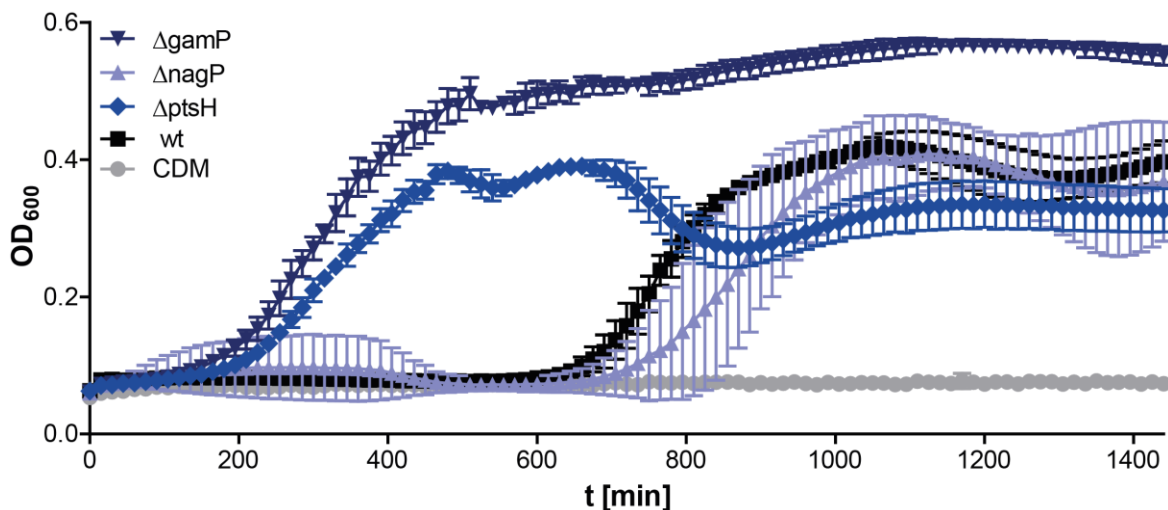


Figure 25: Growth curve analysis of PTS deleted strains in presence of CGlcN monitored for 23.75 h (1425 min)

Growth curve analysis of PTS deleted (ΔgamP , ΔptsH , ΔnagP , shades of blue) strains in comparison to the wt *B. subtilis* 168 strain in black and sterile growth control (CDM) depicted in grey in the presence of 300 μM (64 $\mu\text{g/ml}$) CGlcN (n=3).

To further verify that the mutants are capable of growing normally and that the effect observed is due to CGlcN treatment, bacterial growth was monitored 4.5 h prior to the addition of CGlcN. **Figure 26** clearly shows that while all strains are able to grow normally before addition of CGlcN, the wt and the Δ nagP mutant are not able to proceed growing in the presence of CGlcN.

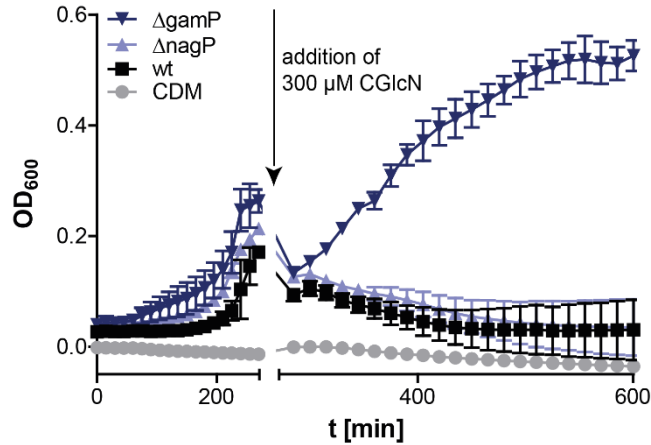


Figure 26: Growth curve analysis of PTS deleted strains with the addition of CGlcN after 270 min

Growth curve analysis of PTS deleted strains (Δ gamP, Δ nagP in shades of blue) is shown in comparison to *B. subtilis* wt in black and the sterile growth control (CDM) depicted in grey. The addition of 300 μ M (64 μ g/ml) CGlcN was carried out after 4.5 h of incubation. The gamP mutant strain is able to grow in the presence of CGlcN while the wildtype and the nagP mutant show a decrease in optical density after the addition of CGlcN (n=3).

3.2.3 Quantitative real-time PCR analysis to determine the intracellular effect of CGlcN on *glmS* levels in *B. subtilis*

Inhibition of *B. subtilis* cell growth is displayed in **section 3.2.1** and the *in vitro* interaction of the *glmS* ribozyme has been shown previously.^{150, 200} This gave rise to the question if these findings correlate to an *in vivo* activation of the *glmS* ribozyme (**Figure 20**).

If CGlcN is transported and phosphorylated by PTS, CGlcN6P *in vivo* would potentially induce self-cleavage of the *glmS* ribozyme. This would lead to degradation of the *glmS* mRNA and as it codes for the essential GlmS enzyme involved in cell wall biosynthesis it would in turn lead to restriction of cell wall precursors. Thereby, this restriction would subsequently cause growth inhibition as hypothesized in **Figure 20**.

Quantitative real-time PCR (qPCR) was performed to analyze the levels of *glmS* ribozyme and gene in the presence and absence of CGlcN. The TaqMan approach utilizing fluorescently labeled probes and the 3'5'-endonuclease activity of the Taq

polymerase, was employed. *B. subtilis* cells were treated with varying concentrations of CGlcN, RNA was extracted and after cDNA synthesis used as template for qPCR experiments (**Figure 27**).

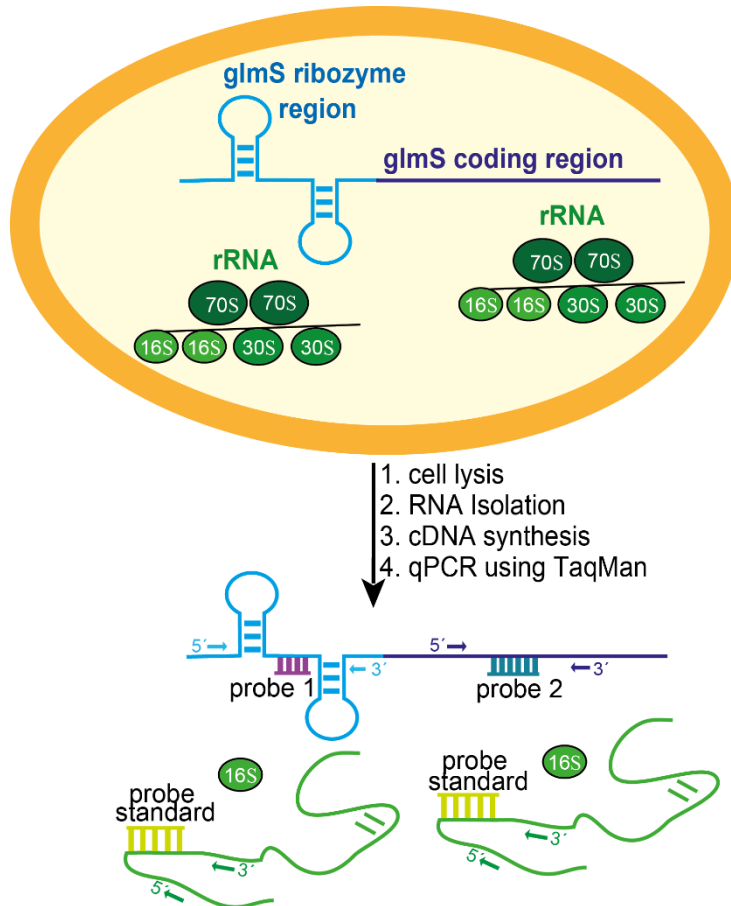


Figure 27: Shema of sample preparation for qPCR analysis

B. subtilis cells were lysed and the RNA isolated followed by cDNA synthesis. The obtained cDNA was used as template for qPCR. The *glmS* ribozyme region, the *glmS* mRNA as well as 16S rRNA as internal standard were amplified. Probes are indicated by the word probe and primers are marked by arrows.

To define the ideal timepoint for RNA extraction, cells were pre-grown to the early exponential phase ($OD_{600} \sim 0.3-0.4$) where metabolic processes are highly regulated and growth was monitored in the presence of CGlcN. The results shown in **Figure 28** indicate inhibition by CGlcN treatment after 60 min. Therefore, the incubation with CGlcN for 60 min was chosen for later RNA isolation experiments.

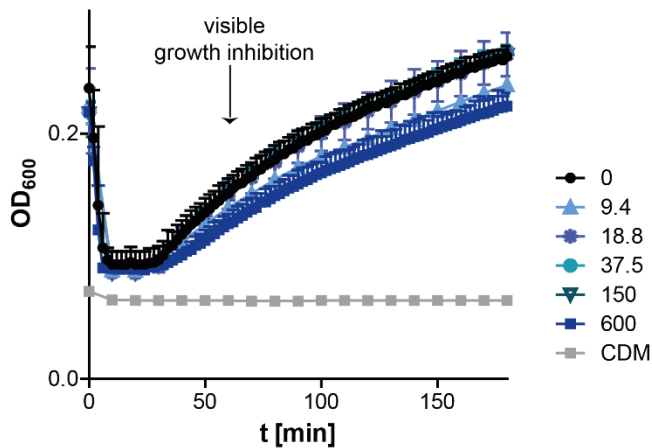


Figure 28: Growth curve of *B. subtilis* pre-grown to $OD_{600} \sim 0.35$ and then incubated in the presence of CGlcN to define the timepoint at which the effect of treatment becomes visible for later RNA extraction experiments

Cells were pre-grown in CDM until an optical density (OD_{600}) of ~ 0.35 was reached. Cells were then transferred to a 96-well plate and the growth in the presence of indicated CGlcN concentrations (shaded in blue) was monitored. For comparison growth of untreated cells is shown in black and a sterile control is shown in grey. As growth inhibition upon addition of CGlcN becomes visible after 60 min (arrow), this time point was chosen to extract the RNA ($n=2$).

To ensure that the isolated RNA is intact and of high quality, samples were analyzed by agarose gel electrophoresis. Intact samples show two dominant bands corresponding to 23S rRNA and 16S rRNA. In some preparations bands of other RNA species, for instance tRNA, are visible. An representative gel of prepared RNA is illustrated in **Figure 29**. This preparation shows intact RNA and was further used to proceed with cDNA synthesis. In the later qPCR experiments, 16S rRNA was used as internal standard and the signals for either *glmS* ribozyme or *glmS* gene were normalized to the expression of 16S rRNA.

Results

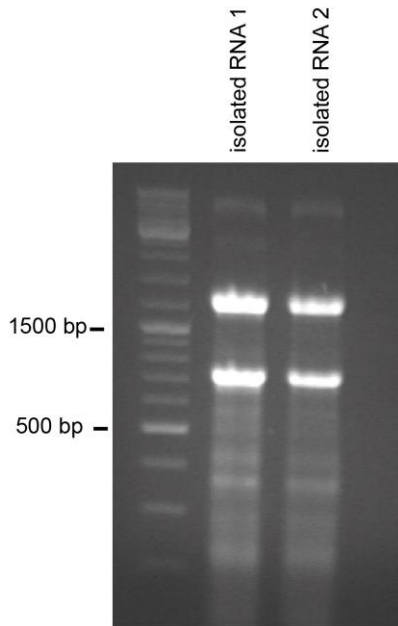


Figure 29: Agarose gel of total RNA isolated from *B. subtilis*

1% Agarose gel depicting 1 kb plus DNA ladder and two samples of isolated total RNA. The bands indicative for ribosomal RNA (23S rRNA 2928 nt and 16S rRNA 1555 nt) are at the expected length considering that a DNA ladder was used to analyze the size of the RNA bands.

A typical result of qPCR analysis obtained by amplifying the cDNA in a real-time PCR cyclor is shown in **Figure 30**. Here, triplicates of a sample and NTC are shown. The threshold (green line) separates the fluorescence signal of the samples from the signal of the NTCs. To ensure that the fluorescence corresponds to the formation of the desired product and to moreover verify that the NTCs have not been contaminated, agarose gel electrophoresis was performed.

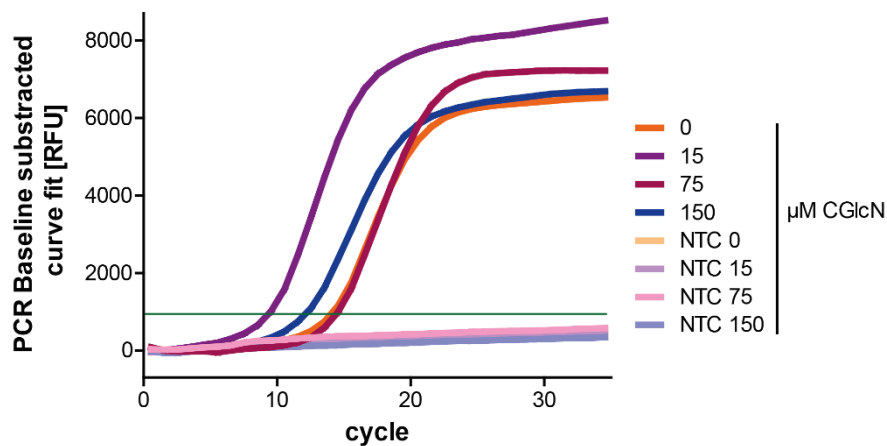


Figure 30: Representative qPCR analysis

Typical qPCR trace obtained by cycling samples in the Bio-Rad iQ5 real-time PCR detection system. Depicted are the results of amplifying 16S rRNA of *B. subtilis*. The green line indicates the threshold, which separates the background fluorescence from the fluorescence arising from the

probe due to amplification. The amplification of 16S rRNA of untreated cells is shown in orange, the amplification of a sample in which no template has been added to the qPCR mix is shown in light orange. The amplification of 16S rRNA of cells treated with 15 μM CGlcN is shown in purple and the corresponding NTC control in light purple. The amplification of 16S rRNA of cells treated with 75 μM CGlcN is shown in pink and the corresponding NTC control in light pink. The amplification of 16S rRNA of cells treated with 150 μM CGlcN is shown in blue and the corresponding NTC control in light blue.

The agarose gel electrophoretic analysis of the qPCR products is shown in **Figure 31** and confirms the fluorescence results of the real-time PCR cyclers; the analysis of all NTCs by agarose gel electrophoresis do not show bands while the samples show one single band of the expected size.

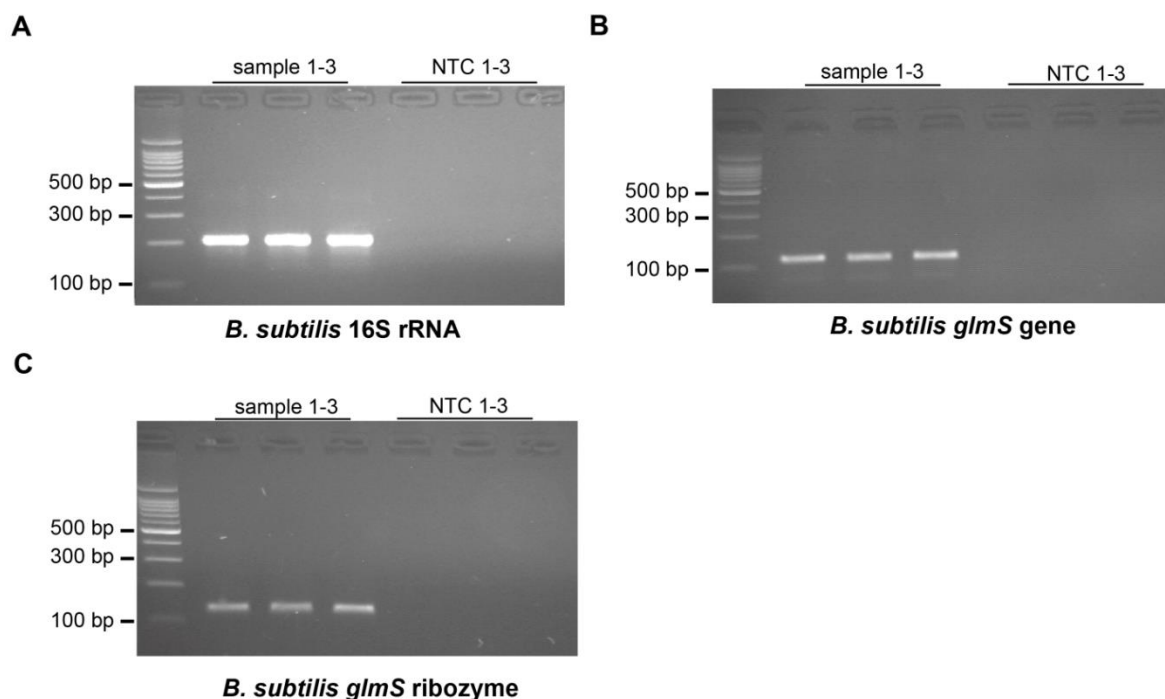


Figure 31: Analysis of qPCR products of *B. subtilis*

2.5% agarose gels depicting the triplicates of the sample and the triplicate NTC after qPCR, the expected lengths of the PCR products (16S rRNA 209 bp, *glmS* gene 120 bp and *glmS* ribozyme 134 bp) could be confirmed.

To compare and normalize the amplification of the three different constructs, 16S rRNA, *glmS* gene and *glmS* ribozyme the amplification efficacy of all constructs was assessed. The amplification efficacy can differ due to the different size and sequence of the amplicon, the different primers and temperature used for cycling. **Figure 32** summarizes the results of the amplification efficacy test. The PCR to amplify the 16S rRNA and the *glmS* ribozyme proceed with efficacies of 80%,

however the construct to monitor the *glmS* gene is amplified with 78% efficacy. For subsequent analysis, this difference was considered as described in 6.2.3.

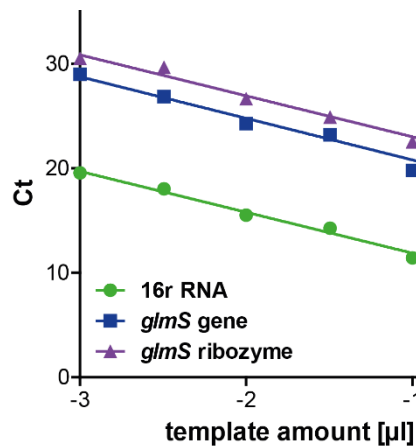


Figure 32: Amplification efficacy of qPCR constructs

Depicted is the amplification efficacy of 16S rRNA (green), *glmS* gene (blue) and *glmS* ribozyme (purple). A cDNA dilution series (of isolated untreated *B. subtilis* RNA) was prepared and qPCR analysis determining the amplification of the constructs was performed independently. By plotting the corresponding Ct's (cycle threshold) against the amount of template used the amplification efficacy can be determined (n=3).

Finally, qPCR analysis to study the effect of CGlcN on *glmS* levels was performed. Expression levels of the cells treated with varying concentrations of CGlcN were compared to untreated cells and the results for the relative expression of the *glmS* ribozyme region are depicted in **Figure 33A**, while the results for the *glmS* gene are depicted in **Figure 33B**. The treatment with CGlcN resulted in a significant and concentration-dependent reduction of *glmS* mRNA and *glmS* ribozyme (**Figure 33**), even at concentration of 1.5 μM (corresponding to 0.01x MIC) CGlcN a significant reduction of *glmS* ribozyme and *glmS* gene levels can be detected. Remarkably, treatment with 300 mM CGlcN caused ~60-fold reduction of the *glmS* mRNA compared to untreated control cells (**Figure 33 A**).

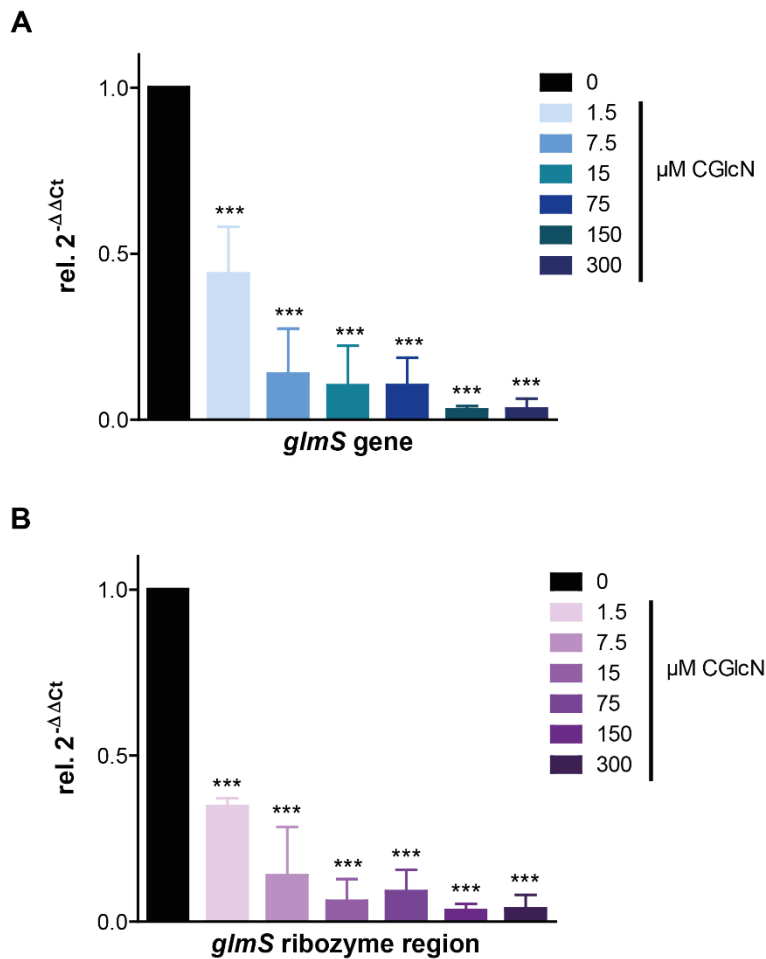


Figure 33: Quantitative real-time PCR analysis of *glmS* gene and *glmS* ribozyme levels in the presence of CGlcN of *B. subtilis*

Shown is the level of *glmS* gene (A) or *glmS* ribozyme (B) in cells where no CGlcN (black) or increasing amounts of CGlcN were added (shades of blue in A and shades of purple in B). The amount of *glmS* gene and *glmS* ribozyme is normalized to the amount of 16S rRNA within the analyzed samples (0, 75, 150 μM n=5, 1.5, 7.5, 15 μM n=2, 300 μM n=3). The data was analyzed by using 1way ANOVA followed by Tukey's test (***) = p-value <0.001).

3.2.4 Quantitative real-time PCR analysis to determine the intracellular effect of CGlcN on *glmS* levels in *S. aureus*

B. subtilis is a non-pathogenic gram-positive bacterium that does not require an S2 laboratory. Moreover, *B. subtilis* is regarded as model gram-positive bacterial organism.⁹ Nevertheless, it would be beneficial to elucidate the exact MoA of antibacterial compounds in human pathogens. Therefore, the effect of CGlcN treatment on *glmS* levels in *S. aureus* was analyzed using the same approach as described in **section 3.2.3** and is illustrated in **Figure 27**. One difference in the approach was that in case of *S. aureus* the sequence of the *glmS* ribozyme did not allow sophisticated design of a primer probe pair. Therefore, in addition to the construct of the *glmS* gene, a separate construct was designed that contains parts of both *glmS* gene and the ribozyme. As described earlier (**section 3.2.3**), growth curve analysis to define the best time point for RNA extraction after CGlcN

treatment was performed. The result can be seen in **Figure 34**. As for *B. subtilis*, 60 min growth in the presence of CGlcN was defined as suitable time point for the RNA extraction.

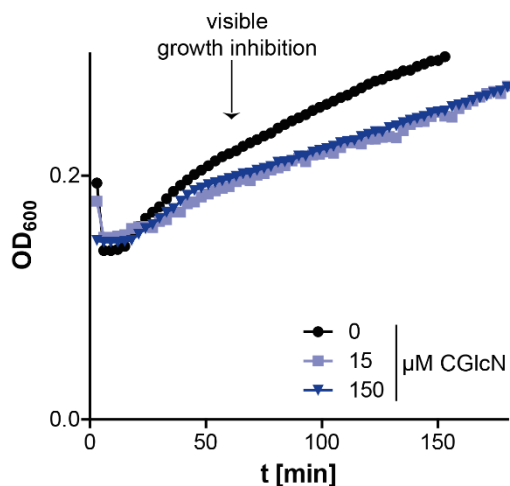


Figure 34: Growth curve of *S. aureus* pre-grown to an OD_{600} ~0.3 and then incubated in the presence of CGlcN to define the timepoint at which the effect of treatment becomes visible for later RNA extraction experiments

Cells were pre-grown in CDM to an optical density (OD_{600}) of ~0.3. Cells were then transferred to a 96-well plate and growth in the presence of the indicated CGlcN concentrations (shaded in blue) was monitored. For comparison, growth of untreated cells is shown in black. As growth inhibition upon addition of CGlcN becomes visible after 60 min (arrow), this time point was chosen to extract the RNA.

However, in case of RNA isolation from *S. aureus* several optimization steps were needed to extract sufficient and intact RNA and even then, several trials with optimized conditions failed due to inefficient lysis. The herein utilized strain, *S. aureus* Mu50 is known to have a very thick cell wall and thereof turns out to be difficult to lyse.²⁰⁴ One of the few experiments where RNA was successfully extracted from *S. aureus* is shown in **Figure 35**. Because cultivation of *S. aureus* requires an S2 laboratory these experiments were performed in the laboratory of Prof. Bierbaum (University of Bonn). Agarose gels prepared there are stained in ethidiumbromid (EtBr) bath after separation, whereas the EtBr is added prior to the run for *B. subtilis* agarose (**Figure 29**). This technical difference results in a higher staining sensitivity for the *S. aureus* preparation. The actual extraction efficacy is later determined by measuring the RNA concentration. This means, that the visible similar amount of isolated RNA in **Figure 29** and **Figure 35** is misleading as at least 10 times less RNA was extracted from the same volume of culture of *S. aureus* cells than in case of the RNA extraction from *B. subtilis*.

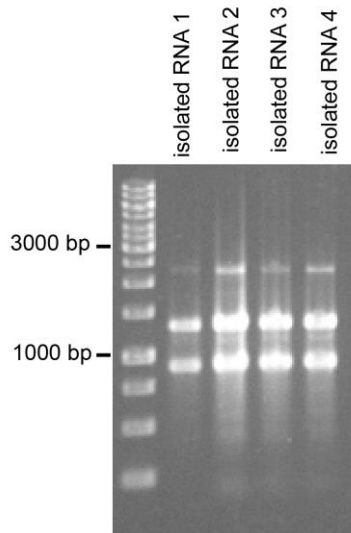


Figure 35: Agarose gel of total RNA isolated from *S. aureus*

Shown is an agarose gel (1%) depicting 1 kb DNA ladder and four samples of isolated total RNA. The bands indicative for ribosomal RNA (23S rRNA 2834 nt and 16S rRNA 1555 nt) can be seen at the expected length considering that a DNA ladder was used to analyze the size of the RNA bands.

The result obtained from the qPCR cyclor for *glmS* gene+ribozyme and 16S rRNA confirms the results displayed in **Figure 30** and the amplification of the product with the correct size could be confirmed by agarose gel electrophoresis (**Figure 36**). The amplification of the *glmS* gene did not show reliable and good fluorescence results. The agarose gel showed a band of the correct size, however the intensity of the band is weak (**Figure 36**). The observations of weaker fluorescence and less production formation are in line and it was decided to skip the amplification of this construct in further studies.

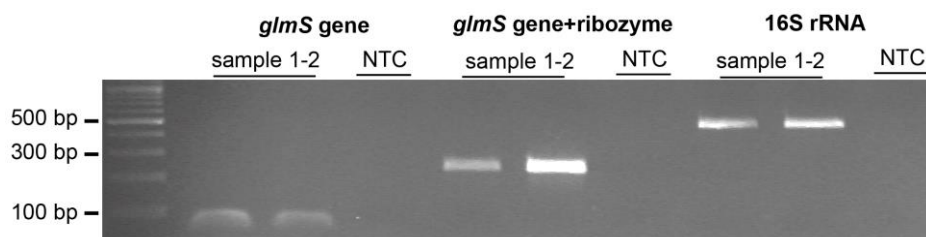


Figure 36: Analysis of qPCR products of *S. aureus*

Shown is an agarose gel (2.5%) depicting the duplicate of the samples and the NTC after qPCR. Shown are the products of *glmS* gene, *glmS* gene+ribozyme and 16S rRNA. The expected lengths of the PCR products (*glmS* gene 71 bp and *glmS* gene+ribozyme 248 bp and 16S rRNA 481 bp) was confirmed. The fact that the bands of sample 1-2 of *glmS* gene+ribozyme have different intensities is due to errors in loading of gel.

The analysis of two independent qPCR experiments is shown in **Figure 37A** and **Figure 37B**. The concentration of CGlcN used for treatment correspond to 1x MIC, 0.1x MIC and 0.01x MIC. The MIC for *S. aureus* was determined to be 625 μM ¹⁹⁹⁻²⁰⁰ and the MIC for *B. subtilis* was determined to be 150 μM . Thereof, the concentrations used for treatment prior to qPCR analysis vary between the two species. For these experiments, independently prepared cDNAs were used for analysis. To save some of the by chemically synthesis limited CGlcN, experiments were also performed with GlcN. This, too, lead to conflicting results as depicted in **Figure 37C** and **Figure 37D**. It was concluded that in case of *S. aureus* this analysis does not yield reliable results.

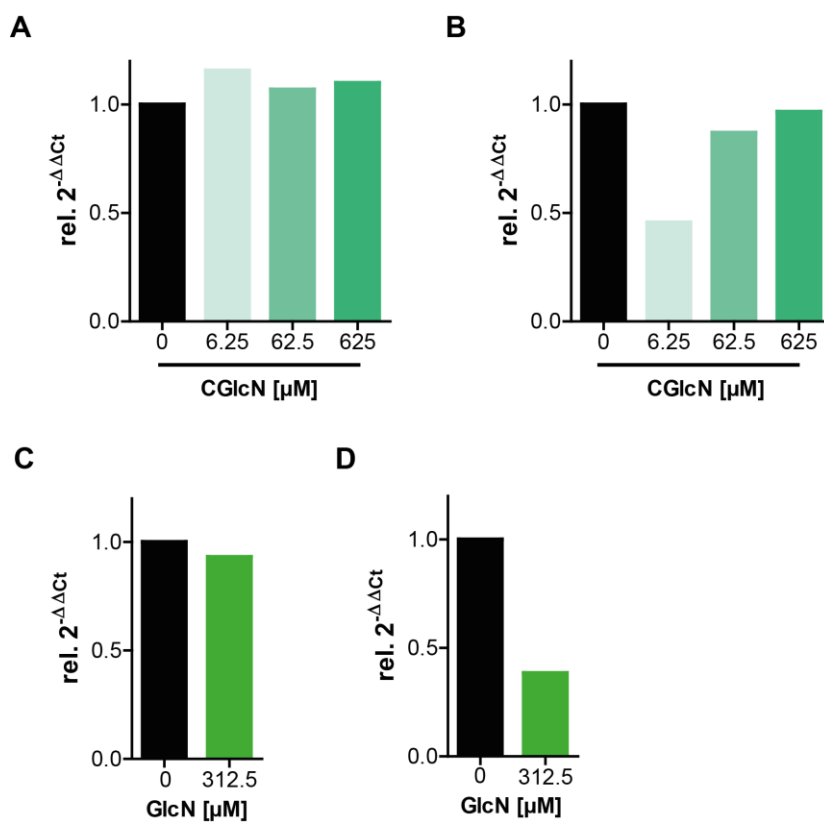


Figure 37: qPCR analysis of *glmS* gene+ribozyme levels in *S. aureus* in the presence of CGlcN or GlcN

Depicted is the level of *glmS* gene+ribozyme in cells where no CGlcN (black) or increasing amounts of CGlcN were added (shades of turquoise) shown in A and B. In C and D levels of *glmS* gene+ribozyme in cells where no GlcN (black) or 312.5 μM GlcN were added (green). The amount of *glmS* gene+ribozyme is normalized to the amount of 16S rRNA within the analyzed samples. A and B as well as C and D depict results obtained utilizing different cDNA preparations.

3.2.5 Induction of stress inducible promoters by CGlcN

The hypothesis on the MoA of CGlcN is illustrated in **Figure 20**. It suggests that upon intracellular availability of CGlcN6P due to uptake and phosphorylation of the

prodrug CGlcN by PTS (**section 3.2.2**), CGlcN6P binds and activates self-cleavage of the *glmS* ribozyme. This event subsequently results in degradation of the *glmS* mRNA (**section 3.2.3**) and therefore the GlmS enzyme. As the GlmS enzyme is essential for the synthesis of the cell wall precursor GlcN, this process would lead to a limited amount of cell wall precursors and therefore impair the bacterial cell wall architecture. If the hypothesis is true, it should be possible to detect the impairment of the bacterial cell wall. The approach utilized here depends on *B. subtilis* strains carrying plasmids of stress inducible promoters. In microarray studies, global regulators whose expression is modulated upon the induction of various stresses have been identified.²⁰⁵ This set of stress inducible promoters can be used to study the induction of differential bacterial stresses. The stress can be correlated to the relative promoter induction of the stress genes under the control of firefly luciferase. For verification of the system, stress induction by reference antibiotics assigned to the cognate promoters is shown in **Figure 38**. The *ypuA* promoter assigns for cell-envelope damage, while the *yorB* promoter recognizes DNA damage, the *bmrC* promoter sense protein damage and the *heID* promoter is induced by RNA damage

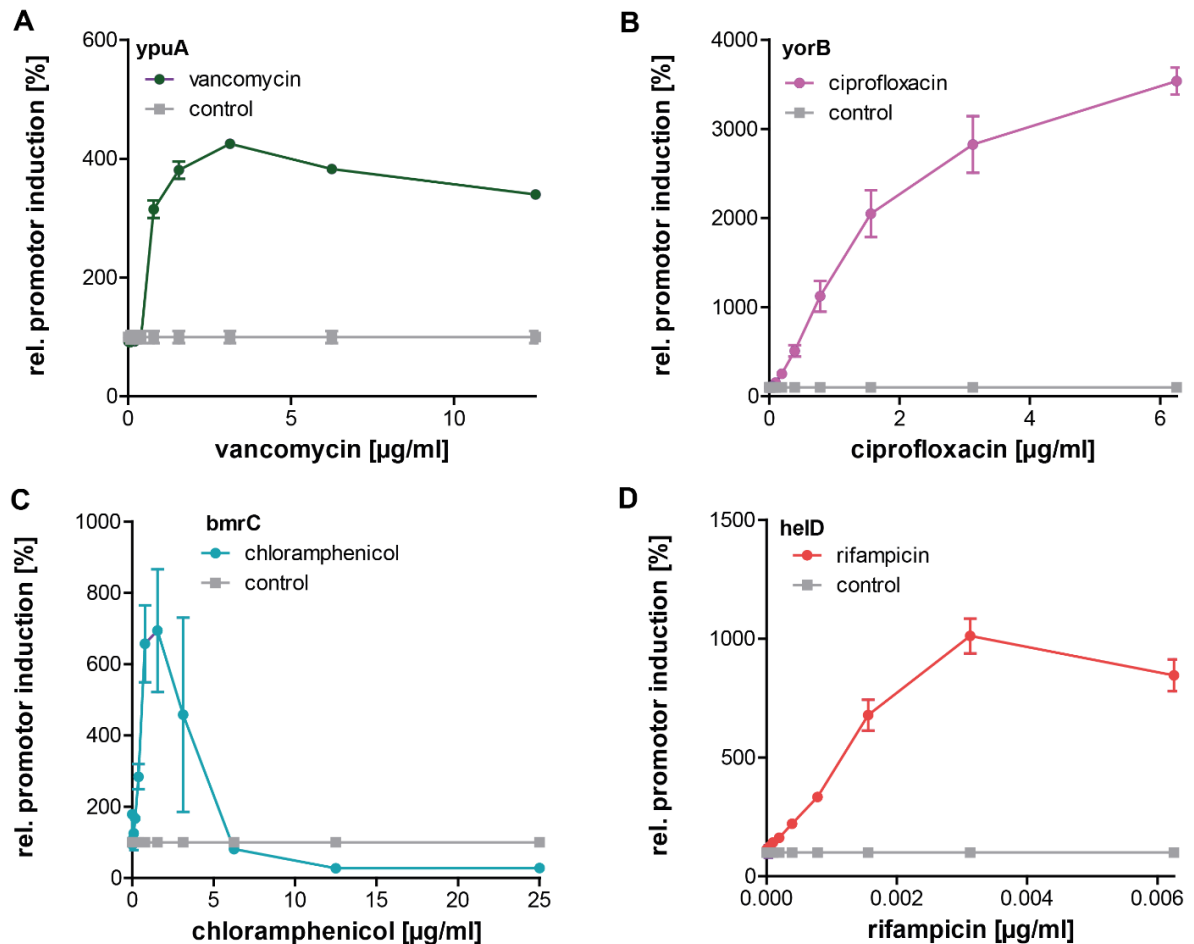


Figure 38: Induction of stress inducible promoters by the corresponding reference antibiotics

Results

Induction of firefly luciferase under the control of stress inducible promoters in *B. subtilis*. In A, the induction of the *ypuA* promoter that is indicative for cell envelope damage by the reference antibiotic vancomycin is shown. B depicts the response of the DNA damage promoter *yorB* to ciprofloxacin. The induction of luciferase due to the stress exhibited by chloramphenicol on the *bmrC* promoter is shown in C. The *bmrC* promoter is indicative of protein damage. In D, the induction of the *helD* promoter by the RNA stress inducing antibiotic rifampicin is displayed. Strains are incubated in the presence (purple) or absence (grey) of the respective reference antibiotic, the controls were adjusted to 100% (n=2).

Luciferase induction by stress inducible promoter strains in the presence of CGlcN is depicted in **Figure 39**. CGlcN treatment selectively induces the *ypuA* promoter linked to cell-envelope stress. Promoters indicative of protein (*helD*), DNA (*yorB*) or RNA (*bmrC*) stress are not induced upon CGlcN treatment (**Figure 39**). This indicates that the antibacterial activity of CGlcN can be conferred by an effect on the cell-wall biosynthesis.

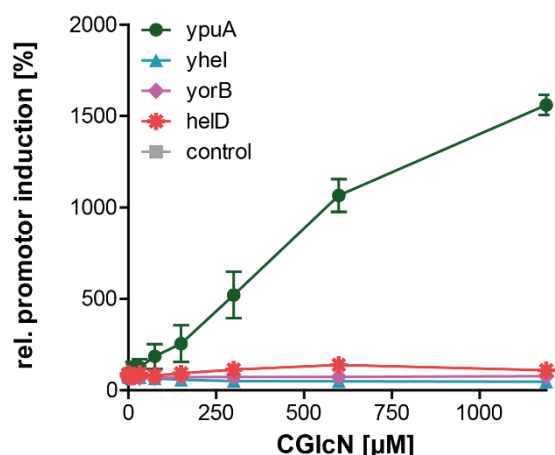


Figure 39: Stress inducible promoter gene assay in the presence of CGlcN

Luciferase induction by stress inducible promoters in the presence of increasing CGlcN concentrations is shown. Depicted are the responses of promoters indicative for cell envelope stress (*ypuA*), protein damage (*bmrC*), DNA damage (*yorB*) and RNA damage (*helD*) (*ypuA* n=6; all others n=4).

3.2.6 Antibacterial effect of CGlcN on *B. subtilis* in LB-medium

To evaluate the influence of the different ingredients of CDM used in previous MoA studies, to a common bacterial medium, growth of *B. subtilis* in the presence of CGlcN in LB medium was analyzed. As depicted in **Figure 40**, CGlcN also shows antibacterial effect in LB-medium. Although the determined MIC (150 µM; 32 µg/ml) is the same as it is for CDM, (**section 3.2.1**), the growth inhibitory effect does not last as long. In LB-medium, the effect of CGlcN treatment starts to vanish after 5 h

(300 min). For comparison, the growth inhibitory effect of CGlcN treatment in CDM lasts more than twice as long with 11.25 h (670 min) (**Figure 25**).

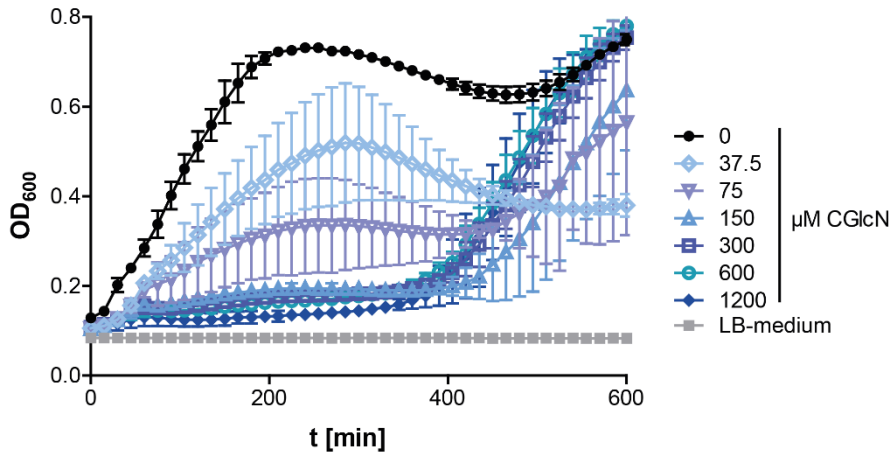


Figure 40: Growth curve of *B. subtilis* in the presence of CGlcN in LB-medium

Depicted is the growth of *B. subtilis* in the presence of different concentrations of CGlcN (shades of blue) in comparison to the sterile control (LB-medium) in grey and cells without addition of CGlcN in black (n=2).

3.3 Experimental validation of *glmS* ribozymes of pathogenic bacteria

In 2011, McCown *et al.* described sequences identified by an *in silico* approach, that are found within the UTR of *glmS* genes in bacterial specimen that from the sequence composition and order look like putative *glmS* ribozymes.¹⁸⁴ Based on these findings, we decided to study the putative ribozymes of the high priority human pathogens *C. difficile*, *L. monocytogenes*, *C. perfringens*, *E. faecium*, *E. faecalis*, *F. peridonticum* and *F. nucleatum* for *glmS* ribozyme self-cleaving properties. Instead of analyzing the predicted sequence region only, we decided to test the whole intergenic region containing the putative ribozymes (6.1.9). This was done on the one hand to have more *in vivo* like conditions and on the other hand to not disrupt potential stabilizing RNA structures.

DNA sequences of the putative *glmS* ribozymes were obtained by gene synthesis and ordered from GENEWIZ (<https://www.genewiz.com/>). Amplification by PCR was performed utilizing the corresponding primer molecules listed in 6.1.8. All forward primers were designed to contain the sequence for the T7 polymerase to allow for *in vitro* transcription afterwards. PCR conditions are described in 6.2.2, the subsequently obtained PCR products range in length from 153 to 499 bp and can be seen in **Figure 41**.

Results

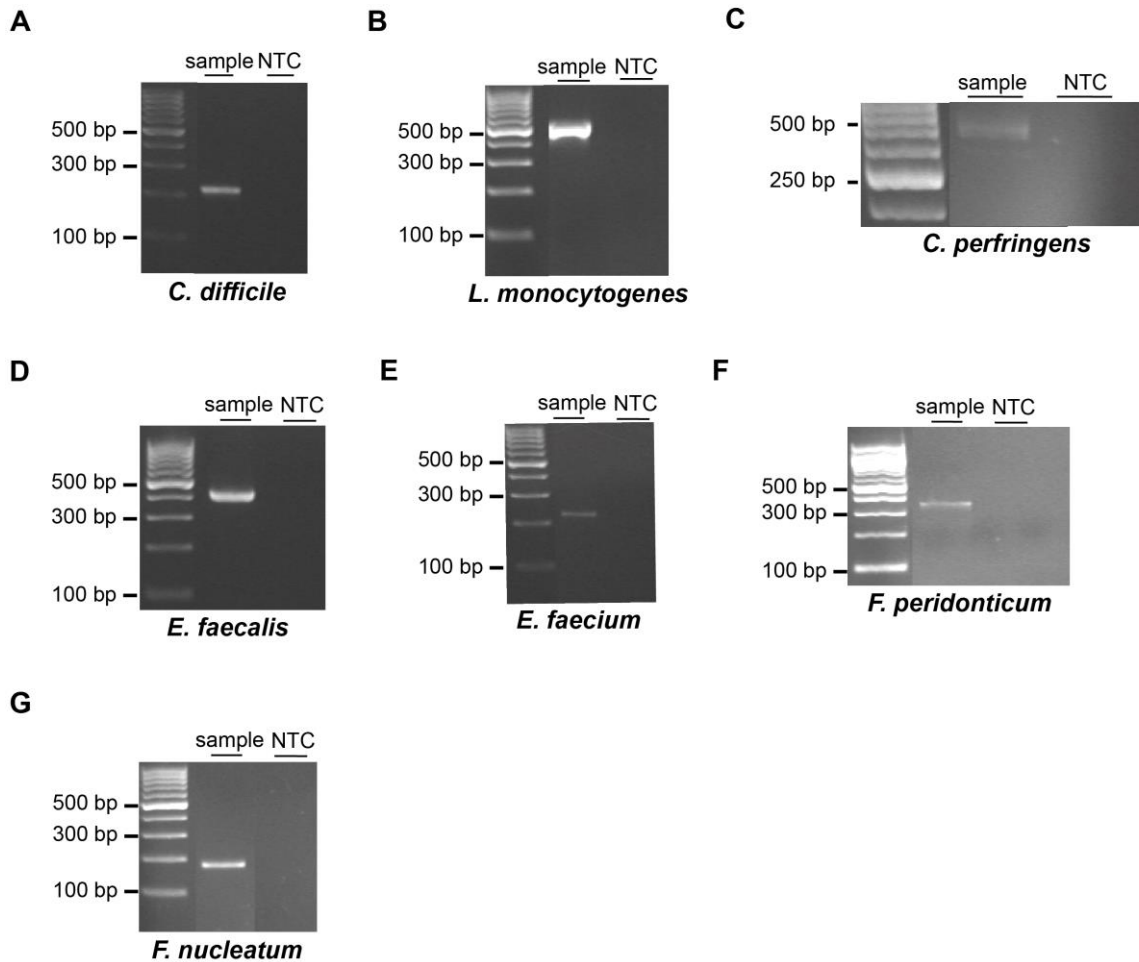


Figure 41: PCR products of *glmS* ribozymes

Depicted are the PCR products of *glmS* ribozymes from *C. difficile* (A), *L. monocytogenes* (B), *C. perfringens* (C), *E. faecalis* (D), *E. faecium* (E), *F. peridonticum* (F) and *F. nucleatum* (G). All amplicons had the expected length; *C. difficile* 266 bp, *L. monocytogenes* 447 bp, *C. perfringens* 499 bp, *E. faecalis* 442 bp, *E. faecium* 217 bp, *F. peridonticum* 350 bp and *F. nucleatum* 153 bp. For all gels but *C. perfringens* a 100 bp ladder was used, for *C. perfringens* a 50 bp ladder was used.

After transcription and radioactive labelling of all constructs a cleavage assay test was performed to analyze *glmS* ribozyme activity under common conditions (50 mM HEPES-200 mM KCl pH 7.5, 10 mM MgCl₂ incubation at 37 °C for 30 min). The radioactive gels showing the upper full-length fraction and the lower cleaved fraction (in case cleavage is induced) are depicted in **Figure 42**.

Results

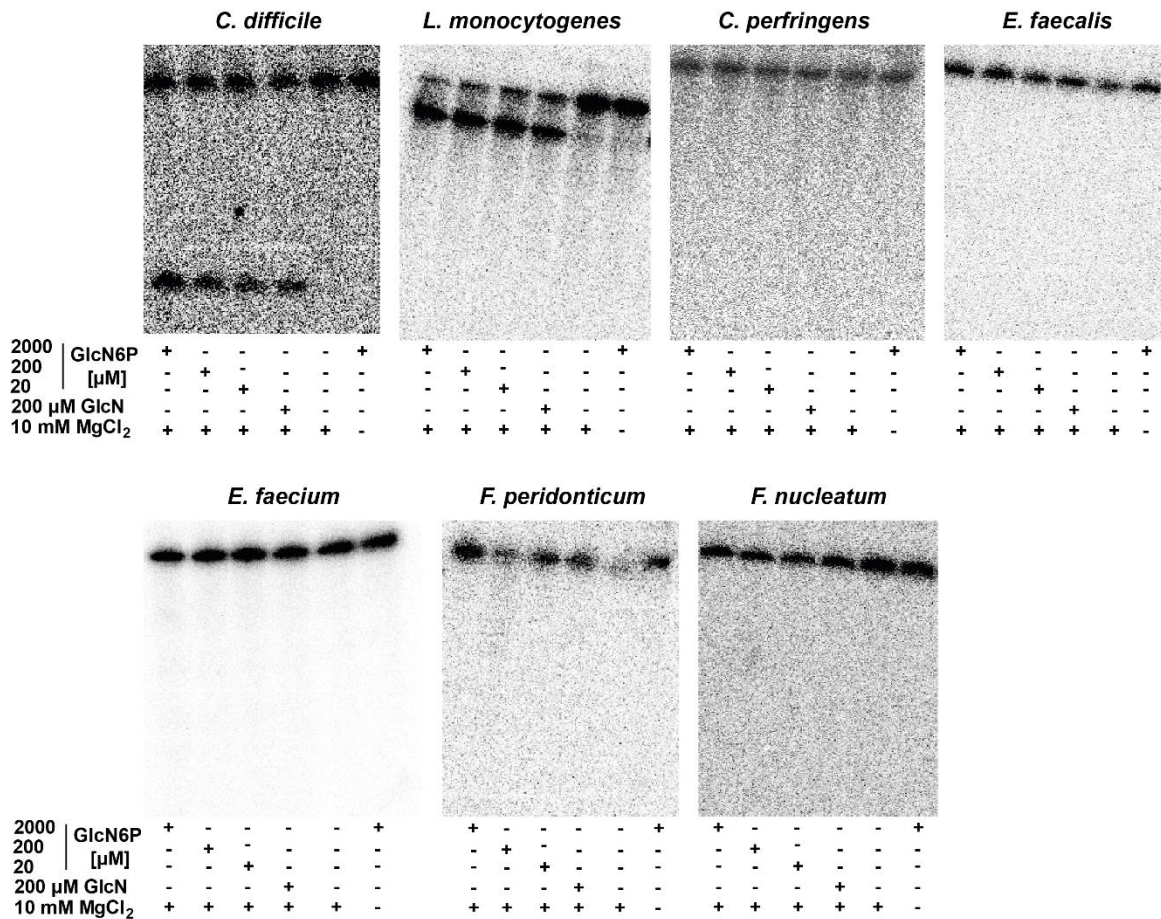


Figure 42: PAGE gel of radioactive metabolite-induced cleavage assay to study *glmS* ribozyme activity

For all herein tested species the results of the cleavage assays are depicted in the following order: in the presence of 2000, 200, or 20 μ M GlcN6P, 200 μ M GlcN, without the addition of the metabolite and in the absence of MgCl₂.

The quantification of this initial screening is shown in **Figure 43**. Cleavage could be observed for the *glmS* ribozyme representatives of *L. monocytogenes* and *C. difficile*. In both cases, cleavage can be clearly observed if 2000, 200 or 20 μ M GlcN6P were added to the sample. However, in the presence of GlcN cleavage of *L. monocytogenes* is not as pronounced as for the *glmS* ribozyme representative of *C. difficile*.

Results

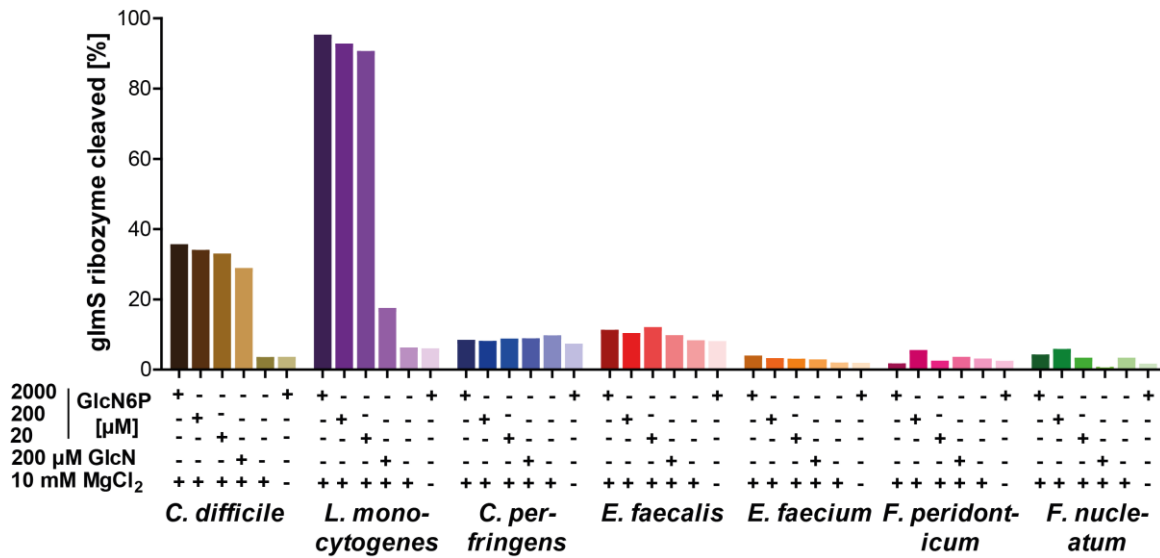


Figure 43: Screening for *glmS* ribozyme activity by radioactive metabolite induced self-cleavage assay

Cleavage was analyzed after 30 min of incubation at 37 °C: The positive sample contained either 2000, 200 or 20 μM GlcN6P. Moreover, a control containing 200 μM GlcN was analyzed, as well as controls lacking any sugar metabolite and a control not containing MgCl₂ (n=1).

Based on the findings of the initial screening the *glmS* ribozyme representatives of *L. monocytogenes* and *C. difficile* were further characterized. The predicted secondary structures of the ribozyme cores of *C. difficile* and *L. monocytogenes* were illustrated according to the consensus secondary structure described by McCown *et al.* and are shown in **Figure 44**.^{184,110}

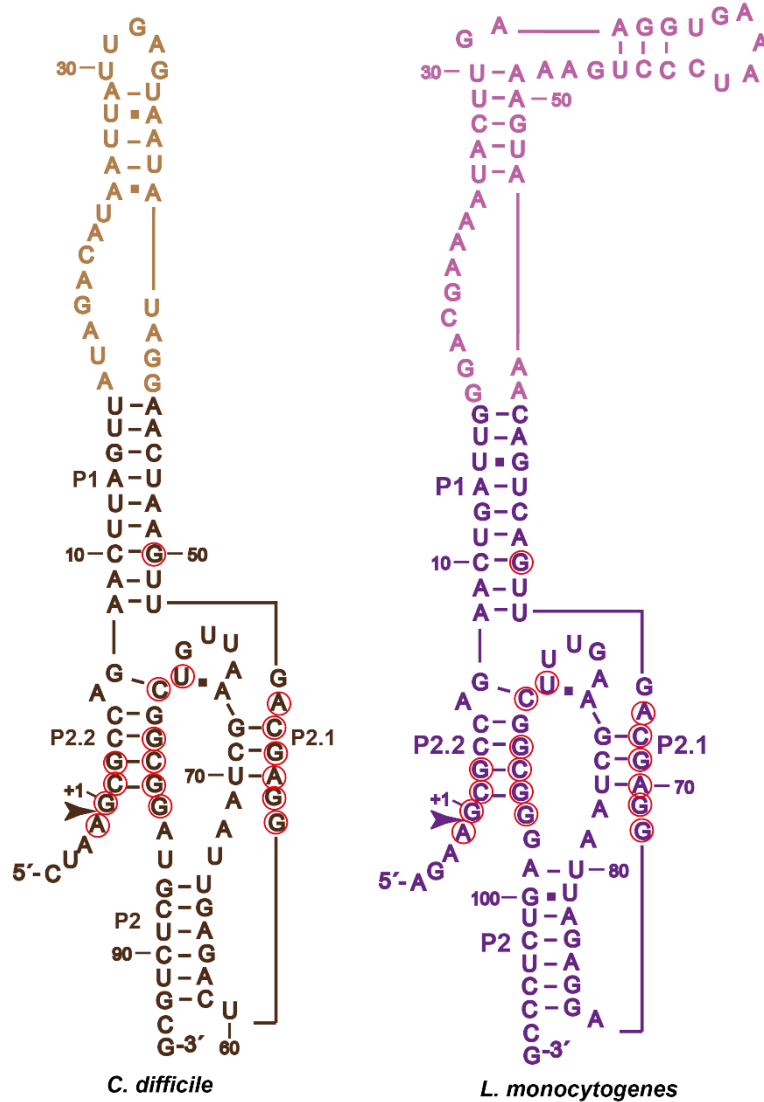


Figure 44: Secondary structure prediction of *glmS* ribozyme cores of *C. difficile* and *L. monocytogenes*

Depicted are the ribozyme cores of *C. difficile* in brown and *L. monocytogenes* in purple. The loop region between P1 and P2.2 are drawn in light brown and light purple, respectively. The cleavage sites are indicated by arrows. Highly conserved residues are marked by red circles according to McCown *et al.*¹⁶⁷

3.3.1 Screening of different sugars to identify activating metabolites of *C. difficile* and *L. monocytogenes* *glmS* ribozyme

Various sugars (**Figure 45**) were analyzed for their ability to induce *glmS* ribozyme cleavage of *C. difficile* and *L. monocytogenes*. The results are displayed in **Figure 46**. These sugars were chosen to allow for comparison to the results obtained for the *glmS* ribozyme of *S. aureus*.¹⁹⁹ For this assay, 200 μ M of the 14 different sugars (**Figure 45**) were incubated in the presence of 10 mM $MgCl_2$ at 37 $^{\circ}$.

Results

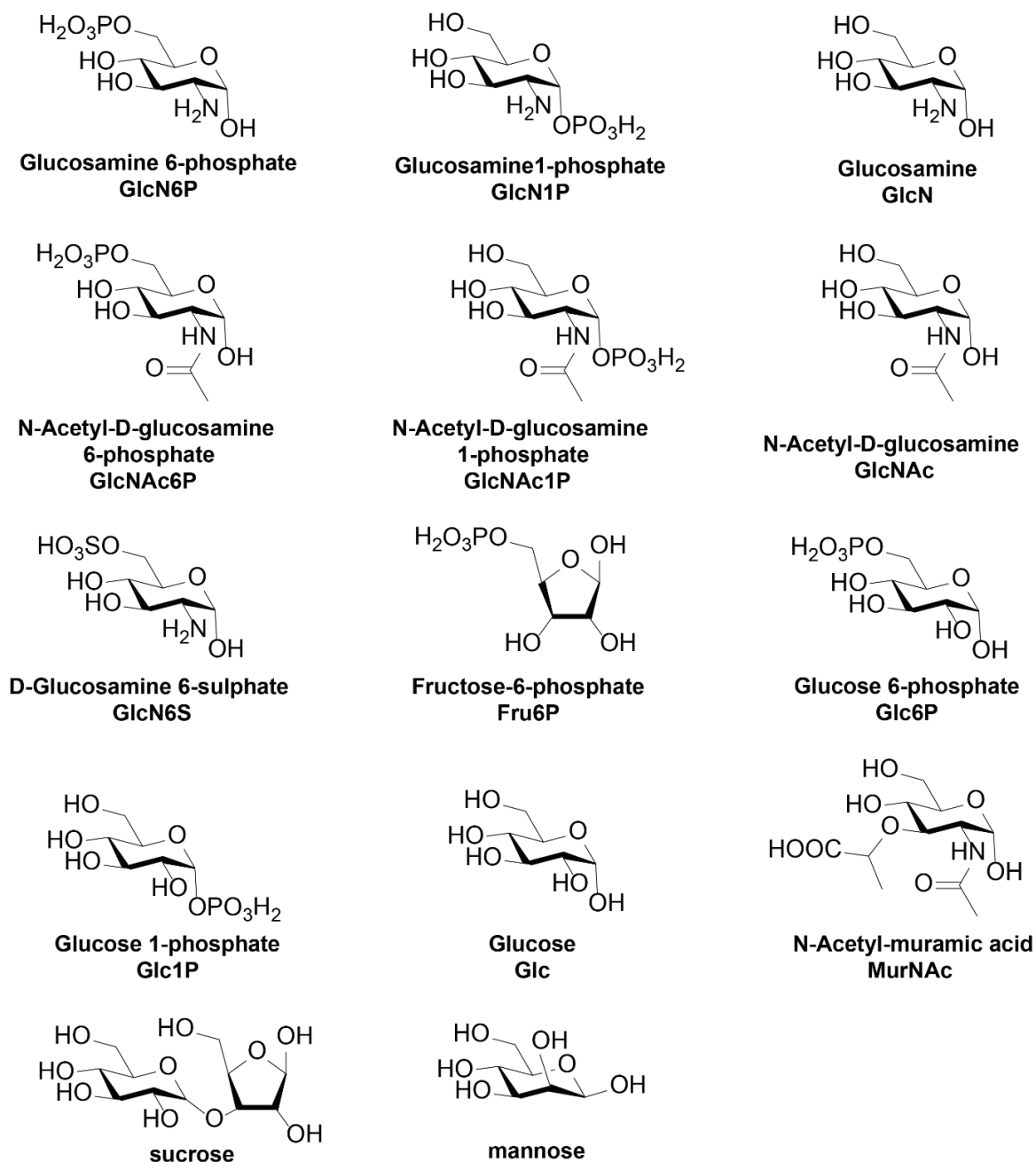


Figure 45: Chemical structures of sugars screened for *C. difficile* and *L. monocytogenes* *glmS* ribozyme self-cleavage induction

Efficient cleavage of both ribozymes was observed for the following sugars: GlcN6P, GlcNAc6P and GlcN6S. In case of the *C. difficile* construct cleavage was also observed in the presence of GlcN.

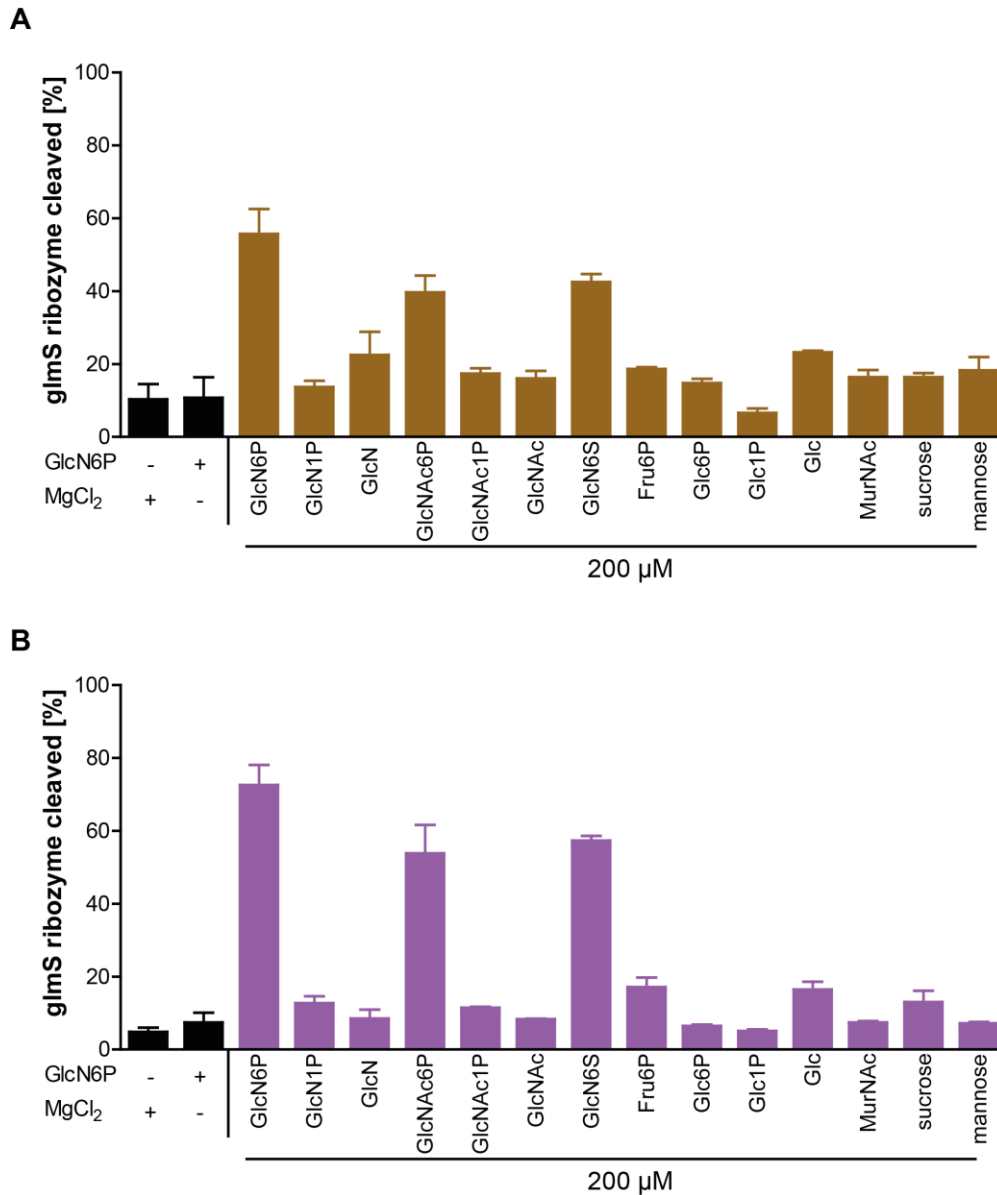


Figure 46: Screening of various sugars for the induction of *glmS* ribozyme cleavage of *C. difficile* and *L. monocytogenes*

Cleavage of the *glmS* ribozyme of *C. difficile* in the presence of 200 μ M sugar is depicted in brown (A) and in purple, cleavage of the *L. monocytogenes* *glmS* ribozyme is shown (B). Cleavage rates are shown in comparison to the controls containing either 200 μ M GlcN6P or GlcN as well as controls lacking the metabolite or MgCl₂ in black (n=2-9). Cleavage was monitored after 30 min of incubation at 37 °C.

Subsequently to the screening of the different sugars, a concentration-dependent analysis regarding the ability of GlcN6P and GlcN to induce *glmS* ribozyme cleavage of *C. difficile* and *L. monocytogenes* was performed. These two sugars were further analysed because GlcN6P and GlcN are commonly known activators of these ribozymes and allow the analysis of the effect of phosphorylated versus non-phosphorylated metabolites.

3.3.2 Concentration-dependent analysis of self-cleavage induction by GlcN6P and GlcN in *C. difficile* and *L. monocytogenes glmS* ribozymes

In **Figure 47A**, *C. difficile glmS* ribozyme cleavage in the presence of concentrations of GlcN6P and GlcN ranging from 10 nM to 100 mM is shown. An EC_{50} value of 0.46 μ M could be determined for GlcN6P-induced cleavage of *C. difficile* (**Figure 47A** and **Table 3**). The same analysis was carried out utilizing the ribozyme of *L. monocytogenes* and revealed an EC_{50} of 0.38 μ M for GlcN6P. Ribozyme cleavage in the presence of GlcN revealed an EC_{50} of ~ 223.1 μ M for *C. difficile* and a high EC_{50} value of ~ 1920 μ M for *L. monocytogenes* (**Figure 47** and **Table 3**). For comparison, the EC_{50} values for *S. aureus* were determined with ~ 3.6 μ M and ~ 189 μ M for GlcN6P and GlcN, respectively.¹⁹⁹

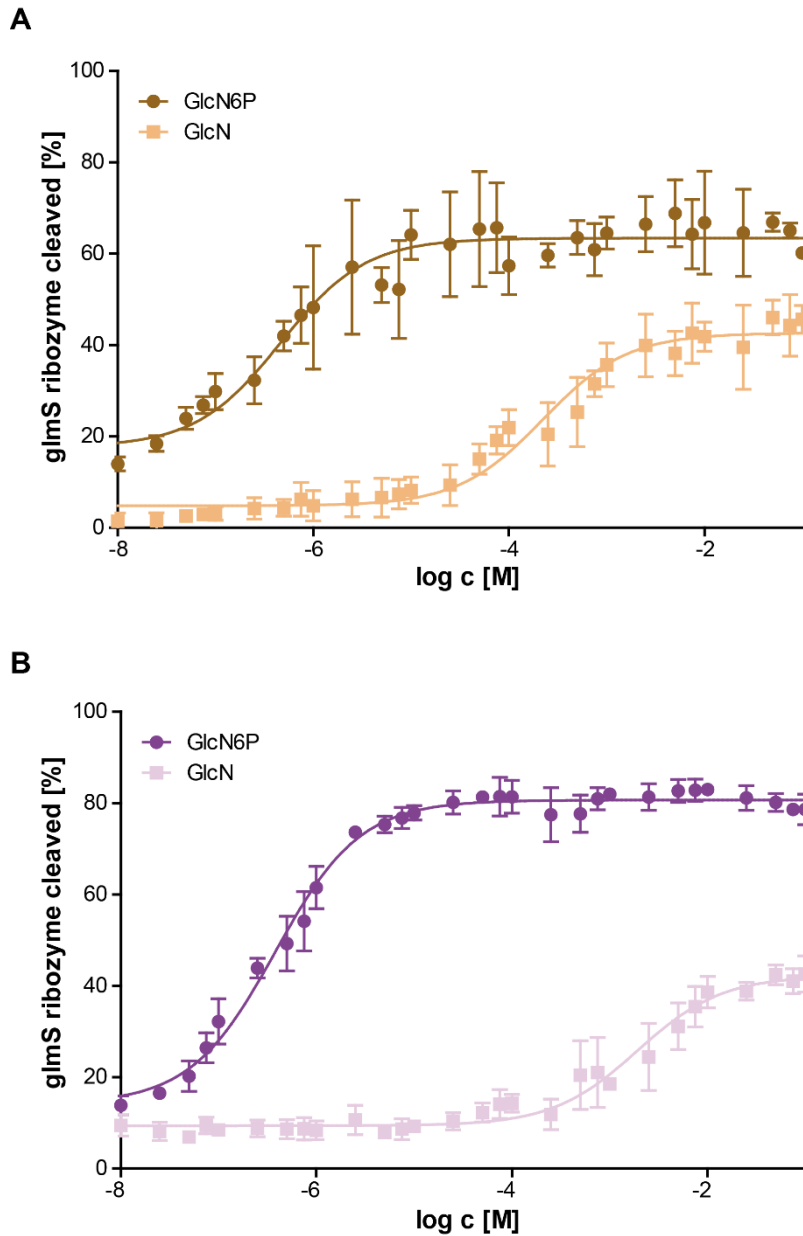


Figure 47: EC₅₀ value determination for GlcN6P- and GlcN-induced self-cleavage of the *glmS* ribozyme of *C. difficile* and *L. monocytogenes*

Cleavage induction by increasing concentrations of GlcN6P and GlcN is depicted. A shows cleavage of the *C. difficile* *glmS* ribozyme and B shows cleavage of *L. monocytogenes* (n=2-4). Cleavage was monitored after 30 min of incubation at 37 °C.

Table 3: EC₅₀ values for GlcN6P- and GlcN-induced cleavage of *glmS* ribozymes of *C. difficile* and *L. monocytogenes*

EC ₅₀ [μ M]	<i>C. difficile</i>	<i>L. monocytogenes</i>
GlcN6P	$\sim 0.46 \pm 0.0001$	$\sim 0.38 \pm$ below 1 nM
GlcN	$\sim 223.1 \pm 0.060$	$\sim 1920 \pm 0.654$

3.3.3 Investigation of different metal ions participating in *glmS* ribozyme self-cleavage of *C. difficile* and *L. monocytogenes*

The initial screening proved that Mg^{2+} is efficient in promoting ribozyme cleavage of ribozyme variants. From the literature, it is evident that other divalent ions are also suitable to coordinate the metabolite.^{94, 150} Therefore, 10 mM of several different divalent ions were screened with regard to self-cleavage induction. The divalent metal ions, Mg^{2+} , Ca^{2+} , and Mn^{2+} were identified as efficient ions for conferring *glmS* ribozyme cleavage of both ribozymes (**Figure 48A** and **Figure 48B**).

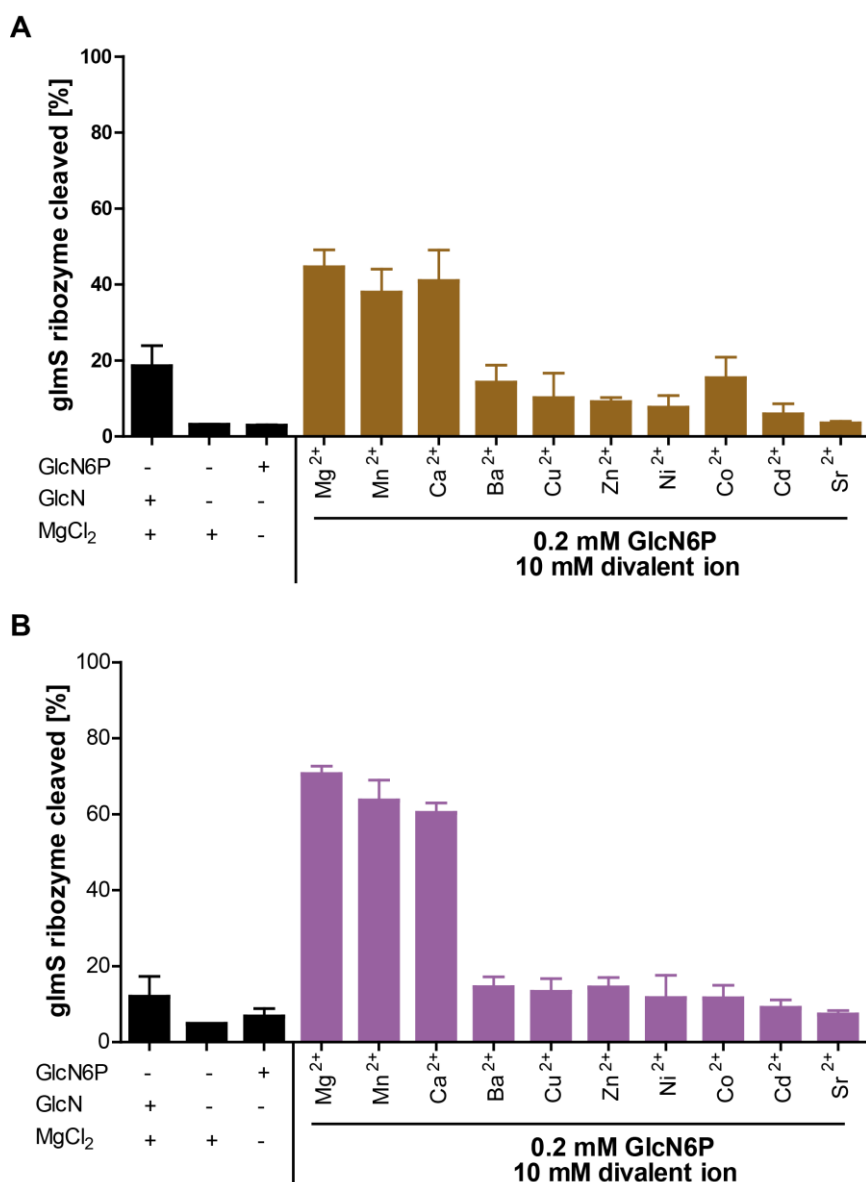


Figure 48: Self-cleavage of *glmS* ribozymes in the presence of GlcN6P and different divalent ions

Radioactive metabolite-induced cleavage assay depicting cleavage of the *C. difficile glmS* ribozyme in the presence of different divalent ions (Mg^{2+} , Mn^{2+} , Ca^{2+} , Ba^{2+} , Cu^{2+} , Zn^{2+} , Ni^{2+} , Co^{2+} , Sr^{2+}) is

shown in brown (A) and cleavage of the *L. monocytogenes* variant is shown in purple (B). Cleavage rates are shown in comparison to controls containing either 200 μM GlcN6P or GlcN as well as controls lacking the metabolite or MgCl_2 in black ($n=2-3$). Cleavage was monitored after 30 min of incubation at 37 $^\circ\text{C}$.

To gain a better understanding concentration-dependent analysis aiming at the determination of EC_{50} values was performed. The concentration-dependent analysis is displayed in **Figure 49A** and **Figure 49B**, the corresponding EC_{50} values can be found in **Table 3**.

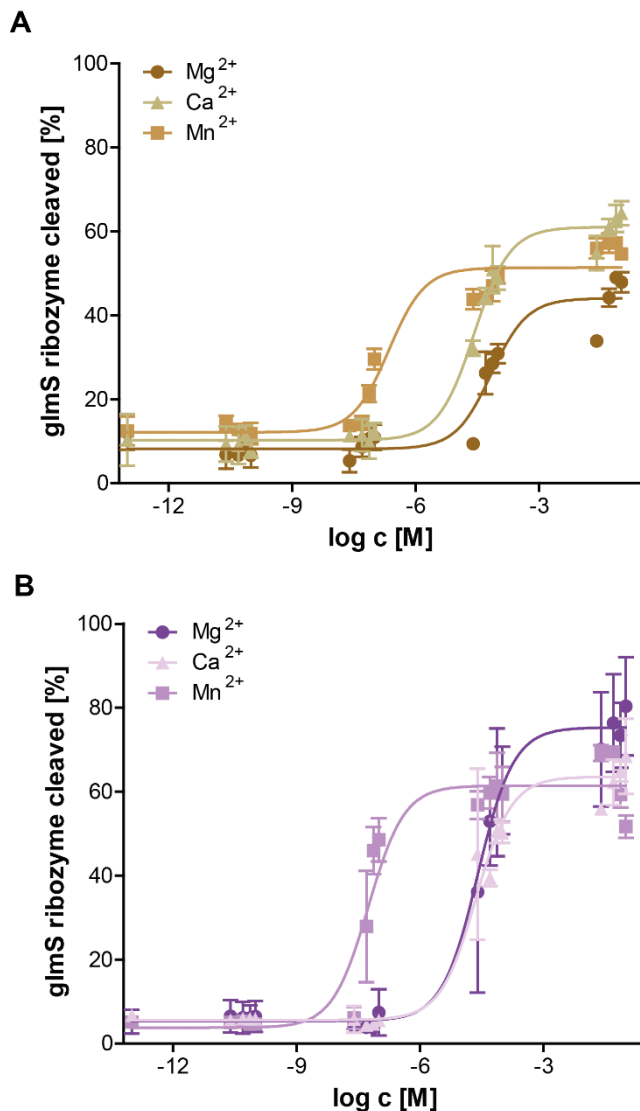


Figure 49: EC_{50} value determination of GlcN6P-induced cleavage of *glmS* ribozymes in the presence of different divalent ions

Radioactive metabolite-induced self-cleavage assay employing concentration-dependent analysis to assess the ability of Mg^{2+} , Mn^{2+} and Ca^{2+} to mediate GlcN6P-induced self-cleavage (200 μM GlcN6P) of *glmS* ribozymes of *C. difficile* illustrated in A in brown and *L. monocytogenes* in B depicted in purple ($n=1-3$). Cleavage was monitored after 30 min of incubation at 37 $^\circ\text{C}$.

The determined EC₅₀ values for cleavage mediated by Mg²⁺, Ca²⁺ and Mn²⁺ reveal that in both cases Mn²⁺ ions are most efficient in cleavage reaction induction followed by Ca²⁺ and Mg²⁺. However, the *glmS* ribozyme variant of *L. monocytogenes* seems to be about three times more sensitive for the induction of cleavage by Mg²⁺ ions than the ribozyme of *C. difficile*.

Table 4: EC₅₀ values for GlcN6P-induced self-cleavage mediated by different divalent ions

EC ₅₀ [μM]	<i>C. difficile</i>	<i>L. monocytogenes</i>
Mg ²⁺	70.067 ± 6.190	25.73 ± 5.452
Ca ²⁺	27.22 ± 3.555	23.03 ± 4.622
Mn ²⁺	0.256 ± 0.963	0.5741 ± 0.0003

3.3.4 pH-dependency of *glmS* ribozyme variants of *C. difficile* and *L. monocytogenes*

The ability of ribozymes to perform self-cleavage reactions is pH-dependent.²⁰⁶ Thereof, the ability of the herein characterized *glmS* ribozymes to perform self-cleavage at different pHs was analyzed. This also allows comparison to other ribozymes, especially the *glmS* ribozyme of other bacterial species. The resulting pH profiles for the *glmS* ribozymes of *C. difficile* are displayed in **Figure 50A**. In **Figure 50B** *L. monocytogenes* *glmS* ribozyme cleavage is shown. For both representatives, cleavage is most efficient in physiological pH ranges of 6-8.5, whereas cleavage is reduced at lower pH.

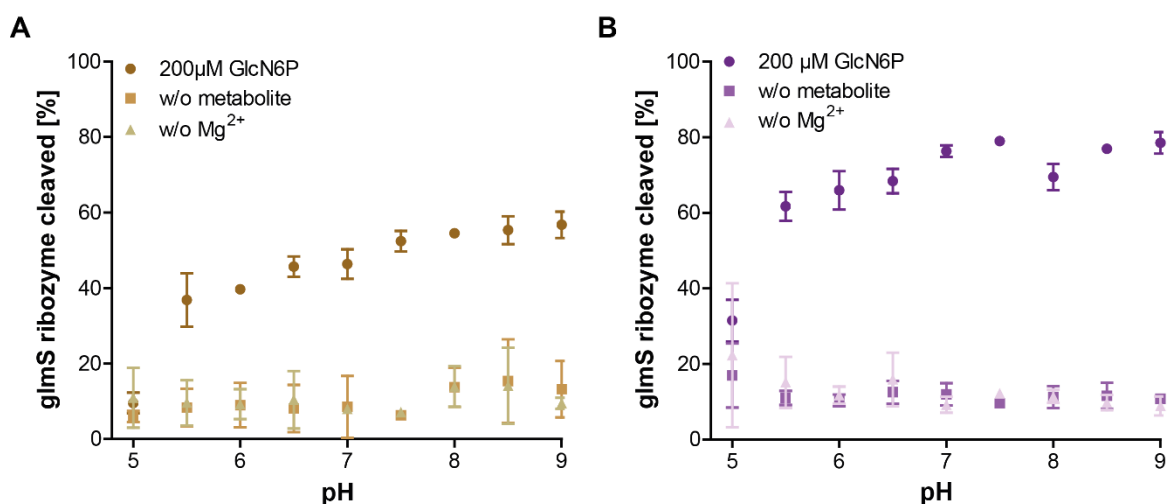


Figure 50: Analysis of pH-dependency of *glmS* ribozyme cleavage

Radioactive metabolite-induced cleavage assay monitoring cleavage at pHs ranging from 5 to 9 analyzed in the presence of 200 μM GlcN6P as well as in the absence of MgCl₂ and metabolite after 30 min incubation at 37 °C. The results for *C. difficile* are shown in A and for *L. monocytogenes* in B (n=3-5).

3.3.5 Determination of *glmS* ribozyme cleavage rates of *C. difficile* and *L. monocytogenes*

To determine the efficiency of the self-cleavage reaction of the *glmS* ribozymes of *C. difficile* and *L. monocytogenes*, kinetic rate constants (k_{obs}) were assessed. The concentrations used to determine rate constants depend on the determined EC_{50} values (**section 3.4.2**). The concentrations equal the initially determined EC_{50} values for both GlcN6P and GlcN (**Figure 47** and **Table 3**) and concentrations by a factor of 10 and 100 higher in case of GlcN6P.

Different RNA preparations show different cleavage capacities, but the overall tendencies in (comparing different activators) are always the same. In case of *C. difficile* the determined k_{obs} values do not agree with the formerly determined EC_{50} value for GlcN6P. For this reason, a new EC_{50} value determination was performed. This re-evaluated EC_{50} value is depicted in **Figure 47** and **Table 3** and explains the deviating concentrations used to determine k_{obs} values.

The GlcN6P-induced cleavage of the *C. difficile* *glmS* ribozyme was found to be faster than the *L. monocytogenes* *glmS* ribozyme (**Figure 51**, **Table 5** and **Table 6**). Comparison of rate constant of the GlcN6P-induced cleavage around the EC_{50} value concentrations (0.2 μM and 0.4 μM GlcN6P for *C. difficile* and *L. monocytogenes*, respectively) shows that the cleavage of *C. difficile* is ~ 5 fold faster than it is the case for the *L. monocytogenes* *glmS* ribozyme (**Table 5** and **Table 6**).

Results

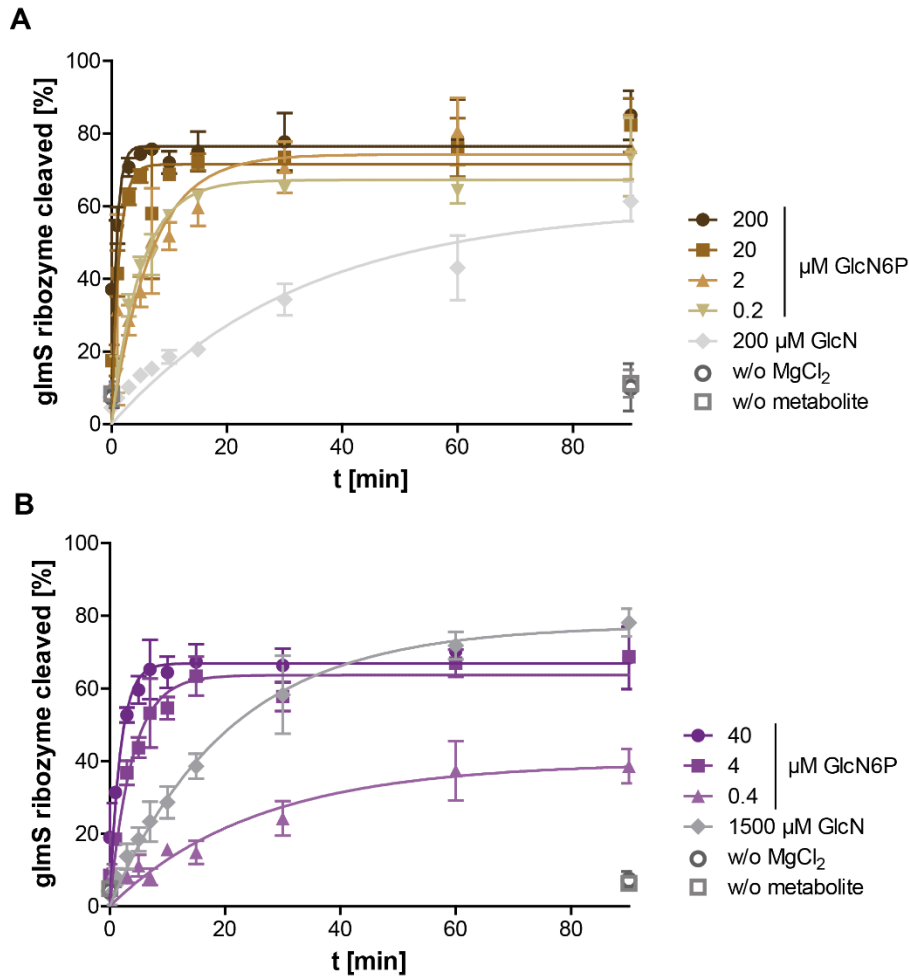


Figure 51: Determination of k_{obs} values for *glmS* ribozymes in the presence of GlcN6P and GlcN

Radioactive metabolite-induced self-cleavage assay monitoring cleavage kinetic of the *C. difficile* *glmS* ribozyme is shown in brown (A) and cleavage of the *L. monocytogenes* variant is shown in purple (B), controls lacking the metabolite or $MgCl_2$ are grey ($n=2-3$).

Table 5: k_{obs} values for *glmS* ribozyme of *C. difficile*

[μ M] GlcN6P	k_{obs} [min^{-1}]
200	1.206 ± 0.372
20	0.786 ± 0.168
2	0.147 ± 0.026
0.2	0.198 ± 0.017
200 GlcN	0.030 ± 0.005

Table 6: k_{obs} values for *glmS* ribozyme of *L. monocytogenes*

[μM] GlcN6P	k_{obs} [min^{-1}]
40	0.548 ± 0.089
4	0.259 ± 0.026
0.4	0.039 ± 0.007
1500 GlcN	0.048 ± 0.004

3.3.6 Influence of the temperature on the *glmS* ribozyme self-cleavage of *C. difficile* and *L. monocytogenes*

Temperature is a parameter that significantly influences the reaction speed and proceeding of cleavage reactions. Therefore, cleavage of the herein validated *glmS* ribozyme variants at temperatures ranging from 6 to 37 °C was analyzed. The results are displayed in **Figure 52A** for the *glmS* ribozyme of *C. difficile* and in **Figure 52B** for the listerial *glmS* ribozyme variant. While the *C. difficile* variant shows dramatically reduced cleavage at temperatures lower than 20 °C, the ribozyme of *L. monocytogenes* remains comparably functional with 60% cleavage activity even at temperatures as low as 6 °C.

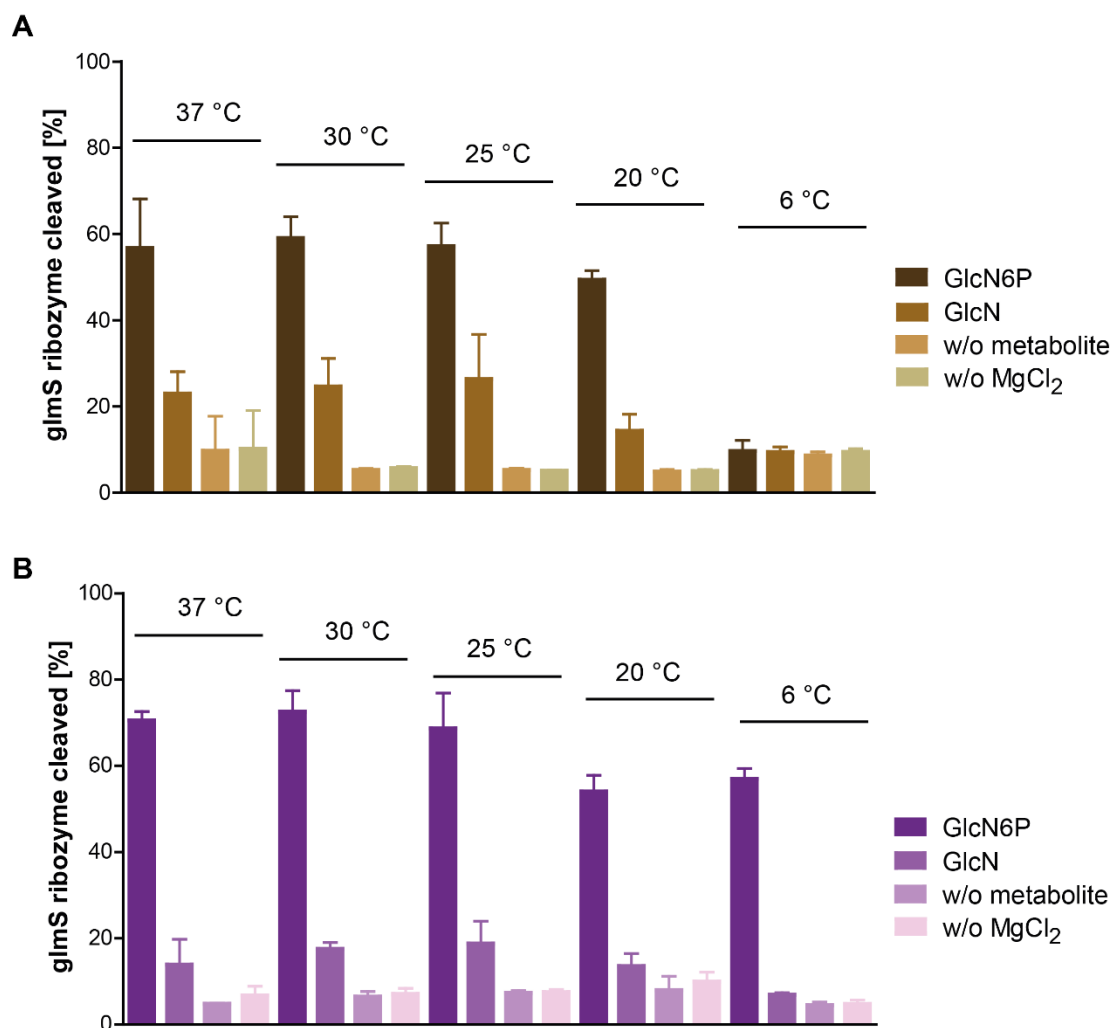


Figure 52: Analysis of the effect of different temperatures on the cleavage of *glmS* ribozymes Radioactive metabolite-induced cleavage assay monitoring cleavage in the presence of 200 μ M GlcN6P, 200 μ M GlcN and in the absence of metabolites as well as in the absence of MgCl₂ is depicted for all tested temperatures (37 °C, 30 °C, 25 °C, 20 °C, 15 °C, 10 °C and 6 °C) assessed after 30 min of incubation. Cleavage of *C. difficile* *glmS* ribozyme is shown in A (shaded in brown) and cleavage of *L. monocytogenes* is shown in B (shaded in purple) (n=3-6).

3.3.7 Kinetics of *L. monocytogenes glmS* self-cleavage at 6 °C

The analysis of cleavage at different temperatures presented in **section 3.3.6** showed the remarkable activity at low temperatures of the *glmS* ribozyme of *L. monocytogenes* compared to *C. difficile*. Based on these findings, the kinetic of the cleavage reaction at 6 °C was analyzed and the results are displayed in **Figure 53**. **Table 7** shows the recorded k_{obs} values in comparison to those obtained at 37 °C (**section 3.3.5**). Interestingly, cleavage rates at 6 °C and at 37 °C are comparable. Only the kinetic obtained with 40 μ M GlcN6P is significantly slower at 6 °C than at 37 °C.

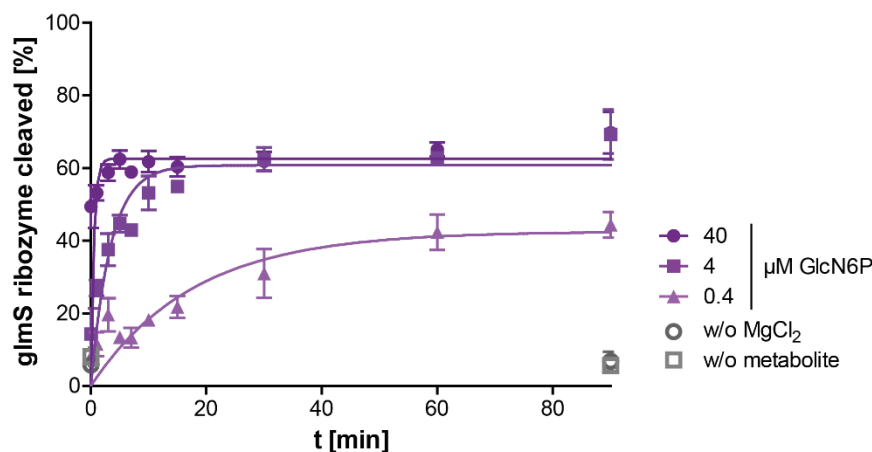


Figure 53: Determination of k_{obs} values for *L. monocytogenes* *glmS* ribozyme in the presence of GlcN6P at 6 °C

Radioactive metabolite-induced cleavage assay depicting the cleavage kinetic of the *L. monocytogenes* *glmS* ribozyme at 6 °C utilizing 40 μM , 4 μM and 0.4 μM GlcN6P is shown in shades of purple, controls lacking the metabolite or MgCl_2 are illustrated in grey ($n=2-3$).

Table 7: k_{obs} values for *glmS* ribozyme of *L. monocytogenes* in the presence of GlcN6P at 6 °C

		k_{obs} [min^{-1}] <i>L. monocytogenes</i>	
		37 °C	6 °C
	[μM]		
GlcN6P	40	0.548 ± 0.089	1.868 ± 1.091
	4	0.259 ± 0.026	0.295 ± 0.051
	0.4	0.039 ± 0.007	0.057 ± 0.012
GlcN	1500	0.048 ± 0.004	n.d

3.4 Screening and Mode of Action analysis of novel carba-sugar variants

Having shown that CGlcN inhibits bacterial growth by targeting the *glmS* ribozyme we wanted to analyze further derivatives of CGlcN(6P) regarding their ability to activate the *glmS* ribozyme *in vitro* and *in vivo* aiming at the identification of a more potent analog. Therefore, Daniel Matzner synthesized further CGlcN derivatives as potential activators of the *glmS* ribozyme. His PhD thesis focused on the chemical synthesis of modified carba-variants of α -D-glucosamine and β -L-idosamine that are mono-fluorinated at the carba-position and the phosphorylated variants of these pseudo-sugars. Moreover, a phosphorylated phenyl carba-sugar variant was synthesized (**Figure 54**).

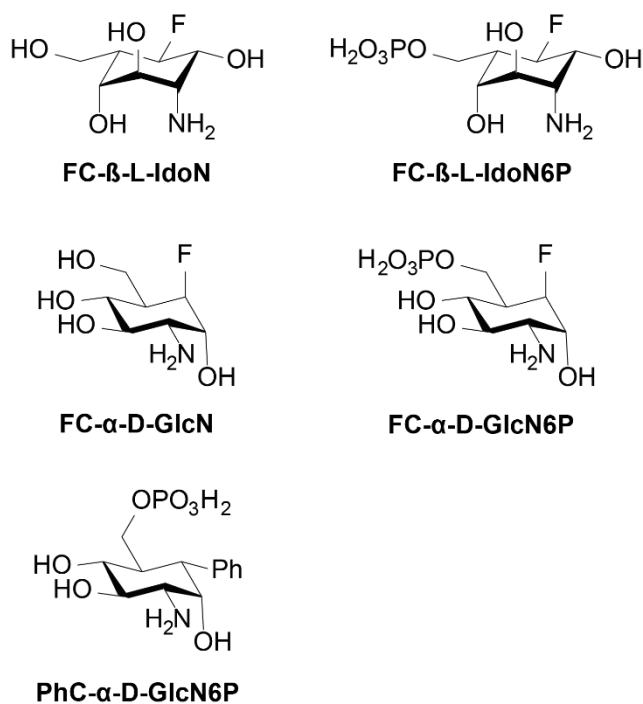


Figure 54: Chemical structures of carba-sugar derivatives

The interaction of the modified carba-sugars with the *glmS* ribozyme *in vitro* as well as modulation of bacterial growth and related *in vivo* studies are presented in the following section.

3.4.1 Screening of carba-sugar derivative for *glmS* ribozyme activation

Metabolite-induced self-cleavage assays were performed to analyze *glmS* ribozyme activation by the different carba-sugar variants. In **Figure 55** the screening of the five different carba-sugar variants regarding cleavage induction of the *glmS* ribozymes of *S. aureus*, *B. subtilis*, *C. difficile* and *L. monocytogenes* is presented.

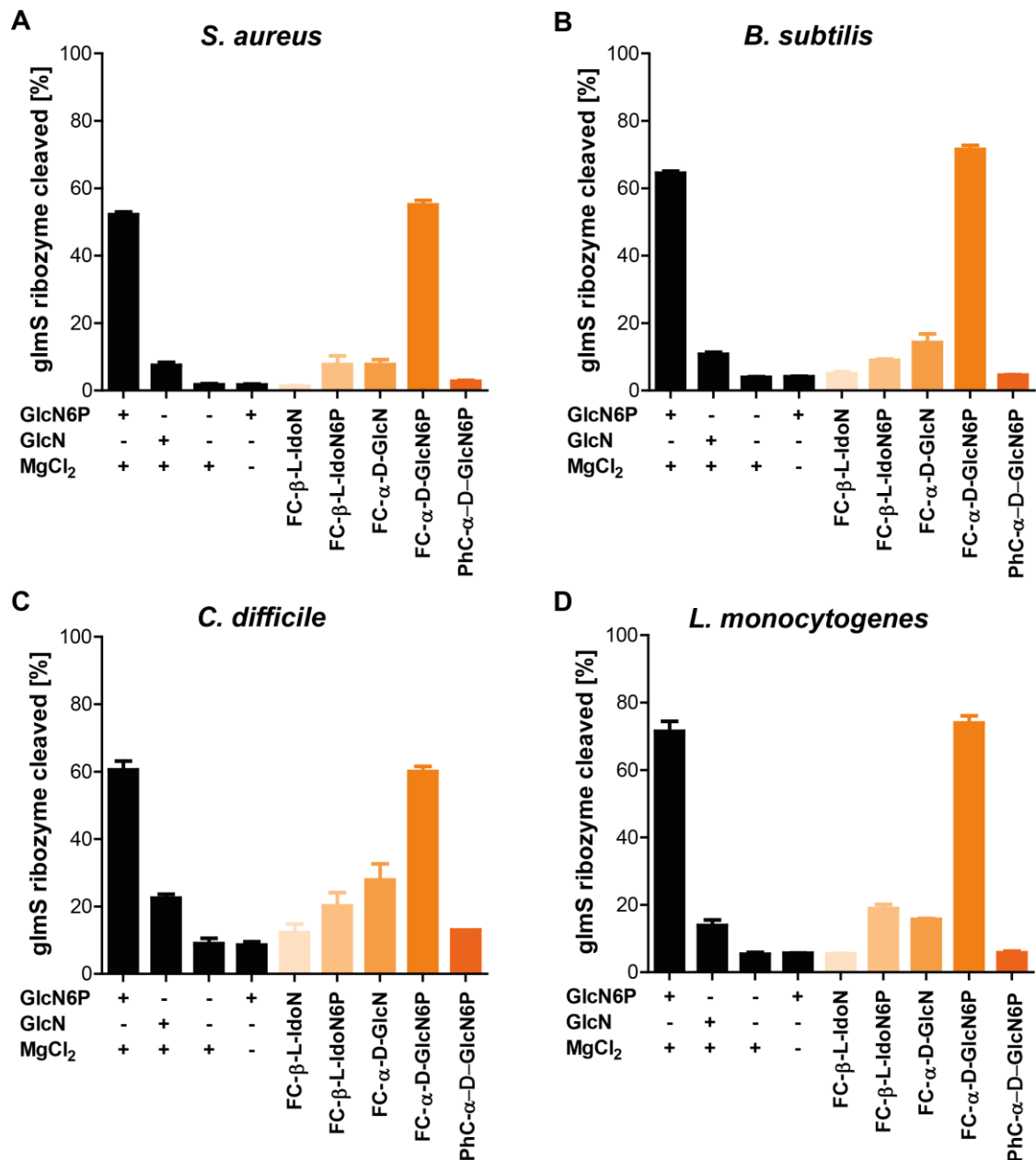


Figure 55: Screening of novel carba-sugar variants for *glmS* ribozyme activation

Shown is the screening for the activation of self-cleavage in the radioactive metabolite-induced cleavage assay for the *glmS* ribozymes of *S. aureus* (A), *B. subtilis* (B), *C. difficile* (C) and *L. monocytogenes* (D) by 2 mM FC-β-L-IdoN, FC-β-L-IdoN6P, FC-α-D-GlcN, FC-α-D-GlcN6P and PhC-α-D-GlcN6P. The percentage of the cleaved fraction is shown (shades of orange) in comparison to the positive control containing 200 μM GlcN6P as well as a control containing 200 μM GlcN and two negative controls either lacking any metabolite or MgCl₂ (n=3-6). Cleavage was monitored after 30 min of incubation at 37 °C.

FC-α-D-GlcN6P induces self-cleavage of all four investigated *glmS* ribozymes while FC-β-L-IdoN6P as well as FC-α-D-GlcN moderately induce self-cleavage and FC-β-L-IdoN as well as PhC-α-D-GlcN6P do not induce self-cleavage. Therefore,

it was decided to further analyze the effect of FC- α -D-GlcN6P in more detail using the *glmS* ribozymes of *S. aureus* and *B. subtilis*.

3.4.2 Concentration-dependent analysis of FC- α -D-GlcN6P-induced cleavage of *glmS* ribozymes

To assess and compare the efficacy of FC- α -D-GlcN6P in inducing *glmS* ribozyme cleavage of *S. aureus* and *B. subtilis*, concentration-dependent analysis was performed. The results can be seen in **Figure 56**. EC₅₀ values of $312 \pm 32 \mu\text{M}$ and $196 \pm 17 \mu\text{M}$ for *S. aureus* and *B. subtilis*, respectively, could be determined. In comparison to the EC₅₀ values obtained in the presence of GlcN6P or CGlcN6P ~ 50 times higher concentrations of FC- α -D-GlcN6P are required to obtain comparable cleavage of the *S. aureus* *glmS* ribozyme variant while in case of *B. subtilis* almost 100 times more FC- α -D-GlcN6P is needed to achieve comparable cleavage ratios (**Table 8**).

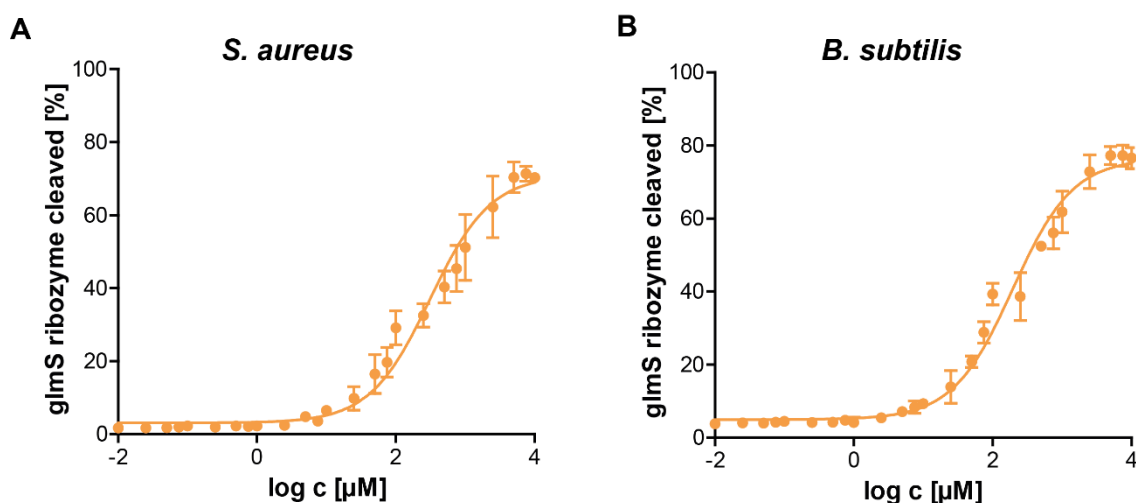


Figure 56: Concentration-dependent analysis of *glmS* ribozyme cleavage induced by FC- α -D-GlcN6P

Radioactive metabolite-induced cleavage assay monitoring cleavage induction of *S. aureus* by FC- α -D-GlcN6P in A, while induction of the *B. subtilis* *glmS* ribozyme is shown in B (n=3). Cleavage was monitored after 30 min of incubation at 37 °C.

Table 8: Comparison of EC₅₀ values regarding the self-cleavage induction by GlcN6P, CGlcN6P and FC- α -D-GlcN6P for *S. aureus* and *B. subtilis* *glmS* ribozymes

*_{150, 199}

<i>glmS</i> ribozyme	EC ₅₀ [μ M]		
	GlcN6P	CGlcN6P	FC- α -D-GlcN6P
<i>S. aureus</i>	3.6 \pm 0.4 *	6.2 \pm 0.7 *	312 \pm 32
<i>B. subtilis</i>	n.d	2.2 \pm 0.4 *	196 \pm 17

3.4.3 Kinetic analysis of FC- α -D-GlcN6P-induced cleavage of *glmS* ribozymes

Kinetic analysis of the FC- α -D-GlcN6P induced *glmS* ribozyme cleavage was performed to assess the kinetic rate constants. The concentrations used to determine rate constants depend on the determined EC₅₀ values (**section 3.4.2**). The concentration equal to the EC₅₀ value, a concentration a factor of 10 higher than the respective EC₅₀ value and 600 μ M as highest concentration were tested. The obtained results for *S. aureus* and *B. subtilis* are depicted in **Figure 57** and **Table 9** and **Table 10**. In accordance with the EC₅₀ value determinations concentration-dependent activation caused by FC- α -D-GlcN6P can be seen. Moreover, the determined k_{obs} values resemble the values determined for CGlcN6P and GlcN6P.¹⁵⁰

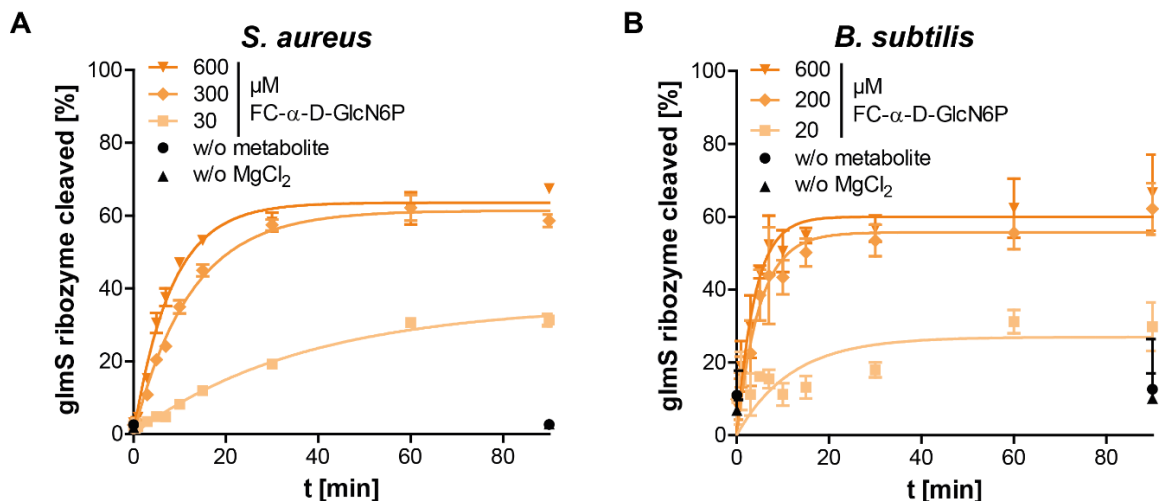


Figure 57: Cleavage kinetics of *glmS* ribozymes in the presence of FC- α -D-GlcN6P
Radioactive metabolite-induced cleavage assay monitoring cleavage rates induced by FC- α -D-GlcN6P for *S. aureus* are shown in A, cleavage rates for *B. subtilis* in B. Controls lacking the metabolite or MgCl₂ are depicted in black (n=3). Cleavage was monitored at the indicated time points while incubating at 37 °C.

Table 9: k_{obs} values for FC- α -D-GlcN6P induced cleavage of *glmS* ribozyme of *S. aureus*

[μM]	k_{obs} [min^{-1}]
600	0.122 ± 0.007
300	0.081 ± 0.003
30	0.027 ± 0.002

Table 10: k_{obs} values for FC- α -D-GlcN6P induced cleavage of *glmS* ribozyme of *B. subtilis*

[μM]	k_{obs} [min^{-1}]
600	0.258 ± 0.036
200	0.204 ± 0.036
20	0.085 ± 0.028

3.4.4 Antibacterial effect of FC- α -D-GlcN on *B. subtilis*

After detailed analysis of the interaction between FC- α -D-GlcN6P and the *glmS* ribozyme *in vitro*, it was analyzed if FC- α -D-GlcN indeed shows antibacterial capacity. The approach equals the one described in **section 3.2.1** for CGlcN and CGlcN6P. The hypothesis presented in **Figure 20** is based on a prodrug approach in which the non-phosphorylated FC- α -D-GlcN is taken up by bacterial cells through the PTS system yielding the molecule FC- α -D-GlcN6P intracellularly. **Figure 20** implies that FC- α -D-GlcN6P activates the *glmS* ribozyme and due to the limitation of cell wall precursors impairs the bacterial cell wall. These different steps of the hypothesis were tested in the following sections. This section analyzes the antibacterial potential of FC- α -D-GlcN regarding *B. subtilis*.

B. subtilis was incubated in the presence of increasing concentrations of FC- α -D-GlcN and bacterial growth was recorded over time. The result of this growth curve analysis can be seen in **Figure 58**. The determined MIC of 150 μM (32 $\mu\text{g/ml}$) matches that observed for CGlcN (**Figure 27**). Comparison of the bacterial growth inhibitory potency of CGlcN and FC- α -D-GlcN therefore reveals equal effectiveness.

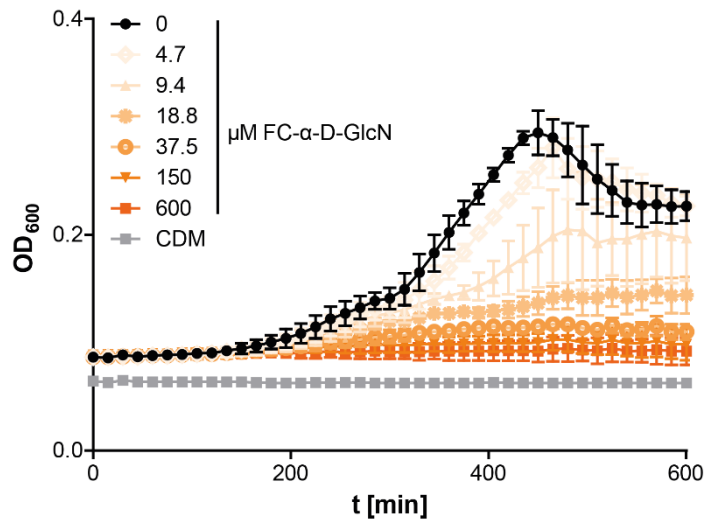


Figure 58: Growth curve analysis of *B. subtilis* in the presence of FC- α -D-GlcN

Increasing concentrations of FC- α -D-GlcN are depicted in shades of orange and compared to the growth of *B. subtilis* without addition of FC- α -D-GlcN in black. The sterile control is shown in grey (n=2).

3.4.5 Analysis of the uptake of FC- α -D-GlcN by PTS

It was analyzed whether the uptake of FC- α -D-GlcN depends on the bacterial PTS. As mentioned earlier, PTSs are responsible for the uptake and phosphorylation of carbohydrates. Here, the same approach that was already used to investigate the uptake of CGlcN (**section 3.1.2**) was followed. Analyzed were the PTS deletion strains NagP and GamP (both deleted in compartment EIII of the PTS) and the PtsH deleted strain which lacks the global kinase involved in all PTSs. For comparison, wt *B. subtilis* was also analyzed. All strains were incubated in CDM as well as in the presence of 2x MIC (300 μ M; 64 μ g/ml) FC- α -D-GlcN (**Figure 59**).

Results

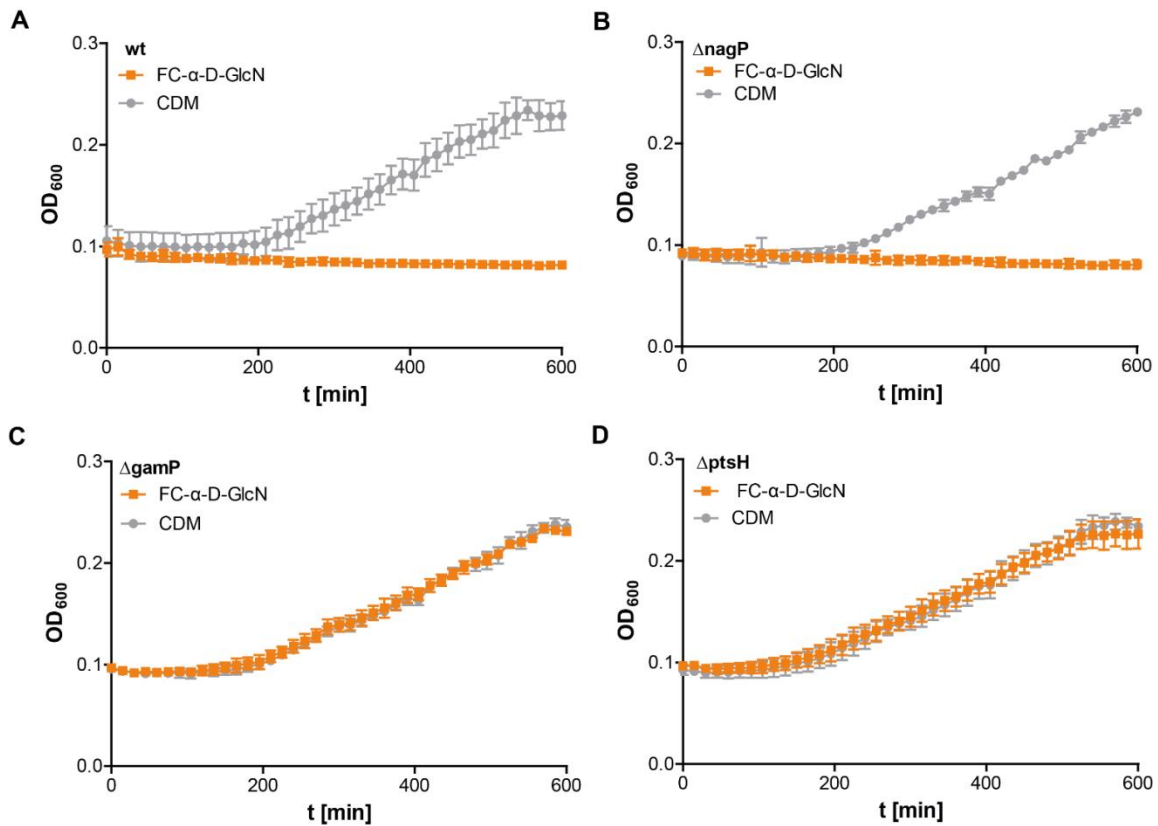


Figure 59: Growth curve analysis of *B. subtilis* 168 wt and PTS knock out strains in the presence of FC- α -D-GlcN

The growth of *B. subtilis* 168 in CDM is depicted in grey. All strains show growth in CDM. Growth of *B. subtilis* in the presence of 300 μ M (64 μ g/ml) FC- α -D-GlcN is represented in orange. Growth of *B. subtilis* wt is shown in A, growth of Δ nagP in B, Δ gamP in C and growth of Δ ptsH is shown in D (n=3).

Figure 60 summarizes the effect of FC- α -D-GlcN on the different *B. subtilis* PTS deletion strains. As observed in **section 3.2.2**, the three deletion strains and the wt are able to grow in CDM. The fact that no increase in optical density can be seen in case of the wt and the nagP mutant incubated in the presence of FC- α -D-GlcN implies that growth of these strains is inhibited by FC- α -D-GlcN. Like the results for CGlcN, the optical density of the gamP and ptsH mutants increase although FC- α -D-GlcN was added to the medium. These results suggest that FC- α -D-GlcN activity depends on the uptake and phosphorylation of the GlcN-specific PTS, GamP, and the global phosphorylation domain PtsH.

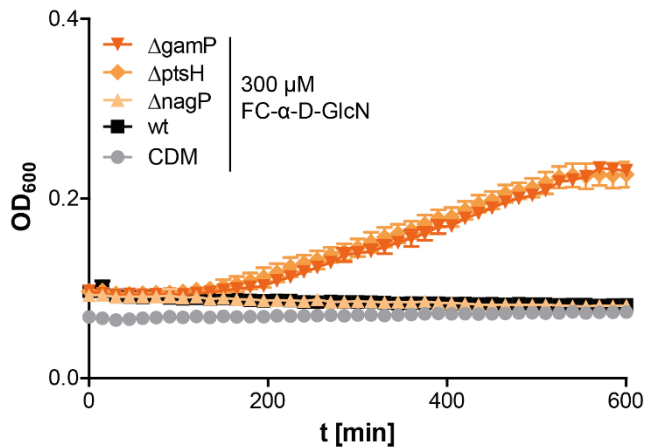


Figure 60: Growth curve analysis of PTS deletion strains in the presence of FC- α -D-GlcN PTS deleted strains (Δ gamP, Δ ptsH, Δ nagP, shades of orange) are shown in comparison to the wt *B. subtilis* strain in black and the sterile growth control (CDM) depicted in grey (n=3).

3.4.6 Induction of stress inducible promoters by FC- α -D-GlcN

The hypothesis presented in **Figure 20** implies that FC- α -D-GlcN treatment impairs the bacterial cell wall. To verify that this hypothesis is also true upon treatment with FC- α -D-GlcN, the same approach as for CGlcN was used to analyze stress induction (**section 3.1.3**). Stress inducible *B. subtilis* promotor strains were used to analyze if induction of these promoters can be detected upon FC- α -D-GlcN treatment. The induction of stress-inducible promoters by the corresponding reference antibiotics is illustrated in **Figure 69**.

The results depicted in **Figure 61** reflect the same tendencies as seen for the treatment with CGlcN. CGlcN and FC- α -D-GlcN treatment both selectively induce the cell envelope stress promotor, *ypuA*. Promoters indicative of protein (*helD*), DNA (*yorB*) or RNA (*bmrC*) stress were not induced by CGlcN and neither by FC- α -D-GlcN. These findings specifically link FC- α -D-GlcN to an impairment of the bacterial cell wall.

Results

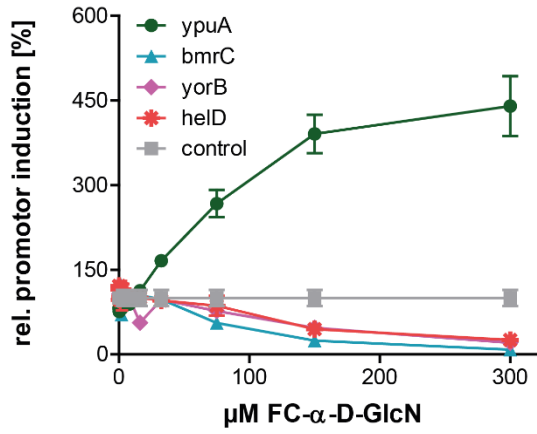


Figure 61: Stress inducible promoter gene assay in the presence of FC-α-D-GlcN

Shown is the luciferase induction by stress inducible promoters in the presence of increasing FC-α-D-GlcN concentrations. Depicted are the responses of promoters indicative for cell envelope stress (*ypuA*), protein damage (*bmrC*), DNA damage (*yorB*) and RNA damage (*helD*) (n=3).

4 Discussion

In this thesis, different aspects of the *glmS* ribozyme were studied. It was aimed at the identification of novel *glmS* ribozyme modulators (**section 3.1 & section 3.4.1**) by either screening commercially available molecules with a similar 3D shape to GlcN6P (**section 3.1**) or a small library of chemically synthesized analogs (**section 3.4.1**). Aspects concerning the *glmS* ribozyme RNA itself were studied by analyzing computer predicted *glmS* ribozyme variants of human pathogens (**section 3.3**). The *glmS* ribozyme variants of *C. difficile* and *L. monocytogenes* were characterized in depth and revealed interesting differences between *glmS* ribozyme variants. The MoA elucidation of CGlcN and the fluorinated derivative FC- α -D-GlcN proves that the *glmS* ribozyme is a suitable antibacterial target structure (**sections 3.2 & section 3.4**).

4.1 *glmS* ribozyme modulators with shape similarity to GlcN6P

Considering all the advantages of virtual screenings (**section 1.2**), an *in silico* search for molecules with a similar 3D shape to GlcN6P, the natural metabolite of the *glmS* ribozyme, was performed by the group of Prof. Reymond (University of Berne). They screened libraries of commercially available compounds and the identified potential hit compounds (1st and 2nd generation Reymond compounds) were analyzed in this thesis regarding their *glmS* ribozyme modulating properties.

4.1.1 *In silico* screening of *glmS* ribozyme modulators

In the first screening, 56 compounds (1st generation Reymond compounds) were identified as potential *glmS* ribozyme modulators. These compounds underwent *in vitro* screenings for activation and inhibition of *glmS* ribozyme cleavage. In the screening for *glmS* ribozyme activators Christina E. Lünse¹⁹⁹ identified the *glmS* ribozyme activators D4, D7, E5, E9 and F5 (**Figure 67**). Afterwards, she performed another screening for activators with a decreased compound concentration of 500 μ M in 0.5% DMSO instead of 2 mM compound in 2% DMSO. In this screening, she identified C1, C11, D1, D3 and F2 as activators. Surprisingly, the hits of the former investigation could not be confirmed. Due to the conflicting data, a screening for activation of *glmS* ribozyme cleavage was also performed in this thesis. Based on the findings of Christina E. Lünse¹⁹⁹ the experiments were performed at a concentration of 500 μ M compounds in 0.5% DMSO, but herein no *glmS* ribozyme self-cleavage activator was identified (**Figure 13**).

The 1st generation Reymond compounds were also tested for inhibition of GlcN6P-induced *glmS* ribozyme self-cleavage. Christina E. Lünse¹⁹⁹ identified the compounds B7, C3, C8, D2, D6, E6, E8, F6, F7+F8 as inhibitors of *glmS* ribozyme

cleavage. In this thesis, an independently performed screening confirmed the previously identified inhibitors except for D6. However, D6 appeared in the screening performed herein close to the cut off and F7 was clarified as inhibitor. Christina E. Lünse¹⁹⁹ also included C9 and D9 as they show structural similarity to the identified inhibitors (**Figure 67**). In the herein performed screening C9, as well as E4, E9, and E11 were identified as additional inhibitors.

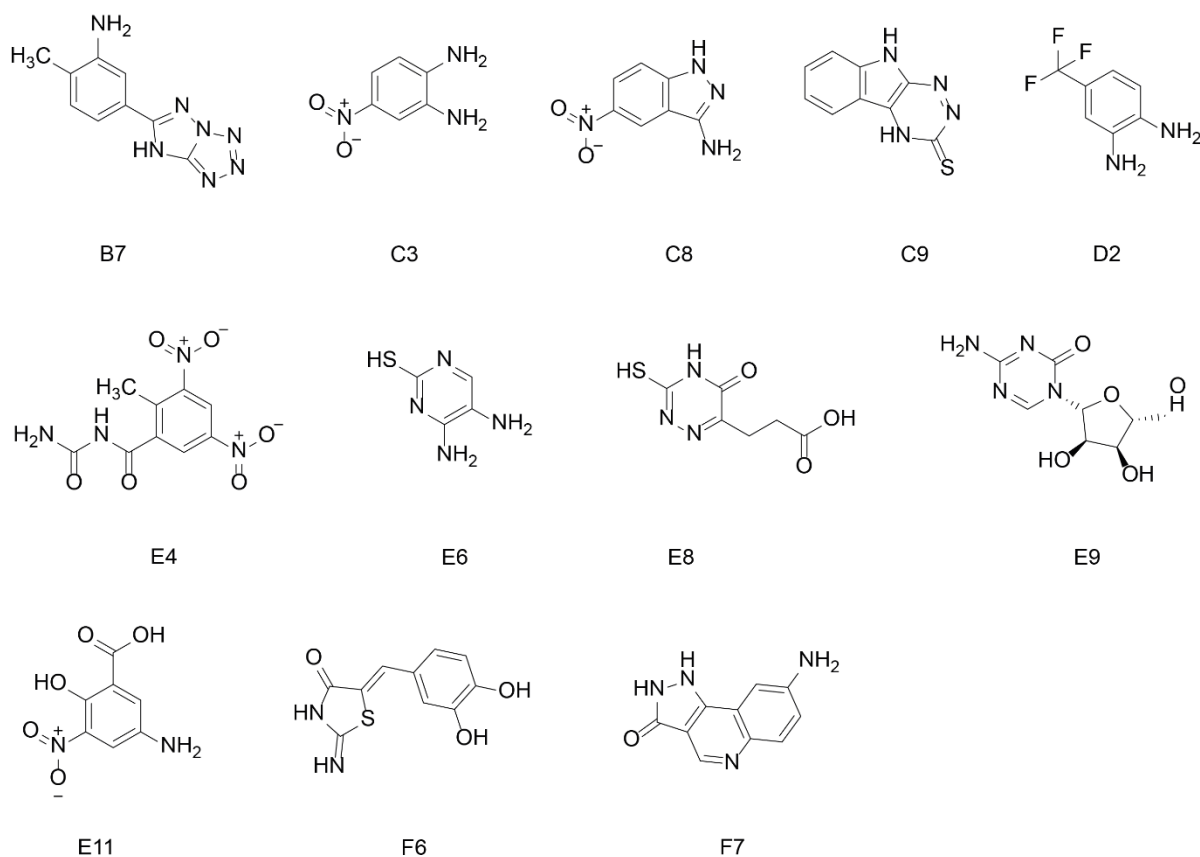


Figure 62: Chemical structures of *glmS* ribozyme self-cleavage inhibitors identified by screening the 1st generation Reymond compounds

Concentration-dependent analysis of the molecules B7, C3, C6, C8, D2 and D4 revealed that D2 is the most efficient inhibitor of *glmS* ribozyme cleavage and determined an IC_{50} value of 488 μ M.¹⁹⁹ The used compounds were obtained from Prof. Reymond's working group (University of Berne). Unfortunately, the obtained compounds were only supposed to be used for screening purposes and thus contained a certain amount of impurities. To address this issue, a concentration-dependent inhibition of GlcN6P-induced self-cleavage by D2 was analyzed utilizing a freshly bought stock of D2 with a purity of 97%. D2 was reconfirmed as concentration-dependent inhibitor of *glmS* ribozyme cleavage. However, a valid IC_{50} value determination was not possible, as the results shown in **Figure 15A** do not allow the calculation of an IC_{50} . Nevertheless, based on the concentration-

dependent inhibition of *glmS* ribozyme cleavage by D2 a search for isomers of D2 was performed. The constitutional isomers of D2, D2.1 and D2.2 (**Figure 63**) were subsequently analyzed regarding their inhibitory capacity in a concentration-dependent manner. While D2.1 (**Figure 15B**) did not show concentration-dependent inhibition of GlcN6P-induced *glmS* ribozyme self-cleavage, D2.2 (**Figure 15C**) did show inhibition. Regarding the data displayed in **Figure 15** it seems that the amino group in meta position to the trifluoromethyl group is crucial for inhibition of *glmS* ribozyme cleavage while the second amino group in *ortho* position (**Figure 15C**) enhances the inhibiting properties over the amino group in meta (**Figure 15A**). To improve understanding of the influence of the substituents on the inhibitory activity, another five derivatives with a benzotrifluoride structure (**Figure 16**) were investigated.

Hydroxyl and amino groups are well known bioisosteres. The definition of bioisosteres was redefined in 1991 by Burger as “compounds or groups that possess near-equal molecular shapes and volumes, approximately the same distribution of electrons, and which exhibit similar physical properties ...”.²⁰⁷ Based on their similar physicochemical properties, bioisosteres are usually comparably recognized in a biological context.²⁰⁷⁻²⁰⁸ The interchangeability of the amino and hydroxyl groups based on their similar steric size, spatial arrangement and their hydrogen donor acceptor properties has been demonstrated in the application of various drug discovery studies.²⁰⁸ Although this bioisosteric pair shares several physicochemical properties, differences as for instance the superior metal ion coordination by the amino group compared to the hydroxyl group²⁰⁷ most likely account for the difference observed for Reymond compounds and structural variants regarding the inhibition of *glmS* ribozyme cleavage.

The amino substituted benzotrifluoride derivatives 4-trifluoromethyl-aniline and 3-trifluoromethyl-aniline did not show any inhibition of *glmS* ribozyme cleavage. It seems that disubstituted benzotrifluoride derivatives are necessary for an inhibition of *glmS* ribozyme cleavage. The other three compounds tested for inhibition are variants of D2 and D2.2 in which one amino substituent has been exchanged for a hydroxyl group. 3-amino-4-hydroxy-benzotrifluoride and 2-amino-5-hydroxy-benzotrifluoride are not capable of inhibiting *glmS* ribozyme cleavage, but 2-hydroxy-4-trifluoromethyl-aniline (**Figure 16**) showed inhibition of GlcN6P-induced *glmS* ribozyme self-cleavage.

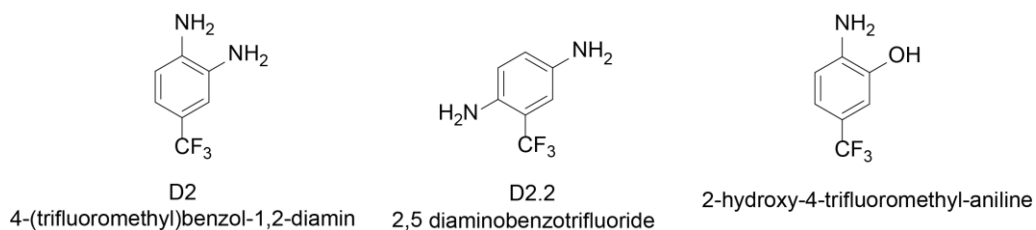


Figure 63: Chemical structures of *glmS* ribozyme self-cleavage inhibitors Reymond compound D2, the isomer D2.2 and the bioisosteres 2-hydroxy-4-trifluoromethyl-aniline

The investigation of those benzotrifluoride based compounds clearly shows the complexity of a structure activity relationship study. Slight chemical alterations decrease or increase the desired inhibitory activity, e.g. 3-amino-4-hydroxy-benzotrifluoride shows no activity and 2-hydroxy-4-trifluoromethyl-aniline shows activity. Regarding the inhibition of GlcN6P-induced *glmS* ribozyme cleavage by the in silico identified Reymond compound D2 and the isomer D2.2 revealed some first hints about the SAR. However, neither the isomer D2.1 nor four chemically related compounds were capable of inhibiting the cleavage of the *glmS* ribozyme. Together with the observation that the fifth tested compound, 2-hydroxy-4-trifluoromethyl-aniline is able to inhibit GlcN6P-induced cleavage this gives first glimpse into tolerated modifications for modulation of *glmS* ribozyme function.

4.1.2 *In silico* screening of *glmS* ribozyme modulators

Based on the findings of the 1st generation Reymond compounds and the analyzed derivatives, a second in silico screening was performed by the group of Prof. Reymond (University of Berne). In this, screening the group of Prof. Reymond used an algorithm that considers the 3D shape of the phosphate and the amine moiety of GlcN6P.^b As it was the case for the screening in the radioactive metabolite-induced cleavage assay, the *glmS* ribozyme of *S. aureus* was studied regarding modulation of self-cleavage by the 2nd generation Reymond compounds (details can be found in **section 6.2.16**). In contrast to the screening of the 1st generation Reymond compounds the potential of the compounds was not assessed by the radioactive metabolite-induced cleavage assay but by a FRET assay. This assay format is suitable for HTS and therefore is less time consuming.²⁰⁹ To evaluate the potential of an assay to be used in HTS screening a Z' value determination is performed. The Z' value quantifies the separation between positive and negative control, Z' value above 0.5 are generally accepted for pharmaceutical screenings. Blount *et al.* analyzed their assay by making use of the equation utilized to determine Z' values (**Equation 2, section 6.2.16**) and reported a Z' value of 0.64. For the herein used FRET assay a Z' value of 0.586 was determined. Although the Z' values determined herein is a bit lower than the one from Blount and coworkers

^b Personal communication of Prof. Reymond and Prof. Mayer

this Z' value still indicates that this assay utilizing the *S. aureus* Mu50 *glmS* ribozyme RNA instead of the *S. aureus* subsp. *aureus* Rosebach *glmS* ribozyme variant would be suitable for HTS. Besides the difference in construct utilized the size of values utilized to determine the Z' value might account for the differences.

The evaluation of the 2nd generation Reymond compounds lead to the identification of 115 putative *glmS* ribozyme modulators. The cut off determining inhibitors or activators of *glmS* ribozyme self-cleavage were chosen that broadly as no *glmS* ribozyme modulator should be overlooked. The compounds utilized for this screening contained a certain amount of impurities and therefore potential modulators of *glmS* ribozyme cleavage require re-evaluation in any way.

The screening for activation of *glmS* ribozyme self-cleavage revealed H6, I3, K6, K8, N1 and N8 (**Figure 17** and **Figure 64**). Moderate induction of self-cleavage was measured in the presence of compounds I8, J1, J3, J9, L7, M1, M5, N5, O1, O4, Q2, and R1 (**Figure 17** and **Figure 64**). Although H6 shows the most efficient activation of *glmS* ribozyme self-cleavage this finding needs to be reconfirmed by a non-fluorescence based assay e.g. the radioactive metabolite-induced cleavage assay, because H6 was shown to exhibit a high amount of fluorescence in buffer per se. The same is true for compounds K6, K8, J3, O1 and R1. Therefore, the remaining initially observed activators I3, N1 and N8 can be regarded as most promising. I3 is a substituted aromatic molecule with methoxy groups in position 1 and 2, a carbonyl group in position 5 and an amino group in position 4 (**Figure 64**). From the known *glmS* ribozyme activators it is evident that the amino group is crucial for activation (**section 1.7.1**). Compound I3 harbors the crucial amino group and, moreover, the methoxy groups in position 1 and 2 might mimic the hydroxyl group found in known *glmS* ribozyme activating compounds. In contrast N8 (**Figure 64**), which does not carry an amino group, in further studies would most likely turn out as false positive hit in further studies. In case of N1, the aromatic ring is functionalized by an acetamide in position 5 and a fluorine in position 2 as well as an amino group in position 1. The fact that N1 (**Figure 64**) carries an amino group might hint at potential activation potential and fluorine is a known bioisostere²⁰⁷⁻²⁰⁸ of hydroxyl groups. Nevertheless, the *glmS* ribozyme discriminates between even closely related molecules and, so far, it is not even known if an aromatic ring can compensate the properties of the sugar ring. Therefore, if I3, N1 or any of the other activators identified herein could function as *glmS* ribozyme activators this would be of utmost interest.

The fact that compound O4 showed up as both *glmS* ribozyme activator and inhibitor (**Figure 17** and **Figure 18**) most likely account for unspecific effects. Whether or not this is due to quenching or modification of the fluorophores or any other artificial effect with the RNA itself could in part be answered by performing radioactive assays.

Although the ability of compounds I8, J1, J9, L7, M1, M5, N5, and Q2 is not as pronounced as for H6, I3, K6, K8, N1 and N8, concentration-dependent analysis could reveal their potential as *glmS* ribozyme activators. From their chemical structure, compounds, which contain an amino group can be regarded as far more promising *glmS* ribozyme activators than those lacking the amino group. Nevertheless, re-screening and concentration-dependent analysis should reveal their potential.

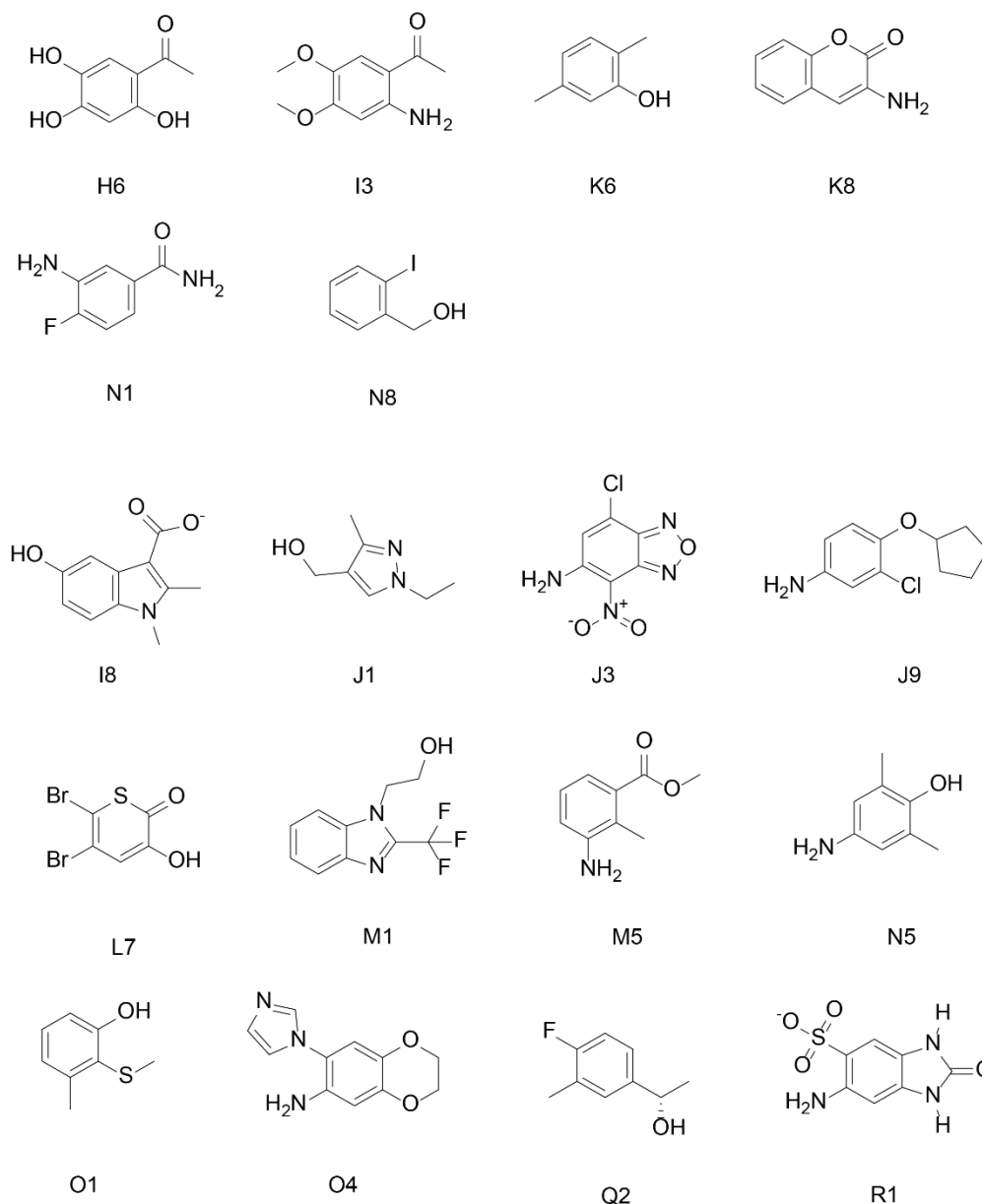


Figure 64: Chemical structures of potential *glmS* ribozyme self-cleavage activators identified by screening the 2nd generation Reymond compounds

From the 115 screened compounds the four compounds G1, H2, O4, and R4 were identified as clear inhibitors of GlcN6P-induced *glmS* ribozyme cleavage (**Figure**

18). As mentioned above, O4 was also identified as *glmS* ribozyme activator and therefore most likely exhibits unspecific effects. Compound G1 lacks an amino group and could be able to compete with GlcN6P for binding as Glc6P is also a known inhibitor. The aromatic ring in compound H2 is functionalized by a nitro group exhibiting a strong negative mesomeric effect (-M effect), whether this substitution is reflecting the physicochemical properties to act as *glmS* ribozyme inhibitor requires reinvestigation. From the identified inhibitors R4 might be the most promising hit. Some inhibitory potential was also observed in the presence of compounds G2, G3, H3, H4, H5, I1, J5, K3, K9, L5, M6, R7, and S1. Compound K3 partially reflects the geometry of D2.2 and therefore might also be functional as *glmS* ribozyme inhibitor. The other identified compounds that have some potential to inhibit *glmS* ribozyme self-cleavage are from a chemical perspective so diverse that at this point of the study there is no explanation for putative interactions with the *glmS* ribozyme.

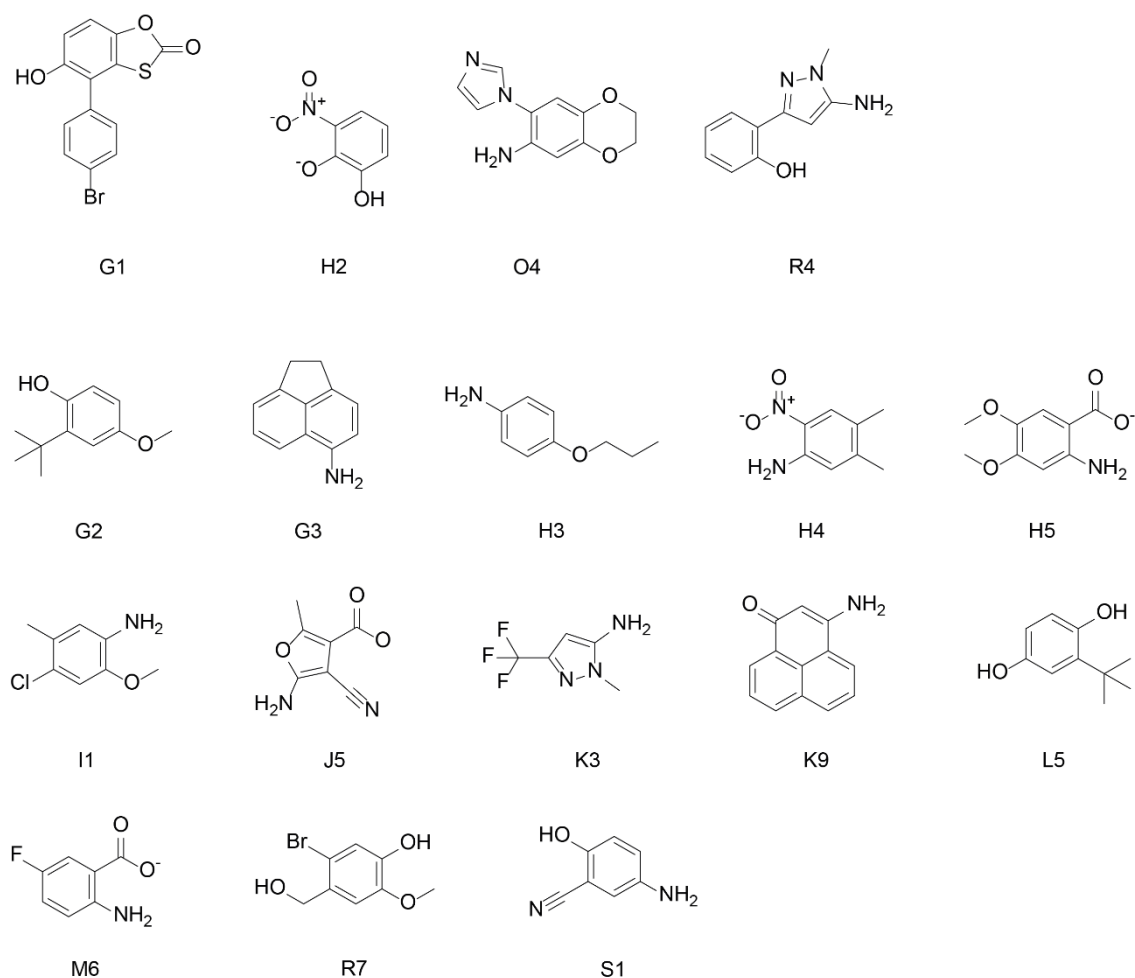


Figure 65: Chemical structures of potential *glmS* ribozyme self-cleavage inhibitors identified by screening the 2nd generation Reymond compounds

In contrast to the previously performed HTS screenings aiming at the identification of *glmS* ribozyme activators^{157, 159} this approach revealed a compound I3 that needs reconfirmation and concentration-dependent analysis, but might turn out as first novel *glmS* ribozyme activator identified by in silico screening.

4.2 MoA analysis CGlcN

To investigate the MoA of CGlcN it was decided to switch the organism studied from *S. aureus* Mu50 to *B. subtilis* 168. As *S. aureus*, *B. subtilis* is known to contain a *glmS* ribozyme in the 5'UTR of the *glmS* gene. Moreover, the *glmS* ribozyme variant of *B. subtilis* was also shown to be activated by CGlcN6P.¹⁵⁰ Although the *in vitro* impact of CGlcN6P is comparable with EC₅₀ values of 6.2 μ M and 2.1 μ M, for *S. aureus* and *B. subtilis*, respectively,^{150, 199} the effect of CGlcN treatment *in vivo* differs tremendously. For *S. aureus*, a rather high MIC value of 625 μ M was determined,¹⁹⁹⁻²⁰⁰ while it was shown in this study that CGlcN inhibits growth of *B. subtilis* 168 with an MIC of 150 μ M. This means that CGlcN treatment is more than 4 times more potent in inhibiting growth of *B. subtilis* as it is in inhibiting *S. aureus* growth. These findings favored the use of *B. subtilis* to study CGlcN activity as the amount of CGlcN available for this investigation was limited by time-consuming chemical synthesis.

B. subtilis is intensively studied and referred to as the gram-positive model organism. Hence, a center of commercially available *B. subtilis* strains was founded in 1978. In this, Bacillus genetic stock center (BGSC), diverse wildtype strains, cloning vectors or mutant strains can be directly ordered. This includes the PTS mutants, Δ GamP, Δ NagP and Δ PtsH utilized in this study. For comparison, modification of the genome of *S. aureus* by allelic replacement would be required. This technique is quite challenging and associated with varying success rates depending on the subspecies used.²¹⁰ Low efficacy of recombination and transduction frequency as well as the intrinsic restriction modification system protecting *S. aureus* from the uptake of foreign DNA as for instance bacteriophages can cause problems, especially if clinical isolates should be genetically manipulated.²¹¹ Moreover, most clinical isolates carry plasmids encoding antibiotic or resistance genes. Prior to genetic manipulation those plasmids should be removed to allow for easier selection and cultivation. Processes to free strains of these plasmids often involve steps utilizing mutagenic substances and therefore potentially manipulate the genetic material.²¹¹ All in all, it is beneficial and easier to use the transformable *B. subtilis* strain 168 that takes up foreign DNA more easily than utilizing the more difficult to manipulate *S. aureus*, of which even genetic competence to allow horizontal gene transfer is not fully understood.²¹¹⁻²¹³

Another more practical aspect corroborating the use of *B. subtilis* in this study regards the cultivation. Herein, CDM was used as growth medium. This minimal medium does not contain glucose or any other sugar component. To grow in CDM

bacteria have to adapt to the use of amino acids and nitrate as sole energy source. Apparently, *B. subtilis* 168 was more capable to adapt to these conditions than *S. aureus* Mu50. Although *S. aureus* was also able to grow in CDM, this turned out to be more difficult and time consuming as well as prone to failure, meaning that cultures did not always start to grow albeit they were efficiently inoculated. In addition, the growth of *S. aureus* in CDM was not always reproducible compared to *B. subtilis*. CDM was already used by Christina E. Lünse¹⁹⁹ as it seems likely that in sugar containing medium CGlcN would need to compete for uptake. This hypothesis is supported by the herein validated uptake route through bacterial sugar transporters, PTS. Even though it has not been analyzed, it seems logical that the uptake of CGlcN would be limited by the presence of sugars, especially GlcNAc in the growth medium.

A standard medium used to grow *B. subtilis* is LB-medium. The effect of CGlcN in LB-medium was analyzed and **section 3.2.6** reports that the growth inhibitory potency of CGlcN remains in LB-medium. LB-medium is usually composed of tryptone (10 g/l), yeast extract (5 g/l) and sodium chloride (5 g/l). Sometimes, sugars or various other components are added. However, the LB-medium used in this study was not supplemented with additional ingredients. Looking at the composition of LB-medium, it becomes clear that it does not contain any additional sugar source except for yeast extract (5 g/l). Yeast extract is mainly composed of amino acids, peptides and vitamins although it also contains carbohydrates. It was shown that LB-medium contains about 0.16% carbohydrates.²¹⁴ Interestingly, glucose, which is the preferred energy source of most bacteria, seems not to be present in significant concentrations.²¹⁴ The data (**section 3.2.6**) are showing that CGlcN is also effective in LB-medium with the same MIC as in CDM. The literature reports limited amount of carbohydrates in LB-medium²¹⁴ and this indicate that there might not be significant competition for the uptake of CGlcN by PTS in LB-medium. Nevertheless, the growth curve (**Figure 40**) reveals that the effect of CGlcN does not last for the same period of time as is the case when recording the same growth curve in CDM (**Figure 21**). This observation most likely correlates with the overall better growth of *B. subtilis* in LB-medium compared to CDM. The fact that the MIC determined after 16-20 h gives the same value in CDM and LB-medium while the growth curves show inhibition for 11.25 h in CDM and only for 5 h in LB-medium is based on the differences in cultivation. In case of the growth curves, plates are shaken. To assess MIC values, plates standstill in the incubator, to allow a better read out of the turbidity. This is associated with decreased airflow, which goes along with limited growth. Therefore, the 16-20 h time point measured in growth curves cannot be correlated to the growth after 16-20 h assessed in MIC determination experiments.

4.2.1 Uptake of CGlcN

CGlcN is charged under physiological conditions and it is therefore unlikely that CGlcN could passively enter bacterial cells. As CGlcN is structurally closely related to GlcN and GlcNAc it was assumed that CGlcN is taken up by bacterial PTS which concomitantly phosphorylate the cognate sugars during the uptake process. It is evident from *in vitro* cleavage assays¹⁵⁰ that the non-phosphorylated CGlcN has only minor *glmS* ribozyme activating properties. Therefore, a central requirement for the hypothesis (**Figure 20**) of CGlcN targeting the *glmS* ribozyme and thereby conferring growth inhibition relies on the uptake and subsequent phosphorylation of CGlcN by bacterial PTS. To address this question, PTS specific knock out strains of the different PTSs were analyzed.

Employing the PTS mutant strains deficient in the GlcN-specific (GamP), the GlcNAc-specific (NagP) or the global kinase domain (PtsH), it was revealed that CGlcN antibacterial activity depends on GamP, the GlcN-specific PTS and the subsequent phosphorylation conferred by the global kinase domain PtsH. Although this prodrug approach is beneficial, it is also prone to resistance development by alterations of the GlcN-specific PTS (GamP). Attempts to equip CGlcN with a phosphate mimicking group that potentially makes CGlcN independent of the bacterial PTS represents a promising strategy to circumvent the dependency on the uptake and eliminate potential resistance mechanisms.

Different phosphate mimicking groups are known in literature and one of the most famous phosphate mimics is the phosphonate. In these old-fashioned phosphate mimics the oxygen building the ester is exchanged for a carbon (**Figure 66**). This chemical replacement does not alter the size and shape much, however, it results in a change of charge.²¹⁵ A CGlcN6P variant carrying a phosphonate instead of a phosphate has been studied in regard to *glmS* ribozyme cleavage activation and could be shown to be capable of *glmS* ribozyme activation. However, the natural metabolite, GlcN6P, is 7 times more effective. The same was observed regarding a malonyl ester containing analog of GlcN6P.¹⁷⁰ A glucosamine 6-phosphate analog bearing a hydroxyphosphonate (**Figure 66**) instead of a phosphate in position 6 was tested and did not induce self-cleavage activity *in vitro*.²¹⁶ In addition, phosphonates are not very well suited for passive penetration of the membrane or bacterial cell walls as they often rely on endocytic uptake.²¹⁵ Although additional chemical groups can be introduced to support the entry of phosphonates, better choices represent phosphate mimics based on sulfonamides or sulfones (**Figure 66**). In case of the TPP riboswitch activator, TT derivatives bearing phosphate mimicks and metal chelating groups were analyzed and it was shown that the introduction of a sulfone group resulted in independency of the bacterial uptake and phosphorylation system.¹¹⁷

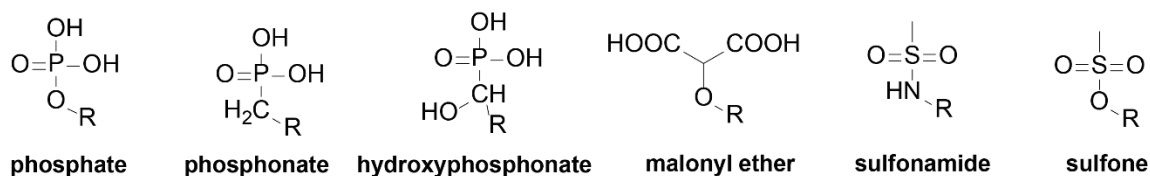


Figure 66: Chemical structure of phosphate and phosphate mimicking moieties

4.2.2 CGlcN reduces glmS ribozyme and gene levels intracellularly

The next step to prove the hypothesis concerning the MoA of CGlcN shown in **Figure 20** was to show that CGlcN treatment actually modulates *glmS* gene and ribozyme expression levels *in vivo*. This goal was achieved by performing quantitative real-time PCR. To analyze the effect of CGlcN on *glmS* mRNA and *glmS* ribozyme RNA, RNA was isolated from CGlcN-treated bacteria and compared to the RNA from untreated cells. Cells were grown to the early exponential phase ($OD_{600} \sim 0.3-0.4$) and then treated with CGlcN for 1 h. A study on *S. aureus* Mu50 revealed increased GlmS expression in the exponential growth phase.²⁰⁴ Other studies analyzing metabolic alterations utilizing qPCR assays or northern blot analysis build on RNA extractions also choose to harvest cells in the exponential growth phase.²¹⁷⁻²¹⁸ Due to the cultivation in CDM and the fact that bacteria did not grow as well in CDM as in common media it was decided to treat cells with an $OD_{600} \sim 0.3-0.4$ (instead of $OD_{600} \sim 0.6-0.7$ as used by others²¹⁷⁻²¹⁸) with CGlcN for 1 h prior to RNA isolation. The timeframe of 1 h for CGlcN treatment was chosen based on the growth curve analysis (**Figure 28** and **Figure 34**), which shows decreased growth after 1h in the presence of CGlcN.

In case of *B. subtilis*, a protocol for RNA isolation, cDNA synthesis, and real-time qPCR analysis could be established after a few optimization steps regarding the amount of lysozyme used to lyse the bacterial cells and the protocol used for efficient cDNA synthesis. The key step of validating the *glmS* ribozyme as antibacterial target is to demonstrate that the ribozyme is the intracellular target of CGlcN treatment. Therefore, the intention was to show the regulation of the *glmS* gene and ribozyme upon CGlcN treatment also for the human pathogen *S. aureus*. However, the isolation of total RNA from *S. aureus* turned out to be difficult and even after experimenting with several different lysis conditions the amount of isolated RNA was much less than that isolated from *B. subtilis*. The fact that the lysis was not efficient is most probably also the reason for the unreproducible qPCR results obtained for different biological replicates/preparations (**Figure 37**). Most likely, the lysis was inefficient because of the thickened cell wall of the *S. aureus* Mu50 strain.²⁰⁴ Other explanations might be found in the general difficulty of *S. aureus* to grow in CDM. This potentially goes along with a breaking down metabolism due to limited availability of resources and thereof associated differences in different experiments.

Concerning the final evaluation of qPCR analysis regarding the expression levels of *glmS* gene and *glmS* ribozyme of *B. subtilis* it could be shown that CGlcN treatment concentration-dependently reduces the expression levels of the gene and the ribozyme (**Figure 33**). Even the treatment of cells with a concentration of 1.5 μ M CGlcN (0.01x MIC) shows significant reduction of the *glmS* ribozyme and gene expression. A tremendous regulation reflected by ~60 fold reduced *glmS* mRNA levels was observed when applying 300 μ M CGlcN (2x MIC). Although potential side effects caused by CGlcN treatment cannot be excluded this data clearly shows that the *glmS* ribozyme and consequentially the *glmS* gene are targets of CGlcN action. These results corroborate the findings that showed that the *glmS* ribozyme regulates *glmS* gene expression *in vivo*.⁷¹

4.2.3 CGlcN treatment can be linked to bacterial cell wall biosynthesis

Nevertheless, it cannot be excluded that CGlcN treatment also causes side effects by addressing other targets. The analysis of stress inducible promotor strains clearly links CGlcN treatment to cell envelope damage. However, targets associated with the bacterial cell envelope and the cell wall, for instance the enzyme GlmM (**section 1.2.2**), might be influenced by CGlcN treatment.

The strain assigned to cell envelope stress harbors a plasmid, in which the *ypuA* promotor is in front of the firefly luciferase. *YpuA* was identified as biomarker of cell wall biosynthesis inhibitors and cell envelope stressing compounds in a transcriptional array analyzing the response of *B. subtilis* to various antibacterials.^{205, 219} It recognizes membrane dependent cell wall stress as well as membrane independent stress.²²⁰ The use of the *ypuA* promotor as indicator for cell envelope and cell wall stress has been validated for HTS assays by screening a library of 14000 compounds. Although the precise function of *ypuA* is unknown, it can be clearly correlated to cell wall and cell envelope stress. Due to its response to several antibacterial compounds as for instance vancomycin, polymyxin B and β -lactams, it can be regarded as key element in the cell wall biosynthesis pathway. The promotors indicative for the inhibition of protein (*heID*), RNA (*bmrC*) or DNA (*yorB*) synthesis (and DNA damage) are not induced upon CGlcN treatment. These marker genes were also identified in the former mentioned transcriptional profiling experiment. These genes are believed to assume important roles in the cognate biosynthetic pathways.

Although no induction of RNA stress was measured, *HeID* (formerly *yvgS*), which interacts with the DNA dependent RNA polymerase with supposed helicase activity, only responds to RNA stresses caused by impairing this key process.²²¹⁻²²² Thus it is still possible that CGlcN interferes with RNA based processes. Whether an sRNA based regulatory system to prevent the accumulation of phosphorylated sugars similar to the sRNA *SgrS* also exists in *Bacillus* and is

potentially an additional target of CGlcN treatment could be revealed by RNA sequencing.

Moreover, it should be determined if antibacterial effects of CGlcN can still be detected if other sugars are present in the bacterial growth medium. This would be especially interesting as sugar rich media are normally used to cultivate the analyzed species. For instance, *S. aureus* is often grown in BHI, a medium containing meat extract, which thus is rich in sugars. The PTS knock out strains analyzed here present only a limited set of transporters. However, from the data collected in this thesis, it cannot be excluded that CGlcN can also be transporter by PTS other than the GlcN specific GamP.

4.2.4 Perspectives based on the findings of CGlcN as antibacterial targeting the *glmS* ribozyme

The study presented in this thesis proves that the *glmS* ribozyme is a suitable antibacterial target. The potency of CGlcN with an MIC of 625 μM (133 $\mu\text{g/ml}$) for the human pathogen *S. aureus* is limited.¹⁹⁹⁻²⁰⁰ The potency of CGlcN in case of the commensal *B. subtilis* with an MIC of 150 μM (32 $\mu\text{g/ml}$) can be regarded as moderate from an antibiotic point of view. For comparison, potent antibiotics such as vancomycin exhibit a MIC of 8 $\mu\text{g/ml}$ in BHI for *S. aureus* Mu50.^{204, 223} However, comparing the potency of CGlcN and FC- α -D-GlcN with the antibacterial potential of other riboswitch activators reveals that overall the potency is comparable. For instance, L-4-oxalysine inhibits the growth of *B. subtilis* with an MIC of 173 μM and the other lysine analog, AEC, inhibits growth of *E. coli* with MIC of 5 μM .¹³⁶⁻¹³⁷ Likewise, the determined MIC value of >128 $\mu\text{g/ml}$ for roseoflavin inhibiting the growth of *E. coli* also falls within the same range as inhibition caused by CGlcN (MIC 133 $\mu\text{g/ml}$ for *S. aureus* and 32 $\mu\text{g/ml}$ for *B. subtilis*).¹⁴⁸ Interestingly, for ribocil an MIC of 2 $\mu\text{g/ml}$ was determined, meaning that ribocil is more potent than roseoflavin in inhibiting the growth of *E. coli* MB5746.¹⁴⁸ The example of the guanine analog PC1, for which it was shown that the guanine riboswitch is indeed not the main target causing the antibacterial effect^{138 139}, illustrates that it is crucial to consistently investigate and proof the central role of the riboswitch mediated gene regulation *in vivo*.

So far there are only a few examples of riboswitch targeting compounds that exhibit antibacterial activity and for which it was shown, all-encompassing, that the riboswitch is the main target. These examples include the study on AEC¹³⁷ and ribocil¹⁴⁸, where sequencing analysis clearly showed that mutations within the riboswitch sequence account for resistance development. The other example overarchingly demonstrating that antibacterial activity can be mediated by targeting a riboswitch consists of the herein described CGlcN, in which qPCR analysis clearly shows that CGlcN treatment affects the *glmS* mRNA and the *glmS* riboswitch region (**Figure 33**).

So far, we can only speculate about the clinical relevance of CGlcN including its oral availability. However, CGlcN and FC- α -D-GlcN potentially pave the way for the application of *glmS* ribozyme targeting drugs in the treatment of pathogenic bacteria. CGlcN and derivatives supposedly have potential in combinational therapy. In a synergistic approach, they might be able to rescue the effectiveness of drugs as for instance the bacterial cell wall targeting vancomycin. By impairing the bacterial cell wall, CGlcN or derivatives could help vancomycin to regain potency lost due to the development of thickened cell walls, one possible resistance mechanism of bacteria. In general, synergistic approaches get more value and are discussed when it comes to antibiotic stewardship. The use of broad spectrum antibiotics is more and more controversially discussed.

Advantages of CGlcN would be that the drug specifically addresses the bacterial GlmS and in contrast to broad spectrum antibiotics would not affect bacteria that do not harbor the *glmS* ribozyme as for instance commensal *E. coli* is in human gut.

4.3 Experimental validation of *in silico* predicted *glmS* ribozymes

As demonstrated in this thesis the *glmS* ribozyme represents a suitable and promising target for antibacterial research (**sections 3.2, 3.4**). For this reason and the general interest in the *glmS* ribozyme it was decided to analyze additional so far only computer predicted *glmS* ribozymes. From the list of predicted *glmS* ribozymes the ones found in bacteria that are most interesting for human health were chosen for validation.¹⁸⁴ This approach led to a list of seven putative *glmS* ribozymes predicted in the UTRs of the *glmS* genes of the following pathogenic bacteria: *C. difficile*, *L. monocytogenes*, *C. perfringens*, *E. faecium*, *E. faecalis*, *F. peridonticum*, and *F. nucleatum* (**section 1.1**). Of note is that the two fusobacteria were chosen due to the fact that they are gram-negative bacteria. Moreover, fusobacteria have implications in human health and are involved in periodontitis and cardiac diseases.²²⁴⁻²²⁵ So far, *glmS* ribozymes have been predicted in gram-negative bacteria but they have not been experimentally validated. The cell walls of gram-negative and positive bacteria have different architectures. Therefore, it would be interesting to analyze the effect of the *glmS* ribozyme on cell wall biosynthesis in gram-negative bacteria. The validation and characterization of *glmS* ribozyme variants in gram-negative bacteria potentially represents a great chance for drug discovery as they are hard to target bacteria.⁵

Although distinct sequences were predicted to have ribozyme function it was decided to use constructs comprising the whole IGR to analyze cleavage capabilities. Reasons for this decision were on the one hand that longer cleaved fragments are easier to separate on PAGE gels ("shorter" fragments might run out

of the gels while the full-length RNA did not even enter the gel). On the other hand, the more important reason for this decision was to ensure that no potential functional or stabilizing RNA is lost. In the beginning of ribozyme research, the reduction of RNA size to the minimal motifs was the goal. However, it was uncovered that the natural sequences of ribozymes as for instance the HHR or hairpin ribozyme contain segments that are indispensable for efficient function.²²⁶⁻²²⁷ Although these minimal motifs are catalytically functional they are impaired in folding and therefore are not fully functional.⁸⁶ Khvorova *et al.* discovered the answer to the conflicting question why the HHR required magnesium concentrations of around 15 mM for activity while in cells concentrations are presumably tenfold lower. They analyzed the natural full-length variant of the HHR and measured comparable cleavage rates at 70 μ M of magnesium.²²⁶ Similar effects regarding the activity of shortened versus full-length ribozyme sequences were discovered in case of the hairpin ribozyme.²²⁷

In a first attempt, the standard conditions utilized for cleavage reactions of the *glmS* ribozymes of *S. aureus* and *B. subtilis* were used to validate the self-cleaving properties of the putative *glmS* ribozymes of *C. difficile*, *L. monocytogenes*, *C. perfringens*, *E. faecium*, *E. faecalis*, *F. peridonticum* and *F. nucleatum*. In this first trial, the RNAs of *C. difficile* and *L. monocytogenes* showed self-cleaving properties. At this point it can only be concluded that the RNAs of *C. perfringens*, *E. faecium*, *E. faecalis*, *F. peridonticum* and *F. nucleatum* did not show cleavage in this experiment.

Besides the possibility that those particular RNA preparations were not intact or incorrectly folded or that any experimental error occurred in this one-time measurement it is also possible that the conditions of the initial screening do not meet those required for cleavage of these *glmS* ribozyme variants or that these proposed sequences are no *glmS* ribozymes.

The precise experimental conditions regarding ions, pH, timeframe, kinetic, temperature folding and metabolites are crucial for ribozyme cleavage.^{95, 153, 228} Therefore, further investigations starting with the novel preparation of RNAs are required to determine the properties of these putative *glmS* ribozymes.

At this point, it was decided to further characterize the sequences of *C. difficile* and *L. monocytogenes* and to postpone the validation of the other putative *glmS* ribozymes. The average maximal cleavage obtained for *L. monocytogenes* was with ~ 80% the highest compared to *C. difficile* with ~ 60% and *S. aureus* with ~ 40%. The constructs analyzed in this thesis all stem from already *in vitro* transcribed RNAs. It is known that cleavage rates of ~ 100% can be obtained if GlcN6P is added during transcription, indicating that the reaction *in vivo* is different from the reaction within the experimental setup.¹⁰⁴ The differences in overall cleavage measured in the herein performed assays most likely accounts for different folding effectivity.

4.3.1 Activators of *C. difficile* and *L. monocytogenes glmS* ribozyme self-cleavage

Paragraph 3.3 describes the experimental validation of the putative *glmS* ribozymes of the two human pathogens *C. difficile* and *L. monocytogenes*. The analysis of *glmS* ribozyme activators revealed the common sugars, GlcN6P, GlcNAc6P, GlcN6S and GlcN as activators of *C. difficile glmS* ribozyme self-cleavage (**Figure 46**). The results resemble the tendencies observed for known *glmS* ribozyme representatives e.g. *B. subtilis*, *B. anthracis* or *S. aureus* albeit a lower EC₅₀ value for the GlcN6P was determined.^{94, 150, 153} The EC₅₀ value for GlcN6P-induced self-cleavage of the *L. monocytogenes glmS* ribozyme represents a similarly high affinity for the natural metabolite as the variant of *C. difficile* with 0.38 µM. Both herein validated *glmS* ribozyme representatives exhibit remarkable affinity for GlcN6P as the affinities are about a factor of 10 higher compared to the *S. aureus glmS* ribozyme variant.¹⁵⁰ Astonishingly, GlcN did not show up as efficient inducer of the *L. monocytogenes glmS* ribozyme variant. Supported by the concentration-dependent analysis revealing an EC₅₀ value of 1920 µM for GlcN induced self-cleavage of the *glmS* ribozyme of *L. monocytogenes* (**Figure 47**), the results suggest that this ribozyme bears a unique discriminatory capacity against non-phosphorylated sugars. At this point, further investigation is required to elucidate the reason for this outstanding finding and it can only be speculated about a potential role of the nucleotides comprising the loop region within the ribozyme core. Besides the fact that the *glmS* ribozyme core region is known to contain all the crucial elements to confer the self-cleavage reaction (**section 1.7.3**), it has been demonstrated for other ribozymes, e.g. the HHR, that the composition and presence of loop regions alter ribozyme function.^{86, 226}

4.3.2 Divalent metal ions participating in *glmS* ribozyme self-cleavage of *C. difficile* and *L. monocytogenes*

The results of the initial screening for divalent cations promoting metabolite-induced *glmS* ribozyme self-cleavage revealed Mg²⁺, Ca²⁺ and Mn²⁺ as cleavage promoting ions (**Figure 48**). These three metal ions commonly show up as *glmS* ribozyme self-cleavage promoting ions.

In case of the initially described variant of *B. subtilis*, Co²⁺ as well as Sr²⁺ were also shown to promote cleavage.⁹⁴ A study on the *B. cereus glmS* ribozyme showed cleavage in the presence of Mg²⁺, Mn²⁺, and Ca²⁺. It is possible that Co²⁺ or Sr²⁺ also are capable of cleavage induction,¹⁵³ but this has not been addressed, probably due to their limited physiological relevance. These results were both obtained by performing assays at 23 °C in Tris buffer and plotting the logarithm of the k_{obs}. This setup differs from the conditions utilized in this thesis, which were HEPES buffer and an endpoint cleavage analysis after 30 min at 37 °C. The same conditions were used to analyze the dependency of *glmS* ribozyme self-cleavage

of *S. aureus*, therefore these data sets are well suited for direct comparison. It was shown that the *S. aureus* variant can utilize the following divalent metal ions for self-cleavage: Mg^{2+} , Ca^{2+} , Mn^{2+} , and Sr^{2+} .¹⁵⁰ In the herein performed analysis Sr^{2+} could not be shown to promote efficient self-cleavage of *C. difficile* and *L. monocytogenes*. However, it was identified as cleavage inducer of the *S. aureus* variant, although the capacity of Sr^{2+} , seems to be limited compared to the cleavage induction by Mg^{2+} , Ca^{2+} , Mn^{2+} . One explanation for the observation that Sr^{2+} is not capable of promoting cleavage of the *glmS* ribozyme variants of *C. difficile* and *L. monocytogenes* might be found when considering the constructs. The analyzed sequences were as formerly mentioned designed to comprise the whole IGR, therefore especially the *L. monocytogenes* construct is almost twice as long as the one that was used to assess the activity of the *S. aureus* variant.

It is assumed that longer RNA sequences benefit from the coordination by hydrated ions as these are capable of bridging larger distances. Moreover, larger RNAs are assumed to adopt more complex folds, which allow for specific interactions with certain metal ions.²²⁹ The comparison of the metal ion properties of Sr^{2+} , Mg^{2+} , Ca^{2+} , and Mn^{2+} uncovers that Sr^{2+} has the biggest ionic radius and exhibits the highest pK_a value of the aqua ion.²²⁹ These properties are potentially unfavorable for the induction of *glmS* ribozyme self-cleavage of *C. difficile* and *L. monocytogenes*.

As all the other domains of life, bacteria require metal ions for their survival. Metal ions function as cofactors for more than 30% of all bacterial proteins. Due to their essential role metal homeostasis is tightly regulated to ensure sufficient metal ion supply and protect the cell from toxic products e.g. hydroxyl radicals.²³⁰⁻²³² Concerning the concentrations of Mg^{2+} required to obtain half-maximal cleavage of the *C. difficile* and *L. monocytogenes* *glmS* ribozyme variants, EC_{50} values of ~ 70 μM and 25 μM , respectively, were determined (**Table 4**). These values are beneath the single-digit mM range of physiological Mg^{2+} concentrations.^{233 234} Intracellular Mn^{2+} concentrations of 100 nM are reported,²³⁵ while EC_{50} values for Mn^{2+} mediated *glmS* ribozyme cleavage of ~ 250 nM for *C. difficile* and more than 500 nM for the *L. monocytogenes* *glmS* ribozyme variant were determined (**Table 4**). Nevertheless, the intracellular amount of metal ions varies between the different bacterial species and environments. For instance, *L. monocytogenes* is found in diverse environments (**section 1.1**) e.g. in soil and food processing environments or inside host macrophages and phagolysosomes, which most likely accounts for the variable requirement of metal ions. The host immune system utilizes diverse metal ion dependent defense mechanisms that are either based on the restriction of metal ions, for instance by the Mn^{2+} chelating protein calprotectin, or by over-exposure of toxic metal ion concentrations.^{230, 232} These diverse and specialized conditions pathogens have to combat thus requires differently and precise control of cellular metal ion concentrations.²³⁰ Therefore, it cannot be ruled out that physiological Mn^{2+} concentration under specialized conditions could promote *glmS*

ribozyme self-cleavage. In case of Ca^{2+} , physiological concentrations in the range of 100-300 nM are reported,²³⁶ while EC_{50} values in the double-digit μM range were determined (**Table 4**). This means that intracellular Ca^{2+} concentrations are presumably not sufficient to promote *glmS* ribozyme self-cleavage. Taken together, it is evident that under physiological conditions *glmS* ribozyme self-cleavage would be promoted by Mg^{2+} and most likely not by Mn^{2+} or Ca^{2+} divalent cations.

4.3.3 pH dependency of *glmS* ribozyme self-cleavage of *C. difficile* and *L. monocytogenes*

The *glmS* ribozyme variants of *C. difficile* and *L. monocytogenes* were both shown to perform most efficiently in the physiological pH range of 6-8.5. These observations are overall in accordance with the published data on other *glmS* ribozyme variants. The *glmS* ribozyme of *B. subtilis* was shown to exhibit increased self-cleavage rates with rising pH until a plateau is attained at a pH of 7.⁹⁴ The study on the pH dependency of the *B. cereus glmS* ribozyme variant showed enhanced cleavage rates in correlation with increased pH.¹⁵¹ The pH dependency determination of the *S. aureus* variant reflects the herein utilized experimental setup in which cleavage was monitored after 30 min of incubation. The studies on the bacillus variants were conducted considering the kinetic of the cleavage reaction. Therefore, the results of *S. aureus glmS* ribozyme are best suited for comparison. The *S. aureus* version showed increased cleavage with increasing pH until a plateau at pH 7 is reached, like the *B. subtilis* variant. However, the two herein characterized *glmS* ribozymes are more responsive at lower pH compared to the *S. aureus* variant, which shows half maximal cleavage at ~ pH 6.5.¹⁵⁰ The *C. difficile* and *L. monocytogenes* variants showed this already at a pH between 5 and 5.5. The ability of these pathogens to grow or persist in environments associated with low pH might explain the observation that these *glmS* ribozymes are capable of cleaving at lower pH. *C. difficile* is causing pseudomembranous colitis (**section 1.1**); in the human intestinal tract where the pH ranges from 1.7-6.²³⁷ *L. monocytogenes* is equipped to persist in the low pH ranges associated with food-processing environments (**section 1.1**).

4.3.4 Kinetic of *glmS* ribozyme self-cleavage of *C. difficile* and *L. monocytogenes*

The observed cleavage rates for *C. difficile* and *L. monocytogenes* (**Figure 51**, **Table 5** and **Table 6**) support the concentration dependency formerly shown in the assays determining the EC_{50} values (**Figure 47** and **Table 3**). The *C. difficile glmS* ribozyme shows faster cleavage rates than the *L. monocytogenes* variant.

By comparing the GlcN6P-induced cleavage rates (k_{obs}), the following sequence starting with the fastest variant can be asserted: *B. subtilis* variant is the fastest so far characterized variant followed by the *C. difficile* and the *L. monocytogenes glmS* ribozyme and the *S. aureus glmS* ribozyme being the slowest (**section 3.3.5**).^{94, 150} Explanations for the observed differences regarding the speed of the cleavage reactions might be uncovered by exchanging parts of the respective nucleotide sequences, for instance exchanging the P1 loops and reassessing the cleavage rates.

4.3.5 Temperature-dependency of *glmS* ribozyme self-cleavage of *C. difficile* and *L. monocytogenes*

The analysis of the impact of different temperatures on GlcN6P-induced self-cleavage of *C. difficile* and *L. monocytogenes glmS* ribozymes lead to the interesting observation that the *L. monocytogenes glmS* ribozyme is almost as active at 6 °C as it is at 37 °C. The *C. difficile glmS* ribozyme showed reduced ability to cleave with decreasing temperature. The results on the *C. difficile glmS* ribozyme resemble the report on the *S. aureus glmS* ribozyme variant.¹⁹⁹ The *glmS* ribozyme of *S. aureus* was shown to dramatically lose cleavage activity at a temperature of 23 °C and below.¹⁵⁰ The *glmS* ribozyme of *B. subtilis* and *B. cereus* were initially characterized at temperatures of 23 °C where they show sufficient cleavage.^{94, 153} However, data on the behavior of those *glmS* ribozymes at lower temperatures is not available. Taking a broader look into other natural ribozymes and their catalytic functions at lower temperatures it turns out that the analyzed ribozymes e.g. CPEB3 and HHR show tremendously decreased activities at lower temperatures. The CPEB3 ribozyme is almost inactive at 22 °C.²³⁸ The same tendency can be seen for the HHR which reveals good activity at 37 °C and above but shows decreased cleavage with decreasing temperatures. Below 20 °C, cleavage activity is almost completely lost.²³⁹

The pathogen *L. monocytogenes* is, unlike the other bacterial species described herein, able to grow at refrigerating temperatures.³⁰ Moreover, *L. monocytogenes* is known to make use of RNA thermometers to control gene expression in a temperature dependent manner (**section 1.4**). Most prominent is the example of the RNA thermometer controlling the expression of the transcriptional activator PrfA involved in virulence induction.²⁴⁰ Therefore, it seems plausible that the *glmS* ribozyme of *L. monocytogenes* is capable of conferring *glmS* ribozyme self-cleavage at temperatures of 6 °C. However, the ability of the *glmS* ribozyme of *L. monocytogenes* to efficiently cleave at temperatures as low as 6 °C is most likely justified by the RNA sequence itself. The construct employed to assess cleavage of the *L. monocytogenes glmS* ribozyme is by far the longest sequence utilized to determine *glmS* ribozyme self-cleavage. The *glmS* ribozyme constructs analyzed in this thesis are composed of the whole IGR. Therefore, the *L. monocytogenes*

sequence contains 164 nt in front of the *glmS* ribozyme sequence and 77 nt afterwards. In contrast, the *C. difficile* construct harbors 31 nt in front and 46 nt after the *glmS* ribozyme sequence. However, the core of *glmS* ribozymes is highly conserved and, therefore, the *L. monocytogenes* ribozyme core resembles the core of other variants within the firmicutes. Nonetheless, *glmS* ribozymes as for instance the one of *Thermoanaerobacter radiovictrix* that show an unusual sequence as well as uncommon features as for instance cleavage at 50 °C are known.¹⁸⁴ The loop within the P1 domain of the *L. monocytogenes* *glmS* ribozyme comprises 39 nt compared to 12 nt for *B. subtilis*, 62 nt for *S. aureus* and 27 nt in case of the *C. difficile* variant. Based on the location within the ribozyme core the differences in nt composition and sequence could account for the different cleavage properties.

4.4 carba-sugar derivatives

The modified carba-sugars was synthesized to identify novel *glmS* ribozyme activators, which could potentially exhibit antibacterial activity (**section 2**). Moreover, the generation of a modified carba-sugars should allow to draw further conclusion on SAR regarding the *glmS* ribozyme and its metabolites. For this purpose, Daniel Matzner performed extensive chemical synthesis of five novel carba-sugar analogs, carba-variants of α -D-glucosamine and β -L-idosamine that are mono-fluorinated at the carba-position and the phosphorylated variants of these pseudo-sugars as well as a phosphorylated phenyl carba sugar. The fluorinated carba-sugars were chosen for synthesis for two reasons: To regain the H-bond between the ribozyme RNA and the GlcN6P ring oxygen that is lost in the carba-sugar, CGlcN6P, and because it was shown that fluorinated pseudo-sugars show improved performance compared to their non-fluorinated-counterparts.²⁴¹⁻²⁴²

In the initial screening for self-cleavage induction of the four different *glmS* ribozymes only FC- α -D-GlcN6P was able to efficiently activate the *glmS* ribozymes. Low *glmS* ribozyme activation was also observed in the presence of FC- β -IdoN6P and FC- α -D-GlcN. However, prominent activation by the two non-phosphorylated compounds, FC- β -L-IdoN, and FC- α -D-GlcN, was not expected as it is evident that the phosphorylation of *glmS* ribozyme activators is required to reach full activation.^{150, 156, 170, 243} The two new, herein characterized *glmS* ribozyme variants show better induction by FC- β -IdoN6P and FC- α -D-GlcN compared to the already known variants from *B. subtilis* and *S. aureus*. This on the one hand can be explained by the higher sensitivity those already exhibit for their natural metabolite, reflected by a difference of a factor of ~ 10 between the EC₅₀ of *S. aureus* and *L. monocytogenes* for GlcN6P (**Table 3**).¹⁵⁰ The sensitivity of the *B. subtilis* variant for the natural metabolite is even less, reflected by a half maximal activity at $\sim 200 \mu\text{M}$.⁹⁴ Interestingly, comparing FC- β -IdoN6P and FC- α -D-GlcN by trend it seems that the phosphorylated FC- β -IdoN6P can more efficiently activate

the *glmS* ribozyme of *L. monocytogenes* than the non-phosphorylated FC- α -D-GlcN, which exhibits the α -anomeric form crucial for *glmS* ribozymes.¹²⁹ The observed tendencies for the *C. difficile* *glmS* ribozyme show a higher cleavage induction by FC- α -D-GlcN than by FC- β -IdoN6P and seem to more closely reflect the situation for the *B. subtilis* *glmS* ribozyme variant (**Figure 55**). The idosamine compounds possess higher flexibility based on the ring-flip conformation, which due to the alteration of the carbon in position 5 influences the carbon in position 6 known to be required for precise positioning of within ribozyme ligand interaction. These properties do explain the overall weak to moderate performance of the idosamine compounds.

The concentration-dependent analysis revealed that ~ 50-100 times higher concentrations of FC- α -D-GlcN6P are needed to achieve cleavage comparable to CGlcN6P (**Figure 56** and **Table 8**). An explanation for this observation is given by molecular docking studies.²⁴⁴ By modeling FC- α -D-GlcN6P into the crystal structure of the *T. tengcongensis* *glmS* ribozyme bound to glucose-6-phosphate (PDB: 2Z74),¹⁵² it could be shown that the modification of CGlcN6P with the fluorine adds steric load that impairs the binding to the metabolite binding pocket. This finding once again highlights how complex it is to design metabolites that induce self-cleavage of the *glmS* ribozyme. Nevertheless, FC- α -D-GlcN6P represents another of the few so far identified artificial *glmS* ribozyme activators (**section 3.4**) and reveals novel insights into the recognition of activators by the *glmS* ribozyme.

Analogous to the studies on CGlcN bacterial assays were performed utilizing the non-phosphorylated FC- α -D-GlcN as prodrug. Interestingly, it could be shown that FC- α -D-GlcN behaves like GlcN in bacterial cell culture. FC- α -D-GlcN inhibits growth of *B. subtilis* with the same effectivity as CGlcN (MICs of 150 μ M) (**Figure 21** and **Figure 58**). Moreover, FC- α -D-GlcN seems to employ the same uptake route by the bacterial GamP PTS as CGlcN (**Figure 24** and **Figure 60**). The analysis of stress-inducible promotor-genes also revealed that CGlcN and FC- α -D-GlcN both selectively induce cell envelope damage. Therefore, the question remains why FC- α -D-GlcN in comparison to CGlcN shows ~ 50 -100 fold worse performance *in vitro* in comparison to CGlcN while the capacity *in vivo* is alike. Several different aspects could explain this. It could be that FC- α -D-GlcN is more efficiently transported by the bacterial GamP transporter or could enter the bacterial cell by another additional entry route yielding an overall higher intracellular concentration compared to the non-fluorinated CGlcN. Another option concerns the cellular MoA: It is possible that FC- α -D-GlcN intracellularly interacts with other targets than the *glmS* ribozyme. These would most likely be involved in cell-wall biosynthesis (**section 1.2.2**) as no DNA, RNA, or protein damage could be detected by the promotor-gene assay. However, further studies are required to address the question why a different *in vitro* performance of FC- α -D-GlcN and CGlcN does not result in a different *in vivo* performance.

5 Outlook

In this thesis, it was clearly proven that the *glmS* ribozyme is a suitable antibiotic target structure (**section 3.2**). Moreover, novel activators of *glmS* ribozyme self-cleavage were identified (**section 3.1** and **section 3.4**) and a SAR study revealed insights into the requirements of *glmS* ribozyme inhibitory compounds (**section 3.1.1** and **section 3.1.1.1**). The characterization of two novel *glmS* ribozyme variants of pathogens of human concern broaden the knowledge on the *glmS* ribozymes and unrevealed unique properties of the *L. monocytogenes glmS* ribozyme (**section 3.3**).

5.1 *glmS* ribozyme modulators with in silico predicted 3D shape similarity to GlcN6P

Commercially available benzotrifluoride based substrates with e.g. nitro, nitrile, fluoro, chloro and iodo substituents (e.g. 2-hydroxy-4-trifluoromethyl-aniline) indicate the broad scope of potential further hits using only benzotrifluoride based compounds. Testing these compounds in future screenings will lead to a better understanding of the mechanism of *glmS* ribozyme inhibition and might therefore enable researchers to predict potential activators of *glmS* ribozyme self-cleavage that might exhibit antibiotic potential.⁹⁷ The 1st generation of Reymond compounds also showed again how challenging the task to identify *glmS* ribozyme activators actually is. Based on these findings and under special consideration of the crucial amino group and the phosphate group of the ribozymes natural metabolite, GlcN6P, analysis of a second generation of compounds lead to the identification of some potential activators of *glmS* ribozyme self-cleavage. The potential of those identified hit compounds should be investigated by concentration-dependent analysis to verify their activity and to rule out artefacts. For this, it would be beneficial to investigate highly pure compound batches. The kinetic analysis of hits compounds that modulate *glmS* ribozyme activity should reveal further insights into the interaction with the *glmS* ribozyme and would allow for comparison with known *glmS* ribozyme modulators. Moreover, due to the fluorescent nature of some herein analyzed compounds re-screening these with the radioactive-metabolite cleavage-assay is inevitable. Finally, SAR studies of isomers and chemically related compounds of verified hit compounds should be conducted to potentially improve their properties regarding *glmS* ribozyme modulation.

5.2 The *glmS* ribozyme activators CGlcN6P and FC- α -D-GlcN6P and their MoA

Having assessed the MoA of CGlcN and FC- α -D-GlcN future studies may focus on the molecular and cellular consequences.

It is evident from qPCR experiments that the *glmS* ribozyme is the intracellular target of CGlcN(6P) (**Figure 33**). However, this has not been proven for FC- α -D-GlcN(6P). To prove the link to the *glmS* ribozyme qPCR experiments analog to the ones performed for the MoA analysis of CGlcN should be performed.

As the GlmS enzyme assumes a fundamental role in carbohydrate metabolism, interfering with the function of this enzyme potentially affects other parts of this pathway. It is of utmost importance to analyze potential other targets of CGlcN(6P) or FC- α -D-GlcN(6P) to verify potential side effects and to gain better understanding of compounds interfering with this essential metabolic process. The most obvious candidate is the enzyme GlmM, which catalyzes the next step in the cell wall biosynthesis pathway (**section 1.2.2**). Besides the identification of catabolic metabolites associated with GlmM function, which could be identified by LC-MS or metabolomics, concerted analysis regarding the function of GlmM in the presence of CGlcN might be performed utilizing purified GlmM protein in enzyme assays.

The analysis of PTS knock-out strains revealed that the action of CGlcN depends on the presence of the GlcN-specific PTS (GamP) and the global phosphorylation domain (PtsH) (**Figure 24**). It is evident from the literature that PTSs phosphorylate the sugar substrate during transport.²⁴⁵ Therefore, the resistance of the PtsH knock out strain against CGlcN treatment implies that the phosphorylated variant CGlcN6P is intracellularly available in the wt strain. Anyway, this data only indirectly provides evidence for the formation of CGlcN6P. By performing metabolomics either employing LC-MS/GC-MS or ESI-TOF analytics the intracellular/*in vivo* formation of CGlcN6P could be proven in CGlcN treated cell extracts. The use of LC-MS/GC-MS techniques potentially also reveals information about the accumulation or reduction of sugar molecules like for instance Fru6P or GlcN1P.

Passaging of *B. subtilis* in the presence of CGlcN will most likely lead to the development of resistances against CGlcN. It would be interesting to search for mutations of the *glmS* ribozyme region that no longer allow the recognition of CGlcN6P. This would be associated with a lack of *glmS* ribozyme self-cleavage in the presence of CGlcN6P and, subsequently, the GlmS enzyme would not be impaired. Alterations of the bacterial PTS that do not allow CGlcN to enter the cell or that permit efficient phosphorylation of CGlcN could also be developed by bacterial cells as protection mechanisms against CGlcN action.

The promotor-gene assays showed that CGlcN and FC- α -D-GlcN treatment induce cell envelope damage (**Figure 39** and **Figure 61**). These findings are in line with the hypothesis of carba-sugars targeting the *glmS* ribozyme, thereby reducing *glmS* mRNA levels and causing growth inhibition (**Figure 20**). Nevertheless, it is of interest to analyze if and how the cell wall is impaired by CGlcN or FC- α -D-GlcN treatment. To address this, the bacterial cell wall should be analyzed by electron-cryomicroscopy in the presence and absence of CGlcN or FC- α -D-GlcN. If labeled

compounds were, used it would be possible to visualize whether CGlcN or FC- α -D-GlcN are implemented in the bacterial cell wall or if the compounds are located elsewhere in the cell.

Proteomics and transcriptomics could be applied to identify proteins or RNAs that are regulated upon CGlcN treatment. In the gram-negative bacterium, *E. coli*, a small RNA, SgrS is known that is regulated upon accumulation of phosphorylated sugars (**section 1.4**). So far, no such analog has been described in gram-positive bacteria, but it would be interesting to either prove or disprove the presence of such a mechanism in gram-positives. Studies on *glmS* ribozyme targeting compounds might contribute to the discovery of such an analog.

Glc is the preferred energy source. Although it was shown herein that CGlcN is transported by the GamP specific PTS, the question whether CGlcN or FC- α -D-GlcN are taken up by bacteria if Glc is present should be addressed by assessing the effect of CGlcN or FC- α -D-GlcN in Glc supplemented medium.

As mentioned, homologs of the prokaryotic GlcN6P-synthase, *GlmS*, can be also found in mammals, e.g. humans. GFAT1 and GFAT2 structurally differ from the prokaryotic *GlmS*.¹⁷⁹ Nevertheless, experiments would be needed to rule out off-target effects of CGlcN with the human enzyme. Toxicity tests in eukaryotic cell culture would hint about the applicability of CGlcN or FC- α -D-GlcN. *In vitro* experiments analyzing the response of GFAT1 and GFAT2 to CGlcN or FC- α -D-GlcN should be performed as the expression of those genes has been shown to vary in different tissues and can therefore only be analyzed to a limited extend in cell culture.

Within this study it could be demonstrated that the *glmS* ribozyme is indeed a suitable antibacterial target. This fact raises hopes with regard to the urgent need of developing novel antibiotics. Moreover, the *glmS* ribozyme represents a target structure that so far is not by addressed drugs, which potentially makes it favorable with regard to resistance development. Nevertheless, the herein identified compounds CGlcN and FC- α -D-GlcN are not at all suitable for antibiotic therapy yet, as several unsolved questions regarding toxicity and bioavailability have to be solved. However, this proof of concept study lays the foundation for further studies and could potentially lead to the discovery of improved GlcN6P analogs targeting the *glmS* ribozyme that might enter clinical trials.

5.3 Validation and characterization of novel *glmS* ribozyme variants

The putative *glmS* ribozymes of the human pathogens *C. perfringens*, *E. faecium*, *E. faecalis*, *F. peridonticum*, and *F. nucleatum* should be validated and characterized in the same kind of fashion as reported herein for the *glmS* ribozyme

of *C. difficile* and *L. monocytogenes*. It should begin with the preparation of fresh RNAs to be analyzed under the common conditions (**section 3.3**). Further studies should also investigate differences in ion dependency, temperature and activating metabolites, kinetic and pH.

The in this thesis validated and characterized *glmS* ribozymes of *C. difficile* and *L. monocytogenes* revealed interesting novel insights into the exhibited sensitivity and selectivity of *glmS* ribozymes for their natural metabolite, GlcN6P. Especially, the high discrimination of the listerial *glmS* ribozyme for phosphorylated versus non-phosphorylated metabolites as well as the tolerance to low temperatures reveals novel unexpected insights into the otherwise highly conserved nature of *glmS* ribozymes. In follow-up studies, it would be of high interest to address these differences and to find explanations for these properties within the RNA sequence. Ways to address this question should include shortening of the employed constructs to the by McCown *et al.* predicted ribozyme sequence.¹⁸⁴ Importantly, comparisons between the P1 loop domains, located within the ribozyme cores, should be made and exchanges of the loop regions of the *glmS* ribozymes should give further insights into the different properties of these *glmS* ribozymes.

It would be very interesting to analyze whether the *in vitro* demonstrated higher sensitivity for GlcN6P of the *glmS* ribozymes of *L. monocytogenes* and *C. difficile* can also be detected for artificial *glmS* ribozyme activators as for instance CGlcN6P or FC- α -D-GlcN6P. If this hypothesis would hold true it would be of relevance to analyze the effect of the corresponding non-phosphorylated prodrugs with regard to inhibition of bacterial growth and MICs.

6 Material & Methods

6.1 Material

6.1.1 Equipment

Equipment	Manufacturer
Agarose gel camera, UV-transilluminator	Bio-Rad Laboratories
Agarose running chamber	In house construction, peqlab
Analytical balances	Sartorius
Autoclave	Systec
Bioscript	Bioline
Centrifuges	Eppendorf, Sigma
Counter	Berthold
Disposable cuvettes	Roth
Electrophoresis Power supply	Consort
Electrophoresis apparatus	In house construction
EnSpire	Perkin Elmer
Eppi racks	Roth
G25 columns	GE healthcare
Glass plates for PAGE	Baack
Glass plates (sequencing gel)	Bio-Rad
Glass pipette tips	Hirschmann
Glasswool silianized	Serva
Heating blocks	Bachhofer
Image eraser	Raytest
Image master VDS	Amersham biosciences
iQ5 real-time PCR detection system	Bio-Rad
Liquid Scintillation counter	PerkinElmer
Membrane filters 25µm, 45µm	Sigma-Aldrich, Whatman
NanoQuant infinite 200	Tecan
NanoDrop	Peqlab
Parafilm	Faust
PCR Thermocycler	Biometra, Eppendorf
pH meter	Inolab
Phosphorimager cassettes	Fuji
Phosphorimager screens	Fuji
Phosphorimager FLA-3000	Fujifilm
Pipettes	Eppendorf, Gilson
Pipette tips	Sarstedt
Pipetteboy Acu-jet Pro	Brand
Plastic foil	Roth
Radioactive protection shield	Nalgene
Random hexamers	Invitrogen
Reaction tubes 0.2 ml, 0.5 ml, 1.5 ml, 2 ml	Eppendorf
PCR multiply µ strip 0.2ml Kette	Sarstedt

PCR 8er Deckelkette flach	Sarstedt
Refrigerators and Freezer 4°C, -20°C, -80°C	AEG, New Brunswick, Liebherr
Scalpel blades	Labormedic
Sequencing gel chamber	Bio-Rad
SpectraMax	Molecular Devices
Sterile hood antair	Thermo scientific
Tecan sunrise	Tecan
Thermomixer 1.5 ml, 2 ml	Eppendorf, HLC
Thermomixer HLC 2 ml	Ditabis
Vortex	Neolab
Water bath	GFL, Julabo
96-well plates black half area	Greiner
96-well plates transparent round bottom	Sarstedt

6.1.2 Chemicals

Reagents	Manufacturer
2,3-Diaminobenzotrifluoride	Abcr
2,5-Diaminobenzotrifluoride	Abcr
2-amino-5-hydroxybenzotrifluoride	Apollo
3-amino-4-hydroxybenzotrifluoride	Abcr
4-Fluoro-2-nitroaniline	Sigma
4-(trifluoromethyl)benzotrifluoride	Abcr
(5a <i>R</i>)-fluoro-carba- α -D-GlcN6P (FC- α -D-GlcN6P)	Synthesized by Daniel Matzner
α -D-carba glucosamine hydrochloride (CGlcN)	Synthesized by Magnus S. Schmidt
α -nicotinamid adenine dinucleotide (NAD)	Sigma
Adenine	Sigma, Alfa Aesar
Agarose	Lonza
Ammoniumpersulfat (APS)	Roth
Bovine serum albumin	Calbiochem
Bioscript	Bioline
Biotin	Fluka
Boric acid	AppliChem
Bromphenol blue	Merck
Calcium chloride dihydrate	Kmf Chem
Calf intestine alkaline phosphatase (CIAP)	Promega
Chloroform	Roth
Chloramphenicol	Sigma
Ciprofloxacin hydrochloride	AppliChem
Cobalamine	Sigma
Columbia blood agar plates	Becton Dickinson
Dibasic potassium phosphate	Sigma
Dichlorodimethylsilane	Acros organics
Diethylpyrocarbonate (DEPC)	Roth

Material & Methods

Dimethylsulfoxide (DMSO)	Sigma
DL-alanine	Sigma
DL-histidine	Sigma
1,4-Dithiothreitol (DTT)	Roth
DNase I	Roche
D-panthoic acid	Serva
Ethanol	VWR
Ethidium bromide	Roth
Ethylendiamintetraacetic acid (EDTA)	AppliChem
fluoro-carba- α -D-GlcN (FC- α -D-GlcN)	Synthesized by Daniel Matzner
fluoro-carba- β -L-IdoN6P (FC- β -L-IdoN6P)	Synthesized by Daniel Matzner
Fluoro-carba- β -L-IdoN (FC- β -L-IdoN)	Synthesized by Daniel Matzner
Folic acid	Serva
D-Fructose-6-phosphate dipotassium salt	Sigma
D-Glucosamine	Sigma
D-Glucosamine 1-phosphate	Sigma
D-Glucosamine 6-phosphate	Sigma
D-Glucosamine 6-sulfate	SantaCruz
D(+)-Glucose	Sigma
D-Glucose 1-phosphate disodium salt hydrate	Sigma
D-Glucose-6-phosphate dipotassium salt hydrate	Sigma
Glycine	Serva
Guanine HCl	Sigma
HEPES Pufferan	Roth
Inorganic pyrophosphatase (IPP)	Roche
Iron(III)nitrate nonahydrate	Sigma
Iron(II)sulfate heptahydrate	Merck
Isopropanol	Merck
L-asparagine	Serva
L-arginine	Merck
L-cysteine	Serva
L-glutamic acid	Merck
L-glutamine	Sigma
L-hydroxyproline	Sigma
L-isoleucine	Sigma
L-leucine	Serva
L-lysine	Serva
L-methionine	Merck
L-phenylalanine	Serva
L-proline	Sigma
L-serine	Merck
L-threonine	Serva
L-tryptophane	Serva
L-tyrosine	Serva
L-valine	Merck

Material & Methods

LB-medium	Roth
Luciferin	Sigma, Serva
Lysostaphin	Sigma, Segenetic
Magnesiumchloride	Roth
Magnesiumsulfate hydrate	Roth
Manganesesulfate	Sigma
Mueller-Hinton agar plates	Oxoid, Becton Dickinson
N-Acetyl-D-Glucosamine	Sigma
N-Acetyl-D-glucosamine 6-phosphate sodium salt	Sigma
N-Acetylmuramic acid	Sigma
N-Acetyl- α -D-glucosamine 1-phosphate disodium salt	Sigma
Nicotinamid	Sigma
p-aminobenzoic acid	Serva
Phenol	Roth
phenyl-carba- α -D-GlcN6P (PhC- α -D-GlcN6P)	Synthesized by Daniel Matzner
Potassium chloride (KCl)	Roth
Potassium dihydrogen phosphate	Fluka
Pfu polymerase	In house production, Ak Famulok; Nicole Krämer
Pyridoxal HCl	Sigma
Pyrodoxamine-di-HCl	Sigma
Random hexamer	Life technologies
Riboflavin	Serva
Rifampicin	AppliChem
RNasin	Promega
RNA protect bacteria	Qiagen
Rotiphorese sequencing gel concentrate Bis-Acrylamid	Roth
Sodium acetate trihydrate	Merck
Sodium hydrogen carbonate	VWR
Spermidine trihydrochlorid	Sigma
sucrose	Acros organics
SuperHot Taq-polymerase für qPCR	Genaxxon bioscience
Thiamine HCl	Serva
T4 Polynucleotide kinase (PNK)	NEB
T7 RNA polymerase	In house production, Ak Famulok; Nicole Krämer
N,N,N,N-Tetramethylethylendiamide (TEMED)	Roth
Uracil	Sigma
Urea	AppliChem
Vancomycin hydrochloride	AppliChem

6.1.3 Solutions, Buffers

Solution	Ingredient
DEPC water	1:500 DEPC
<u>Solutions for PAGE:</u>	
Solution B	8.3 M Urea in 10x TBE
Solution C	Rotiphorese Sequenziergel Konzentrat
Solution D	8.3 M Urea

Buffer	composition
2x Agarose DNA loading buffer	50 mM Tris/HCl 50 mM EDTA 50% Glycerine (v/v) pH 8
2x Agarose RNA loading buffer	9.5 ml Formamide 25 µl 10% SDS 10 µl 0.5 M EDTA 0.5 ml water bromphenol blue
10x Cleavage assay buffer	500 mM HEPES 2 M KCl pH 7.5
Luciferase buffer (promotor-gen assay)	2 mM Luciferin 100 mM Citrate-buffer pH 5
2x PAGE sucrose loading buffer	45 mM HEPES 45 mM Boric acid 4 M Urea 10% sucrose 0.05% SDS 100 mM EDTA
10x TBE buffer	890 mM Tris/HCl 890 mM boric acid 20 mM EDTA pH 8.0

6.1.4 Kits

Product	Manufacturer
PCR clean up kit (NucleoSpin Extract II)	Macherey & Nagel
G25 column	GE HealthCare
PCR purification (cDNA)	Fermentas
GeneJET PCR purification kit	Life technologies
PrestoSpin R Bug	Molzym
RNeasy Min Elute Clean-up	Qiagen
RNeasy protect bacteria Mini kit	Qiagen
Sequenase Version 2.0 PCR product sequencing	USB

6.1.5 Chemically defined medium

Component	Amount [mg]
Group I	
FeSO ₄ x 7 H ₂ O	5
Fe(NO ₃) ₃ x 9 H ₂ O	1
MnSO ₄	5
dissolve in 1 ml H ₂ O	
Group II A	
L-tryptophan	100
L-cystein	50
dissolve in 1 ml 2 N HCl at 55 °C	
Group IIB	
L- leucine	100
DL-alanine	100
L-isoleucine	100
L-methionine	100
L-threonine	200
L-arginine	100
DL-histidine	100
L-valine	100
L-lysine	100
L-glutamine	100
dissolve in 10 ml H ₂ O	
Group IIC	
L-asparagine	100
L-phenylalanine	100
L-serine	100
L-proline	100
L-hydroxyproline	100
L-glutamic acid	100
Glycine	100
L-tyrosine	100
dissolve each amino acid in 1 ml 2.5 N NaOH at 55°C	
Group III	
p-aminobenzoic acid	0.2
Biotin	0.2
Folic acid	0.8
Nicotinamid	1
α-NAD	2.5
D-panthoic acid	2
Pyridoxal HCl	1
Pyrodoxamin-di-HCl	1
Riboflavin	2
Thiamine HCl	1
Cobalamine	0.1
dissolve components in 10 ml H ₂ O and dropwise addition of 2.5 N NaOH until the solution becomes clear	

Group IV	
Adenine	20
Guanine HCl	20
Uracil	20
dissolve in 3 ml 2 N HCl at 90 °C	
Group V	
K ₂ HPO ₄	200
KH ₂ PO ₄	100
	0
MgSO ₄ x H ₂ O	700
CaCl ₂ x 2 H ₂ O	7
NaOAc x 3 H ₂ O	450
	0
NaHCO ₃	250
	0
HEPES	130
	00
dissolve components in 300 ml H ₂ O	
H ₂ O ad 500 ml	

6.1.6 Bacterial strains

Organism	Mutation/Specification	origin
<i>S. aureus</i> Mu50	VISA	Kind gift of K. Hiramatsu
<i>B. subtilis</i> 168 wt		Deutsche Stammsammlung
<i>B. subtilis</i> 1S34 pS 63	helD	kind gift of C. Freiberg, constructed in ²⁰⁵
<i>B. subtilis</i> 1S34 pS 130	yvql	kind gift of C. Freiberg, constructed in ²⁰⁵
<i>B. subtilis</i> 1S34 pS 77	yorB	kind gift of C. Freiberg, constructed in ²⁰⁵
<i>B. subtilis</i> 1S34 pS 107	ypuA	kind gift of C. Freiberg, constructed in ²⁰⁵
<i>B. subtilis</i> 1S34 pS 72	bmrC	kind gift of C. Freiberg, constructed in ²⁰⁵
<i>B. subtilis</i> 168 ΔptsH::erm	Δhpr	BGSC #: BKE13900
<i>B. subtilis</i> 168 ΔgamP::erm	ΔgamP	BGSC #: BKE02350
<i>B. subtilis</i> 168 ΔnagP::erm	ΔnagP	BGSC #: BKE07700

6.1.7 Standards, nucleotides

Type	Length	Manufacturer
DNA ladder	100-10000 bp	PeqLab
DNA ladder	100-1000 bp	PeqLab
RNA ladder	Low range	Fermentas
RNA ladder	High range	Fermentas

γ ³²P-ATP purchased by Perkin Elmer.

6.1.8 Synthetic oligos

Name	Sequence (5'-3')
5' T7 <i>C. difficile</i>	TCGTAATACGACTCACTATAGGTTTAAAGG GTATTCTC
3' <i>C. difficile</i>	TAGGTCATATAAGTTTACTTTGGCTTCCC
5' T7 <i>C. perfringens</i>	TCGTAATACGACTCACTATAGGTAATAAAAGAAGGA AGGG
3' <i>C. perfringens</i>	CAATTTCTATCTATAAATGAATAAGGTTCTAA
5' T7 <i>E. faecalis</i>	TCGTAATACGACTCACTATAGGACGATTAAGGATGA A
3' <i>E. faecalis</i>	CATGAAAGAGAATGATACTCACATGATCTA
5' T7 <i>E. faecium</i>	TCGTAATACGACTCACTATAGGATATTGATAGGAGG A
3' <i>E. faecium</i>	AATGAGGAGGAGATAGGCTAATG
5' T7 <i>F. nucleatum</i>	TCGTAATACGACTCACTATAGGTATCTCTAACAATG
3' <i>F. nucleatum</i>	AATACATTTTCTTCGCGGTC
5' T7 <i>F. peridonticum</i>	TCGTAATACGACTCACTATAGGTAATATATAAACTCA TTATAA
3' <i>F. peridonticum</i>	CAAAAAGGTGATCAAGCTAATTA
5' T7 <i>L. monocytogenes</i>	TCGTAATACGACTCACTATAGGTCAGCTCGCTCCTT TTTGTATC
3' <i>L. monocytogenes</i>	AGTAAACTCCTCCAATAATTAAGTTGAGGGC
5' T7 <i>S. aureus</i>	TCGTAATACGATCACTATAGGTAATGATTAATGGAAA GGGG
3' <i>S. aureus</i>	ATCTTATTAAGTTTGTCCATTAAGTCACCC
5' <i>S. aureus</i> FRET	TAATACGACTCACTATAGGTATTTGTAGACGAGGAG
5' <i>S. aureus</i> FRET substrate	Cy3-AAGCGCCUGUGCAAA-FAM
5' T7 <i>B. subtilis</i>	TCGTAATACGACTCACTTAGGTCTTGTTCTTATTTCT C
3' <i>B. subtilis</i>	GTCCCCTTCCTACATGTTTTTTGGA
RS+ <i>glmS</i> gene <i>S. aureus</i> probe	Cy5-ACGCGTACTATTCCAATATGGAGGA-BHQ
<i>glmS</i> gene <i>S. aureus</i> probe	Cy5-TCGGTCACACACGTTGGGCA-BHQ
16 rRNA <i>S. aureus</i> probe	FAM-CCTTTGACAACCTCTAGAGATAGAGCCTTCCC- BHQ

5' qPCR RS+glmS gene <i>S. aureus</i>	CAAAGTTAATAAGATCGCCAGAA
3' qPCR RS+glmS gene <i>S. aureus</i>	AATATAACCAACAATTCCACACAT
5' qPCR glmS gene <i>S. aureus</i>	GATTTTGGATGGACCTGTTG
3' qPCR glmS gene <i>S. aureus</i>	AGTTTTTCATGATTCGGTACAC
5' qPCR 16 rRNA <i>S. aureus</i>	CGGTCCAGACTCCTACGGGAGGCAGCA
3' qPCR 16 rRNA <i>S. aureus</i>	GCGTGGACTACCAGGGTATCTAATCC
5' T7 RS+gene <i>S. aureus</i>	TCGTAATACGACTCACTATAGGCAAAGTTAATAAGATCGCCAGAA
5' T7 gene <i>S. aureus</i>	TCGTAATACGACTCACTATAGGCGATTTTGGATGGACCTGTTG
5' T7 16rRNA <i>S. aureus</i>	TCGTAATACGACTCACTATAGGCGGTCCAGACTCCTACGGGAGGCAGCA
5' <i>B. subtilis</i> RS	AACTAAGCGCCCGGAAAA
3' <i>B. subtilis</i> RS	TTTGTTCAAGGAGTCACCCC
<i>B. subtilis</i> RS probe	FAM-ACCTCCATCCTCGTCAACTAAGCCT-BHQ
5' <i>B. subtilis</i> gene	GATGCCAATGTAGAAGCGAAAG
3' <i>B. subtilis</i> gene	GTGAACAAGTGTAAGCGGC
<i>B. subtilis</i> gene probe	Cy5-ACACGGCGAACCAAGCTATCTGAA-BHQ
5' <i>B. subtilis</i> 16 rRNA	CGTAAACGATGAGTGCTAAGTGTTAGG
3' <i>B. subtilis</i> 16 rRNA	TATCTCTAGGATTGTCAGAGGATGTCAAG
<i>B. subtilis</i> 16 rRNA probe	Cy5-CTTTGAGTTTCAGTCTTGCGACCGTACTC-BHQ

6.1.9 Sequences of *glmS* ribozymes

S. aureus Mu50

GGUCGUAUACGACUCACUAUAGGUAAUGAUUAAUGGAAAGGGGGAAAGU
 UCGGCAGUACAGUUAAGCGCCUGUGCAAUAAAUAUUUGUAUUUGAAGA
 UAAAGGUUAAUAUAGAGUGGCCUUUAUAGAGUGCAAUUAUGUAUUUG
 UAGACGAGGAGGAUAGUGAUCGAAUAGAUCGGCGGAUGCUAUCCCGGAU
 GUGGCUCAUUCGUUAGCUUAUUAAGUAAAACAUUAGGGUGACUUAUGGA
 CAAAGUUAUAAGAUCGCCAGAA

***B. subtilis* chromosomal DNA strain 1A40 (originate *B. subtilis* 168)**

GGUCUUGUUCUUAUUUUUCUCAAUAGGAAAAGAAGACGGGAUUUAUUGCUUU
ACCUAUAUUUAUAGCGCCCGAACUAAGCGCCCGGAAAAAGGCUUAGUUGA
CGAGGAUGGAGGUUAUCGAAUUUUCGGCGGAUGCCUCCCGGCUGAGUGU
GCAGAUCACAGCCGUAAGGAUUUCUCAAACCAAGGGGGUGACUCCUUGA
ACAAAGAGAAAUCACAUGAUCUCCAAAAACAUGUAGGAAGGGGAC

***C.difficile* 630 IGR**

GGUUUAAAGGGUAUUCUCAGAUUAAAUACUGAGGACACCUUUCUAAGCG
CCAGAACUUAGUUAUAGACAUAAUUAUUGAGUAAUUAUAGGAACUAAGUUG
ACGAGGUCAGAGUUAUUCGAAUUGUCGGCGGAUGCUCUGCGGUGUGUUU
ACCAUCGAAAGACUUCUUUAAAUAUAGGAGCAAUCCUAUGGACAAAGGG
AAGCCAAAGUAAACUUAUUAUGACCUAACUCUUAUUUUUAUUAUUUUUAUU
UUUAGGAGGACACAAAUA

***L. monocytogenes* F2365 IGR**

GGUCAGCUCGCUCCUUUUUGUAUCAUAACUUAUUUAUUAGUCAUUUGUUA
UUUUUUGUCA AUGUAUAGACCAAUUUUAAACAAACGGCUAUAUAUAAUGC
UUGACCUAGUAUACAUAUUUAUUGUAAAAUGAAUUUGUUCCUUGAAAAGU
AGUGAAGGAGGAUCGUACAAUUAUUAGAAGCGCCAGAACUGAUUGGGAC
GAAAUAUCUUGAAGGUGAAAUCCUGAAAAGUAAACAGUCAGUUGACGAG
GAGGAGAUUAAUCGAAGUUUCGGCGGGAGUCUCCCGGCUGUGCAUGCAG
UCGUUAAGUCUUAACUUAACAAAUCACUUGGGUGACCAAGUGGACAGAGUAG
UAAUGAAACAUGUUUUUUUACCCUCCAAGGAAACCAAAAAAUGUAGAGGGC
UUGAAAUUGGAUAAGUCUGCCCUCAAGUUAUUUAUUGGAGGAGUUUUACU

***C. perfringens* ATCC 13124 IGR**

GGUACUGAGAAAUUUUAACAAUGGAAAGCGUCUAUACACUAAUUUAUCU
UUGAAGUUAAAAAUGAAAGAAUAAUUAUAAAAUUUCUUUUUAUAAUAUGG
AAUUUAAAAAGUUAAUUUUUAAAAUCAAAUACUUAUGAUGUCUAUACAACUA
UACAUUAUUAUUAAACAAAAGAAUUAUAGAGGUUAUAGACAGAUAAUUAA
AAUUAUUUCUUAUUUUUAAAUGAAAUAACUAAAAUUGAACUGAAAUAAGCU
UUAAAAGCUUGAAUUUUUUUAAAAAGUGUUAGAUAAGUUUGUGGCCUUU
UUAGAAAGAUGAUGCAUAGAAUUAUUUAACUUUCAAAAUAUAGAUUAAAG
CGCCAGAACUUAAGUUUUUAUUGAUAGACUAAUAAGUAAUUUAACUUUAG
UAGAUUAAAAUGCUUAUUUAAGAUUCUUAUUAAAUUUAAGUUGACGAGGUU
GGGGAGUAUCGAAUUUUCGGCGGAUGCCCCACGGUAAAGCACUAC

***E. faecalis* V583**

GGUAACAAAUUGAUAAAGGUUCUAUAAAUAGAACGGAUUUUUUUUAUUA
UUAAGAAUCUAGUACUUUCUCUACUAUGAGUGUACUAGAUUCUUUUUUU
GCAACUUUAAGAACUAGACCAAUUUUCGGUUUUUAGAUUUUUUGUUGACA
AGUACCUACUUUUAUUGUAUGAUUGUUUAUGUUUCUACGGAAUAUUAUU
ACAAAGGAGGUUAUAGACCAAUAUCGGAUAGCGCCAGACCUGAACGUUC
AGGUGACGAGGAGAGAGCUUAUCGAAGAUUCGGCGGGUGGCUCUAGGGA
CUGCACUCUACAGAUACAAAGAAAACUAAUUGUGAAGUUAGAACAAGC
GGUUAUCACGCAGGUAGAAACAUAUAAUGGGAUUUGCUAGUUAACAGGA
CCUAGUAAAUACAGAAUUUCAAUUGGAAAGUAGGAAUUAGCAUU

***E. faecium* DO**

GGUUUUACUCCUCCUCUAUCCGAUUACUUUCUAUUGUACCGAACUCCUGA
AAAAGAUGAUAGAUAAAAACCAUUAUUUUUUGACAUAAAAAGGACAUUUG
ACAAAGAAUUUGAUUAUACCAAUUUAUUUUUUUAUUCUUUUUUUGUUGAC
AAGAACAUUCGCAAAGGUUAUGAUUUUAAAUGUUUCCAGAUAAAAACAA
AAAGGAGGAUAGUUUA

***F. peridonticum* ATCC 33693 IGR**

GGUAUAUAUAAACUCAUUAUAAAAGAACCAAUUGUAUUACCUAAGGAAGU
AGUUAUAAACGAUUGUUAAGAAGAUUUUCAAAUUGUUUCUAUAGAACUAA
GUAUGAUAGUGGUUGGAUAAAAAUUGUUAUUAUUAGUAAUAAAGAUUAA
AUACAGUUUAUUUUUUUAUUUAUUAUUUUUAUCUUUUUUAGAUACAACUGU
UUCUAUUUUUUUAUCCCAUUUUUAUAAAACCAUUUUUAAGCUAUAAGGCGA
AAUUUUUUUAAUUUACUUAUAGAACUCCUCCUUUCUUUACUUUCUUUUU
AAUUAGCUUGAUCACCUUUUUGUUAUAAAUUCUUGACUAUAAGGUGUUA

***F. nucleatum* ATCC 25586 IGR**

GGUAUCCUCUAACAAUGAUAAUAGAGAAACAUGUGUUUAACGAGACACAA
AAACAACUAUUACCAACAUUGGUGGAAACCUUGUAGGCGGCCUUUUGAAGC
UAUUAAAGGUUAGGAGCAGUUGAGAUUUUUCUCAAGACCGCGAAGAAAUG
UAUU

6.1.10 Software

Software	Manufacture
Adobe Illustrator	Adobe Systems
AIDA Biopackage	Raytest
ChemDraw	PerkinElmer
GraphPad Prism	GraphPad Software
LISCAP image capture software	Amersham biosciences
Magellan data analysis software	Tecan
Microsoft office package	Microsoft
QuantityOne	Bio-Rad

6.2 Methods

6.2.1 Preparation of DEPC water

To ensure RNA integrity DEPC water was used to solubilize buffer components and compounds. Therefore, diethylpyrocarbonate was mixed with dH₂O in a ratio 1:500 this was let sit in the fume hood overnight. The next day the water was autoclaved (121 °C, 60 min) to sterilize and break DEPC to ethanol and CO₂. It functions by covalently modifying the amino acids of potential RNases and thereby leads to inactivation of RNases.

6.2.2 PCR

Polymerase chain reaction (PCR) is used to amplify specific DNA sequences. The desired DNA double stranded template is denatured (95 °C) so that in the second step the complimentary primers can anneal to the template. The exponential amplification by the DNA polymerase proceeds at 72 °C. Due to the thermo-stability of DNA polymerases several cycles of amplification can be performed within the thermocycler. The protocol used to setup PCR reactions is summarized in **Table 11**. A negative control containing no template DNA was always run in parallel to rule out contaminations or unspecific amplification. The conditions and temperature profiles used in PCR reactions are shown in **Table 12** and **Table 13**. The varying temperatures used for the annealing steps to amplify the different PCR products are displayed in **Table 13**. Usually, 2 µl of PCR products were always analyzed by Agarose gel electrophoresis. Afterwards PCR products were purified using NucleoSpin column by Macherey & Nagel.

Table 11: Pipetting scheme for PCR reactions

Reagent	Amount	Stock	Resultant
PCR buffer	10 µl	10x	1x
MgCl ₂	8 µl	25 mM	2 mM
5' primer	1 µl	100 µM	1 µM
3' primer	1 µl	100 µM	1 µM
dNTPs	0.8 µl	25 mM	0.2 mM
DNA template	1 µl	100-1000 nM	1-10 nM
DNA polymerase	1 µl	2.5 U/µl	2.5 U
water	77.2 µl		

Table 12: PCR cycling program

step	temperature	time	Repeat
Initial denaturation	95 °C	1.5-2 min	
denaturation	95 °C	1 min	20-22 cycles
annealing	Table 13	1 min	
elongation	72 °C	1 min	
final elongation	72 °C	1.5-2 min	

Table 13: Annealing temperatures for PCR reactions

PCR	Annealing temperature
<i>B. subtilis</i>	60 °C
<i>S. aureus</i>	60 °C
<i>S. aureus FRET</i>	58 °C
<i>C. difficile</i>	57.9 °C
<i>L. monocytogenes</i>	61.4 °C
<i>C. perfringens</i>	54.4 °C
<i>E. faecalis</i>	57.5 °C
<i>E. faecium</i>	56.6 °C
<i>F. peridonticum</i>	53 °C
<i>F. nucleatum</i>	54.5 °C

6.2.3 Quantitative real-time PCR

Real-time PCR is a method to monitor the amplification of nucleic acids within time. Herein, the TaqMan approach was used, where a fluorescent probe containing a fluorophore as for instance Cy5 or FAM at its 5' end and a quencher on its 3' end was used. The probe anneals to the respective target sequence between the two corresponding primers, if the amplification proceeds the probe is cleaved due to the 5' nuclease activity of taq polymerase(s). The quencher and the fluorophore become separated from each other and the fluorescence of the fluorophore corresponding to an increase in PCR product can be detected. Herein, real time PCR was used to quantify relative RNA levels of the *glmS* gene, the *glmS* ribozyme and 16S-rRNA as internal control to assess the intracellular levels in *B. subtilis*. In another experiment aiming at the determination of the intracellular *glmS* levels in *S. aureus* the *glmS* gene, a construct analyzing *glmS* gen+*glmS* ribozyme and 16S-rRNA as internal control were assayed. The Master mix contains the reactants listed in **Table 14** and the temperatures used for cycling of the different constructs are listed in **Table 15-17** Table 17 for amplification of *B. subtilis* and in **Table 18-20** for *S. aureus*. These were mixed in a sterile PCR workstation.

Table 14: Pipetting scheme real-time PCR reactions

Reagent	Amount	Stock	Resultant
Buffer	5 µl	10x	1x
MgCl ₂	6 µl	25 mM	3 mM
3' primer	0.5 µl	10 µM	0,1 µM
5' primer	0.5 µl	10 µM	0.1 µM
dNTPs	0.4 µl	25 mM	0.2 mM
TaqMan probe	2 µl	20 µM	0.8 µM
Super Hot-start taq	0.5 µl	2.5U/µl	1.25 U
Water	Up to 50µl		
cDNA template	0,75µl usually		

Table 15: PCR cycles for qPCR reactions amplifying *glmS* ribozyme-*B. subtilis*

step	temperature	time	Repeat
initial denaturation	95 °C	10 min	
denaturation	95 °C	1 min	35 cycles
annealing	54.9 °C	1 min	
elongation	72 °C	1 min	
final elongation	72 °C	10 min	

Table 16: PCR cycles for qPCR reactions amplifying the *glmS* gene-*B. subtilis*

step	temperature	time	Repeat
initial denaturation	95 °C	10 min	
denaturation	95 °C	1 min	35 cycles
annealing	54.5 °C	1 min	
elongation	72 °C	1 min	
final elongation	72 °C	10 min	

Table 17: PCR cycles for qPCR reactions amplifying 16S rRNA-*B. subtilis*

step	temperature	time	Repeat
initial denaturation	95 °C	10 min	
denaturation	95 °C	1 min	35 cycles
annealing	43 °C	1 min	
elongation	72 °C	1 min	
final elongation	72 °C	10 min	

Table 18: PCR cycles for qPCR reactions amplifying *glmS* gene-*S. aureus*

step	temperature	time	Repeat
initial denaturation	95 °C	10 min	
denaturation	95 °C	1 min	35--40 cycles
annealing	55 °C	1 min	
elongation	72 °C	1 min	
final elongation	72 °C	10 min	

Table 19: PCR cycles for qPCR reactions amplifying *glmS* gene+ribozyme-*S. aureus*

step	temperature	time	Repeat
initial denaturation	95 °C	10 min	
denaturation	95 °C	1 min	35--40 cycles
annealing	55 °C	1 min	
elongation	72 °C	1 min	
final elongation	72 °C	10 min	

Table 20: PCR cycles for qPCR reactions amplifying 16S rRNA *S. aureus*

step	temperature	time	Repeat
initial denaturation	95 °C	10 min	
denaturation	95 °C	1 min	35--40 cycles
annealing	60°C	1 min	
elongation	72 °C	1 min	
final elongation	72 °C	10 min	

cDNA originating from RNA extractions of *B. subtilis* 168 or *S. aureus* Mu50 were used as templates and added in the other sterile PCR working station. Usually samples were run in triplicates as well as three no-template controls (NTCs). To normalize samples to 16S rRNA and to be able to compare the expression of the different constructs the amplification efficacy was tested using a cDNA dilution series of templates. Afterwards the obtained Ct value was plotted against the template amount used, the gradient reveals than the amplification efficacy. By utilizing the Pfaffl-method and the corresponding equation the amplification efficacy can be considered (**Equation 1**).

Equation 1: Pfaffl-method for efficiency adjusted normalization

$$\frac{Target}{Reference} = \frac{(1 + E)^{\Delta Ct Target}}{(1 + E)^{\Delta Ct Reference}}$$

Results obtained after cycling the real-time PCR cycler were evaluated using GraphPad prism and statistical analysis using 1way ANOVA followed by Tukey's test was performed.

6.2.4 Agarose gel electrophoresis

Agarose gel electrophoresis was used to separate nucleic acids and to analyze their integrity. Agarose was melted in 0.5x TBE buffer and the percentage was adjusted to the length of nucleic acids, percentages ranged from 1-2.5% (w/v). Samples were mixed 1:1 with loading dye and loaded on the gel. Finally, 0.5x TBE buffer was added to the chamber and a power of 150 V was applied for 15-20 min.

The intercalating dye, ethidium bromide (EtBr) was used in a ratio of 1:10000 to visualize nucleic acid using UV light. The size of the separated nucleic acids was compared to RNA or DNA ladders.

When performing agarose gels in order to assess the integrity of RNA isolated from *S. aureus* cells 1x TAE buffer was used to dissolve agarose with a final percentage of 1% (w/v). The electrophoresis chamber was filled with 1x TAE and 0.5 µl of samples were mixed with loading buffer. After loading the pockets of the gel a constant power of 100 V was applied for 1 h. Afterwards, the gel was stained in an EtBr bath (1:10000 diluted in water) for 30 min before the RNA was visualized by UV light.

6.2.5 Polyacrylamide gel electrophoresis (PAGE)

Polyacrylamide gel electrophoresis can be used for preparative and analytical purposes. PAGE was used to clean nucleic acid samples by cutting the bands with the correct size out of the gel and subsequent cleaning by gel filtration. For this purpose, 6-10% gels were used. The preparation of the mixtures used in this thesis are stated in **Table 21**. After the addition of APS and TEMED which are starting the polymerization of the acrylamide; the mixture was filled in the already assembled glass chamber. The glass chamber was assembled by thoroughly cleaned plates and the appropriate spacers and combs. Depending on the purpose the gels should be used; for preparative purposes, thick gels or for analytical purposes thin gels were used. Analytical gels were mainly used to analyze samples of the metabolite induced self-cleavage assay for this purpose 17% PAGE was mostly poured. Polymerized gels were placed into the running chamber and the chamber was filled with 1x TBE buffer. Prior to loading of the samples, the pockets of the gel were rinsed using a syringe and 1Xtbe buffer. The samples were mixed with 2x sucrose buffer in a 1:1 ratio and constant power of 15 W per gel and 370-600 V was applied. After sufficient separation of the samples the gels were disassembled.

<u>Solutions for PAGE:</u>	
Solution B	8.3 M Urea in 10x TBE
Solution C	Rotiphorese Sequenziergel Konzentrat
Solution D	8.3 M Urea

Table 21: Composition of PAGE-PAA gels

%	Solution	Amount [ml] 100	70	50	30
6	B	10	7	5	3
	C	24	16.8	12	7.2
	D	66	46.2	33	19.8
10	B	10	7	5	3
	C	40	28	20	12
	D	50	35	25	15
12	B	10	7	5	3
	C	48	33.6	24	14.4
	D	42	29.4	21	12.6
17	B	10	7	5	3
	C	68	47.6	34	20.4
	D	22	15.4	11	6.6
20	B	10	7	5	3
	C	80	56	40	24
	D	10	7	5	3
Add to all preparations	10% APS	0.8	0.56	0.4	0.24
	TEMED	0.04	0.028	0.02	0.012

6.2.6 *In vitro* transcription

To transcribe DNA templates into RNA *in vitro* transcription using the DNA dependent RNA polymerase of T7 bacteriophage was performed. Prerequisite is that the DNA template does contain the T7 promoter sequence. Usually this condition is met by the introduction of the T7 promoter sequence during PCR namely at the 5' end of the used forward primer. To allow for optimal transcription the first two nucleotides being transcribed should be guanines. The addition of IPP to the transcription mixture prevents inhibitory effects due to the accumulation of pyrophosphates. The reagents listed in **Table 22** were mixed and incubated at 37 °C for at least 4 h or o/n.

Table 22: Pipetting scheme of *in vitro* transcription

Reagent	Amount	Stock	Resultant
HEPES pH7.9	20 µl	200 mM	40 mM
MgCl ₂	25 µl	100 mM	25 mM
DTT	5 µl	100 mM	5 mM
NTPs	10 µl	25 mM	2.5 mM
RNasin	1.24 µl	40 U/µl	50 U
IPP	0.2 µl	2 U/ml	0.4 U
ds DNA template	10 µl	150-300 pmol	1.5-3 µM
T7 RNA polymerase	5 µl	50 U/µl	250 U
DEPC water	23.56 µl		

6.2.7 RNA work up after in vitro transcription

To clean RNA samples after in vitro transcription the samples were incubated in the presence of 2.5 U DNaseI (0.5 μ l) for at least 10 min at 37 °C. Afterwards the samples were mixed with sucrose buffer and loaded onto pre-ran 6-10% PAGE. A constant power of 360 V and 15 W per gel was applied. A marker solution (1x sucrose buffer mixed with the dyes bromphenol blue and xylencyanol) was loaded onto the gel to monitor the separation of the RNA sample. After sufficient separation, the chamber was disassembled, the glass plates were removed and the gel was wrapped into foil. Visualization of the RNA was enabled by using a UV lamp at 245 nm and a fluoro-coated silica plate. The band with the correct size was cut out of the gel using a scalpel blade. The gel piece was placed into a 2 ml Eppendorf tube and crushed with a 1 ml pipette tip. The gel pieces were mixed with 0.3 M NaOAc until the gel pieces could easily move. Passive elution proceeded at 65°C and vigorous shaking for 90 min. Afterwards the mixture was filtered through a syringe prepacked with silanized glass wool. The syringe was washed 5 times with 250 μ l 0.3 M NaOAc. RNA was subsequently precipitated by the addition of 3 volumes EtOH and 1 μ l glycogen to allow for better precipitation. After incubation at – 80 °C for 10 min the samples were centrifuged at 4 °C and full speed for at least 30 min. Then the supernatant was removed and the pellet was washed with 100 μ l 70% EtOH. After centrifugation for 5 min the supernatant was removed and the dried pellet was re-suspended in 10 μ l DEPC water.

6.2.8 RNA work up by electroelution used for non-cleaving *S. aureus* FRET leader strand

The electroelution chamber was used to extract RNA of the non-cleaving *S. aureus* FRET leader strand from PAGE gels. In case of functional ribozyme RNA extraction by electroelution leads to the induction of the cleavage reaction as 8 M NH_4OAc is used in the channels for precipitation, in these cases the protocol described in **section 6.2.7** was used. For electroelution both parts of the electroelution chamber were filled with 1x TBE in such a way as to enable the RNA to migrate through the channel upon the application of electrical power. Prior to loading 180 μ l 8 M NH_4OAc in the channels separating the two halves of the chamber the channel was flushed with 1x TBE to remove potential air bubbles. The gel pieces were applied in the pockets and a constant power of 150 V was applied for 45 min. Afterwards the channel was sealed by cut pipette tips and the TBE buffer was carefully removed from the two halves of the chamber. The NH_4OAc containing the RNA was removed and precipitated by the addition of 3 volumes 100% EtOH. After incubation at – 80 °C for 10 min the samples were centrifuged at full speed for at least 30 min. Then the supernatant was removed and the pellet was washed with 100 μ l 70% EtOH. After centrifugation for 5 min the supernatant

was removed and the dried pellet was re-suspended in a suitable amount of DEPC water.

6.2.9 5' Dephosphorylation

To allow radioactively labelling of 5' ends, dephosphorylation reactions were undertaken. Therefore, 75 pmol of purified nucleic acid were incubated in the presence of calf intestine alkaline phosphatase (CIAP). This enzyme catalysis the hydrolysis of 5' phosphates of RNA or DNA samples. The reaction was mixed as stated in **Table 23** and an incubation step at 37 °C for 15 min was followed by an incubation at 55 °C for 15 min after addition of additional 8.5 U CIAP. The enzyme was inactivated by incubation at 75 °C for 10 min. Finally, dephosphorylated samples were purified by phenol-chloroform extraction (**section 6.2.10**) and precipitated nucleic acids were dissolved in 5 µl water.

Table 23: Pipetting scheme for dephosphorylation reactions

Reagent	Amount	Stock	Resultant
CIAP buffer	5 µl	10x	1x
BSA	5 µl	10 mg/ml	1 mg/ml
nucleic acid			75 pmol
CIAP	0.85 µl	20 U/µl	17 U
RNasin	0.5 µl	40 U/µl	20 U
DEPC water	ad 50 µl		

6.2.10 Phenol-chloroform extraction

To clean nucleic acids samples especially after dephosphorylation reactions phenol-chloroform extraction followed by ethanol precipitation was performed. In this regard samples were mixed with phenol in a 1:1 ratio. Centrifugation at 13000 rpm for 3 min allowed the separation of the phenol and the water based phase. The upper phase containing nucleic acids was transferred in a new reaction tube and mixed with two volumes chloroform. After a second centrifugation step the upper phase was transferred in a new tube and mixed with 3 M NaOAc, 100% ethanol and 1 µl glycogen. The mixture was let stand at – 80 °C for 10 min. Centrifugation for at least 30 min at 13000 rpm and 4 °C led to the formation of a nucleic acid containing pellet which was subsequently cleaned by washing using 70% ethanol. The dried pellet was dissolved in 5 µl DEPC water. 2 µl of the cleaned samples were used to analyze the integrity by agarose gel electrophoresis (**section 6.2.4**). The remaining 3 µl were used for radioactive phosphorylation (**section 6.2.11**).

6.2.11 5' radioactive phosphorylation

In order to radioactively label nucleic acids, the reagents stated in **Table 24** were mixed and an incubation step of 30 min at 37 °C allowed incorporation of γ^{32} ATP by T4-polynucleotide kinase. Radioactively labeled RNA was purified using G25 columns applying manufactures instructions.

Table 24: Pipetting scheme for radioactive phosphorylation

Reagent	Amount	Stock	Resultant
PNK buffer	2 μ l	10x	1x
CIAP nucleic acid	3 μ l	0.5 μ M	45 pmol
γ^{32} ATP	2 μ l	10 μ Ci/ μ l	20 μ Ci
T4 PNK	2 μ l	10 U/ μ l	20 U
RNasin	0.3 μ l	40 U/ μ l	12 U
DEPC water	9.7 μ l		

6.2.12 Determination of nucleic acid concentration

Concentrations of nucleic acids (dsDNA or RNA) were determined using either the NanoQuant infinite 200 (Tecan) or the nanodrop (peqlab). Prior measuring the samples 2 μ l of DEPC water were used for blanking.

6.2.13 RNA isolation of Gram-positive bacteria

In order to prepare cDNA that can be used for real-time PCR experiments RNA was isolated from either *S. aureus* Mu50 or *B. subtilis* 168. For cultivation of *B. subtilis* 5 ml LB-medium was inoculated from a glycerol stock and pre-grown at 150 rpm and 37°C o/n. The next day the appropriate volume of 1x CDM was inoculated 1:100 with the pre-culture and while shaking at 37 °C allowed to grow till the desired optical density (usually ~0.35-0.4). In case of *S. aureus* Mu50, cells were streaked on Columbia blood agar and incubated at 37 °C for at least 6 h. One of the colonies formed was used to inoculate 5 ml ½ MH medium. This pre-culture was grown for at least 8 h at 170 rpm and 37 °C (usually o/n). The appropriate volume 1x CDM was inoculated 1:100 and cultures were grown to the desired OD₆₀₀ (usually ~ 0.32). Then cells were harvested and the OD₆₀₀ was determined. Cells were mixed with RNA protect (qiagen) in 2:1 ratio calculating the OD₆₀₀ as 1. After immediate vortexing for 10 sec. the mixture was incubated at RT for 10 min. Cells were subsequently centrifuged for 10 min at 5000 g. The supernatant was removed the remaining volume should not exceed 500 μ l. The pellet was either stored at -20 °C or directly re-suspended in 500 μ l 10 mM HEPES-10 mM EDTA. After the addition of 40 μ l lysostaphin (10mg/ml >3000 U/mg) in case of *S. aureus* and 32 μ l lysozyme (10 mg/ml 40000 U/mg) in case of *B. subtilis* the mixture was immediately vortexed for 5 sec. and incubated at 37°C lysis was monitored and eventually 16 μ l lysozyme

were added after 30 min of incubation for *B. subtilis* the incubation was set to 1 h in total. To lyse *S. aureus* Mu50 cells were incubated at 37 °C for 15 min in the presence of lysostaphin. During this incubation step vortexing was performed every 2 min for 10 sec. Purification of the samples was performed using PrestoSpinR e.g. RNeasy protect bacteria Mini kit according to the manufactures instructions. To reduce the volume of the sample and to clean the sample more thoroughly the eluate was purified using RNeasy Min elute clean up kit and eluted in 14 µl DEPC water per column (to purify 50 ml culture OD₆₀₀ > 0.5 two columns were used resulting in ~ 26 µl eluate). The integrity of the RNA was analyzed by loading 0.5 µl per sample on an agarose gel (**section 6.2.4**) detection of the desired bands for ribosomal RNA at ~ 1500 nt and ~ 2900 nt confirmed intact RNA. Moreover, the concentration was determined using the nanodrop or nanoquant (**section 6.2.12**). Intact RNA was later used for reverse transcription and quantitative PCR.

6.2.14 Reverse Transcription for real-time PCR

RNA isolated from *B. subtilis* 168 or *S. aureus* Mu50 was transcribed into cDNA to use it as template in real time PCR applications. First, intact RNA was mixed with random hexamers and dNTPs and incubated at 70 °C to allow for priming. The premix containing RNasin and reverse transcriptase was pipetted on ice and mixed to the priming mixture. cDNA synthesis was enabled by incubation at 42 °C for 30 min. The mixture and protocol can be found in **Table 25**.

Table 25: Pipetting and reaction scheme for reverse transcription

Reagent	Amount	Stock	Resultant
RNA			up to 3 µg
Random hexamer primer	1 µl	50 µM	1.25 µM
dNTPs	1 µl	10 mM	0.25 mM
DEPC water	Up to 10 µl		
incubation 5 min at 70°C chill on ice at least 1 min			
Reaction buffer	4 µl	5x	1x
Bioscript	1 µl	200 U/µl	200 U
RNasin	1 µl	40 U/µl	40 U
DEPC water	4 µl		
incubation 10 min at 25 °C			
incubation 30 min at 42 °C			
incubation 5 min at 85 °C chill on ice			

6.2.15 Radioactive metabolite induced *glmS* ribozyme self-cleavage assay

Radioactively labeled ribozyme RNA was folded for 1 min at 95 °C. Incubation at RT for 5 min allowed for the correct folding. The integrity and properties of the RNA were studied; therefore, RNA was incubated in the presence of 10 mM MgCl₂ and 200 μM GlcN6P (for better estimation of cleavage properties it is recommended to analyze cleavage at lower GlcN6P concentrations as well) or 200 μM GlcN. In another tube the RNA was incubated without MgCl₂ here no cleavage is supposed to occur as divalent ions are needed to confer the self-cleavage reaction. RNA incubated in the presence of MgCl₂ but in the absence of any metabolite is also supposed to not show a cleaved fraction after PAGE separation. To assess the general induction of cleavage endpoint determinations were performed. In these cases, RNA was incubated in cleavage buffer (50 mM HEPES, 200 mM KCl pH 7.5) and in the presence of 10 mM MgCl₂ and the compound to be tested for 30 min at 37 °C. Competition assays to investigate inhibition of GlcN6P-induced cleavage were assayed in the presence of 200 μM GlcN6P. Afterwards, cleavage reactions were stopped by the addition of EDTA containing sucrose buffer. Subsequently full-length and cleavage product were separated by PAGE. After sufficient separation gels were disassembled and wrapped in plastic foil. Radioactivity was usually detected o/n utilizing phosphorimager screens stored at -80 °C or -20 °C. The radioactivity was read by the phosphorimager and quantified by the AIDA image analyzer. The analysis was performed using the of GraphPad Prism for EC₅₀ value determinations the nonlinear fit log(agonist) vs response (three parameter) was used.

To determine k_{obs} values the cleavage kinetic was analyzed over time. Therefore, master mixes of the compound to be tested (usually different concentrations) as well as the negative controls either lacking the metabolite or the MgCl₂ were prepared. These master mixes were incubated at 37 °C or 6 °C depending on the assay and samples (10 μl) were withdrawn at the following timepoints: 0 min, 1 min, 3 min, 5 min, 7 min, 10 min, 15 min, 30 min, 60 min, 90 min. The samples taken were transferred into tubes that already contained EDTA containing sucrose buffer to stop the reaction. Samples were afterwards analyzed by PAGE. After sufficient separation gels were disassembled and wrapped in plastic foil. Radioactivity was usually detected o/n utilizing phosphorimager screens stored at -80 °C or -20 °C. The radioactivity was read by the phosphorimager and quantified by the AIDA image analyzer. The analysis was performed using the pseudo-first order association kinetics fit of GraphPad Prism

6.2.16 Fluorescence based *glmS* ribozyme self-cleavage assays utilizing Förster resonance energy transfer (FRET) assay

The assay used herein is based on a publication by Blount et al. in 2006.²⁰⁹ They used a fluorescence based assay utilizing FRET and validated this assay format for high-throughput application and identified known ribozyme metabolites by screening a library of 960 compounds, however confirmation by common gel electrophoretic tests using radioactively labeled RNA was needed to identify false positive activators.²⁰⁹ The ribozyme is split in a substrate strand containing the cleavage site a fluorophore at its 5' end and the rest of the ribozyme sequence (leader sequence). In their assay, Blount et al. analyzed the *glmS* ribozyme of *S. aureus* subsp. *aureus* Rosebach, herein the cleavage of *S. aureus* subsp. *aureus* Mu50 was investigated. The substrate used herein has the following sequence (5'-Cy3-AAGCGCCUGUGCAAA-FAM-3'). The 5-Cy3 represents the FRET acceptor group and the 3' FAM functions as the FRET donor. This substrate can be hybridized to the truncated P1 stem of the ribozyme. Binding of compounds to the fully assembled ribozyme induces the cleavage reaction and results in an increase in fluorescence. Prior to fluorescence-based *glmS* ribozyme self-cleavage assays the *glmS* leader sequence and the *glmS* substrate strand had to be annealed. This construction of the full-length *glmS* ribozyme was achieved by following the scheme presented in **Table 26**. Pipetted were three different master mixes (MM), the MM for the positive control later containing 200 μ M GlcN6P (**Table 27**), one mix for the later negative control without GlcN6P (**Table 28**) and a mixture lacking the leader sequence of the *glmS* ribozyme (**Table 29**). To establish the assay a control where no MgCl₂ was added was analyzed the pipetting scheme is shown in **Table 30**, as this control did never show any fluorescence signal to be correlated with *glmS* ribozyme cleavage this control was not used in later assays. 40 μ l of the mixtures were separately placed in wells of a 96-well plate (U shaped black half area) and the fluorescence was monitored at 37 °C. After this first read 10 μ l GlcN6P and/or 10 μ l of the compounds to be tested were added and the fluorescence was recorded over 30 min at 37 °C. Plates were measured either every 30 or 90 sec. The first read was used in the evaluation for background normalization utilizing GraphPad Prism. The Z' value is used to assess the potential of assay to be used in HTS screenings. According to the equation for Z' value determinations, a Z' value of 0.586 was determined for the FRET assay used in this thesis.

Table 26: Temperature profile for annealing of fluorescence-based cleavage assay of *S. aureus glmS* ribozyme

temperature	time	ramp [°/s]
95 °C	1 min	2.0
50 °C	pause	0.25
20 °C	pause	0.25
72 °C	1.5 min	2.0
4 °C	pause	

Table 27: Pipetting scheme for positive control FRET reactions

reagent	amount	temperature	time
500 mM HEPES, 2 M KCl (buffer) 2.5 µM <i>glmS</i> leader sequence	1.1 µl 10 µl	95 °C	1 min
100 mM MgCl ₂	1.2 µl	50 °C	pause
10 µM <i>glmS</i> ribozyme substrate	2.5 µl	20 °C	pause
		72 °C	1.5 min
buffer 100 mM MgCl ₂ DEPC water	3.9 µl 3.8 µl 17.5µl	4 °C	pause

Table 28: Pipetting scheme for control of FRET reactions without GlcN6P

reagent	amount	temperature	time
500 mM HEPES, 2 M KCl (buffer) 2.5 µM <i>glmS</i> leader sequence	1.1 µl 10 µl	95 °C	1 min
100 mM MgCl ₂	1.2 µl	50 °C	pause
10 µM <i>glmS</i> ribozyme substrate	2.5 µl	20 °C	pause
		72 °C	1.5 min
buffer 100 mM MgCl ₂ DEPC water	3.9 µl 3.8 µl 17.5µl	4 °C	pause

Table 29: Pipetting scheme for FRET reactions without *glmS* leader sequence

reagent	amount	temperature	time
500 mM HEPES, 2 M KCl (buffer)	1.1 µl	95 °C	1 min
100 mM MgCl ₂	1.2 µl	50 °C	pause
10 µM <i>glmS</i> ribozyme substrate	2.5 µl	20 °C	pause
		72 °C	1.5 min
buffer 100 mM MgCl ₂ DEPC water	3.9 µl 3.8 µl 27.5µl	4 °C	pause

Table 30: Pipetting scheme for FRET reactions without MgCl₂

reagent	amount	temperature	time
500 mM HEPES, 2 M KCl (buffer) 2.5 μM <i>glmS</i> leader sequence	1.1 μl 10 μl	95 °C	1 min
		50 °C	pause
10 μM <i>glmS</i> ribozyme substrate	2.5 μl	20 °C	pause
		72 °C	1.5 min
buffer DEPC water	3.9 μl 22.5 μl	4 °C	pause

Equation 2: Determination of Z' values. ²⁴⁶

$$1 - \frac{3 * SD \text{ positive} + SD \text{ negative}}{\text{mean positive} - \text{mean negative}}$$

6.2.17 Cultivation of *S. aureus* Mu50

S. aureus Mu50 was streaked on Columbia blood agar plates, after incubation at 37 °C overnight single colonies were picked and pre-grown in ½ MH for at least 8 h. Afterwards, 1x CDM was inoculated 1:100 with *S. aureus* Mu50 and grown at 37 °C and 170 rpm till an OD₆₀₀ of ~0.3-0.35 was reached and further processing was undertaken (**section 6.2.13**).

6.2.18 Cultivation of *B. subtilis* 168

3-5 ml LB-medium or CDM was inoculated with *B. subtilis* either from an agar plate (assays performed in AKs Broetz-Oesterhelt and C. Mayer) or of a glycerol culture stored at -80 °C and incubated at 37 °C and 130 rpm o/n. The next day the desired amount of CDM was inoculated with *B. subtilis* pre-culture and allowed to grow at 37C and vigorous shaking. For detailed information on cultivation see specified **sections (6.2.13, 6.2.19, 6.2.20, 6.2.22 and 6.2.21)**.

6.2.19 Minimal inhibitory concentration (MIC)

To investigate the potency of (potential) antibacterial substances MIC determinations were performed. The bacterial strain of interest was streaked on agar plates (either Mueller-Hinton agar for *B. subtilis* or Columbia blood agar for *S. aureus*) and incubated for 12-24 h at 37 °C. The next day 5 ml of CDM were inoculated with 3-5 morphologically similar colonies, the culture was allowed to grow for 18 -24 h at 37 °C. A serial twofold dilution of the potential antibiotic substance was prepared. 100 μl of the two-times concentrated stock was added to the first well of a transparent, round bottom 96-well plate. Into the wells 2-12 50 μl of medium was added by mixing 50 μl of the first well with the second well and

taking 50 μl of the second well and mixing with the third well and so on a serial dilution series was accomplished. The plate was then inoculated with 50 μl 1×10^6 CFU/ml. A sterility control containing 100 μl medium and a growth control containing only bacterial suspension without the addition of test antibiotic were prepared as well. The plate was incubated for 16-20 h at 37 °C. After this incubation, the turbidity of the medium was analyzed by eye and the MIC was read as the lowest concentration of antimicrobial substance inhibiting bacterial growth.

6.2.20 Growth curve

Growth curve analysis was performed to investigate the growth of *B. subtilis* and *S. aureus* in the presence of CGlcN or FC- α -D-GlcN. This analysis was performed in clear U-shaped 96-well plates with a clear lid. The outer wells (row A and H and wells 1 and 12) have not been used for analysis but instead were filled with medium to minimize evaporation. In all assays growth controls containing untreated bacteria as well as sterile controls containing only medium e.g. compound have been analyzed in parallel. The total volume in each well being analyzed was 200 μl .

To validate the optimal time-course of incubation in later mRNA expression studies bacterial cells were pre-cultured in either 5 ml LB-medium for *B. subtilis* or 1/2 MH for *S. aureus* overnight at 37 °C and 130 rpm or 170 rpm respectively. The next day 5 ml 1xCDM were inoculated 1:100 with bacterial cells and allowed to grow till early exponential phase ($\text{OD}_{600} \sim 0.3$). Subsequently bacterial cells were transferred in 96-well plates and growth was monitored in the presence of CGlcN. CGlcN concentrations in concentration-ranges corresponding to those that later on will be used in mRNA expression studies were chosen. Growth curve analysis were performed in the Tecan Sunrise plate reader monitoring the absorbance at 600 nm over several hours. The plate was shaken for 3 sec. prior to each measurement and growth was determined every 180 sec. As suitable time-course (for later on mRNA expression studies) the timepoint at which CGlcN treated cells decrease in growth compared to untreated cell was defined (in both cases ~ 60 min). Evaluation of the data was performed using GrapPad Prism.

Furthermore, growth curve analysis was used to monitor the growth of *B. subtilis* PTS deletion mutants (**section 6.2.21**).

6.2.21 Δ PTS mutants

To study whether CGlcN or FC- α -D-GlcN are taken up by the phosphoenolpyruvate system strains deleted in the GlcN-specific, GlcNAc-specific transporter as well as a deletion mutant lacking the global kinase (were analyzed and compared to wildtype cells. This study was carried out using *B. subtilis* 168 strains

ordered by the BGSC and being available in the working group of Prof. C. Mayer in Tübingen. The deletion mutations were constructed by inserting an erythromycin resistance cassette in the coding region of the cognate transporter subunit. Analyzed were the following strains: *B. subtilis* 168 wildtype, *B. subtilis* 168 Δ hpr:erm, *B. subtilis* 168 Δ gamP:erm and *B. subtilis* 168 Δ nagP:erm. 3 ml CDM were inoculated with the different strains and grown over night at 37 °C. The next day 20 μ l of the preculture were mixed with 100 μ l CDM and 80 μ l of either CGlcN/ FC- α -D-GlcN, GlcN or CDM to gain a total volume of 200 μ l (OD₆₀₀ ~0.1). The final concentrations of CGlcN and GlcN/ FC- α -D-GlcN were adjusted to 64 μ g/ml which equals 2xMIC for CGlcN/ FC- α -D-GlcN. The growth was monitored for 24 h and the optical density was measured every 45 sec (CGlcN) or every 15 min (FC- α -D-GlcN). The plate was shaken for 3 sec. prior to each measurement. Evaluation of the data was performed using GrapPad Prism.

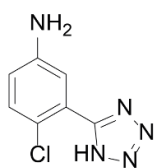
6.2.22 Promotor-gene assay

In cooperation with the AK Broetz-Oesterhelt *B. subtilis* 168 reporter strains which are selectively inducible upon certain stresses were analyzed looking at the induction after CGlcN treatment.

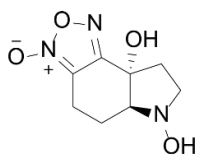
These stress inducible promoters have been identified by Hutter et al. and were further validated by Hutter et al. and Urban et al. Hutter et al. performed microarray studies and analyzed the transcription profile of *B. subtilis* in the presence of 37 known antibiotics.^{205, 219} Based on these findings *B. subtilis* reporter strains were constructed carrying stress inducible promoter regions in front of a luciferase cassette. Thereafter, Urban et al. generated similar reporter strains that complement the former ones. Moreover, validation of the reporter strains screening a library of 14.000 compounds at Bayer HealthCare was undertaken. Resulting in a collection of reporter strains that can be used to analyze fundamental bacterial metabolic pathways as for instance protein biosynthesis.

Herein, *B. subtilis* reporter strains indicative for cell envelope stress (*ypuA*) as well as protein (*bmrC*), DNA (*yorB*) and RNA (*helD*) damage were analyzed to analyze induction upon CGlcN treatment. All *B. subtilis* strains were pre-grown in 10 ml LB-Erythromycin o/n at 37 °C. Then the optical density was measured and the culture was diluted to an OD₆₀₀ of 0.05 in 5 ml of CDM. The culture was allowed to grow till an OD₆₀₀ of 0.2 was reached. Meanwhile a serial dilution series of reference antibiotics (vancomycin, rifampicin, chloramphenicol and ciprofloxacin) as well as a dilution series of CGlcN or FC- α -D-GlcN was prepared in a 96-well plate. At the timepoint the culture reached an optical density of 0.2 the culture was diluted till an OD₆₀₀ of 0.02 and the plate was inoculated with cells finally leading to an OD₆₀₀ of 0.01. The plate was incubated for max. 3.5 h at 37 °C then 60 μ l citrate buffer containing luciferin was injected and the bioluminescence was read in the plate reader. Evaluation of the data was performed using GrapPad Prism.

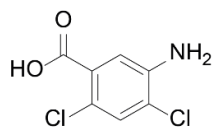
7 Appendix



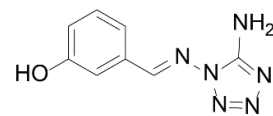
B1



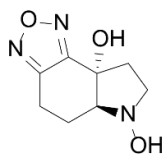
B2



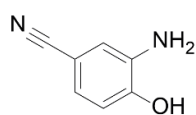
B3



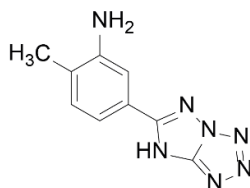
B4



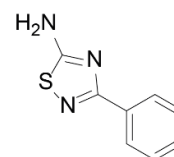
B5



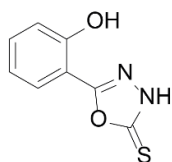
B6



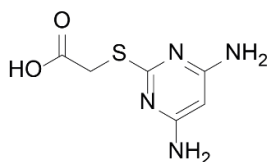
B7



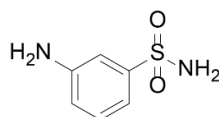
B8



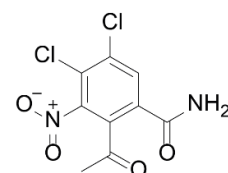
B9



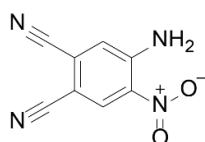
B10



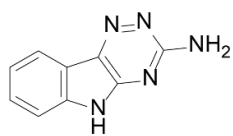
B11



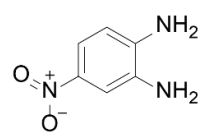
B12



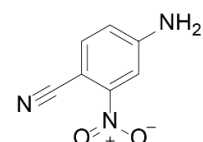
C1



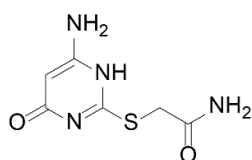
C2



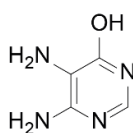
C3



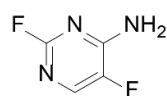
C4



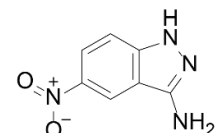
C5



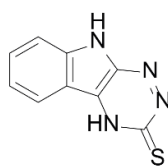
C6



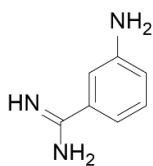
C7



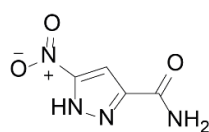
C8



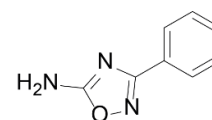
C9



C10

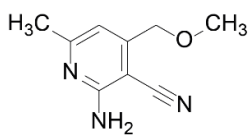


C11

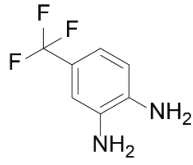


C12

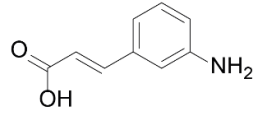
Appendix



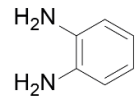
D1



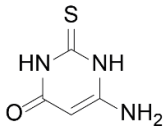
D2



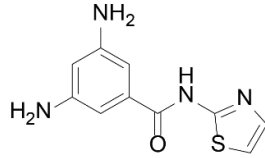
D3



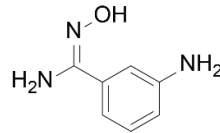
D4



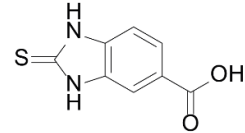
D5



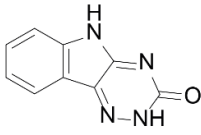
D6



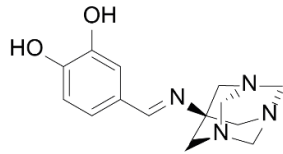
D7



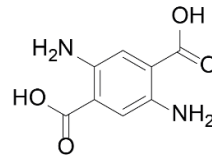
D8



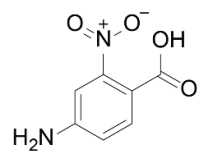
D9



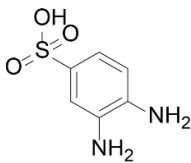
D10



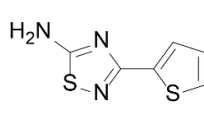
D11



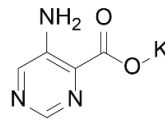
D12



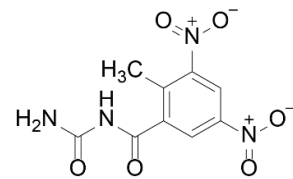
E1



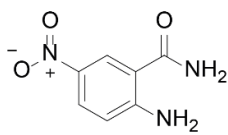
E2



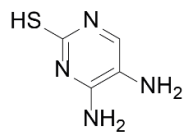
E3



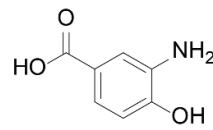
E4



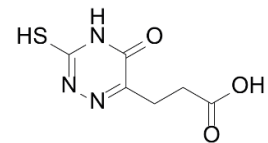
E5



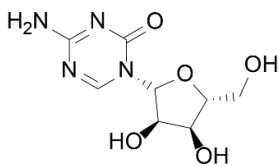
E6



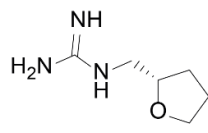
E7



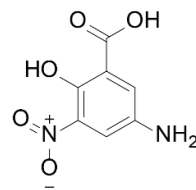
E8



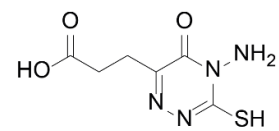
E9



E10



E11



E12

Appendix

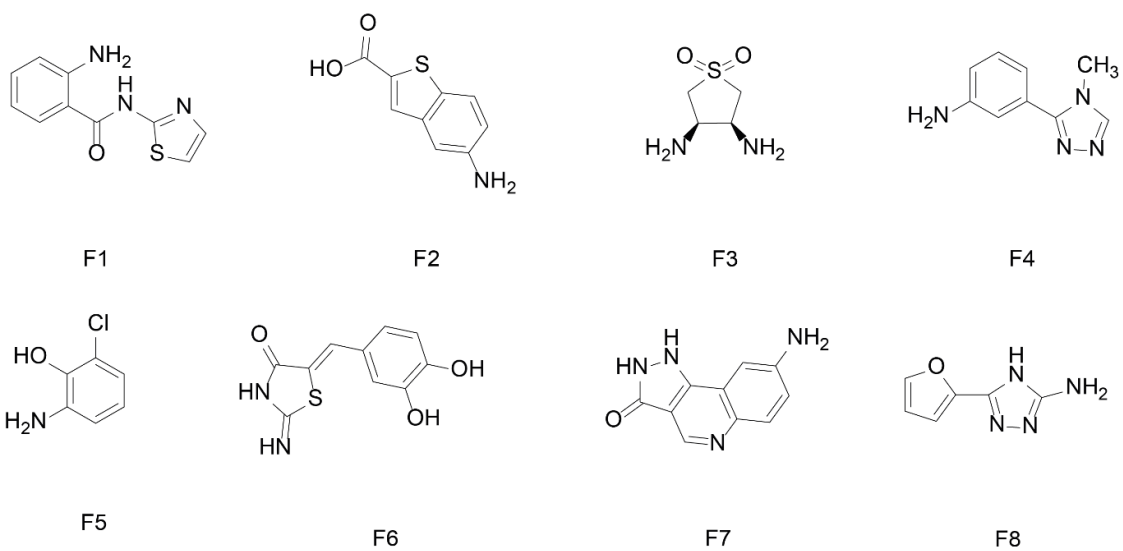
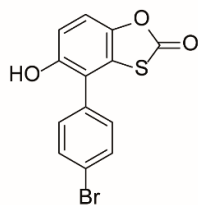
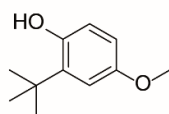


Figure 67: Chemical structures of 1st generation Reymond compounds

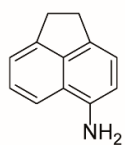
Appendix



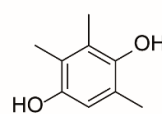
G1



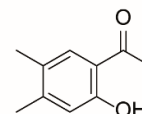
G2



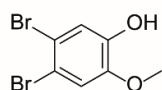
G3



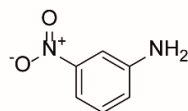
G4



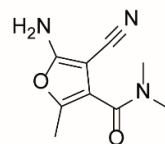
G5



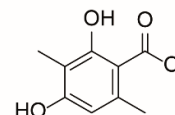
G6



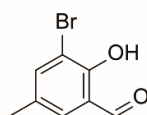
G7



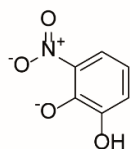
G8



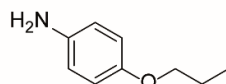
G9



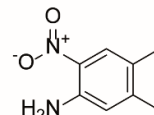
H1



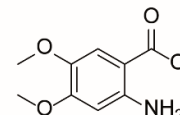
H2



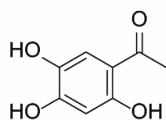
H3



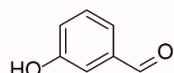
H4



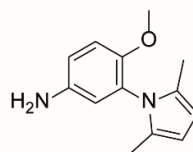
H5



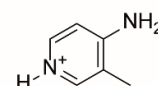
H6



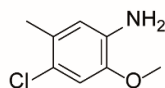
H7



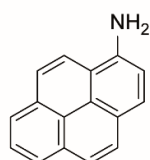
H8



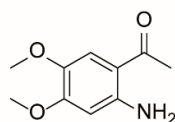
H9



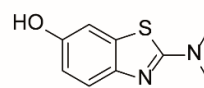
I1



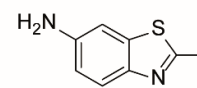
I2



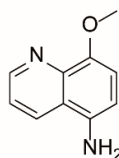
I3



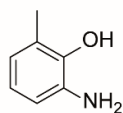
I4



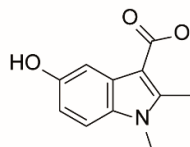
I5



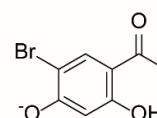
I6



I7

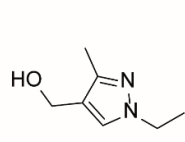


I8

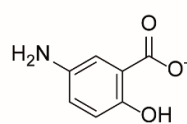


I9

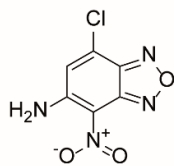
Appendix



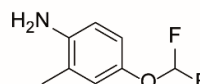
J1



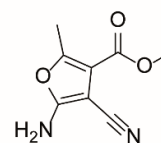
J2



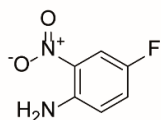
J3



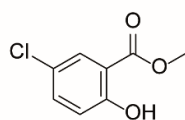
J4



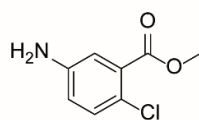
J5



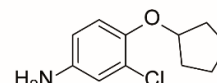
J6



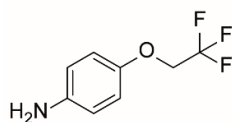
J7



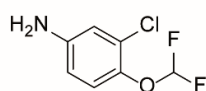
J8



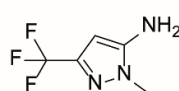
J9



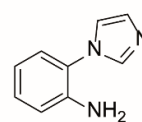
K1



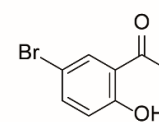
K2



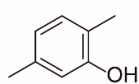
K3



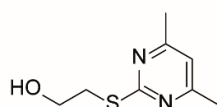
K4



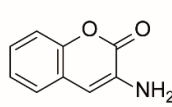
K5



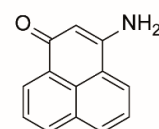
K6



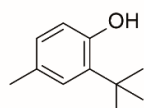
K7



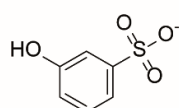
K8



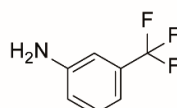
K9



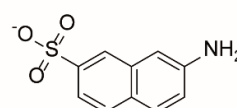
L1



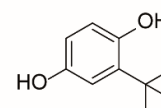
L2



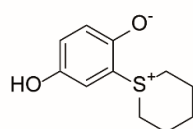
L3



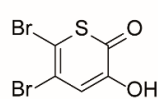
L4



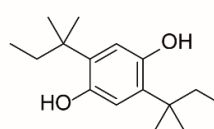
L5



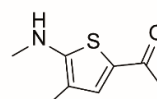
L6



L7

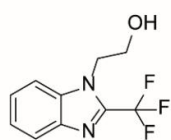


L8

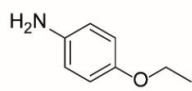


L9

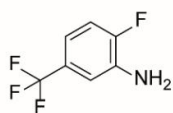
Appendix



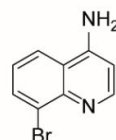
M1



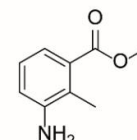
M2



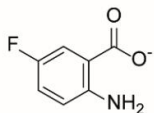
M3



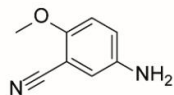
M4



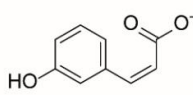
M5



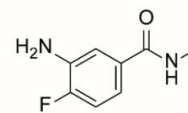
M6



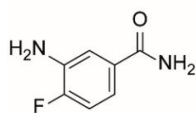
M7



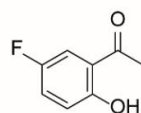
M8



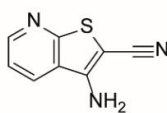
M9



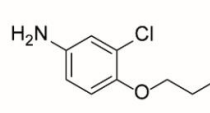
N1



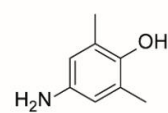
N2



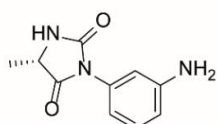
N3



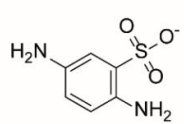
N4



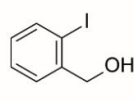
N5



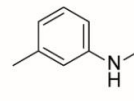
N6



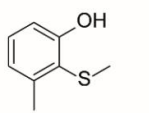
N7



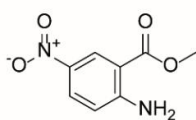
N8



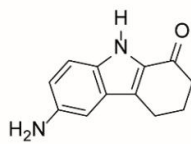
N9



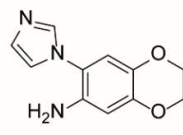
O1



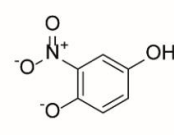
O2



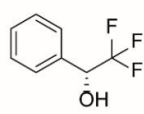
O3



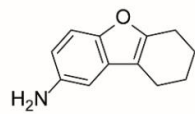
O4



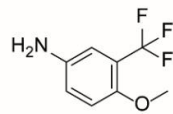
O5



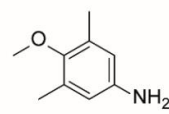
O6



O7

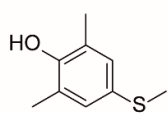


O8

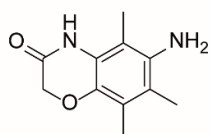


O9

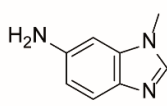
Appendix



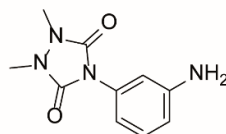
P1



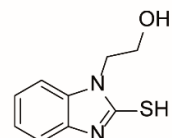
P2



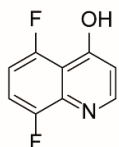
P3



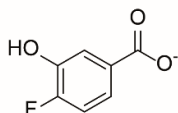
P4



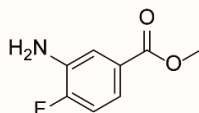
P5



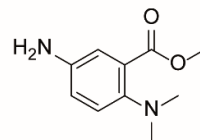
P6



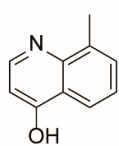
P7



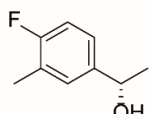
P8



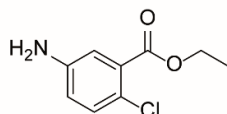
P9



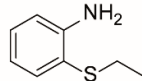
Q1



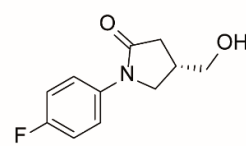
Q2



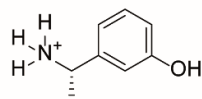
Q3



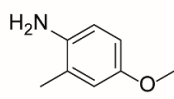
Q4



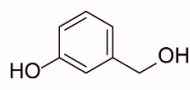
Q5



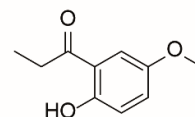
Q6



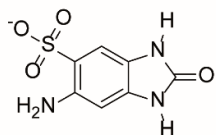
Q7



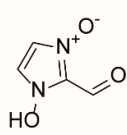
Q8



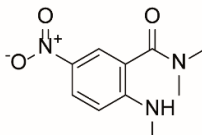
Q9



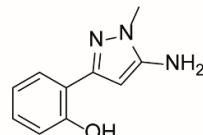
R1



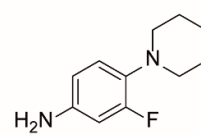
R2



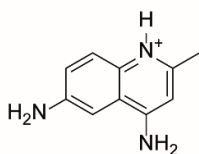
R3



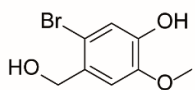
R4



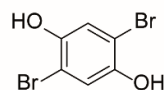
R5



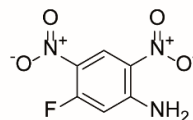
R6



R7



R8



R9

Appendix

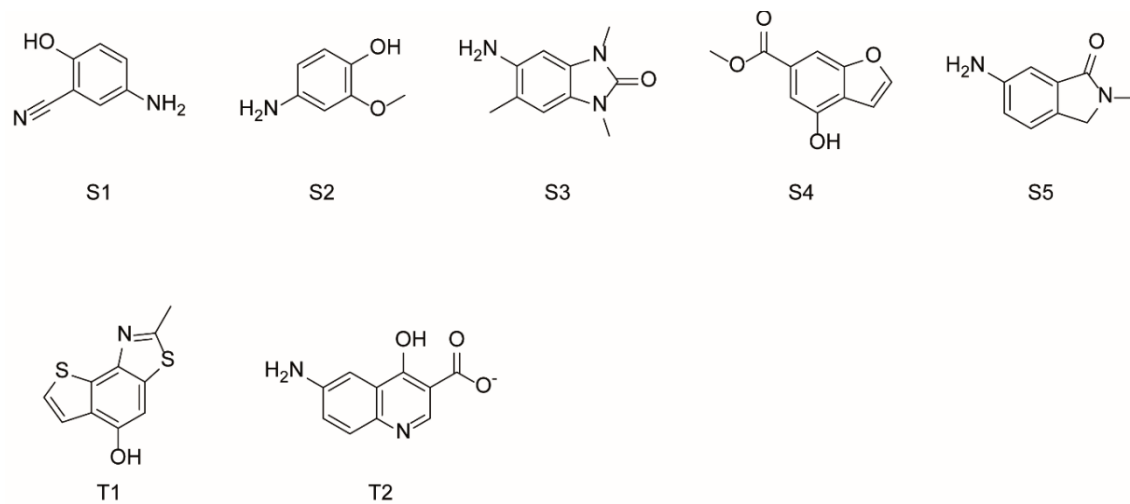


Figure 68: Chemical structures of 2nd generation Reymond compounds

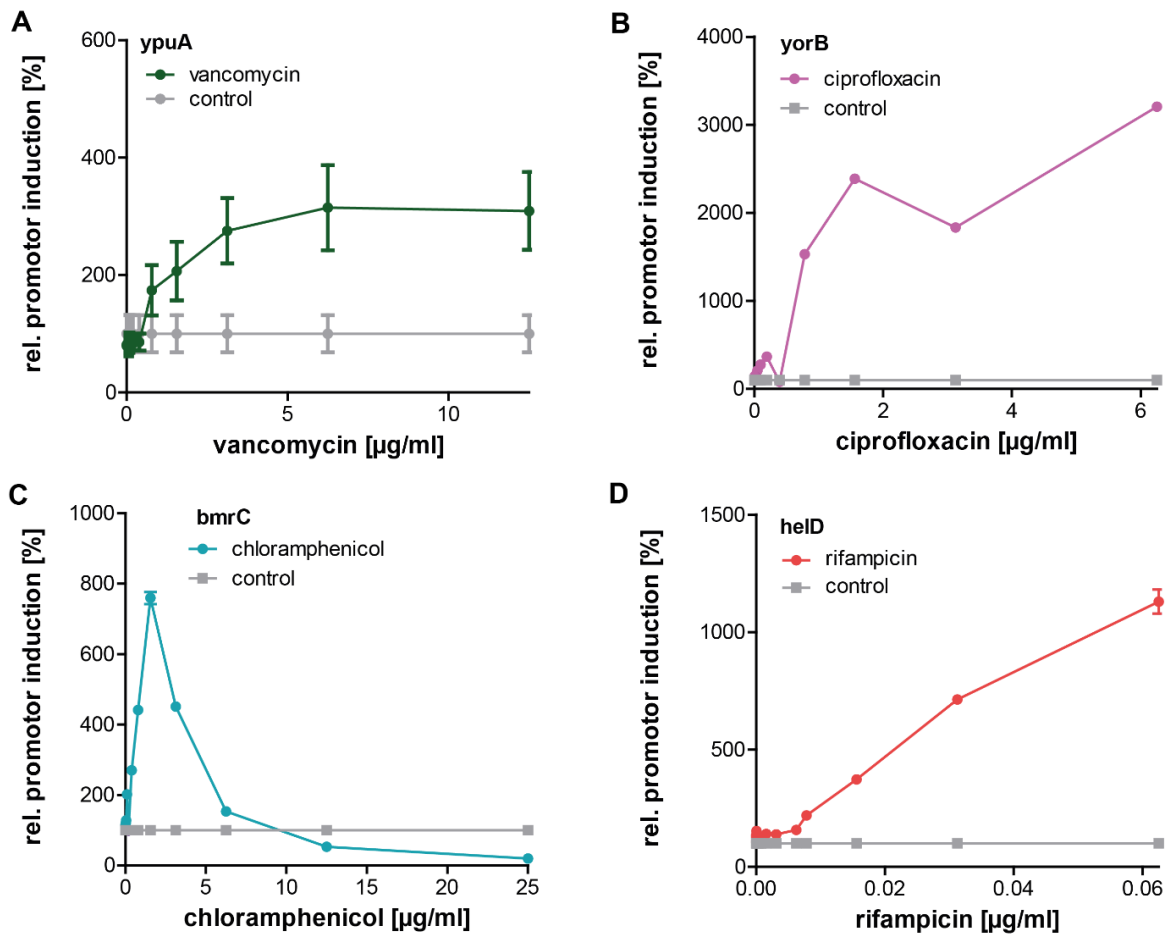


Figure 69: Induction of stress inducible promoters by the corresponding reference antibiotics

Shown is the induction of firefly luciferase under the control of stress inducible promoters in *B. subtilis*. In A, the induction of the *ypuA* promoter that is indicative for cell envelope damage by the reference antibiotic vancomycin is shown. B depicts the response of the DNA damage promoter *yorB* to ciprofloxacin. The induction of luciferase due to the stress exhibited by chloramphenicol on the *bmrC* promoter is shown in C. It is indicative of protein damage. In D, the induction of the *helD* promoter by the RNA stress inducing antibiotic rifampicin is displayed. Strains are incubated in the presence (purple) or absence (grey) of the respective reference antibiotic, the controls were adjusted to 100% (n=2).

8 References

1. Talbot, G. H.; Bradley, J.; Edwards, J. E., Jr.; Gilbert, D.; Scheld, M.; Bartlett, J. G.; Antimicrobial Availability Task Force of the Infectious Diseases Society of America, Bad bugs need drugs: an update on the development pipeline from the Antimicrobial Availability Task Force of the Infectious Diseases Society of America. *Clin Infect Dis* **2006**, *42* (5), 657-68.
2. Aminov, R., History of antimicrobial drug discovery: Major classes and health impact. *Biochem Pharmacol* **2017**, *133*, 4-19.
3. O'Neill, J. C., The review on antimicrobial resistance. **2014**.
4. Rice, L. B., Federal Funding for the Study of Antimicrobial Resistance in Nosocomial Pathogens: No ESKAPE. *J Infect Dis* **2008**, *197* (8), 1079-1081.
5. Boucher, H. W.; Talbot, G. H.; Bradley, J. S.; Edwards, J. E.; Gilbert, D.; Rice, L. B.; Scheld, M.; Spellberg, B.; Bartlett, J., Bad bugs, no drugs: no ESKAPE! An update from the Infectious Diseases Society of America. *Clin Infect Dis* **2009**, *48* (1), 1-12.
6. Berdy, J., Thoughts and facts about antibiotics: Where we are now and where we are heading. *J Antibiot* **2012**, *65* (8), 385-395.
7. Norrby, S. R.; Nord, C. E.; Finch, R.; European Society of Clinical, M.; Infectious, D., Lack of development of new antimicrobial drugs: a potential serious threat to public health. *Lancet Infect Dis* **2005**, *5* (2), 115-9.
8. Levy, S. B.; Marshall, B., Antibacterial resistance worldwide: causes, challenges and responses. *Nat Med* **2004**, *10* (12 Suppl), S122-9.
9. Michna, R. H.; Commichau, F. M.; Todter, D.; Zschiedrich, C. P.; Stulke, J., SubtiWiki-a database for the model organism *Bacillus subtilis* that links pathway, interaction and expression information. *Nucleic Acids Res* **2014**, *42* (Database issue), D692-8.
10. Lin, Y.-C.; Peterson, M. L., New insights into the prevention of staphylococcal infections and toxic shock syndrome. *Expert review of clinical pharmacology* **2010**, *3* (6), 753-767.
11. Kluytmans, J.; van Belkum, A.; Verbrugh, H., Nasal carriage of *Staphylococcus aureus*: epidemiology, underlying mechanisms, and associated risks. *Clinical Microbiology Reviews* **1997**, *10* (3), 505-520.
12. CDC, C. f. D. C. a. P., Antibiotic resistance threats in the United States, 2013.
<http://www.cdc.gov/drugresistance/threat-report-2013> **2013**.
13. Gonzales, P. R.; Pesesky, M. W.; Bouley, R.; Ballard, A.; Bidy, B. A.; Suckow, M. A.; Wolter, W. R.; Schroeder, V. A.; Burnham, C. A.; Mobashery, S.; Chang, M.; Dantas, G., Synergistic, collaterally sensitive beta-lactam combinations suppress resistance in MRSA. *Nat Chem Biol* **2015**, *11* (11), 855-61.
14. Cui, L.; Ma, X.; Sato, K.; Okuma, K.; Tenover, F. C.; Mamizuka, E. M.; Gemmell, C. G.; Kim, M.-N.; Ploy, M.-C.; El Solh, N.; Ferraz, V.; Hiramatsu, K., Cell Wall Thickening Is a Common Feature of Vancomycin Resistance in *Staphylococcus aureus*. *J Clin Microbiol* **2003**, *41* (1), 5-14.
15. Cui, L.; Iwamoto, A.; Lian, J. Q.; Neoh, H. M.; Maruyama, T.; Horikawa, Y.; Hiramatsu, K., Novel mechanism of antibiotic resistance originating in vancomycin-intermediate *Staphylococcus aureus*. *Antimicrob Agents Chemother* **2006**, *50* (2), 428-38.

16. Paredes-Sabja, D.; Shen, A.; Sorg, J. A., Clostridium difficile spore biology: sporulation, germination, and spore structural proteins. *Trends Microbiol* **2014**, *22* (7), 406-16.
17. Nelson, R. L.; Suda, K. J.; Evans, C. T., Antibiotic treatment for Clostridium difficile-associated diarrhoea in adults. *The Cochrane database of systematic reviews* **2017**, *3*, Cd004610.
18. Rupnik, M.; Wilcox, M. H.; Gerding, D. N., Clostridium difficile infection: new developments in epidemiology and pathogenesis. *Nat Rev Microbiol* **2009**, *7* (7), 526-36.
19. Miller, B. A.; Chen, L. F.; Sexton, D. J.; Anderson, D. J., Comparison of the Burdens of Hospital-Onset, Healthcare Facility-Associated Clostridium difficile Infection and of Healthcare-Associated Infection due to Methicillin-Resistant Staphylococcus aureus in Community Hospitals. *Infection Control & Hospital Epidemiology* **2015**, *32* (4), 387-390.
20. Napolitano, L. M.; Edmiston, C. E., Jr., Clostridium difficile disease: Diagnosis, pathogenesis, and treatment update. *Surgery* **2017**.
21. Baines, S. D.; O'Connor, R.; Saxton, K.; Freeman, J.; Wilcox, M. H., Activity of vancomycin against epidemic Clostridium difficile strains in a human gut model. *J Antimicrob Chemother* **2009**, *63* (3), 520-5.
22. Paredes-Sabja, D.; Sarker, M. R., Interactions between Clostridium perfringens spores and Raw 264.7 macrophages. *Anaerobe* **2012**, *18* (1), 148-56.
23. Kelly, C. P.; LaMont, J. T., Clostridium difficile--more difficult than ever. *N Engl J Med* **2008**, *359* (18), 1932-40.
24. Chaturongakul, S.; Raengpradub, S.; Wiedmann, M.; Boor, K. J., Modulation of stress and virulence in Listeria monocytogenes. *Trends Microbiol* **2008**, *16* (8), 388-96.
25. NicAogain, K.; O'Byrne, C. P., The Role of Stress and Stress Adaptations in Determining the Fate of the Bacterial Pathogen Listeria monocytogenes in the Food Chain. *Front Microbiol* **2016**, *7*, 1865.
26. Gahan, C. G.; Hill, C., Listeria monocytogenes: survival and adaptation in the gastrointestinal tract. *Front Cell Infect Microbiol* **2014**, *4*, 9.
27. Vázquez-Boland, J. A.; Kuhn, M.; Berche, P.; Chakraborty, T.; Domínguez-Bernal, G.; Goebel, W.; González-Zorn, B.; Wehland, J.; Kreft, J., Listeria Pathogenesis and Molecular Virulence Determinants. *Clinical Microbiology Reviews* **2001**, *14* (3), 584-640.
28. Welshimer, H. J., Survival of Listeria monocytogenes in soil. *J Bacteriol* **1960**, *80*, 316-20.
29. Stoll, R.; Goebel, W., The major PEP-phosphotransferase systems (PTs) for glucose, mannose and cellobiose of Listeria monocytogenes, and their significance for extra- and intracellular growth. *Microbiology* **2010**, *156* (Pt 4), 1069-83.
30. Walker, S. J.; Archer, P.; Banks, J. G., Growth of Listeria monocytogenes at refrigeration temperatures. *The Journal of applied bacteriology* **1990**, *68* (2), 157-62.
31. Angelidis, A. S.; Smith, G. M., Role of the glycine betaine and carnitine transporters in adaptation of Listeria monocytogenes to chill stress in defined medium. *Appl Environ Microbiol* **2003**, *69* (12), 7492-8.
32. Shahamat, M.; Seaman, A.; Woodbine, M., Survival of Listeria monocytogenes in high salt concentrations. *Zentralblatt fur Bakteriologie. 1. Abt.*

- Originale. A: Medizinische Mikrobiologie, Infektionskrankheiten und Parasitologie* **1980**, 246 (4), 506-11.
33. Farber, J. M.; Peterkin, P. I., *Listeria monocytogenes*, a food-borne pathogen. *Microbiological Reviews* **1991**, 55 (3), 476-511.
 34. Siegman-Igra, Y.; Levin, R.; Weinberger, M.; Golan, Y.; Schwartz, D.; Samra, Z.; Konigsberger, H.; Yinnon, A.; Rahav, G.; Keller, N.; Bisharat, N.; Karpuch, J.; Finkelstein, R.; Alkan, M.; Landau, Z.; Novikov, J.; Hassin, D.; Rudnicki, C.; Kitzes, R.; Ovadia, S.; Shimoni, Z.; Lang, R.; Shohat, T., *Listeria monocytogenes* infection in Israel and review of cases worldwide. *Emerging infectious diseases* **2002**, 8 (3), 305-10.
 35. Bassetti, M. M., M., Temperoni, C., Astilean, A., New antibiotics for bad bugs: where are we? **2013**.
 36. Bush, K.; Page, M. G., What we may expect from novel antibacterial agents in the pipeline with respect to resistance and pharmacodynamic principles. *Journal of pharmacokinetics and pharmacodynamics* **2017**, 44 (2), 113-132.
 37. Alekshun, M. N.; Levy, S. B., Molecular Mechanisms of Antibacterial Multidrug Resistance. *Cell* **2007**, 128 (6), 1037-1050.
 38. Dersch, P.; Khan, M. A.; Mühlen, S.; Görke, B., Roles of Regulatory RNAs for Antibiotic Resistance in Bacteria and Their Potential Value as Novel Drug Targets. *Front Microbiol* **2017**, 8 (803).
 39. Lewis, K., New approaches to antimicrobial discovery. *Biochem Pharmacol* **2017**, 134, 87-98.
 40. Andries, K.; Verhasselt, P.; Guillemont, J.; Gohlmann, H. W.; Neefs, J. M.; Winkler, H.; Van Gestel, J.; Timmerman, P.; Zhu, M.; Lee, E.; Williams, P.; de Chaffoy, D.; Huitric, E.; Hoffner, S.; Cambau, E.; Truffot-Pernot, C.; Lounis, N.; Jarlier, V., A diarylquinoline drug active on the ATP synthase of *Mycobacterium tuberculosis*. *Science* **2005**, 307 (5707), 223-7.
 41. Starkey, M.; Lepine, F.; Maura, D.; Bandyopadhyaya, A.; Lesic, B.; He, J.; Kitao, T.; Righi, V.; Milot, S.; Tzika, A.; Rahme, L., Identification of anti-virulence compounds that disrupt quorum-sensing regulated acute and persistent pathogenicity. *PLoS Pathog* **2014**, 10 (8), e1004321.
 42. Payne, D. J.; Gwynn, M. N.; Holmes, D. J.; Pompliano, D. L., Drugs for bad bugs: confronting the challenges of antibacterial discovery. *Nat Rev Drug Discov* **2007**, 6 (1), 29-40.
 43. Lavecchia, A.; Di Giovanni, C., Virtual screening strategies in drug discovery: a critical review. *Curr Med Chem* **2013**, 20 (23), 2839-60.
 44. Vyas, V., Jain, A., Jain, A., Gupta, A., Virtual Screening: A Fast Tool for Drug Design. *Sci Pharm.* **2008**, 76: 333–360.
 45. Nichols, D.; Cahoon, N.; Trakhtenberg, E. M.; Pham, L.; Mehta, A.; Belanger, A.; Kanigan, T.; Lewis, K.; Epstein, S. S., Use of ichip for high-throughput in situ cultivation of "uncultivable" microbial species. *Appl Environ Microbiol* **2010**, 76 (8), 2445-50.
 46. Walsh, C., Where will new antibiotics come from? *Nat Rev Micro* **2003**, 1 (1), 65-70.
 47. Schneider, T.; Sahl, H. G., An oldie but a goodie - cell wall biosynthesis as antibiotic target pathway. *Int J Med Microbiol* **2010**, 300 (2-3), 161-9.
 48. Bush, K., Introduction to Antimicrobial Therapeutics Reviews: The bacterial cell wall as an antimicrobial target. *Ann N Y Acad Sci* **2013**, 1277 (1), v-vii.
 49. Crandon, J. L.; Nicolau, D. P., Pharmacodynamic Approaches to Optimizing Beta-Lactam Therapy. *Critical Care Clinics* 27 (1), 77-93.

50. Vu, H.; Nikaido, H., Role of beta-lactam hydrolysis in the mechanism of resistance of a beta-lactamase-constitutive *Enterobacter cloacae* strain to expanded-spectrum beta-lactams. *Antimicrob Agents Chemother* **1985**, *27* (3), 393-398.
51. Périchon, B.; Courvalin, P., VanA-Type Vancomycin-Resistant *Staphylococcus aureus*. *Antimicrob Agents Chemother* **2009**, *53* (11), 4580-4587.
52. Leclercq, R.; Derlot, E.; Duval, J.; Courvalin, P., Plasmid-mediated resistance to vancomycin and teicoplanin in *Enterococcus faecium*. *N Engl J Med* **1988**, *319* (3), 157-61.
53. Sievert, M. D. B., M. L.; Stolman, G.; Johnson, D.; Stobierski, M. G.; Downes, F. P.; Somsel, P. A.; Rudrik, J. T.; Brown, W.; Hafeez, W.; Lundstrom, T.; Flanagan, E.; Johnson, R.; Mitchell, J.; Chang, S., *Staphylococcus aureus* resistant to vancomycin. . *MMWR Morb. Mortal. Wkly. Rep* **2002**, *51*:565–567.
54. Ling, L. L.; Schneider, T.; Peoples, A. J.; Spoering, A. L.; Engels, I.; Conlon, B. P.; Mueller, A.; Schaberle, T. F.; Hughes, D. E.; Epstein, S.; Jones, M.; Lazarides, L.; Steadman, V. A.; Cohen, D. R.; Felix, C. R.; Fetterman, K. A.; Millett, W. P.; Nitti, A. G.; Zullo, A. M.; Chen, C.; Lewis, K., A new antibiotic kills pathogens without detectable resistance. *Nature* **2015**, *517* (7535), 455-459.
55. Karageorgopoulos, D. E.; Wang, R.; Yu, X.-h.; Falagas, M. E., Fosfomycin: evaluation of the published evidence on the emergence of antimicrobial resistance in Gram-negative pathogens. *Journal of Antimicrobial Chemotherapy* **2012**, *67* (2), 255-268.
56. Deutscher, J.; Francke, C.; Postma, P. W., How phosphotransferase system-related protein phosphorylation regulates carbohydrate metabolism in bacteria. *Microbiol Mol Biol Rev* **2006**, *70* (4), 939-1031.
57. Reizer, J.; Saier, M. H., Jr.; Deutscher, J.; Grenier, F.; Thompson, J.; Hengstenberg, W., The phosphoenolpyruvate:sugar phosphotransferase system in gram-positive bacteria: properties, mechanism, and regulation. *Crit Rev Microbiol* **1988**, *15* (4), 297-338.
58. Cordaro, J. C.; Melton, T.; Stratis, J. P.; Atagün, M.; Gladding, C.; Hartman, P. E.; Roseman, S., Fosfomycin resistance: selection method for internal and extended deletions of the phosphoenolpyruvate:sugar phosphotransferase genes of *Salmonella typhimurium*. *J Bacteriol* **1976**, *128* (3), 785-793.
59. Lambert, M. P.; Neuhaus, F. C., Mechanism of d-Cycloserine Action: Alanine Racemase from *Escherichia coli* W. *J Bacteriol* **1972**, *110* (3), 978-987.
60. Prosser, G. A.; de Carvalho, L. P. S., Kinetic mechanism and inhibition of *Mycobacterium tuberculosis* d-alanine:d-alanine ligase by the antibiotic d-cycloserine. *FEBS Journal* **2013**, *280* (4), 1150-1166.
61. Pearson, N. D.; Prescott, C. D., RNA as a drug target. *Chem Biol* **1997**, *4* (6), 409-414.
62. Vicens, Q.; Westhof, E., RNA as a drug target: the case of aminoglycosides. *Chembiochem* **2003**, *4* (10), 1018-23.
63. Taylor, B. S.; Sobieszczyk, M. E.; McCutchan, F. E.; Hammer, S. M., The challenge of HIV-1 subtype diversity. *N Engl J Med* **2008**, *358* (15), 1590-602.
64. Mitsuyasu, R. T.; Merigan, T. C.; Carr, A.; Zack, J. A.; Winters, M. A.; Workman, C.; Bloch, M.; Lalezari, J.; Becker, S.; Thornton, L.; Akil, B.; Khanlou, H.; Finlayson, R.; McFarlane, R.; Smith, D. E.; Garsia, R.; Ma, D.; Law, M.; Murray, J. M.; von Kalle, C.; Ely, J. A.; Patino, S. M.; Knop, A. E.; Wong, P.; Todd, A. V.; Haughton, M.; Fuery, C.; Macpherson, J. L.; Symonds, G. P.; Evans, L. A.; Pond,

- S. M.; Cooper, D. A., Phase 2 gene therapy trial of an anti-HIV ribozyme in autologous CD34+ cells. *Nat Med* **2009**, *15* (3), 285-92.
65. He, P.; Zhu, D.; Hu, J. J.; Peng, J.; Chen, L. S.; Lu, G. X., pcDNA3.1(-)-mediated ribozyme targeting of HER-2 suppresses breast cancer tumor growth. *Molecular biology reports* **2010**, *37* (3), 1597-604.
66. Fei, Q.; Zhang, H.; Fu, L.; Dai, X.; Gao, B.; Ni, M.; Ge, C.; Li, J.; Ding, X.; Ke, Y.; Yao, X.; Zhu, J., Experimental cancer gene therapy by multiple anti-survivin hammerhead ribozymes. *Acta biochimica et biophysica Sinica* **2008**, *40* (6), 466-77.
67. Schroeder, R.; Waldsich, C.; Wank, H., Modulation of RNA function by aminoglycoside antibiotics. *Embo J* **2000**, *19* (1), 1-9.
68. Colameco, S.; Elliot, M. A., Non-coding RNAs as antibiotic targets. *Biochem Pharmacol* **2017**, *133*, 29-42.
69. Hu, X.; Sood, A. K.; Dang, C. V.; Zhang, L., The role of long noncoding RNAs in cancer: the dark matter matters. *Current opinion in genetics & development* **2017**, *48*, 8-15.
70. Dar, D.; Sorek, R., Regulation of antibiotic-resistance by non-coding RNAs in bacteria. *Curr Opin Microbiol* **2017**, *36*, 111-117.
71. Collins, J. A.; Irnov, I.; Baker, S.; Winkler, W. C., Mechanism of mRNA destabilization by the glmS ribozyme. *Genes Dev* **2007**, *21* (24), 3356-68.
72. Lalaouna, D.; Eyraud, A.; Chabelskaya, S.; Felden, B.; Massé, E., Regulatory RNAs Involved in Bacterial Antibiotic Resistance. *PLoS Pathog* **2014**, *10* (8), e1004299.
73. Storz, G.; Vogel, J.; Wassarman, Karen M., Regulation by Small RNAs in Bacteria: Expanding Frontiers. *Mol Cell* **2011**, *43* (6), 880-891.
74. Erdmann, V. A.; Barciszewska, M. Z.; Hochberg, A.; de Groot, N.; Barciszewski, J., Regulatory RNAs. *Cell Mol Life Sci* **2001**, *58* (7), 960-77.
75. Waters, L. S.; Storz, G., Regulatory RNAs in Bacteria. *Cell* **2009**, *136* (4), 615-628.
76. Roßmanith, J.; Narberhaus, F., Exploring the modular nature of riboswitches and RNA thermometers. *Nucleic Acids Res* **2016**, *44* (11), 5410-5423.
77. Kortmann, J.; Narberhaus, F., Bacterial RNA thermometers: molecular zippers and switches. *Nat Rev Micro* **2012**, *10* (4), 255-265.
78. Dar, D.; Shamir, M.; Mellin, J. R.; Koutero, M.; Stern-Ginossar, N.; Cossart, P.; Sorek, R., Term-seq reveals abundant ribo-regulation of antibiotics resistance in bacteria. *Science* **2016**, *352* (6282).
79. Dambach, M. D.; Winkler, W. C., Expanding roles for metabolite-sensing regulatory RNAs. *Curr Opin Microbiol* **2009**, *12* (2), 161-9.
80. Mellin, J. R.; Cossart, P., The non-coding RNA world of the bacterial pathogen *Listeria monocytogenes*. *RNA Biol* **2012**, *9* (4), 372-378.
81. Görke, B.; Vogel, J., Noncoding RNA control of the making and breaking of sugars. *Genes Dev* **2008**, *22* (21), 2914-2925.
82. Rice, J. B.; Vanderpool, C. K., The small RNA SgrS controls sugar-phosphate accumulation by regulating multiple PTS genes. *Nucleic Acids Res* **2011**, *39* (9), 3806-19.
83. Papenfort, K.; Sun, Y.; Miyakoshi, M.; Vanderpool, Carin K.; Vogel, J., Small RNA-Mediated Activation of Sugar Phosphatase mRNA Regulates Glucose Homeostasis. *Cell* **2013**, *153* (2), 426-437.
84. Vogel, J.; Luisi, B. F., Hfq and its constellation of RNA. *Nat Rev Micro* **2011**, *9* (8), 578-589.

85. Urban, J. H.; Papenfort, K.; Thomsen, J.; Schmitz, R. A.; Vogel, J., A conserved small RNA promotes discoordinate expression of the *glmS* operon mRNA to activate GlmS synthesis. *J Mol Biol* **2007**, *373* (3), 521-8.
86. Lilley, D. M. J., Ribozymes[mdash]a snip too far? *Nat Struct Mol Biol* **2003**, *10* (9), 672-673.
87. Kruger, K.; Grabowski, P. J.; Zaug, A. J.; Sands, J.; Gottschling, D. E.; Cech, T. R., Self-splicing RNA: autoexcision and autocyclization of the ribosomal RNA intervening sequence of *Tetrahymena*. *Cell* **1982**, *31* (1), 147-57.
88. Weinberg, Z.; Kim, P. B.; Chen, T. H.; Li, S.; Harris, K. A.; Lünse, C. E.; Breaker, R. R., New classes of self-cleaving ribozymes revealed by comparative genomics analysis. *Nat Chem Biol* **2015**, *11* (8), 606-610.
89. Serganov, A.; Patel, D. J., Ribozymes, riboswitches and beyond: regulation of gene expression without proteins. *Nat Rev Genet* **2007**, *8* (10), 776-790.
90. Lilley, D. M. J., How RNA acts as a nuclease: some mechanistic comparisons in the nucleolytic ribozymes. *Biochem Soc Trans* **2017**, *45* (3), 683-691.
91. Pyle, A., Metal ions in the structure and function of RNA. *JBIC Journal of Biological Inorganic Chemistry* **2002**, *7* (7), 679-690.
92. Pyle, A., Ribozymes: a distinct class of metalloenzymes. *Science* **1993**, *261* (5122), 709-714.
93. Guerrier-Takada, C.; Gardiner, K.; Marsh, T.; Pace, N.; Altman, S., The RNA moiety of ribonuclease P is the catalytic subunit of the enzyme. *Cell* **1983**, *35* (3 Pt 2), 849-57.
94. Winkler, W. C.; Nahvi, A.; Roth, A.; Collins, J. A.; Breaker, R. R., Control of gene expression by a natural metabolite-responsive ribozyme. *Nature* **2004**, *428* (6980), 281-6.
95. Hanna, R.; Doudna, J. A., Metal ions in ribozyme folding and catalysis. *Curr Opin Chem Biol* **2000**, *4* (2), 166-70.
96. Nakano, S.; Chadalavada, D. M.; Bevilacqua, P. C., General acid-base catalysis in the mechanism of a hepatitis delta virus ribozyme. *Science* **2000**, *287* (5457), 1493-7.
97. Soukup, J. K., Chapter Five - The Structural and Functional Uniqueness of the *glmS* Ribozyme. In *Prog Mol Biol Transl Sci*, Garrett, A. S., Ed. Academic Press: 2013; Vol. Volume 120, pp 173-193.
98. Weinberg, Z.; Wang, J. X.; Bogue, J.; Yang, J.; Corbino, K.; Moy, R. H.; Breaker, R. R., Comparative genomics reveals 104 candidate structured RNAs from bacteria, archaea, and their metagenomes. *Genome Biol* **2010**, *11* (3), R31.
99. Cheah, M. T.; Wachter, A.; Sudarsan, N.; Breaker, R. R., Control of alternative RNA splicing and gene expression by eukaryotic riboswitches. *Nature* **2007**, *447* (7143), 497-500.
100. Sudarsan, N.; Lee, E. R.; Weinberg, Z.; Moy, R. H.; Kim, J. N.; Link, K. H.; Breaker, R. R., Riboswitches in eubacteria sense the second messenger cyclic di-GMP. *Science* **2008**, *321* (5887), 411-3.
101. Wachter, A.; Tunc-Ozdemir, M.; Grove, B. C.; Green, P. J.; Shintani, D. K.; Breaker, R. R., Riboswitch control of gene expression in plants by splicing and alternative 3' end processing of mRNAs. *Plant Cell* **2007**, *19* (11), 3437-50.
102. Blount, K. F.; Breaker, R. R., Riboswitches as antibacterial drug targets. *Nat Biotechnol* **2006**, *24* (12), 1558-64.

103. Mandal, M.; Lee, M.; Barrick, J. E.; Weinberg, Z.; Emilsson, G. M.; Ruzzo, W. L.; Breaker, R. R., A glycine-dependent riboswitch that uses cooperative binding to control gene expression. *Science* **2004**, *306* (5694), 275-9.
104. Barrick, J. E.; Corbino, K. A.; Winkler, W. C.; Nahvi, A.; Mandal, M.; Collins, J.; Lee, M.; Roth, A.; Sudarsan, N.; Jona, I.; Wickiser, J. K.; Breaker, R. R., New RNA motifs suggest an expanded scope for riboswitches in bacterial genetic control. *Proc Natl Acad Sci U S A* **2004**, *101* (17), 6421-6.
105. Nahvi, A.; Sudarsan, N.; Ebert, M. S.; Zou, X.; Brown, K. L.; Breaker, R. R., Genetic control by a metabolite binding mRNA. *Chem Biol* **2002**, *9* (9), 1043.
106. Mironov, A. S.; Gusarov, I.; Rafikov, R.; Lopez, L. E.; Shatalin, K.; Kreneva, R. A.; Perumov, D. A.; Nudler, E., Sensing small molecules by nascent RNA: a mechanism to control transcription in bacteria. *Cell* **2002**, *111* (5), 747-56.
107. Winkler, W.; Nahvi, A.; Breaker, R. R., Thiamine derivatives bind messenger RNAs directly to regulate bacterial gene expression. *Nature* **2002**, *419* (6910), 952-6.
108. Winkler, W. C.; Cohen-Chalamish, S.; Breaker, R. R., An mRNA structure that controls gene expression by binding FMN. *Proc Natl Acad Sci U S A* **2002**, *99* (25), 15908-13.
109. Breaker, R. R., Prospects for riboswitch discovery and analysis. *Mol Cell* **2011**, *43* (6), 867-79.
110. McCown, P. J.; Corbino, K. A.; Stav, S.; Sherlock, M. E.; Breaker, R. R., Riboswitch Diversity and Distribution. *Rna* **2017**.
111. Mandal, M.; Breaker, R. R., Adenine riboswitches and gene activation by disruption of a transcription terminator. *Nat Struct Mol Biol* **2004**, *11* (1), 29-35.
112. Winkler, W. C.; Nahvi, A.; Sudarsan, N.; Barrick, J. E.; Breaker, R. R., An mRNA structure that controls gene expression by binding S-adenosylmethionine. *Nat Struct Biol* **2003**, *10* (9), 701-7.
113. Sudarsan, N.; Cohen-Chalamish, S.; Nakamura, S.; Emilsson, G. M.; Breaker, R. R., Thiamine pyrophosphate riboswitches are targets for the antimicrobial compound pyrithiamine. *Chem Biol* **2005**, *12* (12), 1325-1335.
114. Serganov, A.; Polonskaia, A.; Phan, A. T.; Breaker, R. R.; Patel, D. J., Structural basis for gene regulation by a thiamine pyrophosphate-sensing riboswitch. *Nature* **2006**, *441* (7097), 1167-71.
115. Thore, S.; Leibundgut, M.; Ban, N., Structure of the eukaryotic thiamine pyrophosphate riboswitch with its regulatory ligand. *Science* **2006**, *312* (5777), 1208-11.
116. Edwards, T. E.; Ferre-D'Amare, A. R., Crystal structures of the thi-box riboswitch bound to thiamine pyrophosphate analogs reveal adaptive RNA-small molecule recognition. *Structure* **2006**, *14* (9), 1459-68.
117. Mayer, G.; Lünse, C.; Suckling, C.; Scott, F., Novel TPP-riboswitch activators bypass metabolic enzyme dependency. *Frontiers in Chemistry* **2014**, *2*.
118. Roth, A. M., P.J.; Zhang, K.; Lee, J.; Breaker, R.R. , Natural structural variations in TPP riboswitches result in altered ligand binding. *in preparation* **2017**.
119. Peselis, A.; Serganov, A., Themes and variations in riboswitch structure and function. *Biochim Biophys Acta* **2014**.
120. Trausch, J. J.; Ceres, P.; Reyes, F. E.; Batey, R. T., The structure of a tetrahydrofolate-sensing riboswitch reveals two ligand binding sites in a single aptamer. *Structure* **2011**, *19* (10), 1413-23.

121. Huang, L.; Ishibe-Murakami, S.; Patel, D. J.; Serganov, A., Long-range pseudoknot interactions dictate the regulatory response in the tetrahydrofolate riboswitch. *Proc Natl Acad Sci U S A* **2011**, *108* (36), 14801-6.
122. Serganov, A.; Huang, L.; Patel, D. J., Coenzyme recognition and gene regulation by a flavin mononucleotide riboswitch. *Nature* **2009**, *458* (7235), 233-7.
123. Kang, M.; Peterson, R.; Feigon, J., Structural Insights into riboswitch control of the biosynthesis of queuosine, a modified nucleotide found in the anticodon of tRNA. *Mol Cell* **2009**, *33* (6), 784-90.
124. Liberman, J. A.; Salim, M.; Krucinska, J.; Wedekind, J. E., Structure of a class II preQ1 riboswitch reveals ligand recognition by a new fold. *Nat Chem Biol* **2013**, *9* (6), 353-5.
125. Serganov, A.; Yuan, Y. R.; Pikovskaya, O.; Polonskaia, A.; Malinina, L.; Phan, A. T.; Hobartner, C.; Micura, R.; Breaker, R. R.; Patel, D. J., Structural basis for discriminative regulation of gene expression by adenine- and guanine-sensing mRNAs. *Chem Biol* **2004**, *11* (12), 1729-41.
126. Batey, R. T.; Gilbert, S. D.; Montange, R. K., Structure of a natural guanine-responsive riboswitch complexed with the metabolite hypoxanthine. *Nature* **2004**, *432* (7015), 411-5.
127. Garst, A. D.; Heroux, A.; Rambo, R. P.; Batey, R. T., Crystal structure of the lysine riboswitch regulatory mRNA element. *J Biol Chem* **2008**, *283* (33), 22347-51.
128. Serganov, A.; Huang, L.; Patel, D. J., Structural insights into amino acid binding and gene control by a lysine riboswitch. *Nature* **2008**, *455* (7217), 1263-7.
129. Klein, D. J.; Ferre-D'Amare, A. R., Structural basis of glmS ribozyme activation by glucosamine-6-phosphate. *Science* **2006**, *313* (5794), 1752-6.
130. Cochrane, J. C.; Lipchock, S. V.; Strobel, S. A., Structural investigation of the GlnS ribozyme bound to its catalytic cofactor. *Chem Biol* **2007**, *14* (1), 97-105.
131. Ren, A.; Rajashankar, K. R.; Patel, D. J., Fluoride ion encapsulation by Mg²⁺ ions and phosphates in a fluoride riboswitch. *Nature* **2012**, *486* (7401), 85-9.
132. Dann, C. E., 3rd; Wakeman, C. A.; Sieling, C. L.; Baker, S. C.; Irnov, I.; Winkler, W. C., Structure and mechanism of a metal-sensing regulatory RNA. *Cell* **2007**, *130* (5), 878-92.
133. Smith, K. D.; Lipchock, S. V.; Ames, T. D.; Wang, J.; Breaker, R. R.; Strobel, S. A., Structural basis of ligand binding by a c-di-GMP riboswitch. *Nat Struct Mol Biol* **2009**, *16* (12), 1218-23.
134. Hengge, R., Principles of c-di-GMP signalling in bacteria. *Nat Rev Microbiol* **2009**, *7* (4), 263-73.
135. Sudarsan, N.; Wickiser, J. K.; Nakamura, S.; Ebert, M. S.; Breaker, R. R., An mRNA structure in bacteria that controls gene expression by binding lysine. *Genes Dev* **2003**, *17* (21), 2688-97.
136. Blount, K. F.; Wang, J. X.; Lim, J.; Sudarsan, N.; Breaker, R. R., Antibacterial lysine analogs that target lysine riboswitches. *Nat Chem Biol* **2007**, *3* (1), 44-9.
137. Ataide, S. F.; Wilson, S. N.; Dang, S.; Rogers, T. E.; Roy, B.; Banerjee, R.; Henkin, T. M.; Ibbra, M., Mechanisms of resistance to an amino acid antibiotic that targets translation. *ACS Chem Biol* **2007**, *2* (12), 819-27.
138. Mulhbachter, J.; Brouillette, E.; Allard, M.; Fortier, L. C.; Malouin, F.; Lafontaine, D. A., Novel riboswitch ligand analogs as selective inhibitors of guanine-related metabolic pathways. *PLoS Pathog* **2010**, *6* (4), e1000865.

139. Ster, C.; Allard, M.; Boulanger, S.; Lamontagne Boulet, M.; Mulhbacher, J.; Lafontaine, D. A.; Marsault, E.; Lacasse, P.; Malouin, F., Experimental treatment of *Staphylococcus aureus* bovine intramammary infection using a guanine riboswitch ligand analog. *J Dairy Sci* **2013**, *96* (2), 1000-8.
140. Kofoed, E. M.; Yan, D.; Katakam, A. K.; Reichelt, M.; Lin, B.; Kim, J.; Park, S.; Date, S. V.; Monk, I. R.; Xu, M.; Austin, C. D.; Maurer, T.; Tan, M.-W., De Novo Guanine Biosynthesis but Not the Riboswitch-Regulated Purine Salvage Pathway Is Required for *Staphylococcus aureus* Infection In Vivo. *J Bacteriol* **2016**, *198* (14), 2001-2015.
141. Woolley, D. W.; White, A. G. C., SELECTIVE REVERSIBLE INHIBITION OF MICROBIAL GROWTH WITH PYRITHIAMINE. *The Journal of Experimental Medicine* **1943**, *78* (6), 489-497.
142. Robbins, W. J., A Pyrimidine Analog of Thiamine and the Growth of Fungi. *Proc Natl Acad Sci U S A* **1942**, *28* (9), 352-355.
143. Chen, L.; Cressina, E.; Leeper, F. J.; Smith, A. G.; Abell, C., A fragment-based approach to identifying ligands for riboswitches. *ACS Chem Biol* **2010**, *5* (4), 355-8.
144. Chen L, C. E., Dixon N, Erixon K, Agyei-Owusu K, Micklefield J, Smith AG, Abell C, Leeper FJ, Probing riboswitch-ligand interactions using thiamine pyrophosphate analogues. *Org Biomol Chem* **2012**, 5924-5931.
145. Cressina, E.; Chen, L.; Moulin, M.; Leeper, F. J.; Abell, C.; Smith, A. G., Identification of novel ligands for thiamine pyrophosphate (TPP) riboswitches. *Biochem Soc Trans* **2011**, *39* (2), 652-7.
146. Cressina, E.; Chen, L.; Abell, C.; Leeper, F. J.; Smith, A. G., Fragment screening against the thiamine pyrophosphate riboswitchthiM. *Chemical Science* **2011**, *2* (1), 157-165.
147. Ott, E.; Stolz, J.; Lehmann, M.; Mack, M., The RFN riboswitch of *Bacillus subtilis* is a target for the antibiotic roseoflavin produced by *Streptomyces davawensis*. *RNA Biol* **2009**, *6* (3), 276-80.
148. Howe, J. A.; Wang, H.; Fischmann, T. O.; Balibar, C. J.; Xiao, L.; Galgoci, A. M.; Malinverni, J. C.; Mayhood, T.; Villafania, A.; Nahvi, A.; Murgolo, N.; Barbieri, C. M.; Mann, P. A.; Carr, D.; Xia, E.; Zuck, P.; Riley, D.; Painter, R. E.; Walker, S. S.; Sherborne, B.; de Jesus, R.; Pan, W.; Plotkin, M. A.; Wu, J.; Rindgen, D.; Cummings, J.; Garlisi, C. G.; Zhang, R.; Sheth, P. R.; Gill, C. J.; Tang, H.; Roemer, T., Selective small-molecule inhibition of an RNA structural element. *Nature* **2015**.
149. Brooks, K. M.; Hampel, K. J., Rapid steps in the glmS ribozyme catalytic pathway: cation and ligand requirements. *Biochemistry* **2011**, *50* (13), 2424-33.
150. Lunse, C. E.; Schmidt, M. S.; Wittmann, V.; Mayer, G., Carba-sugars activate the glmS-riboswitch of *Staphylococcus aureus*. *ACS Chem Biol* **2011**, *6* (7), 675-8.
151. McCarthy, T. J.; Plog, M. A.; Floy, S. A.; Jansen, J. A.; Soukup, J. K.; Soukup, G. A., Ligand requirements for glmS ribozyme self-cleavage. *Chem Biol* **2005**, *12* (11), 1221-6.
152. Klein, D. J.; Wilkinson, S. R.; Been, M. D.; Ferre-D'Amare, A. R., Requirement of helix P2.2 and nucleotide G1 for positioning the cleavage site and cofactor of the glmS ribozyme. *J Mol Biol* **2007**, *373* (1), 178-89.
153. Roth, A.; Nahvi, A.; Lee, M.; Jona, I.; Breaker, R. R., Characteristics of the glmS ribozyme suggest only structural roles for divalent metal ions. *Rna* **2006**, *12* (4), 607-19.

154. Viladoms, J.; Fedor, M. J., The glmS ribozyme cofactor is a general acid-base catalyst. *J Am Chem Soc* **2012**, *134* (46), 19043-9.
155. Davis, J. H.; Dunican, B. F.; Strobel, S. A., glmS Riboswitch binding to the glucosamine-6-phosphate alpha-anomer shifts the pKa toward neutrality. *Biochemistry* **2011**, *50* (33), 7236-42.
156. Lim, J.; Grove, B. C.; Roth, A.; Breaker, R. R., Characteristics of ligand recognition by a glmS self-cleaving ribozyme. *Angew Chem Int Ed Engl* **2006**, *45* (40), 6689-93.
157. Blount, K.; Puskarz, I.; Penchovsky, R.; Breaker, R., Development and application of a high-throughput assay for glmS riboswitch activators. *RNA Biol* **2006**, *3* (2), 77-81.
158. Lunse, C. E.; Schuller, A.; Mayer, G., The promise of riboswitches as potential antibacterial drug targets. *Int J Med Microbiol* **2013**.
159. Mayer, G.; Famulok, M., High-throughput-compatible assay for glmS riboswitch metabolite dependence. *ChemBiochem* **2006**, *7* (4), 602-4.
160. Klawuhn, K.; Jansen, J. A.; Soucek, J.; Soukup, G. A.; Soukup, J. K., Analysis of metal ion dependence in glmS ribozyme self-cleavage and coenzyme binding. *ChemBiochem* **2010**, *11* (18), 2567-71.
161. Lau, M. W.; Ferre-D'Amare, A. R., An in vitro evolved glmS ribozyme has the wild-type fold but loses coenzyme dependence. *Nat Chem Biol* **2013**, *9* (12), 805-10.
162. Lau, M. W.; Trachman, R. J., 3rd; Ferre-D'Amare, A. R., A divalent cation-dependent variant of the glmS ribozyme with stringent Ca²⁺ selectivity co-opts a preexisting nonspecific metal ion-binding site. *Rna* **2017**, *23* (3), 355-364.
163. Jansen, J. A.; McCarthy, T. J.; Soukup, G. A.; Soukup, J. K., Backbone and nucleobase contacts to glucosamine-6-phosphate in the glmS ribozyme. *Nat Struct Mol Biol* **2006**, *13* (6), 517-23.
164. Hampel, K. J.; Tinsley, M. M., Evidence for preorganization of the glmS ribozyme ligand binding pocket. *Biochemistry* **2006**, *45* (25), 7861-71.
165. Tinsley, R. A.; Furchak, J. R.; Walter, N. G., Trans-acting glmS catalytic riboswitch: locked and loaded. *Rna* **2007**, *13* (4), 468-77.
166. Cochrane, J. C.; Lipchock, S. V.; Smith, K. D.; Strobel, S. A., Structural and chemical basis for glucosamine 6-phosphate binding and activation of the glmS ribozyme. *Biochemistry* **2009**, *48* (15), 3239-46.
167. McCown, P. J.; Winkler, W. C.; Breaker, R. R., Mechanism and distribution of glmS ribozymes. *Methods Mol Biol* **2012**, *848*, 113-29.
168. Schwalbe, H.; Buck, J.; Fürtig, B.; Noeske, J.; Wöhnert, J., Structures of RNA Switches: Insight into Molecular Recognition and Tertiary Structure. *Angewandte Chemie International Edition* **2007**, *46* (8), 1212-1219.
169. Dubecky, M.; Walter, N. G.; Sponer, J.; Otyepka, M.; Banas, P., Chemical feasibility of the general acid/base mechanism of glmS ribozyme self-cleavage. *Biopolymers* **2015**, *103* (10), 550-62.
170. Fei, X.; Holmes, T.; Diddle, J.; Hintz, L.; Delaney, D.; Stock, A.; Renner, D.; McDevitt, M.; Berkowitz, D. B.; Soukup, J. K., Phosphatase-Inert Glucosamine 6-Phosphate Mimics Serve as Actuators of the glmS Riboswitch. *ACS Chem Biol* **2014**.
171. Kath-Schorr, S.; Wilson, T. J.; Li, N. S.; Lu, J.; Piccirilli, J. A.; Lilley, D. M., General acid-base catalysis mediated by nucleobases in the hairpin ribozyme. *J Am Chem Soc* **2012**, *134* (40), 16717-24.

172. Bevilacqua, P. C.; Brown, T. S.; Nakano, S.; Yajima, R., Catalytic roles for proton transfer and protonation in ribozymes. *Biopolymers* **2004**, *73* (1), 90-109.
173. Klein, D. J.; Been, M. D.; Ferre-D'Amare, A. R., Essential role of an active-site guanine in glmS ribozyme catalysis. *J Am Chem Soc* **2007**, *129* (48), 14858-9.
174. Soukup, G. A., Core requirements for glmS ribozyme self-cleavage reveal a putative pseudoknot structure. *Nucleic Acids Res* **2006**, *34* (3), 968-75.
175. Fedor, M. J.; Williamson, J. R., The catalytic diversity of RNAs. *Nat Rev Mol Cell Biol* **2005**, *6* (5), 399-412.
176. Xin, Y.; Hamelberg, D., Deciphering the role of glucosamine-6-phosphate in the riboswitch action of glmS ribozyme. *Rna-a Publication of the Rna Society* **2010**, *16* (12), 2455-63.
177. Viladoms, J.; Scott, L. G.; Fedor, M. J., An active-site guanine participates in glmS ribozyme catalysis in its protonated state. *J Am Chem Soc* **2011**, *133* (45), 18388-96.
178. Even, S.; Pellegrini, O.; Zig, L.; Labas, V.; Vinh, J.; Brechemmier-Baey, D.; Putzer, H., Ribonucleases J1 and J2: two novel endoribonucleases in *B.subtilis* with functional homology to *E.coli* RNase E. *Nucleic Acids Res* **2005**, *33* (7), 2141-52.
179. Milewski, S., Glucosamine-6-phosphate synthase—the multi-facets enzyme. *Biochimica et Biophysica Acta (BBA) - Protein Structure and Molecular Enzymology* **2002**, *1597* (2), 173-192.
180. Ghosh, S.; Blumenthal, H. J.; Davidson, E.; Roseman, S., Glucosamine metabolism. V. Enzymatic synthesis of glucosamine 6-phosphate. *J Biol Chem* **1960**, *235*, 1265-73.
181. Yki-Jarvinen, H.; Nyman, T.; Rissanen, E.; Leino, M.; Hamalainen, S.; Virkamaki, A.; Hauguel-de Mouzon, S., Glutamine: fructose-6-phosphate amidotransferase activity and gene expression are regulated in a tissue-specific fashion in pregnant rats. *Life Sci* **1999**, *65* (2), 215-23.
182. Bates, C. J.; Adams, W. R.; Handschumacher, R. E., Control of the formation of uridine diphospho-N-acetyl-hexosamine and glycoprotein synthesis in rat liver. *J Biol Chem* **1966**, *241* (8), 1705-12.
183. Whelan, W. L.; Ballou, C. E., Sporulation in *D-glucosamine* auxotrophs of *Saccharomyces cerevisiae*: meiosis with defective ascospore wall formation. *J Bacteriol* **1975**, *124* (3), 1545-57.
184. McCown, P. J.; Roth, A.; Breaker, R. R., An expanded collection and refined consensus model of glmS ribozymes. *Rna* **2011**, *17* (4), 728-36.
185. Komatsuzawa, H.; Fujiwara, T.; Nishi, H.; Yamada, S.; Ohara, M.; McCallum, N.; Berger-Bachi, B.; Sugai, M., The gate controlling cell wall synthesis in *Staphylococcus aureus*. *Mol Microbiol* **2004**, *53* (4), 1221-31.
186. Sarvas, M., Mutant of *Escherichia coli* K-12 defective in *D-glucosamine* biosynthesis. *J Bacteriol* **1971**, *105* (2), 467-71.
187. Freese, E. B.; Cole, R. M.; Klofat, W.; Freese, E., Growth, sporulation, and enzyme defects of glucosamine mutants of *Bacillus subtilis*. *J Bacteriol* **1970**, *101* (3), 1046-62.
188. Wu, H. C.; Wu, T. C., Isolation and characterization of a glucosamine-requiring mutant of *Escherichia coli* K-12 defective in glucosamine-6-phosphate synthetase. *J Bacteriol* **1971**, *105* (2), 455-66.

189. Imada, A.; Nozaki, Y.; Kawashima, F.; Yoneda, M., Regulation of glucosamine utilization in *Staphylococcus aureus* and *Escherichia coli*. *J Gen Microbiol* **1977**, *100* (2), 329-37.
190. Ferre-D'Amare, A. R., Use of a coenzyme by the glmS ribozyme-riboswitch suggests primordial expansion of RNA chemistry by small molecules. *Philos Trans R Soc Lond B Biol Sci* **2011**, *366* (1580), 2942-8.
191. Vogler, A. P.; Trentmann, S.; Lengeler, J. W., Alternative route for biosynthesis of amino sugars in *Escherichia coli* K-12 mutants by means of a catabolic isomerase. *J Bacteriol* **1989**, *171* (12), 6586-92.
192. Chmara, H.; Zahner, H.; Borowski, E., Anticapsin, an active-site directed irreversible inhibitor of glucosamine-6-phosphate synthetase from *Escherichia coli*. *J Antibiot (Tokyo)* **1984**, *37* (9), 1038-43.
193. Kaminski, K.; Sokolowska, T., Letter: The probable identity of bacilysin and tetaïne. *J Antibiot (Tokyo)* **1973**, *26* (3), 184-5.
194. Barreteau, H.; Kovac, A.; Boniface, A.; Sova, M.; Gobec, S.; Blanot, D., Cytoplasmic steps of peptidoglycan biosynthesis. *FEMS Microbiol Rev* **2008**, *32* (2), 168-207.
195. Chmara, H.; Milewski, S.; Andruszkiewicz, R.; Mignini, F.; Borowski, E., Antibacterial action of dipeptides containing an inhibitor of glucosamine-6-phosphate isomerase. *Microbiology* **1998**, *144* (Pt 5), 1349-58.
196. Rogers, H. J. P., H.R.; Ward, J.B., *Microbial Cell Walls and Membranes*. Chapman and Hall, London. **1980**.
197. Ghuysen, J. M.; Hakenbeck, R., *Bacterial Cell Wall*. Elsevier Science: 1994.
198. Urban, J. H.; Vogel, J., Two seemingly homologous noncoding RNAs act hierarchically to activate glmS mRNA translation. *PLoS Biol* **2008**, *6* (3), e64.
199. Lünse, C. E., Dissertation. *University of Bonn* **2012**.
200. Schuller, A.; Matzner, D.; Lunse, C. E.; Wittmann, V.; Schumacher, C.; Unsleber, S.; Brotz-Oesterhelt, H.; Mayer, C.; Bierbaum, G.; Mayer, G., Activation of the glmS Ribozyme Confers Bacterial Growth Inhibition. *Chembiochem* **2017**, *18* (5), 435-440.
201. Montalbetti, N.; Simonin, A.; Simonin, C.; Awale, M.; Reymond, J.-L.; Hediger, M. A., Discovery and characterization of a novel non-competitive inhibitor of the divalent metal transporter DMT1/SLC11A2. *Biochemical Pharmacology* **2015**, *96* (3), 216-224.
202. Gundlach, J.; Mehne, F. M. P.; Herzberg, C.; Kampf, J.; Valerius, O.; Kaefer, V.; Stülke, J., An Essential Poison: Synthesis and Degradation of Cyclic Di-AMP in *Bacillus subtilis*. *J Bacteriol* **2015**, *197* (20), 3265-3274.
203. Wilson, D. B., Cellular transport mechanisms. *Annu Rev Biochem* **1978**, *47*, 933-65.
204. Cui, L.; Murakami, H.; Kuwahara-Arai, K.; Hanaki, H.; Hiramatsu, K., Contribution of a Thickened Cell Wall and Its Glutamine Nonamidated Component to the Vancomycin Resistance Expressed by *Staphylococcus aureus* Mu50. *Antimicrob Agents Chemother* **2000**, *44* (9), 2276-2285.
205. Urban, A.; Eckermann, S.; Fast, B.; Metzger, S.; Gehling, M.; Ziegelbauer, K.; Rubsamen-Waigmann, H.; Freiberg, C., Novel whole-cell antibiotic biosensors for compound discovery. *Appl Environ Microbiol* **2007**, *73* (20), 6436-43.
206. Soukup, G. A., *Catalytic RNA*. Elsevier Science: 2013.
207. Burger, A., Isosterism and bioisosterism in drug design. *Progress in drug research. Fortschritte der Arzneimittelforschung. Progres des recherches pharmaceutiques* **1991**, *37*, 287-371.

208. Patani, G. A.; LaVoie, E. J., Bioisosterism: A Rational Approach in Drug Design. *Chem Rev* **1996**, *96* (8), 3147-3176.
209. Blount, K.; Puskarz, I.; Penchovsky, R.; Breaker, R., Development and application of a high-throughput assay for glmS riboswitch activators. *RNA Biol* **2006**, *3* (2), 77-81.
210. Prax, M.; Lee, C. Y.; Bertram, R., An update on the molecular genetics toolbox for staphylococci. *Microbiology* **2013**, *159* (Pt 3), 421-35.
211. McNamara, P. J., Staphylococcus: Molecular Genetics. *Caister Academic Press* **2008**.
212. Morikawa, K.; Inose, Y.; Okamura, H.; Maruyama, A.; Hayashi, H.; Takeyasu, K.; Ohta, T., A new staphylococcal sigma factor in the conserved gene cassette: functional significance and implication for the evolutionary processes. *Genes to cells : devoted to molecular & cellular mechanisms* **2003**, *8* (8), 699-712.
213. Morikawa, K.; Takemura, A. J.; Inose, Y.; Tsai, M.; Nguyen Thi le, T.; Ohta, T.; Msadek, T., Expression of a cryptic secondary sigma factor gene unveils natural competence for DNA transformation in Staphylococcus aureus. *PLoS Pathog* **2012**, *8* (11), e1003003.
214. Baev, M. V.; Baev, D.; Radek, A. J.; Campbell, J. W., Growth of Escherichia coli MG1655 on LB medium: monitoring utilization of sugars, alcohols, and organic acids with transcriptional microarrays. *Appl Microbiol Biotechnol* **2006**, *71* (3), 310-6.
215. Wiemer, A. J.; Wiemer, D. F., Prodrugs of phosphonates and phosphates: crossing the membrane barrier. *Topics in current chemistry* **2015**, *360*, 115-160.
216. Wang, G. N.; Lau, P. S.; Li, Y. F.; Ye, X. S., Synthesis and evaluation of glucosamine-6-phosphate analogues as activators of glmS riboswitch. *Tetrahedron* **2012**, *68* (46), 9405-9412.
217. Sass, P.; Jansen, A.; Szekat, C.; Sass, V.; Sahl, H. G.; Bierbaum, G., The lantibiotic mersacidin is a strong inducer of the cell wall stress response of Staphylococcus aureus. *BMC Microbiol* **2008**, *8*, 186.
218. Kalamorz, F.; Reichenbach, B.; Marz, W.; Rak, B.; Gorke, B., Feedback control of glucosamine-6-phosphate synthase GlmS expression depends on the small RNA GlmZ and involves the novel protein YhbJ in Escherichia coli. *Mol Microbiol* **2007**, *65* (6), 1518-33.
219. Hutter, B.; Fischer, C.; Jacobi, A.; Schaab, C.; Loferer, H., Panel of Bacillus subtilis reporter strains indicative of various modes of action. *Antimicrob Agents Chemother* **2004**, *48* (7), 2588-94.
220. Wenzel, M.; Chiriac, A. I.; Otto, A.; Zweytick, D.; May, C.; Schumacher, C.; Gust, R.; Albada, H. B.; Penkova, M.; Kramer, U.; Erdmann, R.; Metzler-Nolte, N.; Straus, S. K.; Bremer, E.; Becher, D.; Brotz-Oesterhelt, H.; Sahl, H. G.; Bandow, J. E., Small cationic antimicrobial peptides delocalize peripheral membrane proteins. *Proc Natl Acad Sci U S A* **2014**, *111* (14), E1409-18.
221. Delumeau, O.; Lecointe, F.; Muntel, J.; Guillot, A.; Guédon, E.; Monnet, V.; Hecker, M.; Becher, D.; Polard, P.; Noirot, P., The dynamic protein partnership of RNA polymerase in Bacillus subtilis. *Proteomics* **2011**, *11* (15), 2992-3001.
222. Wiedermannová, J.; Sudzinová, P.; Kovaľ, T.; Rabatinová, A.; Šanderová, H.; Ramaniuk, O.; Rittich, Š.; Dohnálek, J.; Fu, Z.; Halada, P.; Lewis, P.; Krásný, L., Characterization of HelD, an interacting partner of RNA polymerase from Bacillus subtilis. *Nucleic Acids Res* **2014**, *42* (8), 5151-5163.
223. Hiramatsu, K.; Aritaka, N.; Hanaki, H.; Kawasaki, S.; Hosoda, Y.; Hori, S.; Fukuchi, Y.; Kobayashi, I., Dissemination in Japanese hospitals of strains of

- Staphylococcus aureus heterogeneously resistant to vancomycin. *Lancet* **1997**, 350 (9092), 1670-3.
224. Leishman, S. J.; Do, H. L.; Ford, P. J., Cardiovascular disease and the role of oral bacteria. *Journal of Oral Microbiology* **2010**, 2, 10.3402/jom.v2i0.5781.
225. Li, X.; Kolltveit, K. M.; Tronstad, L.; Olsen, I., Systemic Diseases Caused by Oral Infection. *Clinical Microbiology Reviews* **2000**, 13 (4), 547-558.
226. Khvorova, A.; Lescoute, A.; Westhof, E.; Jayasena, S. D., Sequence elements outside the hammerhead ribozyme catalytic core enable intracellular activity. *Nat Struct Biol* **2003**, 10 (9), 708-12.
227. Zhao, Z. Y.; Wilson, T. J.; Maxwell, K.; Lilley, D. M., The folding of the hairpin ribozyme: dependence on the loops and the junction. *Rna* **2000**, 6 (12), 1833-1846.
228. Treiber, D. K.; Rook, M. S.; Zarrinkar, P. P.; Williamson, J. R., Kinetic intermediates trapped by native interactions in RNA folding. *Science* **1998**, 279 (5358), 1943-6.
229. Feig, A. L. U., O. C., The role of metal ions in biochemistry. *Cold Spring Harbor Laboratory Press* **1999**.
230. Jesse, H. E.; Roberts, I. S.; Cavet, J. S., Metal ion homeostasis in *Listeria monocytogenes* and importance in host-pathogen interactions. *Advances in microbial physiology* **2014**, 65, 83-123.
231. Palmer, L. D.; Skaar, E. P., Transition Metals and Virulence in Bacteria. *Annual review of genetics* **2016**, 50, 67-91.
232. Juttukonda, L. J.; Skaar, E. P., Manganese Homeostasis and Utilization in Pathogenic Bacteria. *Mol Microbiol* **2015**, 97 (2), 216-228.
233. Groisman, E. A.; Hollands, K.; Kriner, M. A.; Lee, E.-J.; Park, S.-Y.; Pontes, M. H., Bacterial Mg(2+) Homeostasis, Transport, and Virulence. *Annual review of genetics* **2013**, 47, 625-646.
234. Ramesh, A.; Winkler, W. C., Magnesium-sensing riboswitches in bacteria. *RNA Biol* **2010**, 7 (1), 77-83.
235. Lin, Y. P.; Kuo, C. J.; Koleci, X.; McDonough, S. P.; Chang, Y. F., Manganese binds to *Clostridium difficile* Fbp68 and is essential for fibronectin binding. *J Biol Chem* **2011**, 286 (5), 3957-69.
236. Dominguez, D. C., Calcium signalling in bacteria. *Mol Microbiol* **2004**, 54 (2), 291-7.
237. Ovesen, L.; Bendtsen, F.; Tage-Jensen, U.; Pedersen, N. T.; Gram, B. R.; Rune, S. J., Intraluminal pH in the stomach, duodenum, and proximal jejunum in normal subjects and patients with exocrine pancreatic insufficiency. *Gastroenterology* **1986**, 90 (4), 958-62.
238. Webb, C. H.; Luptak, A., HDV-like self-cleaving ribozymes. *RNA Biol* **2011**, 8 (5), 719-27.
239. El-Murr, N.; Maurel, M. C.; Rihova, M.; Vergne, J.; Herve, G.; Kato, M.; Kawamura, K., Behavior of a hammerhead ribozyme in aqueous solution at medium to high temperatures. *Naturwissenschaften* **2012**, 99 (9), 731-8.
240. Johansson, J.; Mandin, P.; Renzoni, A.; Chiaruttini, C.; Springer, M.; Cossart, P., An RNA thermosensor controls expression of virulence genes in *Listeria monocytogenes*. *Cell* **2002**, 110 (5), 551-61.
241. Unione, L.; Xu, B.; Díaz, D.; Martín-Santamaría, S.; Poveda, A.; Sardinha, J.; Rauter, A. P.; Blériot, Y.; Zhang, Y.; Cañada, F. J.; Sollogoub, M.; Jiménez-Barbero, J., Conformational Plasticity in Glycomimetics: Fluorocarbamethyl-L-idopyranosides Mimic the Intrinsic Dynamic Behaviour of Natural Idose Rings. *Chemistry – A European Journal* **2015**, 21 (29), 10513-10521.

242. Xu, B.; Unione, L.; Sardinha, J.; Wu, S.; Ethève-Quellejeu, M.; Pilar Rauter, A.; Blériot, Y.; Zhang, Y.; Martín-Santamaría, S.; Díaz, D.; Jiménez-Barbero, J.; Sollogoub, M., gem-Difluorocarbadisaccharides: Restoring the exo-Anomeric Effect. *Angewandte Chemie International Edition* **2014**, *53* (36), 9597-9602.
243. Posakony, J. J.; Ferre-D'Amare, A. R., Glucosamine and glucosamine-6-phosphate derivatives: catalytic cofactor analogues for the glmS ribozyme. *J Org Chem* **2013**, *78* (10), 4730-43.
244. Matzner, D.; Schuller, A.; Seitz, T.; Wittmann, V.; Mayer, G., Fluoro-Carba-Sugars are Glycomimetic Activators of the glmS Ribozyme. *Chemistry* **2017**, *23* (51), 12604-12612.
245. Deutscher, J.; Aké, F. M. D.; Derkaoui, M.; Zébré, A. C.; Cao, T. N.; Bouraoui, H.; Kentache, T.; Mokhtari, A.; Milohanic, E.; Joyet, P., The Bacterial Phosphoenolpyruvate:Carbohydrate Phosphotransferase System: Regulation by Protein Phosphorylation and Phosphorylation-Dependent Protein-Protein Interactions. *Microbiol Mol Biol Rev* **2014**, *78* (2), 231-256.
246. Zhang, J.-H.; Chung, T. D. Y.; Oldenburg, K. R., A Simple Statistical Parameter for Use in Evaluation and Validation of High Throughput Screening Assays. *J Biomol Screen* **1999**, *4* (2), 67-73.

Acknowledgment

There are many people without whom this work would not have been possible, who contributed in one way or another to this thesis and it is a pleasure to thank those who made this possible.

First, I would like to express my sincere thankfulness to Professor Dr. Günter Mayer for the opportunity to work on this exciting project. His support and encouraging personal guidance has provided the basis for my scientific career from the very beginning.

I sincerely thank Prof. Dr. Tanja Schneider for her fruitful input within the Forschergruppe, which contributed to this thesis. Moreover, I highly appreciate the scientific example she gave.

I am very grateful to Prof. Dr. Sven Burgdorf and Prof. Dr. Ulrich Kubitscheck for their willingness to be referees on this thesis.

There are many collaborators whose contributions has been invaluable and I am grateful for their scientific input and the conversations during coffee breaks. This includes the working group of Prof. Gabriele Bierbaum who have supported me in performing studies of *S. aureus* and as a sign of confidence allowed me continuous access to their labs by my own pair of keys. I am sincerely thankful to Prof. Heike Brötz-Oesterhelt and Prof. Christoph Mayer and their working groups, especially Catherine Schumacher, Anne Berscheid and Sandra Unsleber, for their help on the MoA analysis of the herein analyzed Carba-sugars. Besides their irreplaceable scientific support, I want to thank them for the great time I was spending in their labs in Düsseldorf and Tübingen. I would like to thank PD Dr. Jens Müller for his kind advices and support in setting up qPCR experiments. The group of Prof. Reymond kindly provided the Reymond compounds and performed a second screening.

Moreover, I would like to thank the riboswitch team, Günter Mayer, Christina Lünse, Daniel Matzner, Yamel Cardona and the other interns for their valuable work.

I highly appreciate the work of my proof reading team which included Silvana Hassel, Franziska Pfeiffer, Gerd Brändle, Malte Rosenthal, Julia Siegl and Daniel Matzner I am thankful for their helpful comments and suggestions.

It is my great pleasure to thank the current and former members of the Mayer, Famulok and Kath-Schorr labs for their constant help and support. This in particular includes Gerd Brändle, Martina Bettio, Laia Civit, Christoph Domnick, Frank Eggert, Jörg Ewers, Franziska Frey, Annika Gebauer, Silvana Hassel, Mohamed Hussein, Mark Kehrzner Nicole Krämer, Sabine Lennarz, Christina Lünse, Daniel Matzner Björn Niebel, Franziska Pfeiffer, Malte Rosenthal, Justina Stark, Katia

Schöler, Julia Siegl, Julian Valero, Anna Weber, Benjamin Weiche, Olga Wolter and Christine Wosnitza.

I am grateful to the DFG for funding and would like to thank all the members of the FOR 854 for their support and the scientific opportunities that were given to me. Moreover, I want to thank all the current and former members of the Friday meeting and the aptamer meeting for their scientific input.

This PhD thesis laid the foundation for my scientific career. However, the chemistry building in the Gerhard-Domagk-Straße is a place where I meet several people that I now call my friends, this especially includes all the members of F²ACM as well as Annika Gebauer, Malte Rosenthal and Julia Siegl I am so thankful for your friendship and support in all matters.

Finally, I am truly indebted and want to express my deepest gratitude to my partner in good and bad times, Basti Esser for his partnership, love and constant support over the last years. It is my inner desire to express my heartfelt gratitude to my family, particularly my mother Margret Schüller, my brother Alexander Schüller, Basti Esser and my almost family in law, especially my almost parents in law, Monika & Wolfgang Esser for love support and understanding and for believing in me whenever I did not.